NASA Technical Memorandum 74079

Aerodynamic Characteristics of a Monoplanar Missile Concept With Bodies of Circular and Elliptical Cross Sections

Ernald B. Graves
Langley Research Center
Hampton, Virginia

NASA
National Aeronautics
and Space Administration
Scientific and Technical
Information Office
1977

SUMMARY

An investigation has been conducted to compare the experimental aerodynamic characteristics of a low-drag missile concept with a body of circular cross section to one with a body of 3:1 elliptical cross section, the bodies having identical cross-section area distributions. The concepts were of monowing design with constant wing span. Tail surfaces were located flush at the body base with ±90° dihedral. Wind-tunnel tests were performed at Mach numbers from 0.5 to 4.63 and at angles of attack from about -5° to 28°.

The comparison shows no significant subsonic normal-force differences at low angles of attack; however, at supersonic speeds, the elliptical concept increasingly provides greater normal force up to Mach 2.5 to 3.0, beyond which an incremental increase of about 25 percent holds through the angle-of-attack range. More pronounced nonlinearities in pitching moment occur at subsonic speeds for the elliptical concept, as well as less longitudinal stability at all test Mach numbers. However, levels of directional and lateral stability are increased, especially at the higher angles of attack. For comparable deflections of the tail surfaces of the circular and elliptical concepts, comparable moment control is indicated, with some apparent superiority in yaw control at supersonic speeds for the elliptical concepts.

INTRODUCTION

The National Aeronautics and Space Administration maintains a continuing research effort in missile related aerodynamics. In this effort, monoplanar missile concepts have been considered, in part, because of the relatively low geometric profile that can be achieved for convenient carriage (ref. 1). A lower geometric profile combined with increased maneuverability at high angles of attack appears naturally suited for missile bodies with elliptical cross sections.

Considerable research on elliptical cross-section bodies has been conducted, but on configurations primarily designed for hypersonic cruise (refs. 2 to 8). The purpose of the present effort is to examine, from the standpoint of stability, performance, and control, the relative merits of the elliptical body in a monoplanar missile concept. Thus, wind-tunnel tests of a monoplanar missile concept with circular body cross sections and with 3:1 elliptical body cross sections were conducted. The concepts had bodies with a fineness ratio of 7 and wing and tail components designed to make the concepts comparable. Test Mach numbers varied from 0.5 to 4.63, and angles of attack varied from about -5° to 28°.

SYMBOLS

The basic aerodynamic data are presented about the body system of axes. All moments are referenced to a point 60.0 percent of the body length when measured from the nose apex.

A reference area (based on maximum body cross-section area), 0.008107 m^2

C_A axial-force coefficient, $\frac{\text{Axial force}}{qA}$

$C_{A,total}$ gross axial-force coefficient, $\frac{\text{Gross axial force}}{qA}$

C_l rolling-moment coefficient, $\frac{\text{Rolling moment}}{qAd}$

C_{l_β} effective dihedral parameter, $\left(\frac{\Delta C_l}{\Delta \beta}\right)_{\alpha=0^\circ,3^\circ}$, per degree

C_m pitching-moment coefficient, $\frac{\text{Pitching moment}}{qAd}$

C_{m_α} longitudinal stability parameter, $\frac{\partial C_m}{\partial \alpha}$, per degree

C_N normal-force coefficient, $\frac{\text{Normal force}}{qA}$

C_n yawing-moment coefficient, $\frac{\text{Yawing moment}}{qAd}$

C_{n_β} directional stability parameter, $\left(\frac{\Delta C_n}{\Delta \beta}\right)_{\alpha=0^\circ,3^\circ}$, per degree

C_Y side-force coefficient, $\frac{\text{Side force}}{qA}$

C_{Y_β} side-force parameter, $\left(\frac{\Delta C_Y}{\Delta \beta}\right)_{\alpha=0^\circ,3^\circ}$, per degree

d	body maximum diameter, 0.1016 m
M	free-stream Mach number
q	free-stream dynamic pressure
α	angle of attack, deg
β	angle of sideslip, deg
δ_{pitch}	deflection of four tail panels to give change in C_m (positive sign denotes desired positive change in C_m), deg
δ_{roll}	deflection of four tail panels to give change in C_l (positive sign denotes desired positive change in C_l), deg
δ_{yaw}	deflection of four tail panels to give change in C_Y (positive sign denotes desired positive change in C_Y), deg

Model component designations:

B	body
T	tail (four panels)
W	wing (two panels)
O	circular body (see figs. 23 to 29)
⬭	elliptical body (see figs. 23 to 29)
	circular missile concept (see figs. 23 to 29)
	elliptical missile concept (see figs. 23 to 29)

TEST FACILITIES

Wind-tunnel tests at Mach numbers from 0.5 to 1.3 were conducted in the Aerodynamic Wind Tunnel (4T), Propulsion Wind Tunnel Facility (PWT) at Arnold Engineering Development Center. This facility is a variable-pressure, continuous-flow wind tunnel with perforated test-section wall.

Tests at Mach numbers from 1.6 to 4.63 were conducted in both the low and high Mach number test sections of the Langley Unitary Plan wind tunnel. This facility is a variable-pressure, continuous-flow wind tunnel with an asymmetric sliding-block nozzle ahead of each test section to permit continuous variation in Mach number.

MODELS

Model drawings are presented in figure 1, and a photograph of the models is shown as figure 2. The circular cross-sectional body was designed in accordance with the theories in references 9 and 10 for minimum wave drag with boattail. An afterbody closure ratio $A_{base}/A_{maximum}$ of 0.69 was used, with $A_{maximum}$ occurring at 68.0 percent body length. (This provided a nominal afterbody closure not exceeding 7°.) The body fineness ratio of 7 was based on maximum body diameter. The elliptical body had an exact 3:1 elliptical cross section that was identical to the area distribution of the circular body.

The wing area and span for the circular concept was chosen as typical of current maneuvering missiles (ref. 11). The wing for the elliptical concept was determined by projecting the elliptical body on the circular body-wing planform. The resultant exposed wing planform then became the wing for the elliptical body.

The tails were identical for both concepts and were located flush with the body base with ±30° dihedral. The tails were located at a 30° angle from the horizontal plane since analysis of the appropriate experimental data in reference 7 indicated that this arrangement would enhance the stability and control characteristics (ref. 12). In order for tail deflection to be compatible with the complex surfaces of the afterbody of the elliptical configuration, the tail hinge line was skewed such that a 10° deflection measured at the body-tail juncture had a resultant 7.04° surface deflection. (See fig. 1(b).)

TEST CONDITIONS

Tests were performed at the following nominal conditions:

Mach number	Stagnation temperature, K	Stagnation pressure, Pa	Reynolds number per meter
0.5	316	86 184.46	7.87×10^6
.7	316	68 947.57	7.87
.9	316	59 946.08	7.87
1.3	316	57 456.31	7.87
1.60	339	54 606.48	6.56
2.00	339	63 569.66	6.56
2.50	339	81 358.13	6.56
2.96	339	104 110.83	6.56
3.95	353	184 779.49	6.56
4.63	353	252 348.11	6.56

Boundary-layer transition grit consisting of sand particles was affixed to the nose, wing, and tail surfaces of the models. Transition bands were

placed a nominal 0.03556 m aft on the nose and 0.00254 m aft streamwise of the leading edges of both wing and tail surfaces. Transition was affixed as follows:

Mach number	ASTM size	Nominal diameter, m	Method	Band width, m
0.5 to 1.3	80	0.0001930	Sprinkle	0.0015875
1.60 to 2.00	60	.0004699	Sprinkle	.0015875
2.50 to 4.63	35	.0005461	Spaced 0.0013653 m apart	.0005461

All aerodynamic forces and moments were measured by means of an internally mounted electrical strain-gage balance, which in turn was rigidly fastened to a sting-tunnel support system. Static pressures in the model chamber and at the model base were also measured.

Angles of attack have been adjusted for tunnel airflow misalignment and model deflection due to aerodynamic loads. Axial-force data have been adjusted to free-stream conditions acting at the base of the models.

PRESENTATION OF DATA AND RESULTS

The data are plotted in comparative form so that the effect of various configuration changes can readily be seen. The following list of abbreviated figure legends is presented as an aid in locating specific experimental data and results.

Experimental Data

Configuration Comparisons

DISCUSSION

Longitudinal Aerodynamics

Comparisons of pitching-moment behavior of the circular and elliptical bodies alone as well as the respective complete configuration concepts are shown in figure 21 at typical subsonic (M = 0.7) and supersonic (M = 2.00) speeds. The data show a more positive C_{m_α} associated with the elliptical body than with the circular body, with no significant discontinuities associated with bodies of either circular or elliptical cross section. A more positive C_{m_α} is also characterized with the elliptical concept. For the 60-percent moment reference location, both concepts exhibit longitudinal stability at subsonic and supersonic speeds; however, significant nonlinearities in C_m ($\alpha > 8^o$) exist for the elliptical concept at subsonic speeds. Flow-visualization observations (vapor screen) tend to substantiate the belief that the low-profile elliptical forebody generates strong vortices which influence the flow about the top tail surfaces at angles of attack. This flow phenomenon results in the noticeable pitch-up observed in the M = 0.7 data.

The relative development of normal force (fig. 22) shows substantially more normal force associated with the elliptical body at subsonic and low supersonic speeds. This increased C_N can be attributed, in part, to the

larger planform area and higher aspect ratio and, in part, to the greater vortex induced normal force on the elliptical body (as can be noted by the reflex in the C_N curves in fig. 12). The reduction in the ratio of normal forces at the higher Mach numbers indicates a diminishing effect of vortex flow, leaving the difference in planform as the dominating factor. The relative C_N values for the complete missile concepts are reduced considerably since the larger wing on the circular concept provides a more efficient lifting surface at subsonic speeds (where vortex lift has more dominance). The difference in concept planform area is about 20 percent, which tends to substantiate the 25-percent increase in C_N (fig. 22) for the elliptical concept at higher speeds where planform area becomes more dominant.

The zero-lift axial force for the body-alone configurations is generally the same regardless of the body cross section. (See fig. 23(a).) A comparison of gross axial force at $\alpha = 0^\circ$ (fig. 23(b)) indicates that at supersonic speeds the average pressures acting at the body base were greater for the elliptical body than for the circular body. Less axial force is exhibited with the elliptical concept and can, in part, be attributed to the somewhat smaller overall cross-section area of the elliptical concept with its smaller wing volume. (See fig. 24.)

A comparison of center-of-pressure behavior can be seen in figure 25. The center of pressure at $\alpha = 0^\circ$ for the bodies is farther forward for the elliptical body at subsonic speeds and generally more aft at supersonic speeds. More center-of-pressure travel with angle of attack is associated with the elliptical body at subsonic speeds, with no appreciable difference occurring between the bodies at supersonic speeds. The center of pressure at $\alpha = 0^\circ$ always acts farther forward on the elliptical concept than on the circular one. The center-of-pressure change with angle of attack shows no appreciable difference between the complete concepts over the test Mach number range.

Figure 26 shows that an increase in cruise efficiency is also associated with the elliptical concept, as indicated by the higher lift-drag ratios (maximum untrimmed) that can be obtained.

Lateral-Directional Aerodynamics

Figure 27 summarizes the lateral-directional data. The parameters in figure 27(a) show the expected neutral dihedral effect of the circular body; the elliptical body displays a positive effective dihedral $\left(-C_{l_\beta}\right)$ at angles of attack. The elliptical body exhibits more significant increases in directional stability (more positive values of C_{n_β}) than does the circular body. The data (fig. 27(b)) show effective dihedral, as well as directional stability, for both concepts. More important, however, is the increase in the levels of both lateral and directional stability for the elliptical concept over the circular concept, especially at angles of attack. (The elliptical concept is directionally stable throughout the entire test angle-of-attack and Mach number range.) Data in figure 28 also show more longitudinal and directional stability compatibility for the elliptical concept than for the circular concept (i.e., the values of $-C_{m_\alpha}$ and C_{n_β} are more nearly equal).

Moment Control Parameters

A summary of control moments provided by deflection of the four tail surfaces at $\alpha = 0^\circ$ is shown in figure 29. The dash line represents wind-tunnel data for the elliptical concept; it is representative of 10° rotational deflection of an actuator mechanism located flush with the body surface and, correspondingly, a 7.04° deflection of the tail surface. The dash-dot line represents a linear extrapolation of 0° deflection and 7.04° deflection data to represent a surface deflection of 10.0°. The data indicate that when the tail surfaces are deflected to the same increment, the elliptical concept can provide more yaw control than can the comparable circular concept.

CONCLUSIONS

A wind-tunnel investigation has been conducted at Mach numbers from 0.5 to 4.63 to determine if a monoplanar missile concept with elliptical cross-section body has aerodynamic advantages over a comparable concept with circular body. The concepts had identical spans and body cross-section area distributions. The elliptical body had an eccentricity of 3:1. The tails for each design had a dihedral of ±30°.

Comparison of the elliptical cross-section concept with the circular cross-section concept indicates the following:

1. About 25 percent more normal force that is nearly independent of angle of attack can be achieved at supersonic speeds.

2. Values of the longitudinal stability parameter C_{m_α} are more positive, with more pronounced nonlinearities in pitching moment occurring at subsonic speeds.

3. Levels of directional stability are increased and are more compatible with levels of longitudinal stability.

4. Noticeably more yaw control is available, although suitable locations for tails on the body are more limited because of the geometry of the elliptical body.

Langley Research Center
National Aeronautics and Space Administration
Hampton, VA 23665
October 26, 1977

REFERENCES

1. Sawyer, Wallace C.; Jackson, Charlie M., Jr.; and Blair, A. B., Jr.: Aerodynamic Technologies for the Next Generation of Missiles. Paper presented at the AIAA/ADPA Tactical Missile Conference (Gaithersburg, Maryland), Apr. 27-28, 1977.

2. Spencer, Bernard, Jr.; and Phillips, W. Pelham: Effects of Cross-Section Shape on the Low-Speed Aerodynamic Characteristics of a Low-Wave-Drag Hypersonic Body. NASA TN D-1963, 1963.

3. Spencer, Bernard, Jr.; and Phillips, W. Pelham: Transonic Aerodynamic Characteristics of a Series of Bodies Having Variations in Fineness Ratio and Cross-Sectional Ellipticity. NASA TN D-2622, 1965.

4. Fournier, Roger H.; Spencer, Bernard, Jr.; and Corlett, William A.: Supersonic Aerodynamic Characteristics of a Series of Related Bodies With Cross-Sectional Ellipticity. NASA TN D-3539, 1966.

5. Spencer, Bernard, Jr.; Phillips, W. Pelham; and Fournier, Roger H.: Supersonic Aerodynamic Characteristics of a Series of Bodies Having Variations in Fineness Ratio and Cross-Section Ellipticity. NASA TN D-2389, 1964.

6. Nelms, Walter P., Jr.: Effects of Body Shape on the Aerodynamic Characteristics of an All-Body Hypersonic Aircraft Configuration at Mach Numbers From 0.65 to 10.6. NASA TN D-6821, 1972.

7. Spencer, Bernard, Jr.; and Fournier, Roger H.: Supersonic Aerodynamic Characteristics of Hypersonic Low-Wave-Drag Elliptical-Body—Tail Combinations as Affected by Changes in Stabilizer Configuration. NASA TM X-2747, 1973.

8. Fox, Charles H., Jr.; and Spencer, Bernard, Jr.: Hypersonic Aerodynamic Characteristics of Low-Wave-Drag Elliptical-Body—Tail Combinations as Affected by Changes in Stabilizer Configuration. NASA TM X-1620, 1968.

9. Adams, Mac C.: Determination of Shapes of Boattail Bodies of Revolution for Minimum Wave Drag. NACA TN 2550, 1951.

10. Bromm, August F., Jr.; and Goodwin, Julia M.: Investigation at Supersonic Speeds of the Wave Drag of Seven Boattail Bodies of Revolution Designed for Minimum Wave Drag. NACA TN 3054, 1953.

11. Friedman, R. F.: Aerodynamic Stability and Control Report for the Sparrow III Model XAAM-N-6b and YAAM-N-6b Missile. BR-1018 (Contract No. NOas-59-0317), Missile & Space Div., Raytheon Co., Nov. 1962. (Available from DDC as AD 511 006.)

12. Graves, Ernald B.: A Monoplanar Missile - The Aerodynamics With Bodies of Circular and Elliptical Cross Section. Blacks in Technology - Beyond the Bicentennial, CP 101, Natl. Tech. Assoc., Aug. 1977.

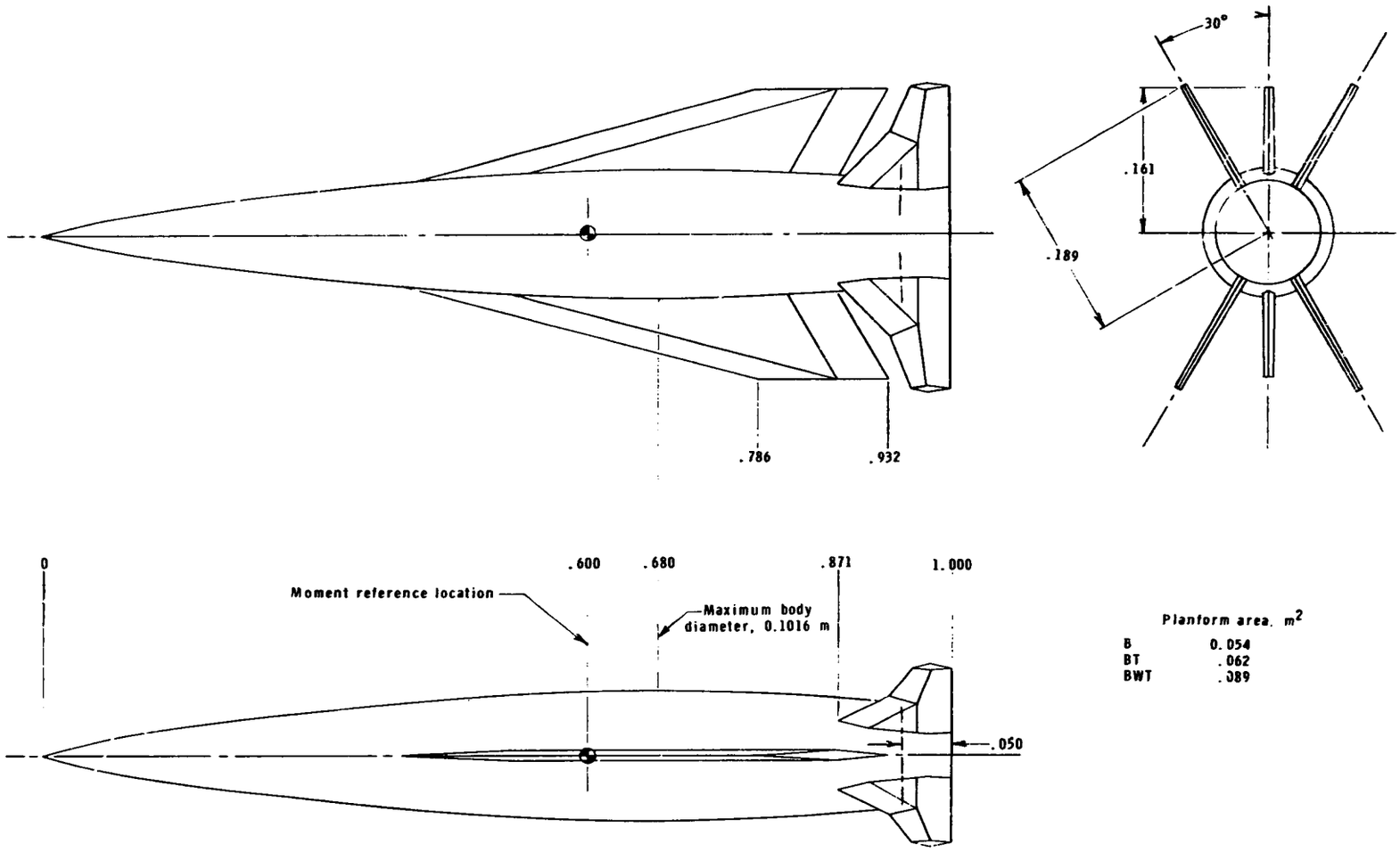

(a) Circular BWT (reference length, 0.7112 m).

Figure 1.- Details of model configurations. Linear dimensions are given in fractions of reference length.

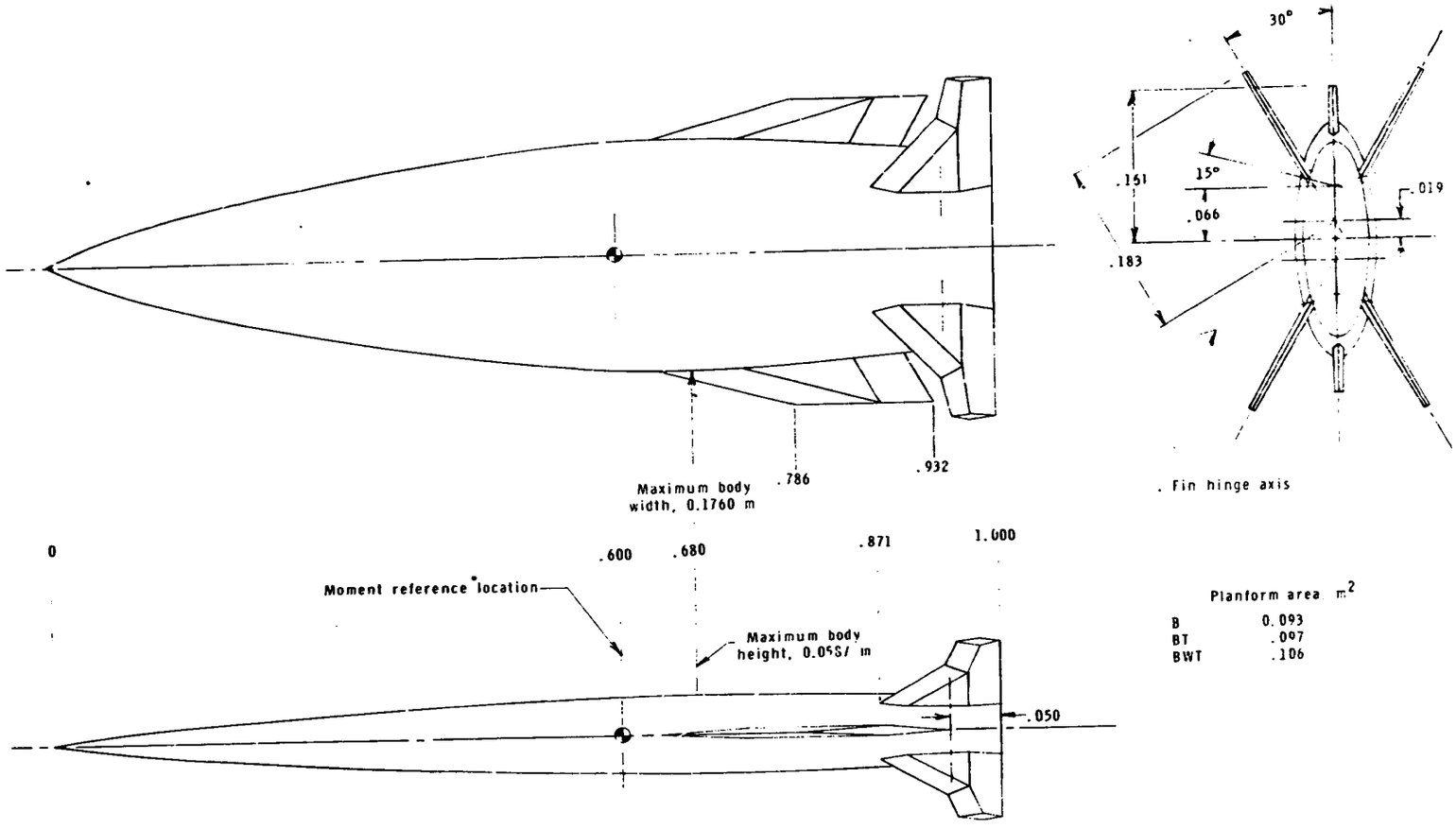

(b) Elliptical BWT (reference length, 0.7112 m).

Figure 1.- Continued.

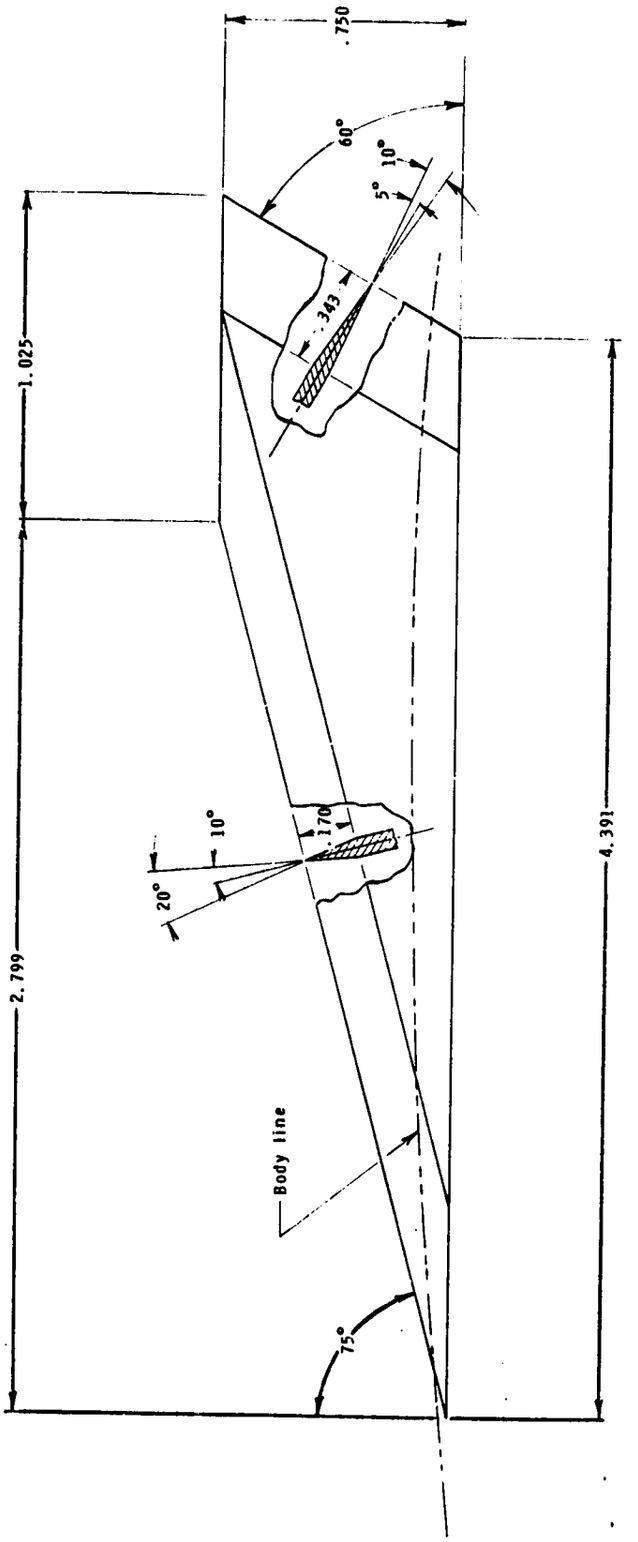

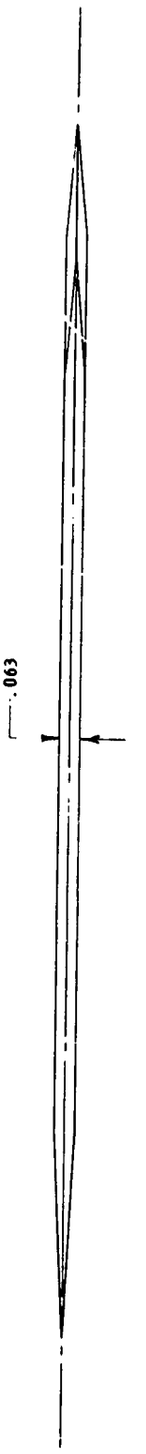

(c) Circular W (reference length, 0.1016 m).

Figure 1.- Continued.

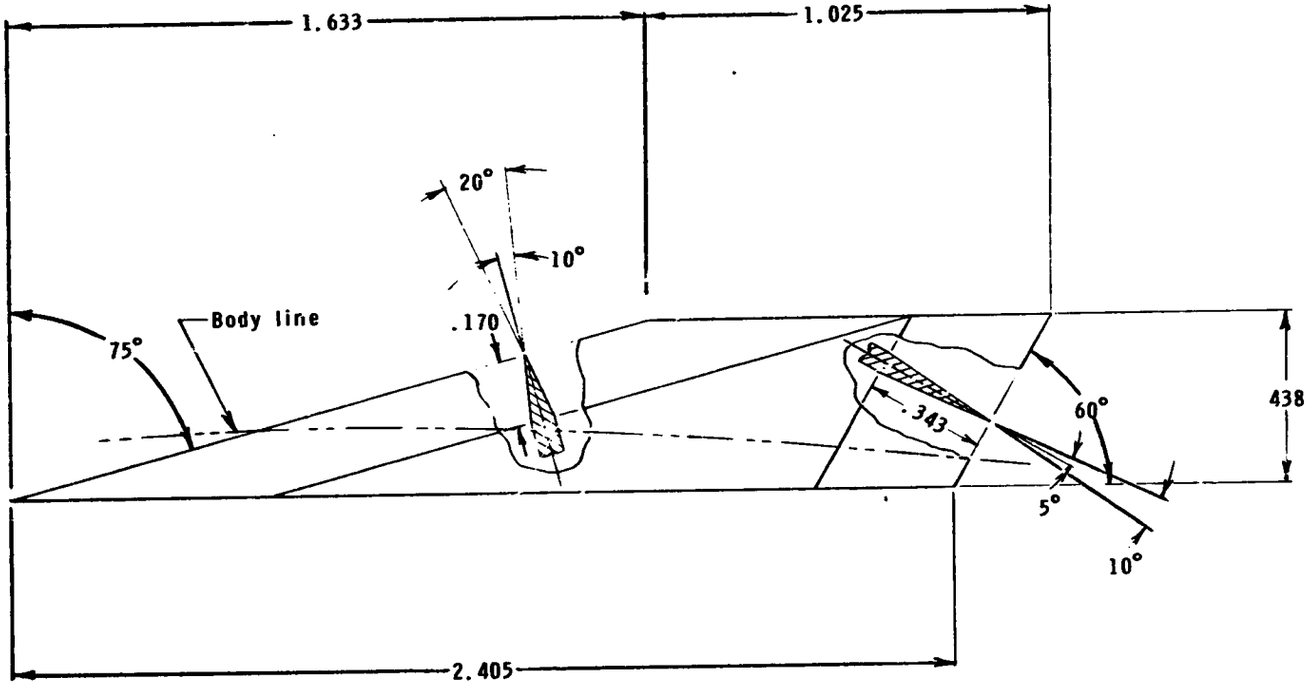

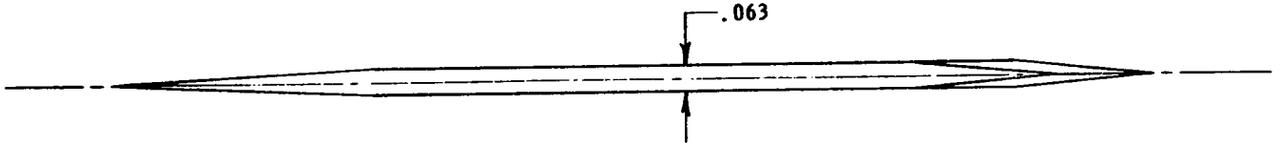

(d) Elliptical W (reference length, 0.1016 m).

Figure 1.- Continued.

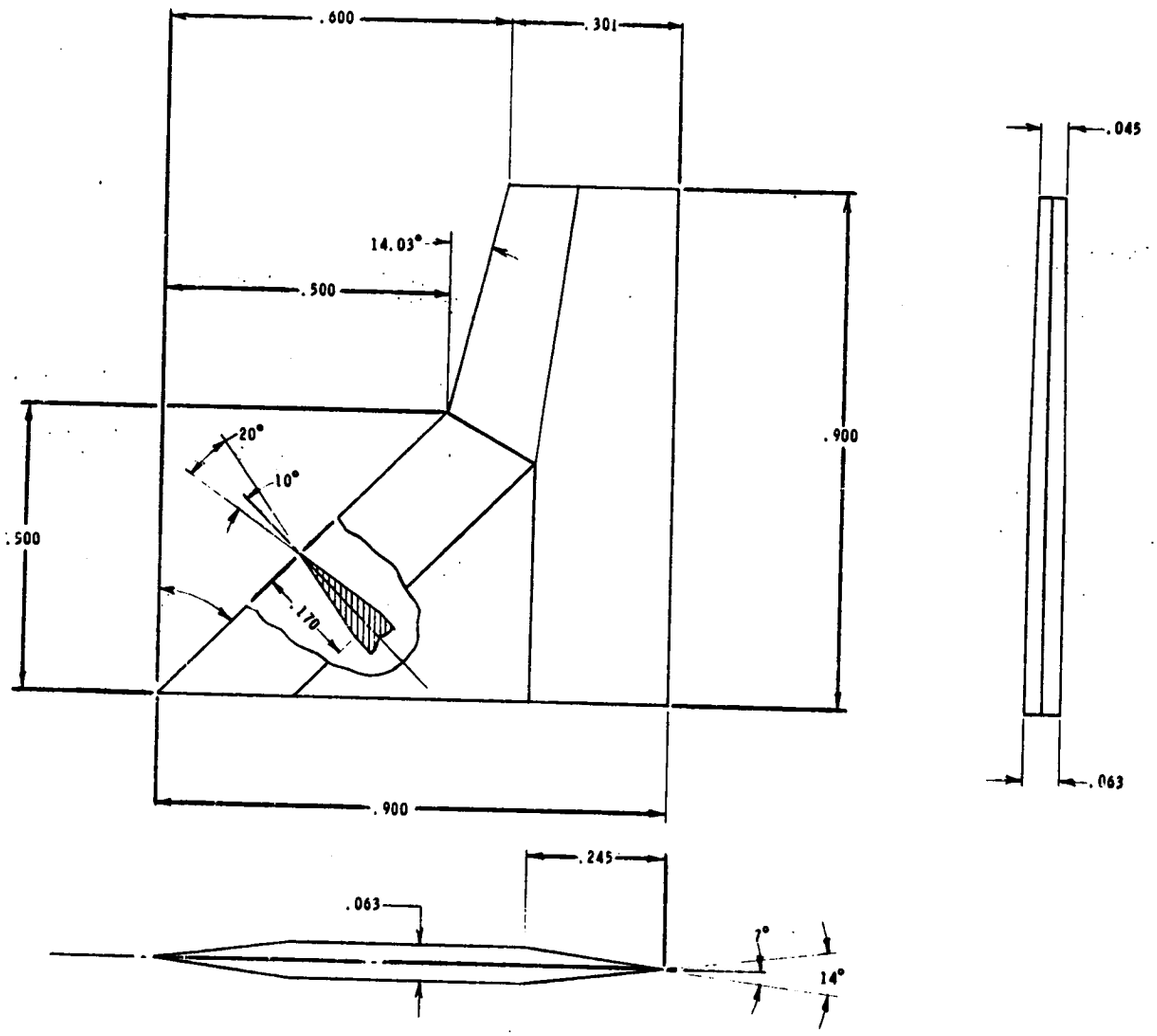

(e) Circular and elliptical T (reference length, 0.1016 m).

Figure 1.- Concluded.

L-76-4125

(a) Circular. (b) Elliptical.

Figure 2.- Photograph of models.

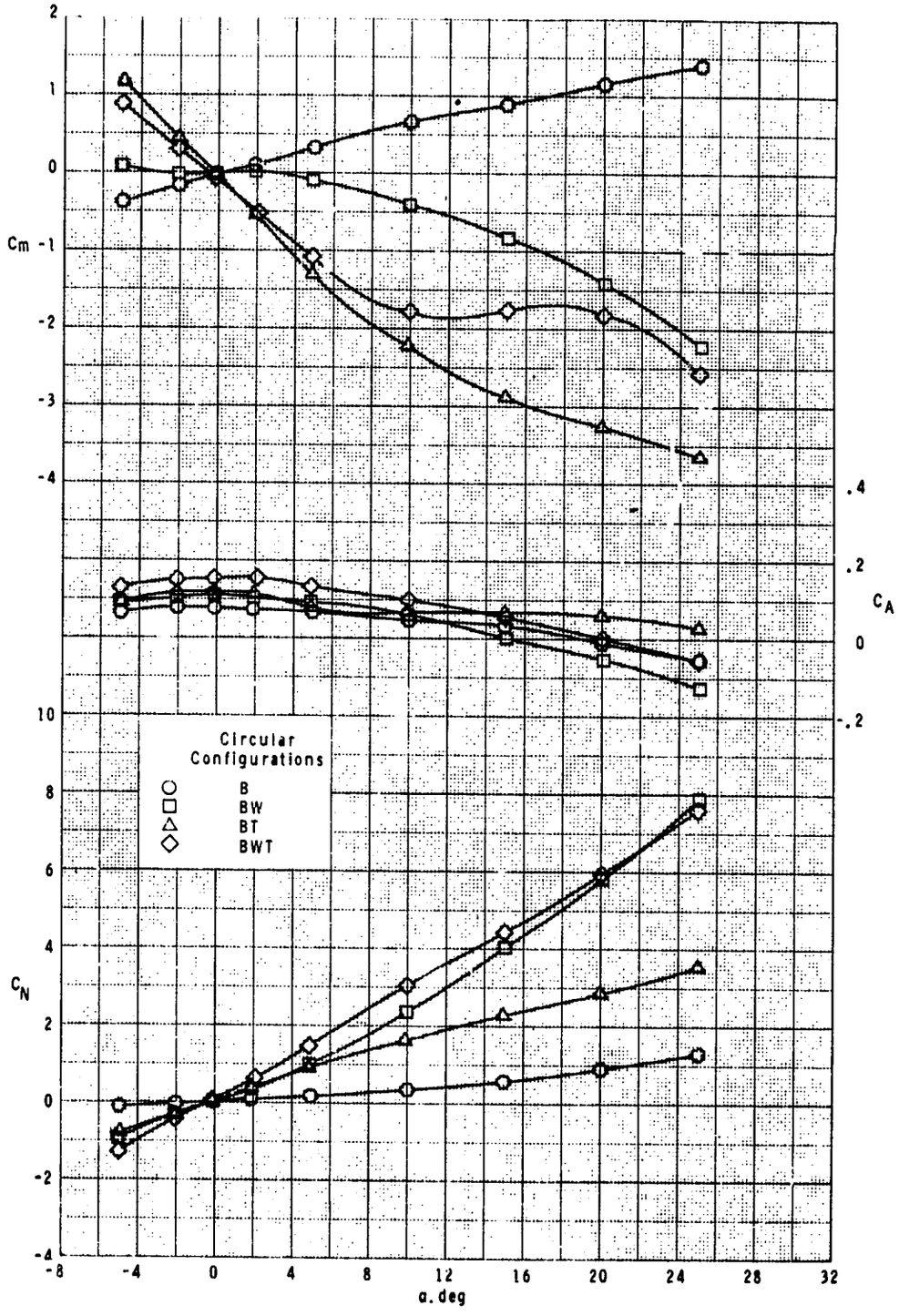

(a) M = 0.5.

Figure 3.- Effect of components on longitudinal aerodynamic characteristics of circular cross-section model with variation in angle of attack.

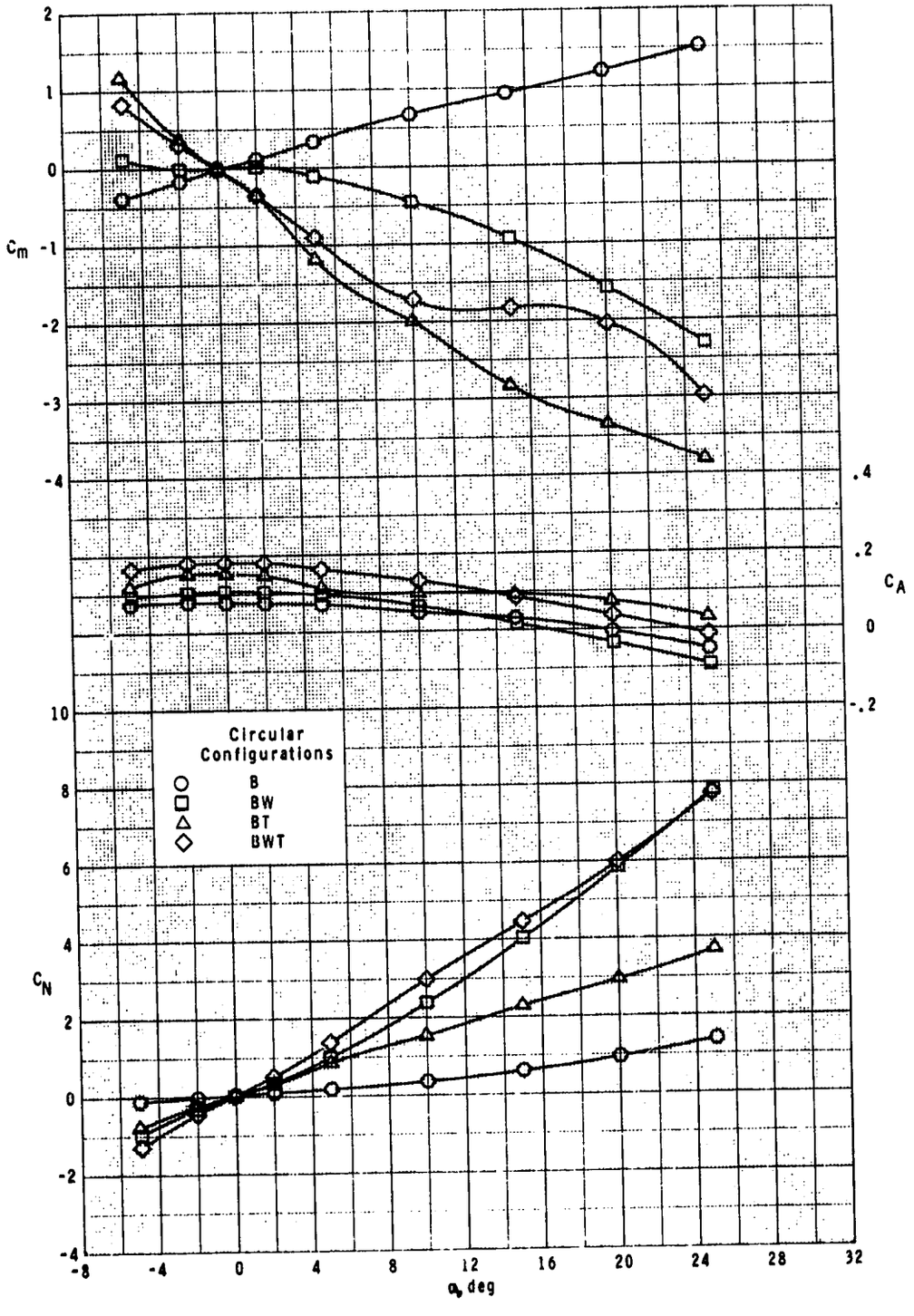

(b) M = 0.7.

Figure 3.- Continued.

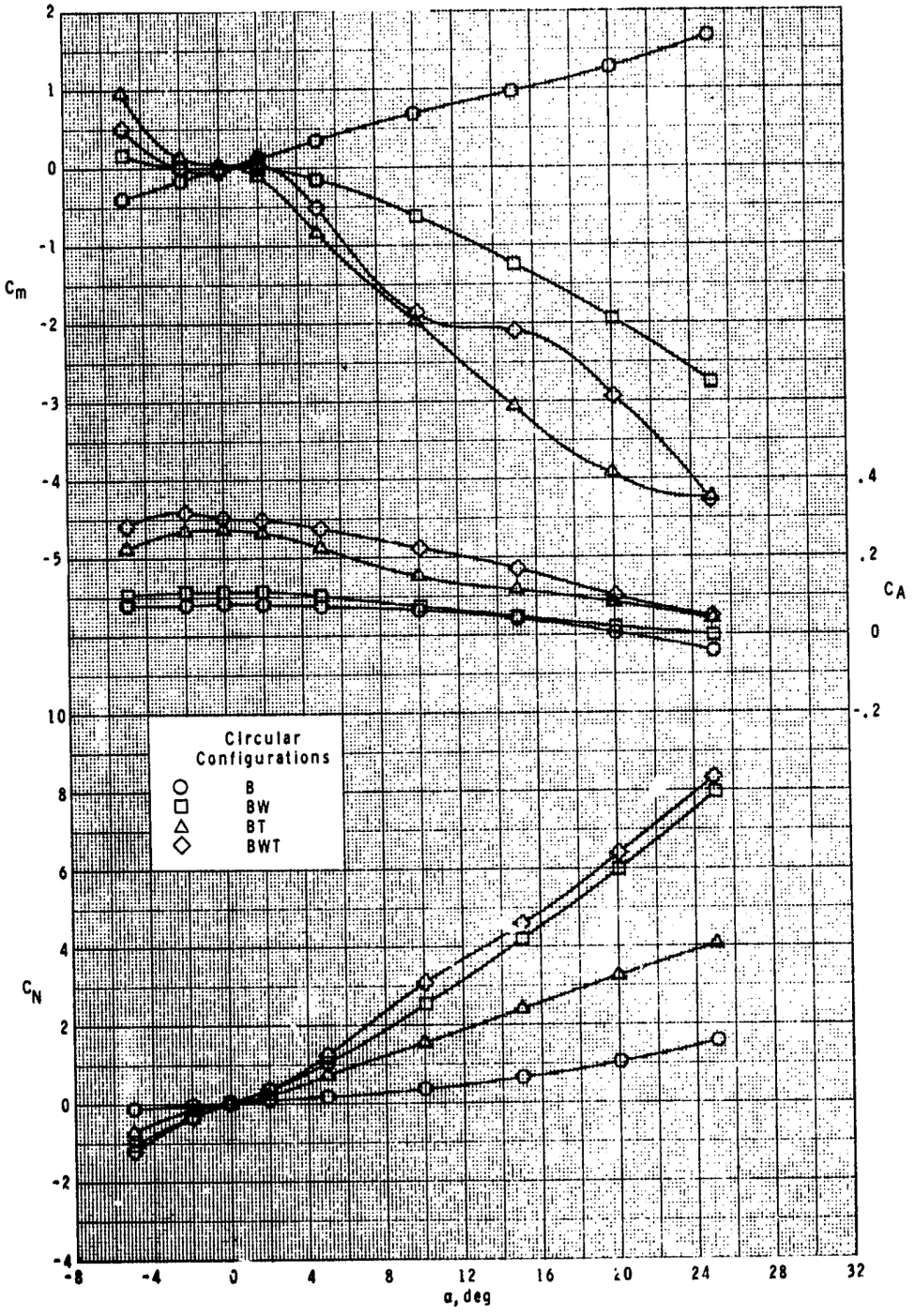

(e) M = 0.9.

Figure 3.- Continued.

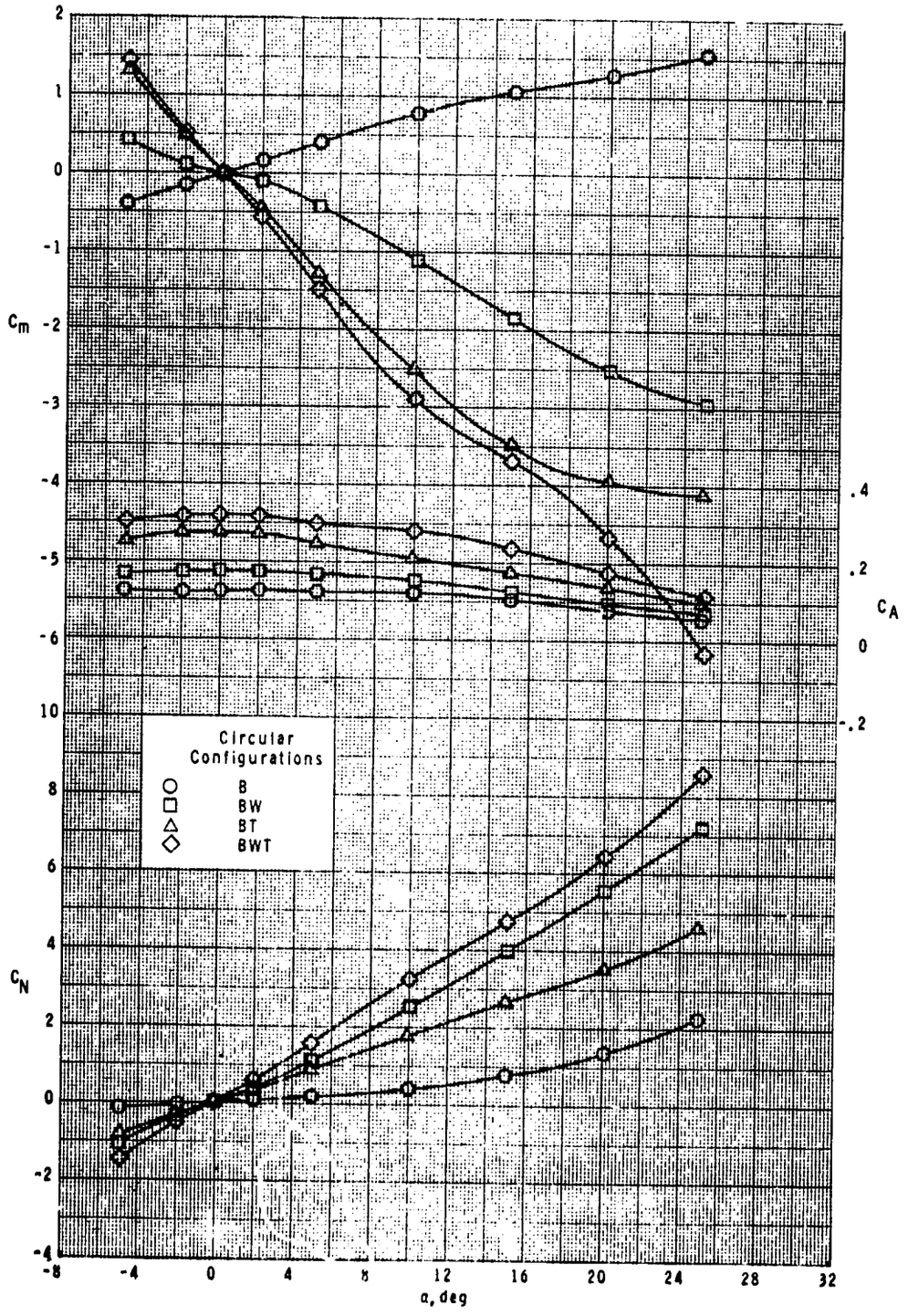

(d) M = 1.3.

Figure 7.- Continued.

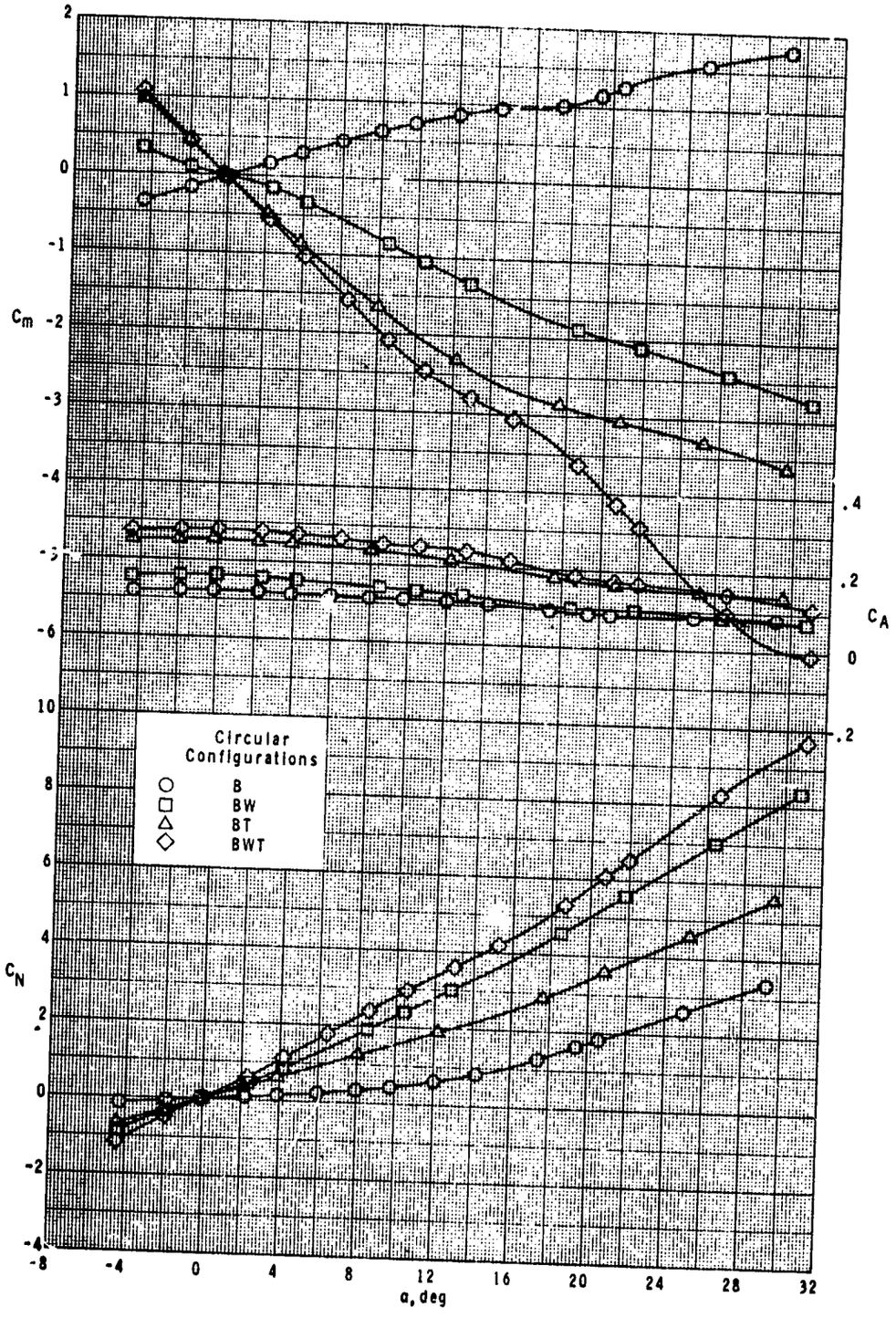

(e) M = 1.60.

Figure 2.- Continued.

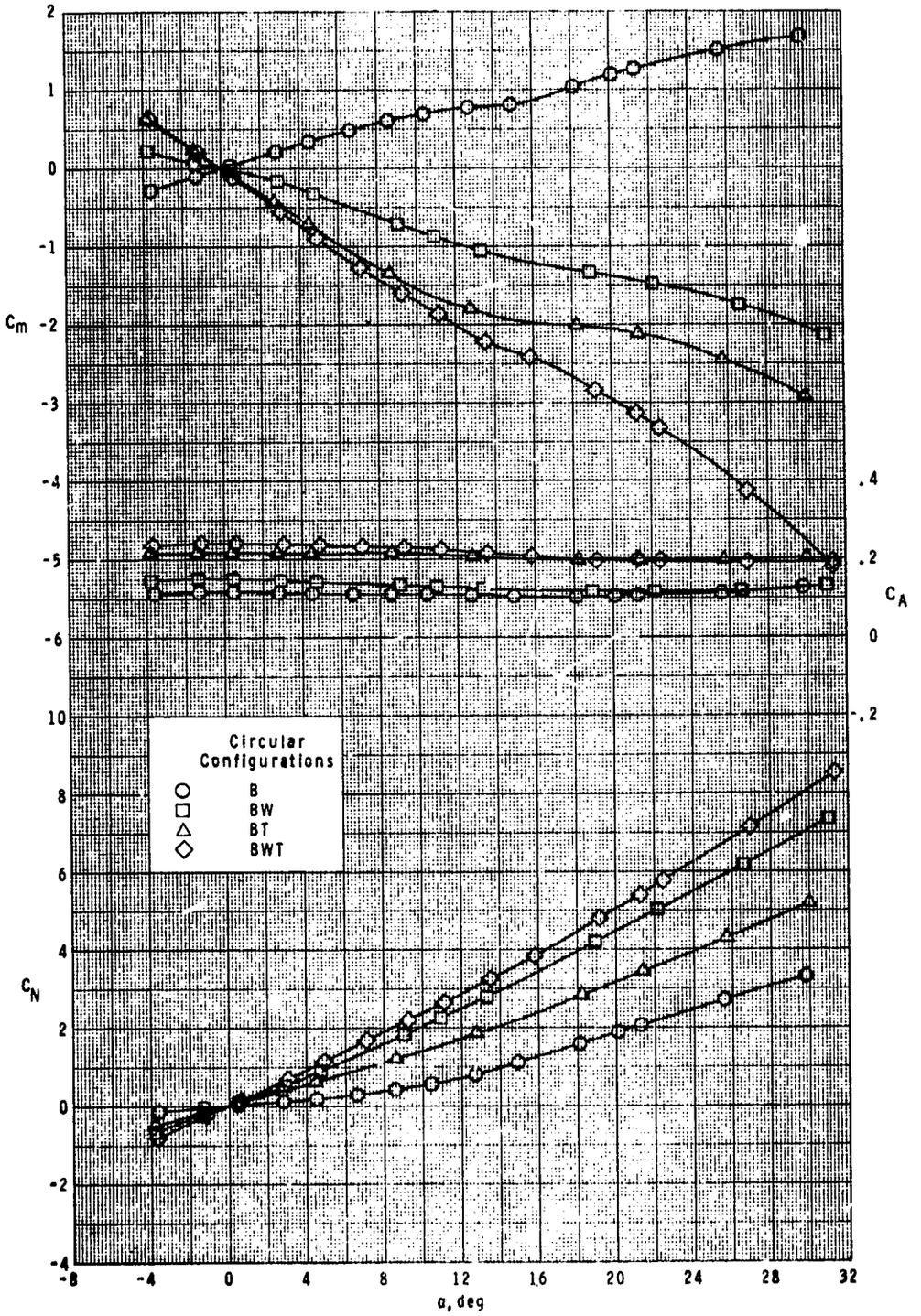

(f) M = 2.00.

Figure 3.- Continued.

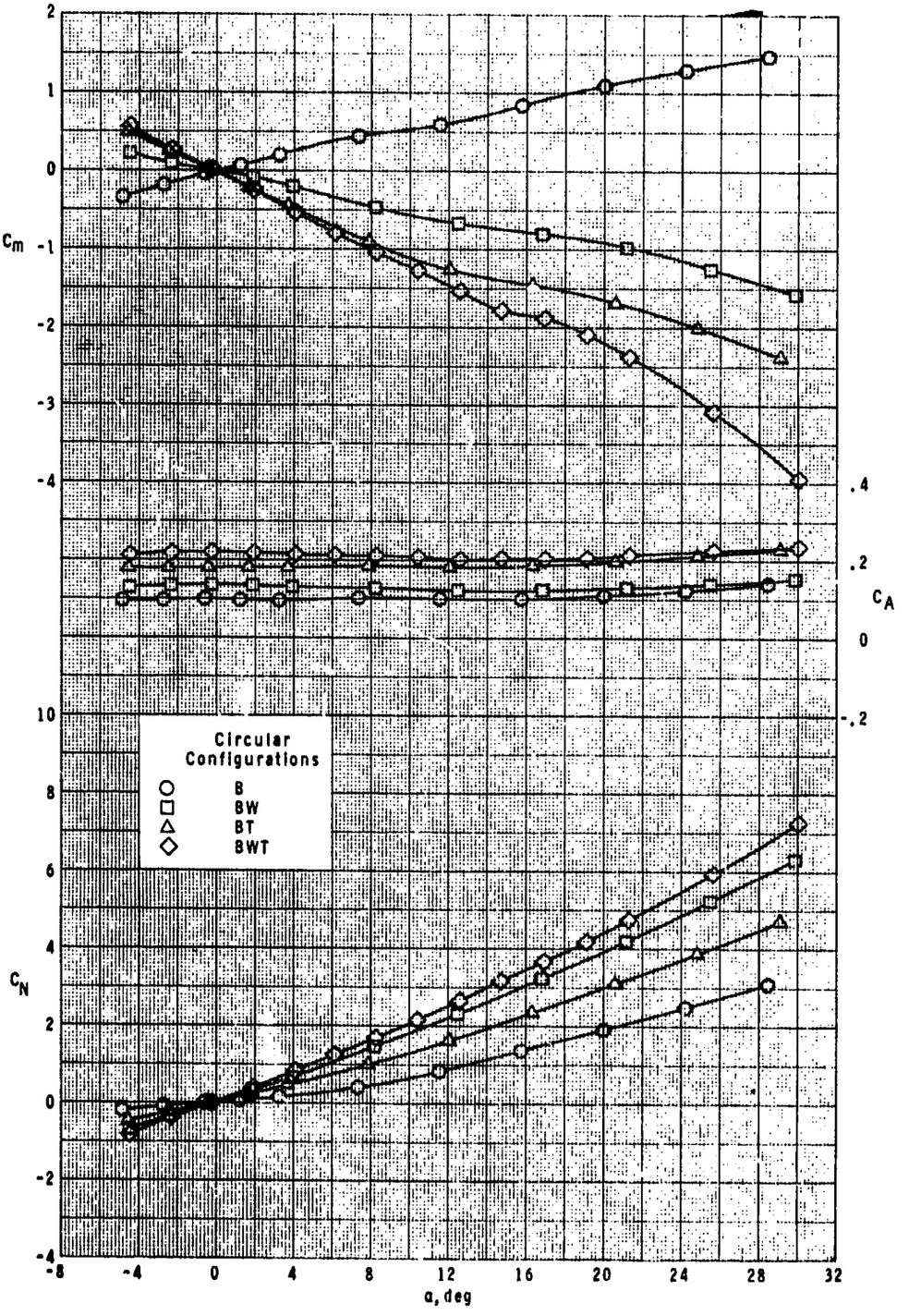

(g) M = 2.50.

Figure 3.- Continued.

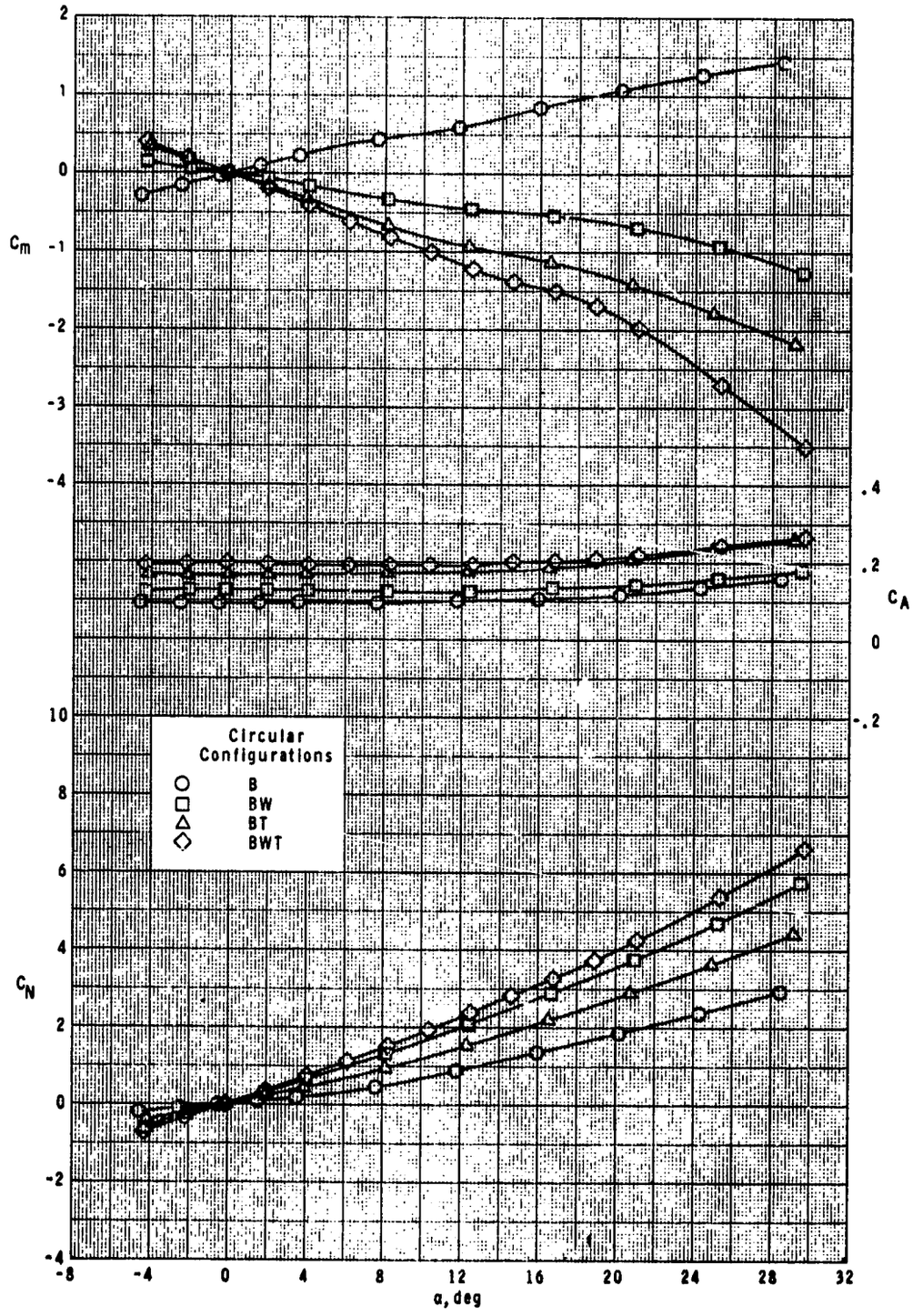

(h) M = 2.96.

Figure 3.- Continued.

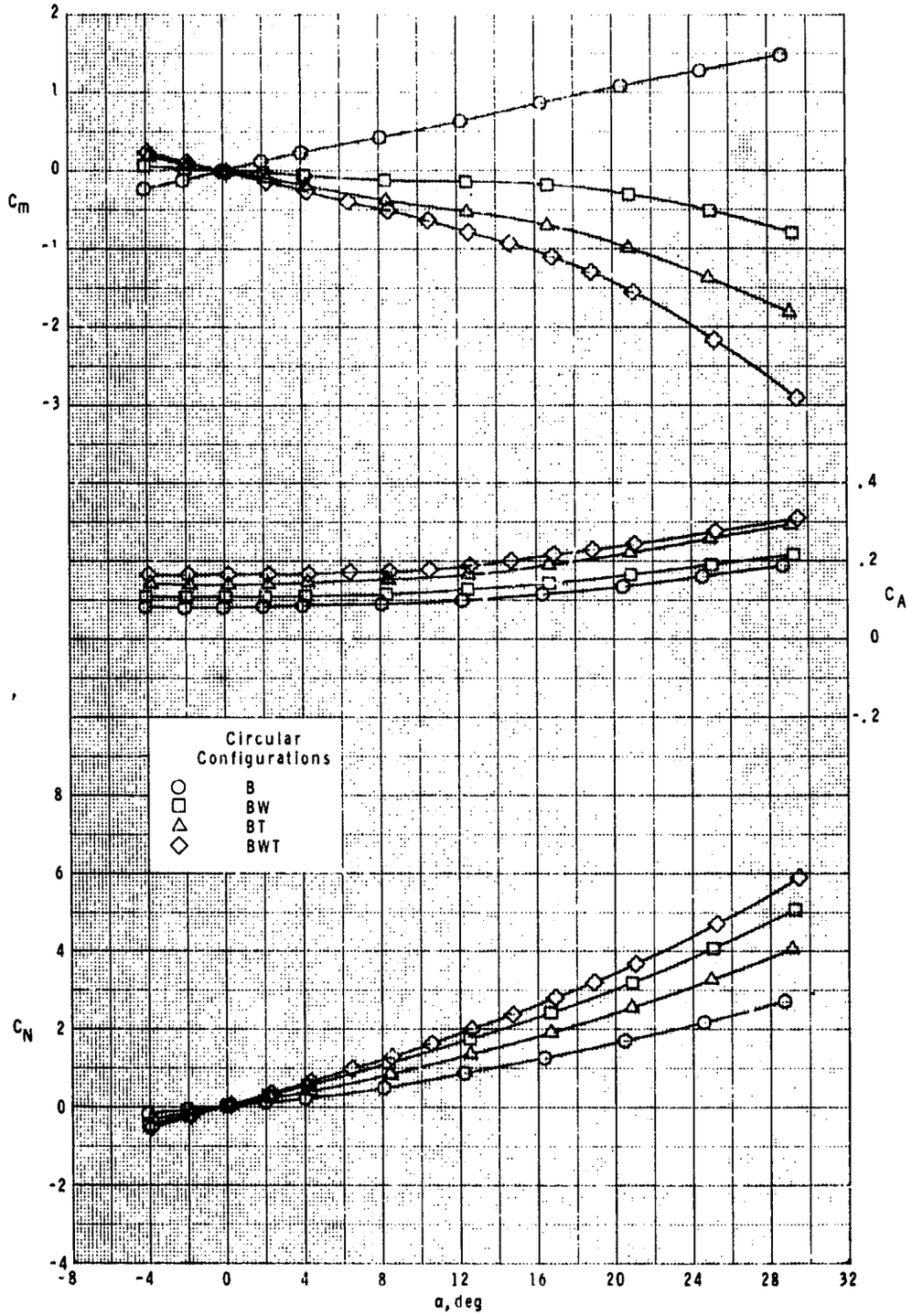

(i) M = 3.95.

Figure 3.- Continued.

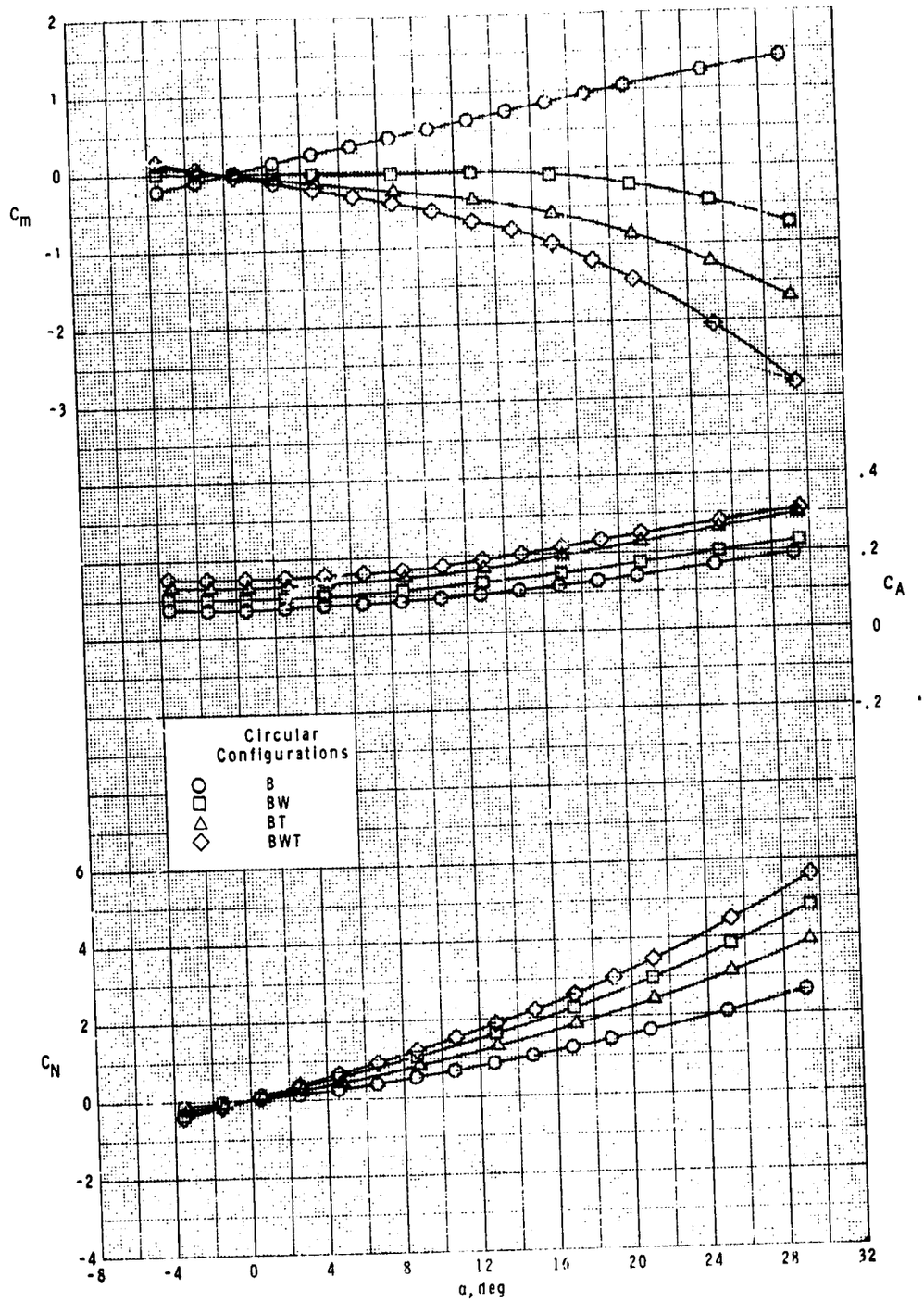

(j) M = 1.63.

Figure 3.- Concluded.

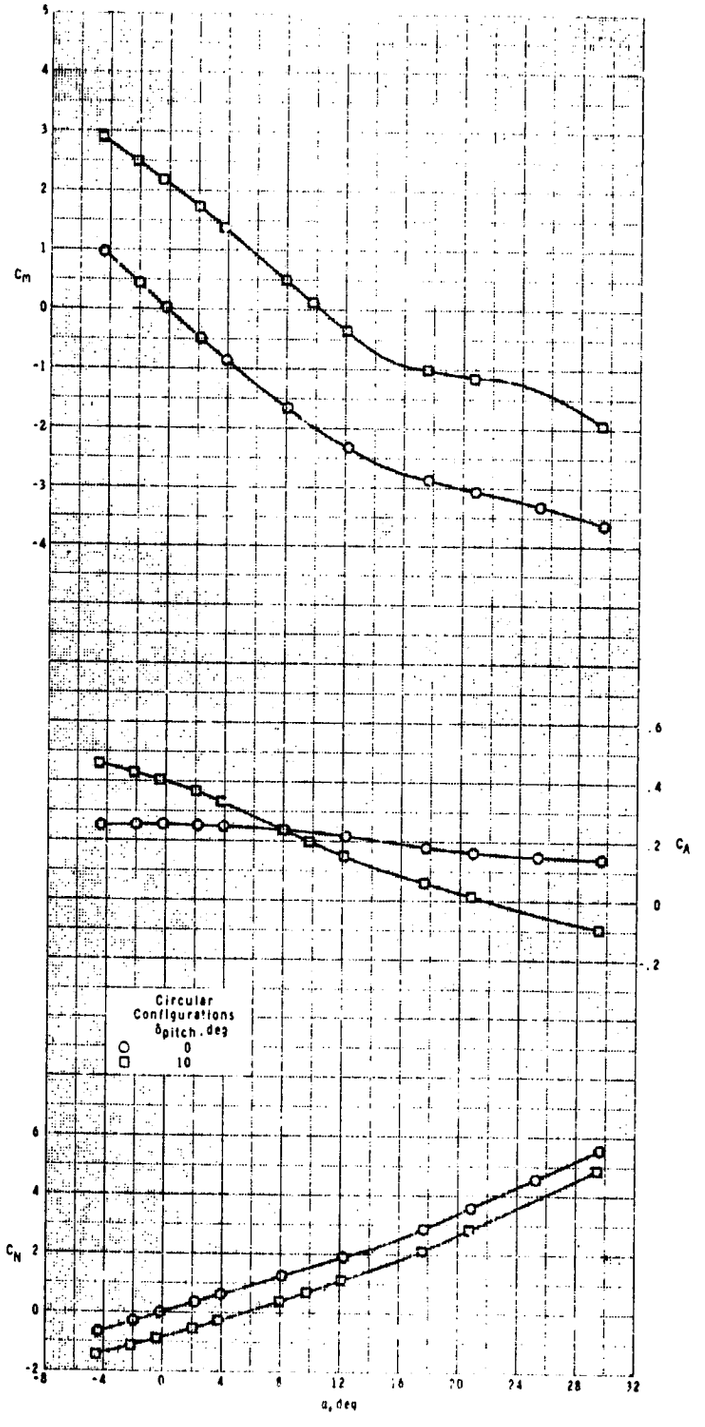

(a) M = 1.60.

Figure 4.- Pitch-control effectiveness of circular cross-section body-tail configuration with variation in angle of attack.

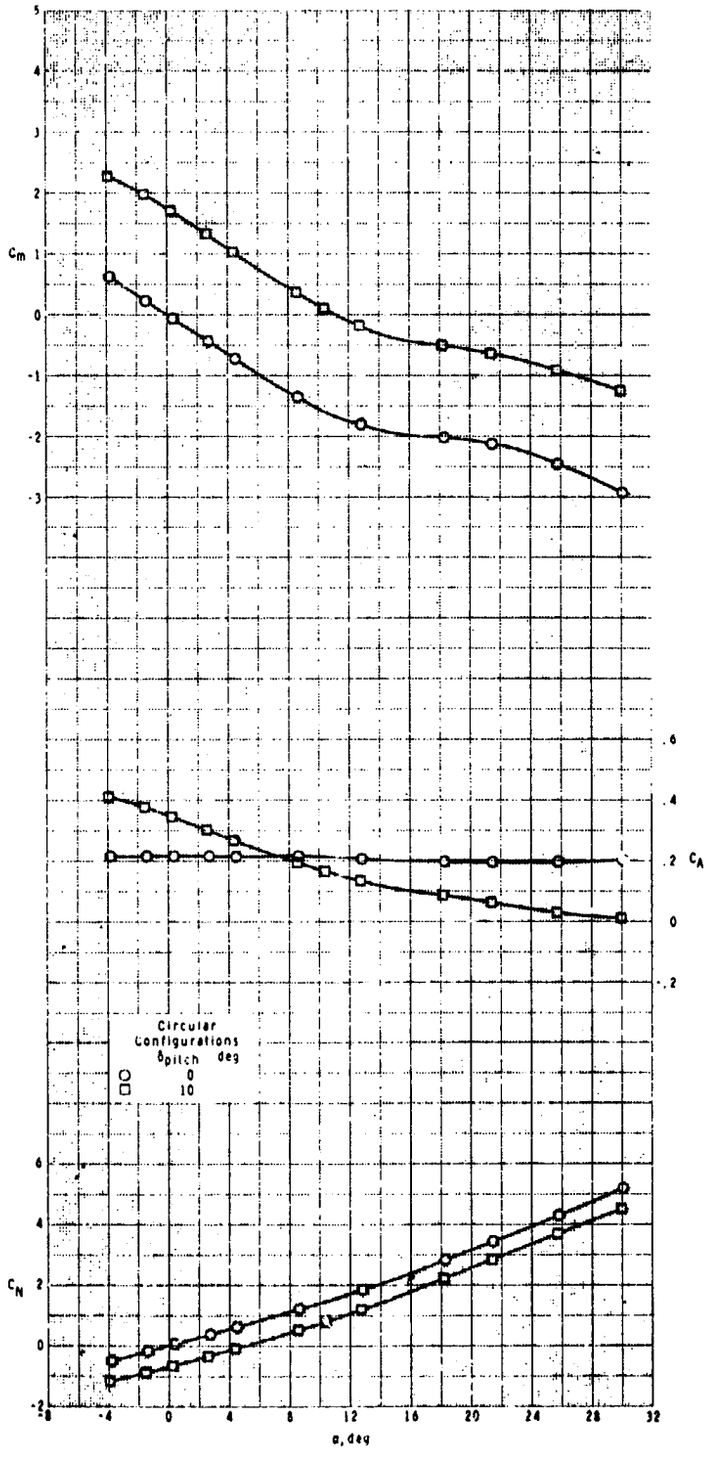

(b) M = 2.00.

Figure 4.- Continued.

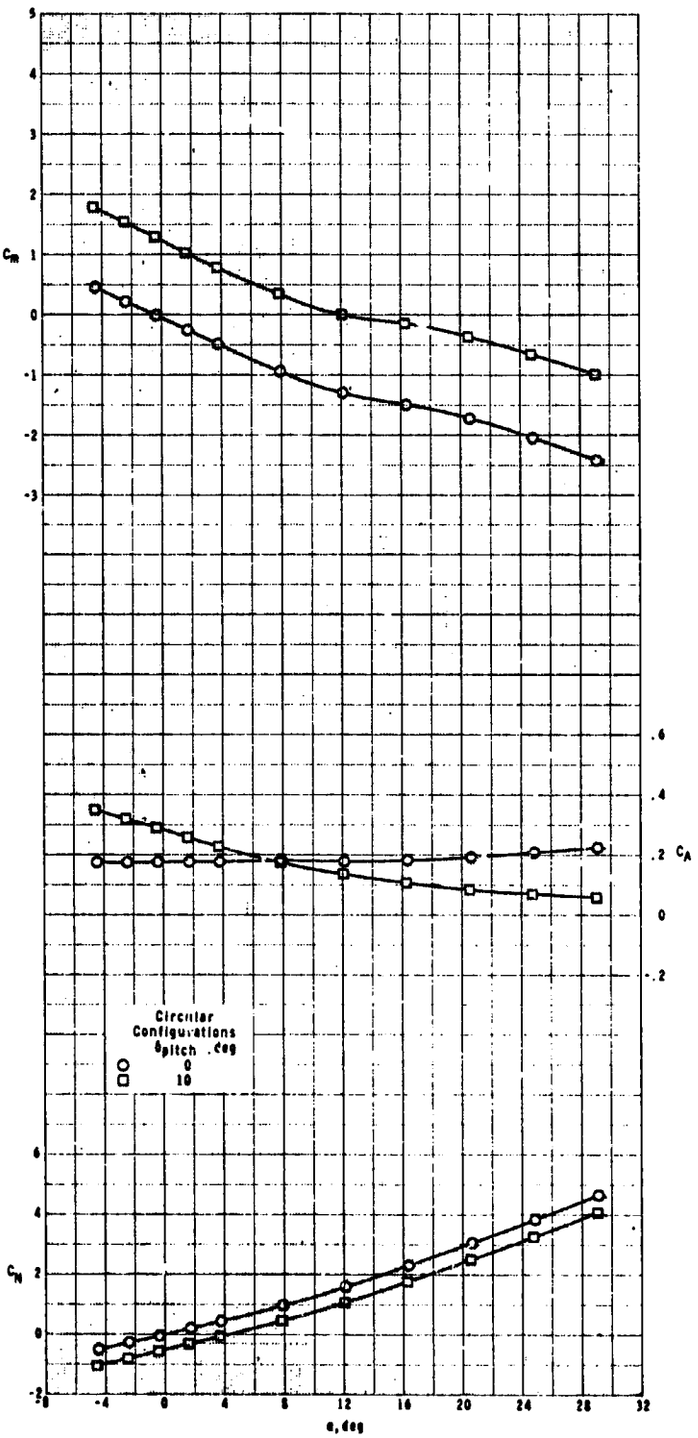

(c) M = 2.50.

Figure 4.- Continued.

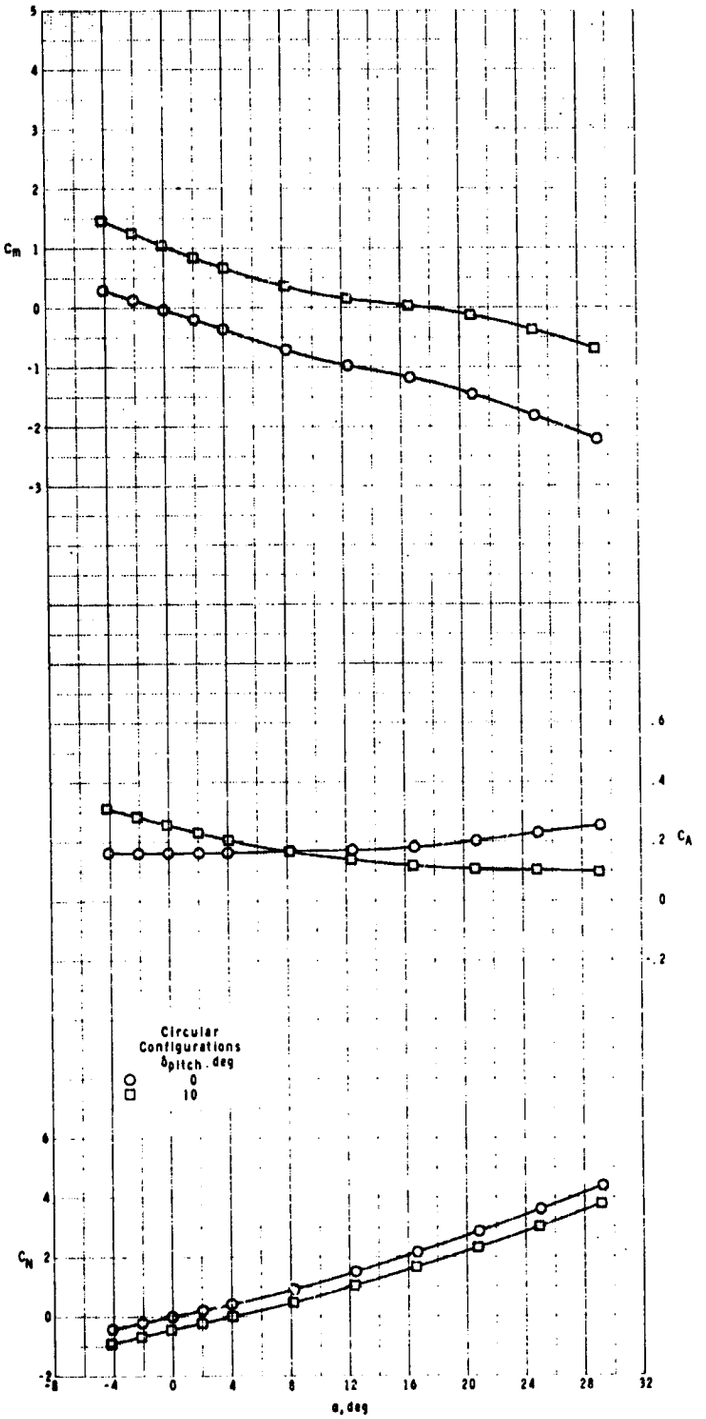

(d) M = 2.96.

Figure 4.- Continued.

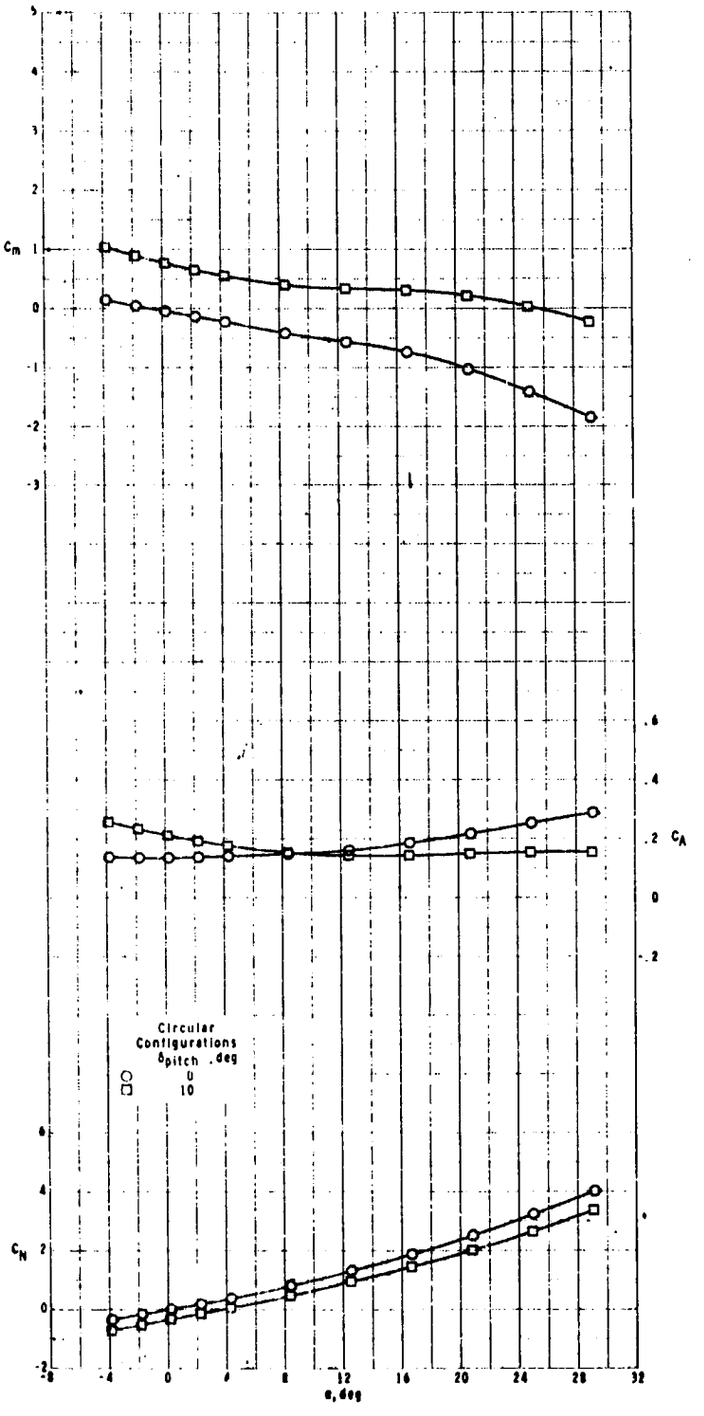

(e) M = 3.95.

Figure 4.- Continued.

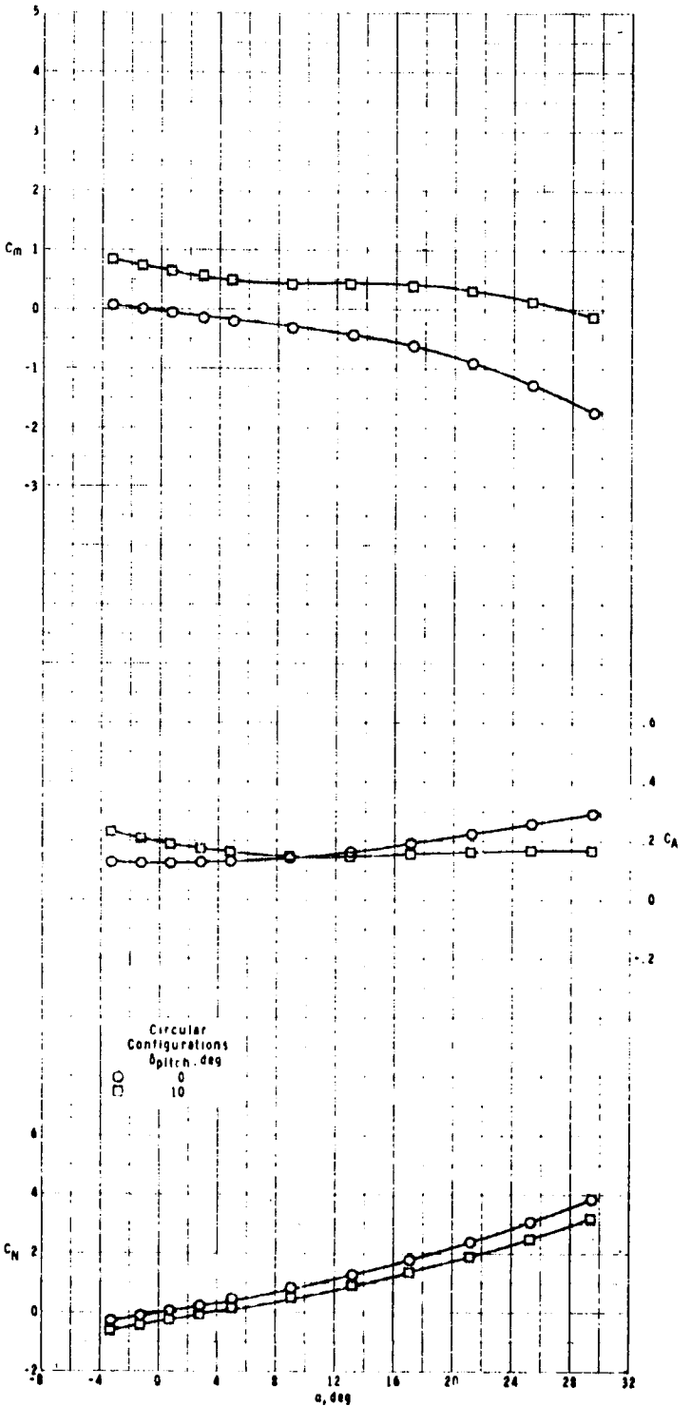

(f) M = 4.63.

Figure 4.- Concluded.

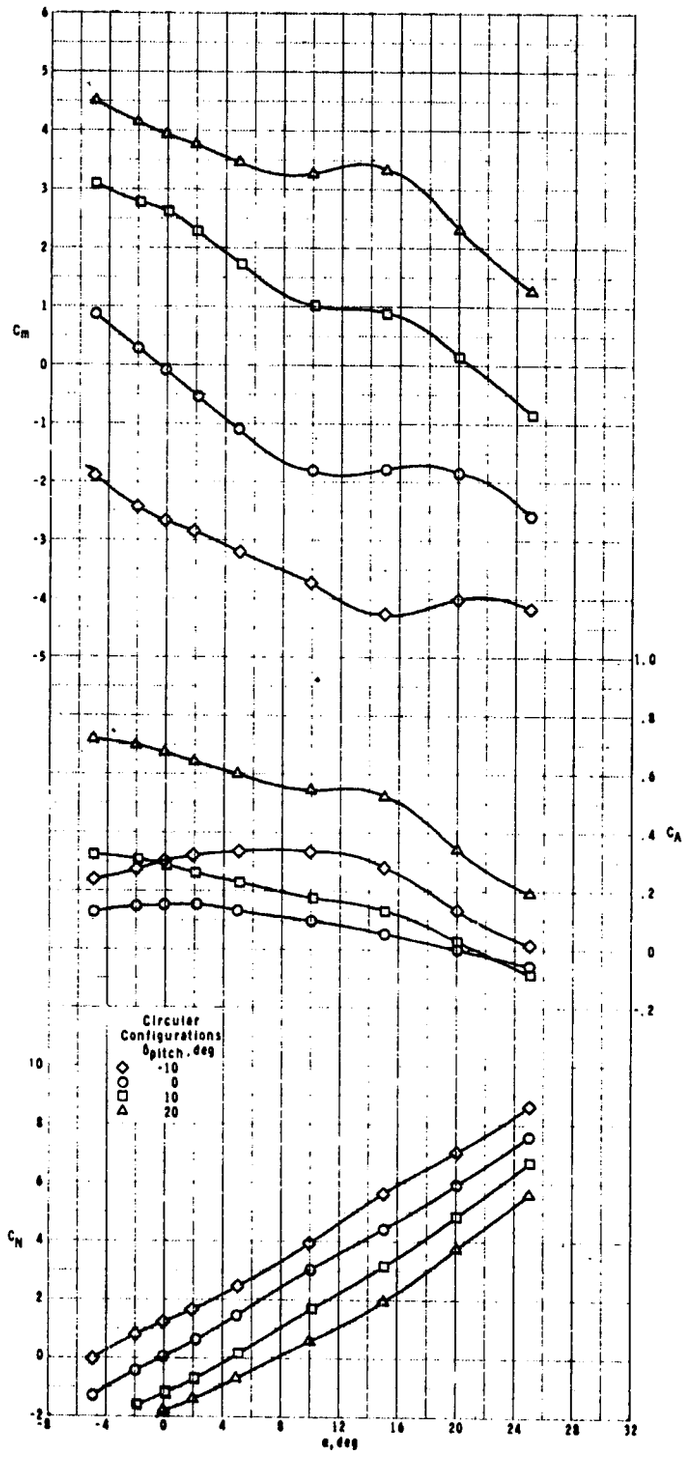

(a) M = 0.5.

Figure 5.- Pitch-control effectiveness of circular cross-section wing-tail configuration with variation in angle of attack.

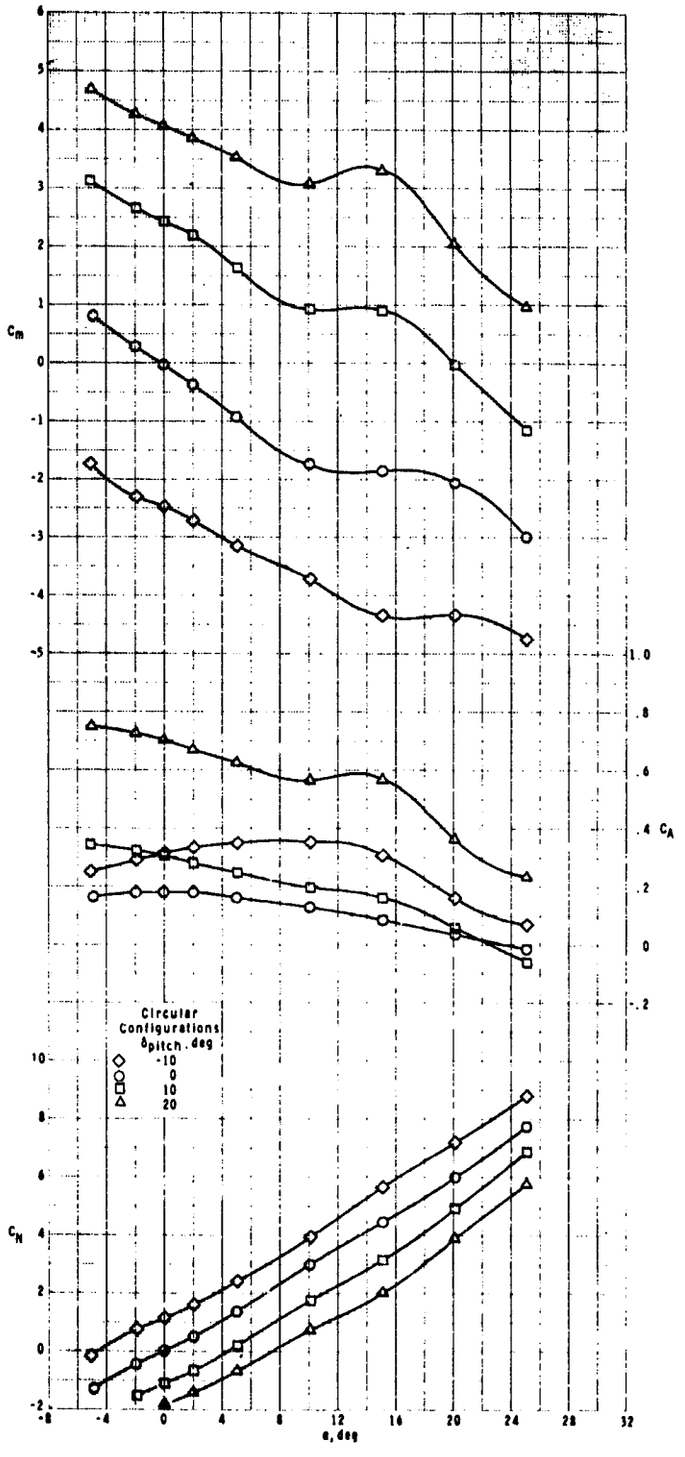

(b) M = 0.7.

Figure 5.- Continued.

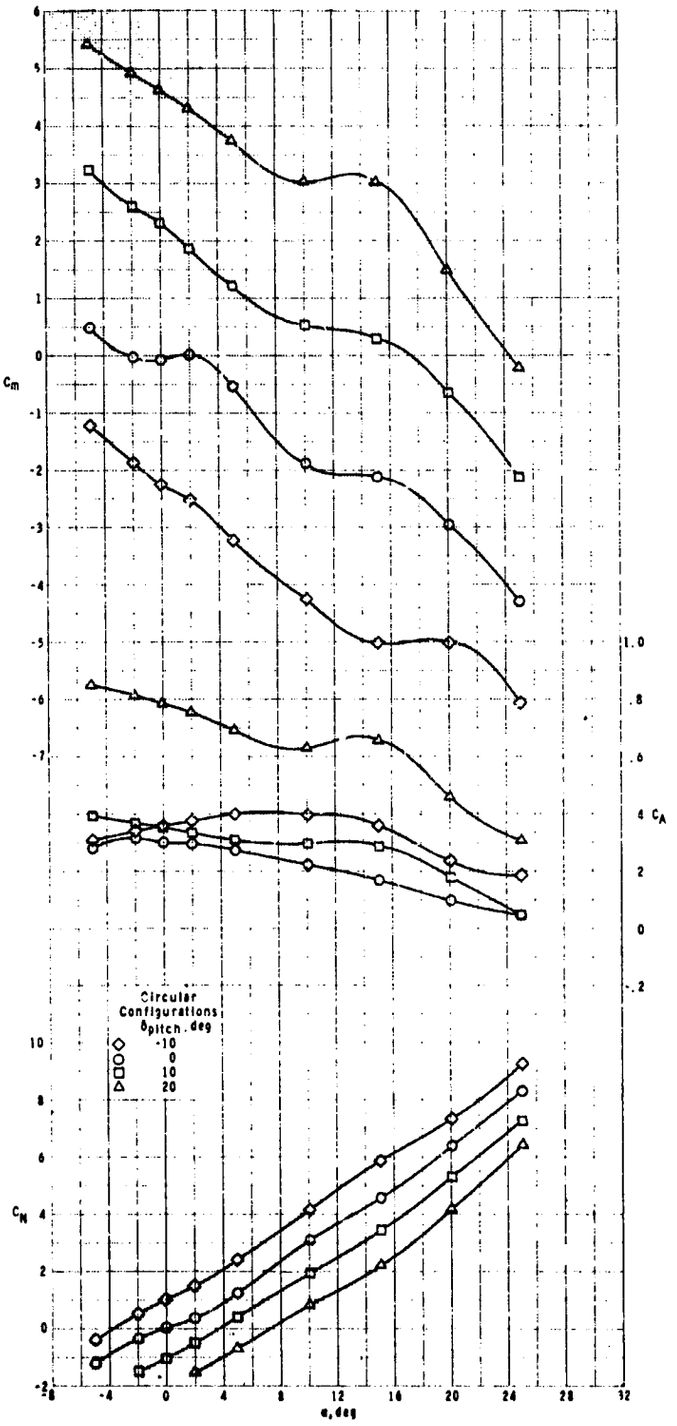

(c) M = 0.9.

Figure 5.- Continued.

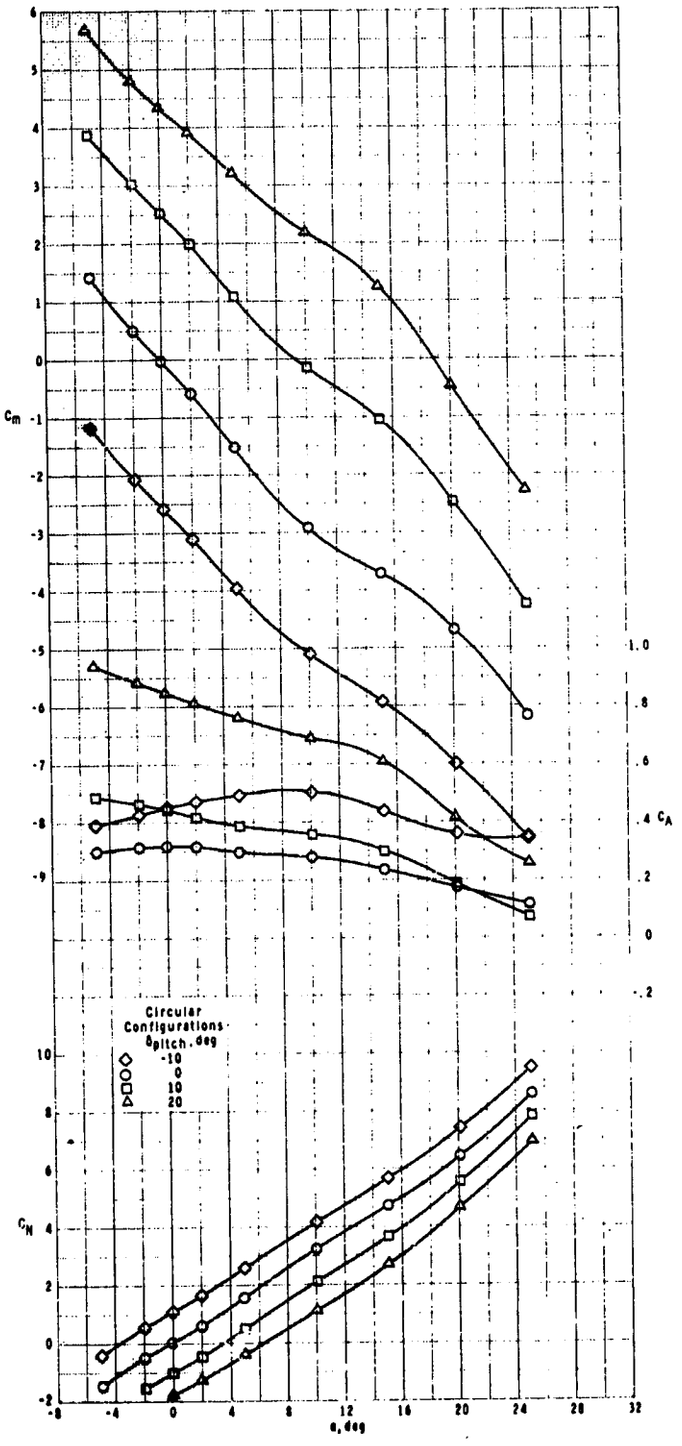

(d) M = 1.3.

Figure 5.- Continued.

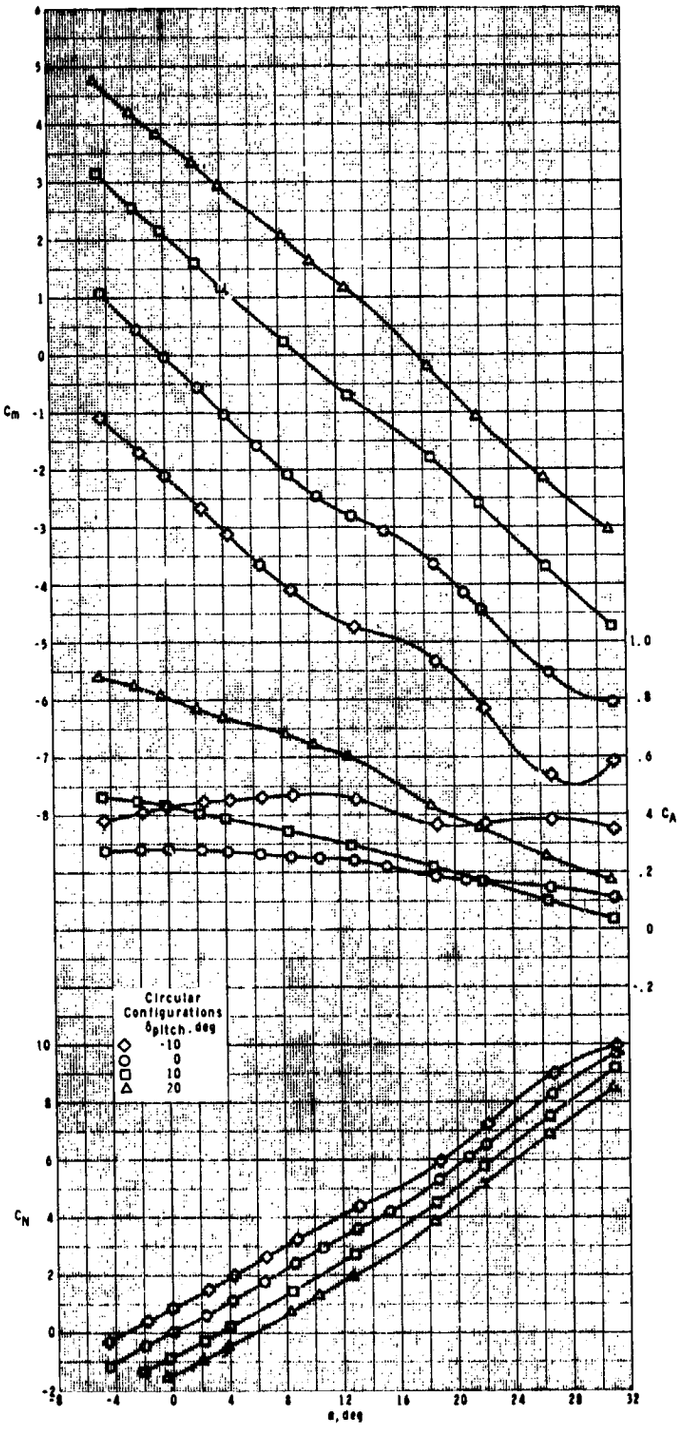

(e) M = 1.60.

Figure 5.- Continued.

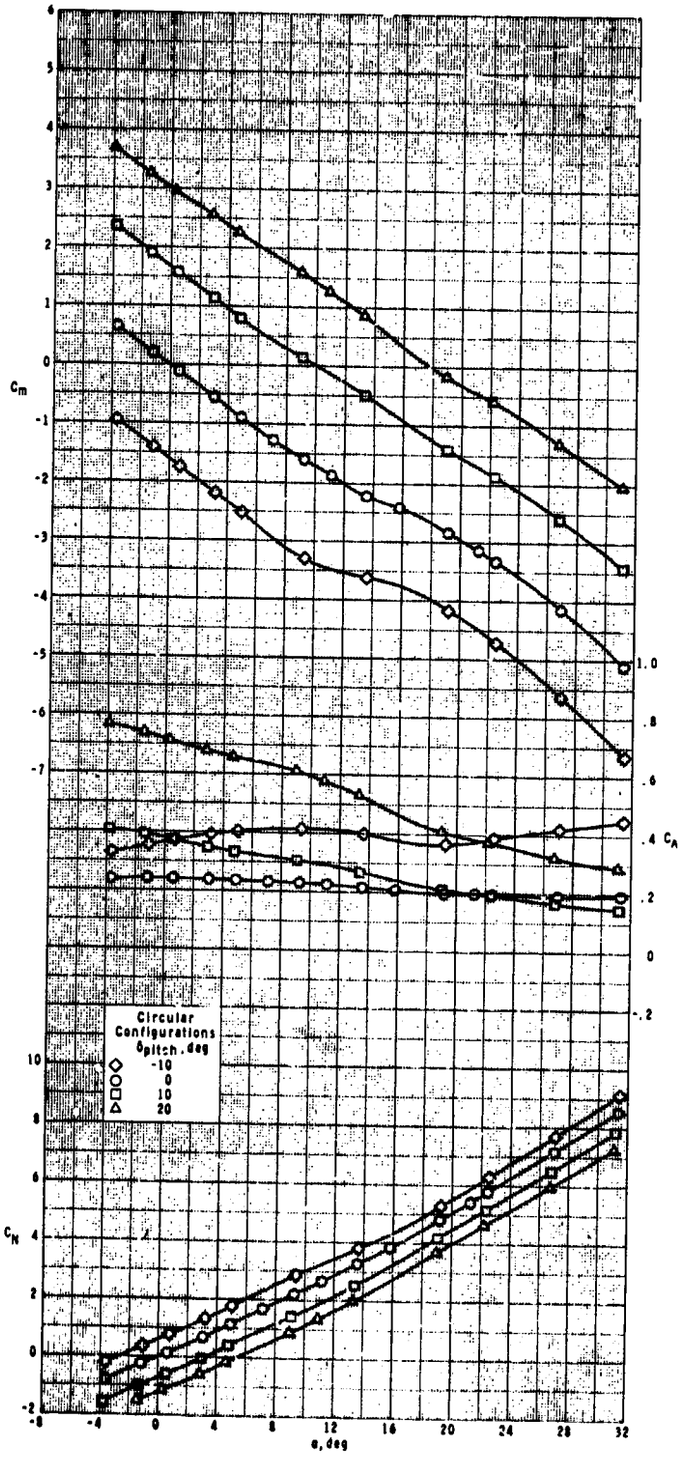

(f) M = 2.00.

Figure 5.- Continued.

ORIGINAL PAGE IS
OF POOR QUALITY

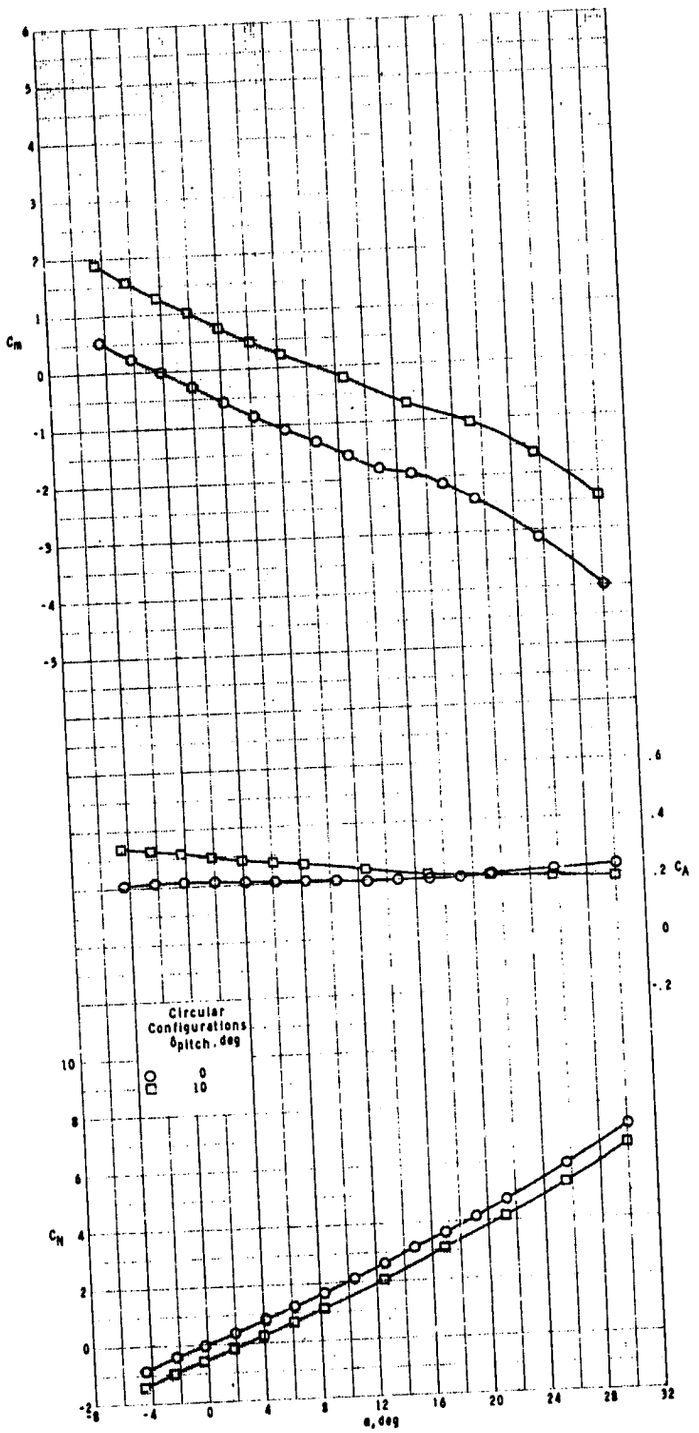

(g) M = 2.50.

Figure 5.- Continued.

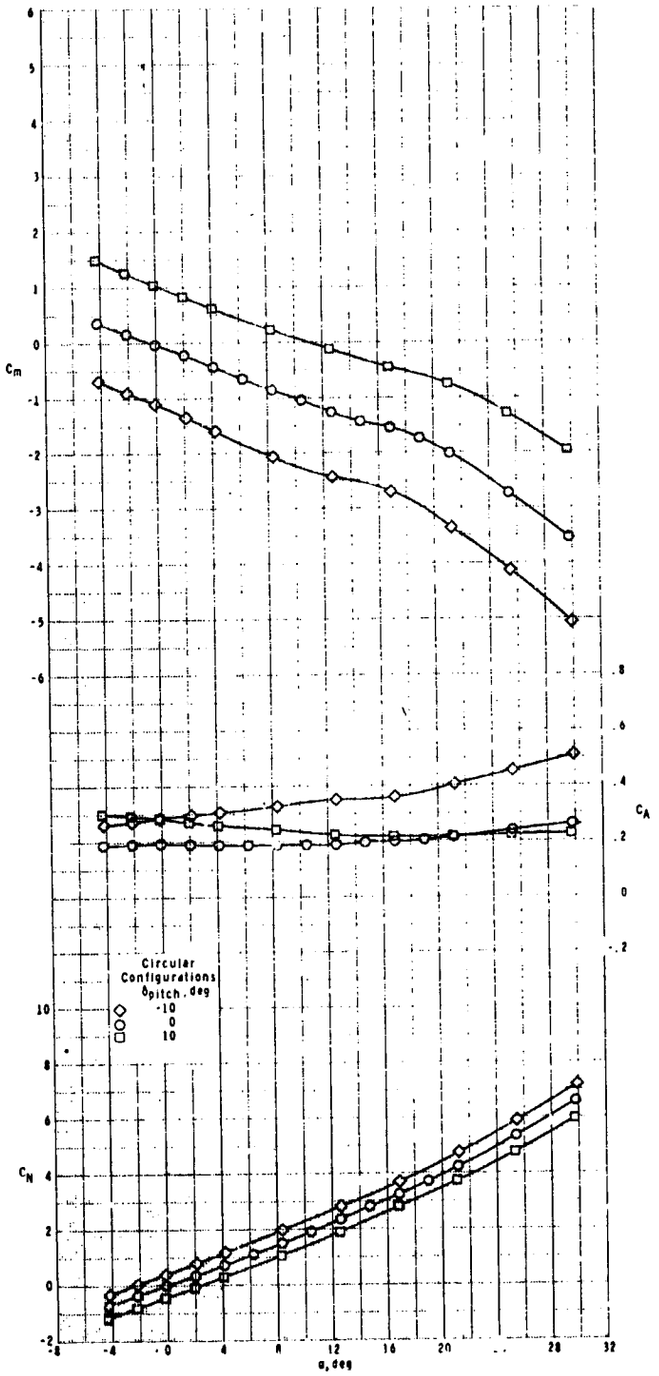

(h) M = 2.96.

Figure 5.- Continued.

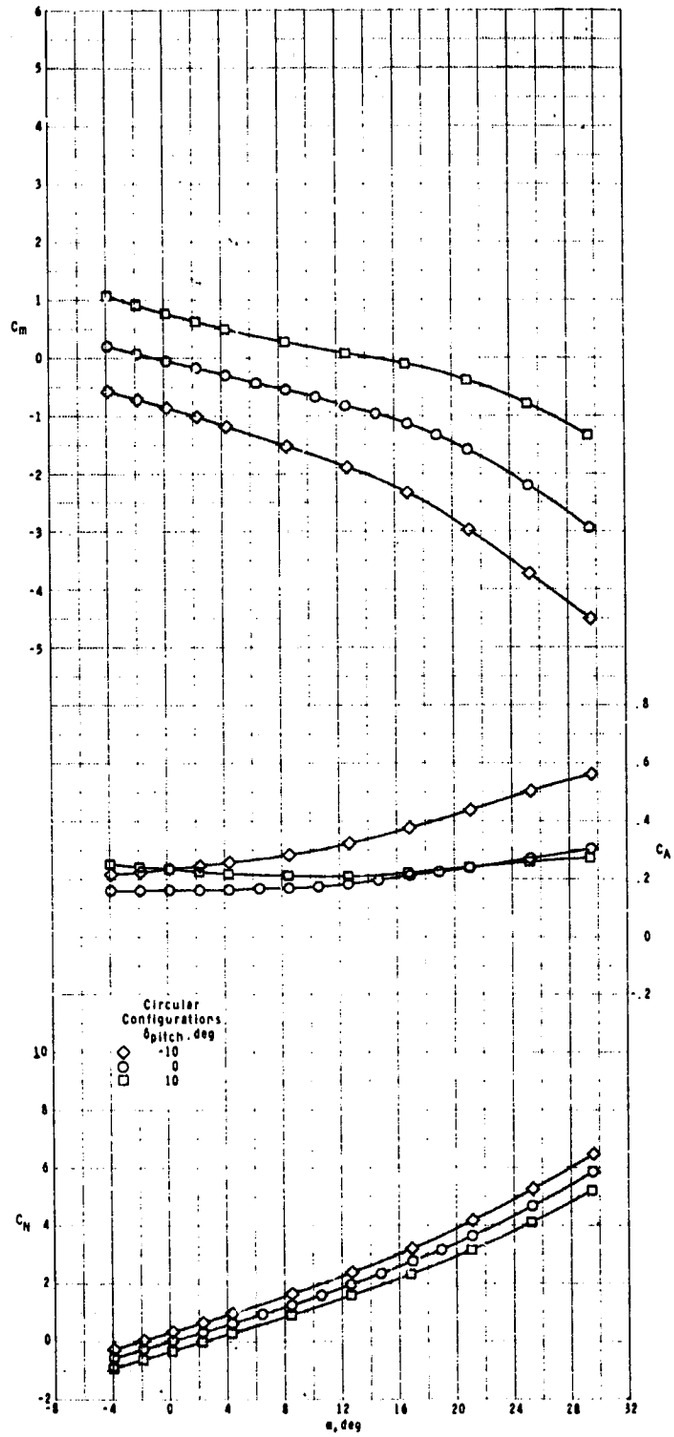

(i) M = 3.95.

Figure 5.- Continued.

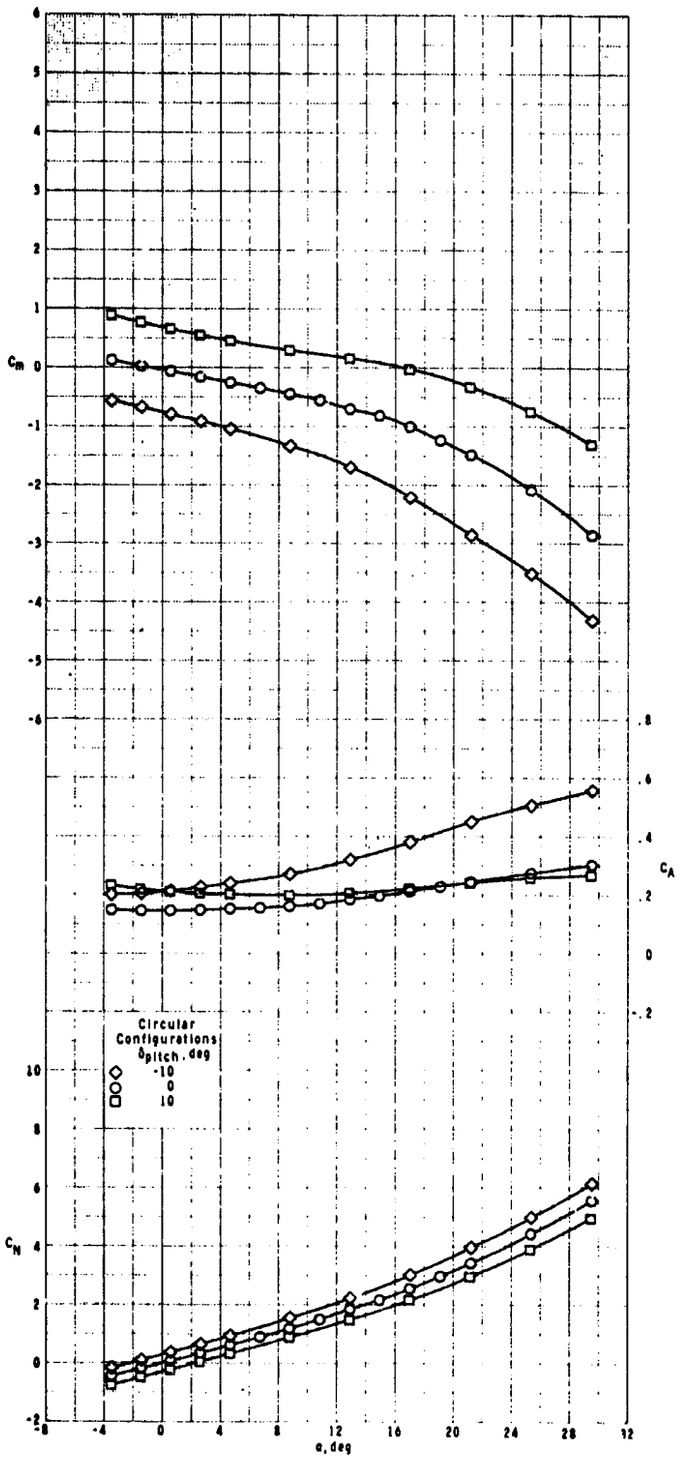

(j) M = 4.63.

Figure 5.- Concluded.

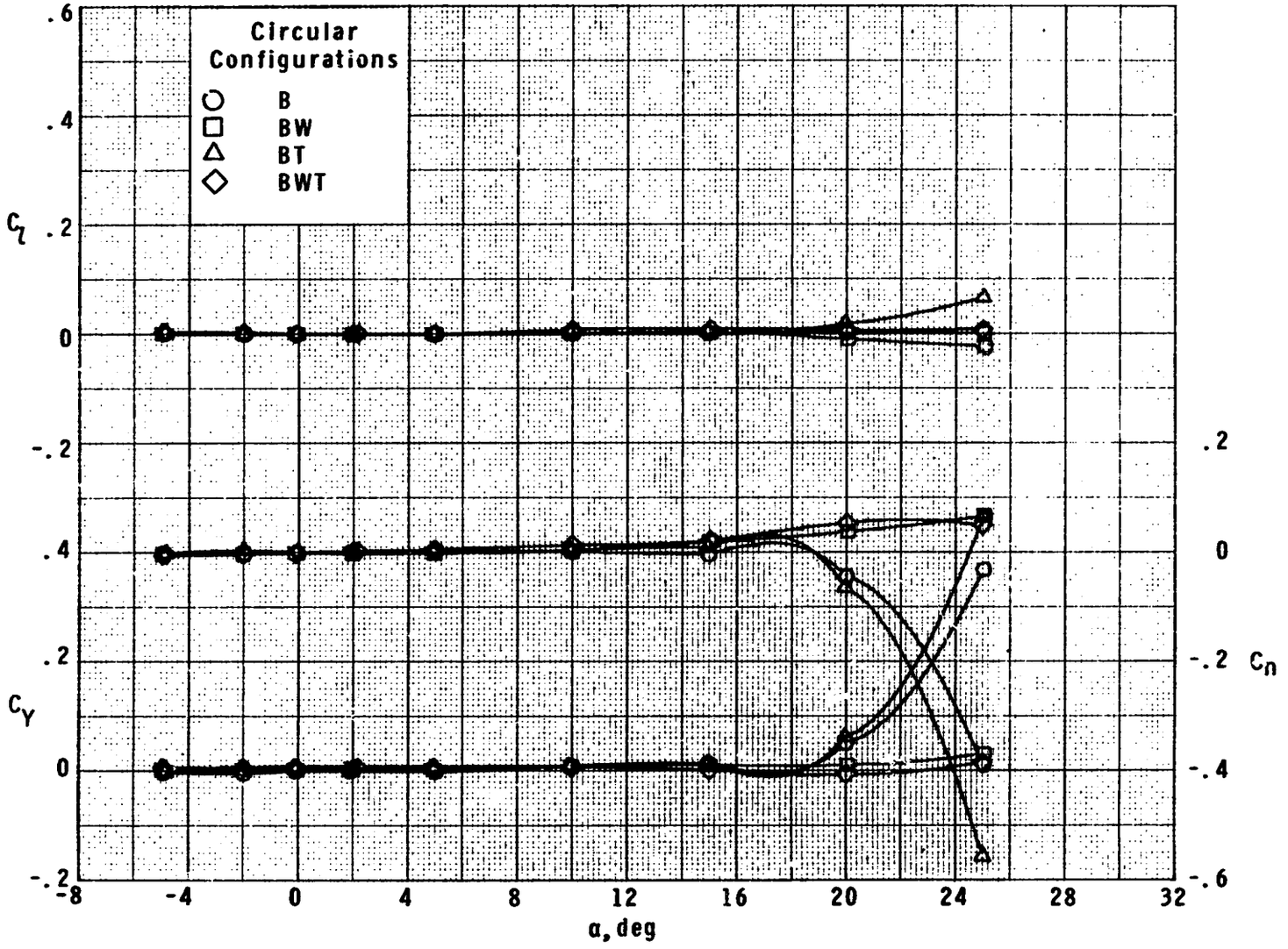

(a) M = 0.5.

Figure 6.- Effect of components on lateral aerodynamic characteristics of circular cross-section model with variation in angle of attack.

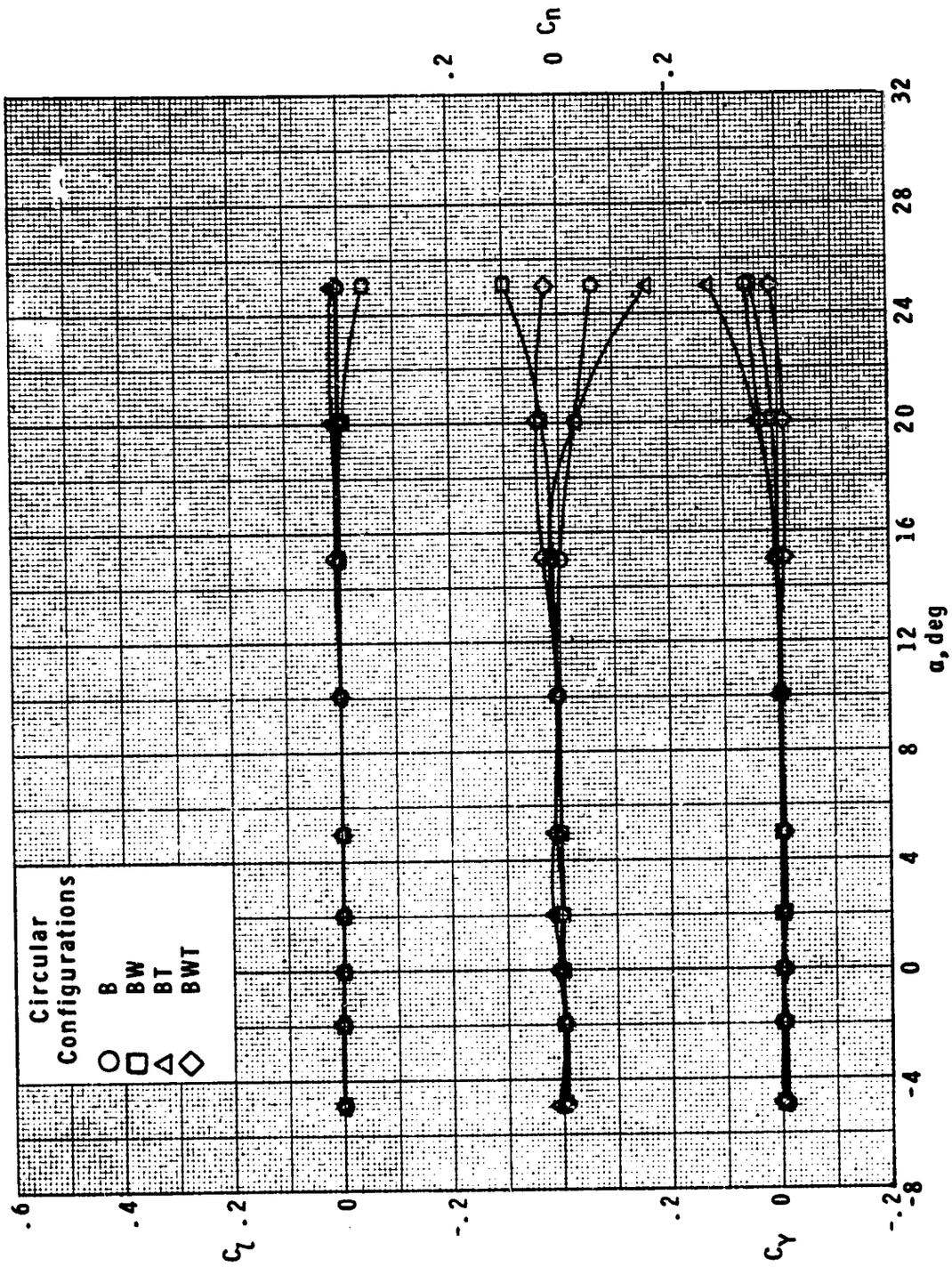

(b) M = 0.7.

Figure 6.- Continued.

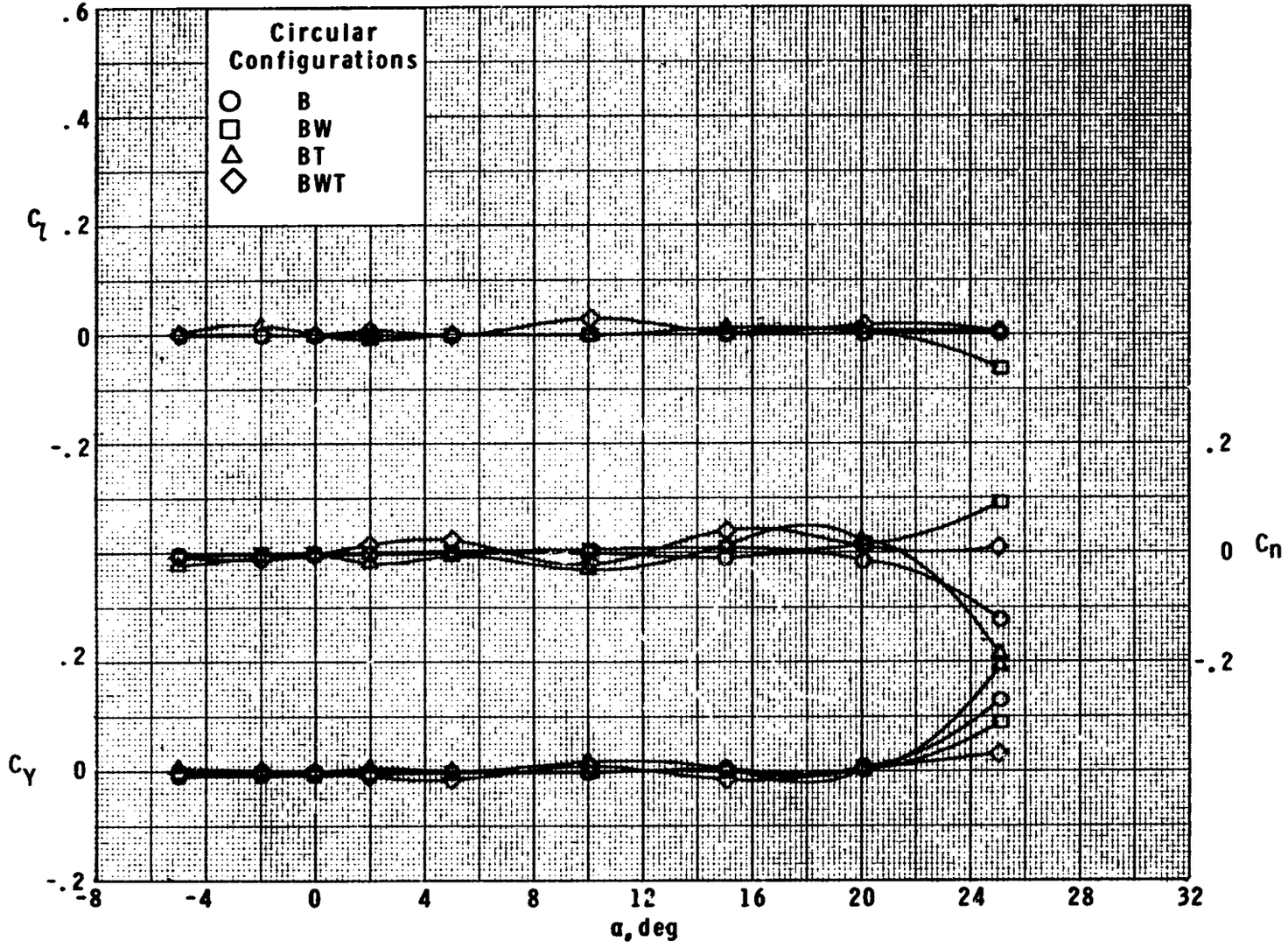

(c) M = 0.9.

Figure 6.- Continued.

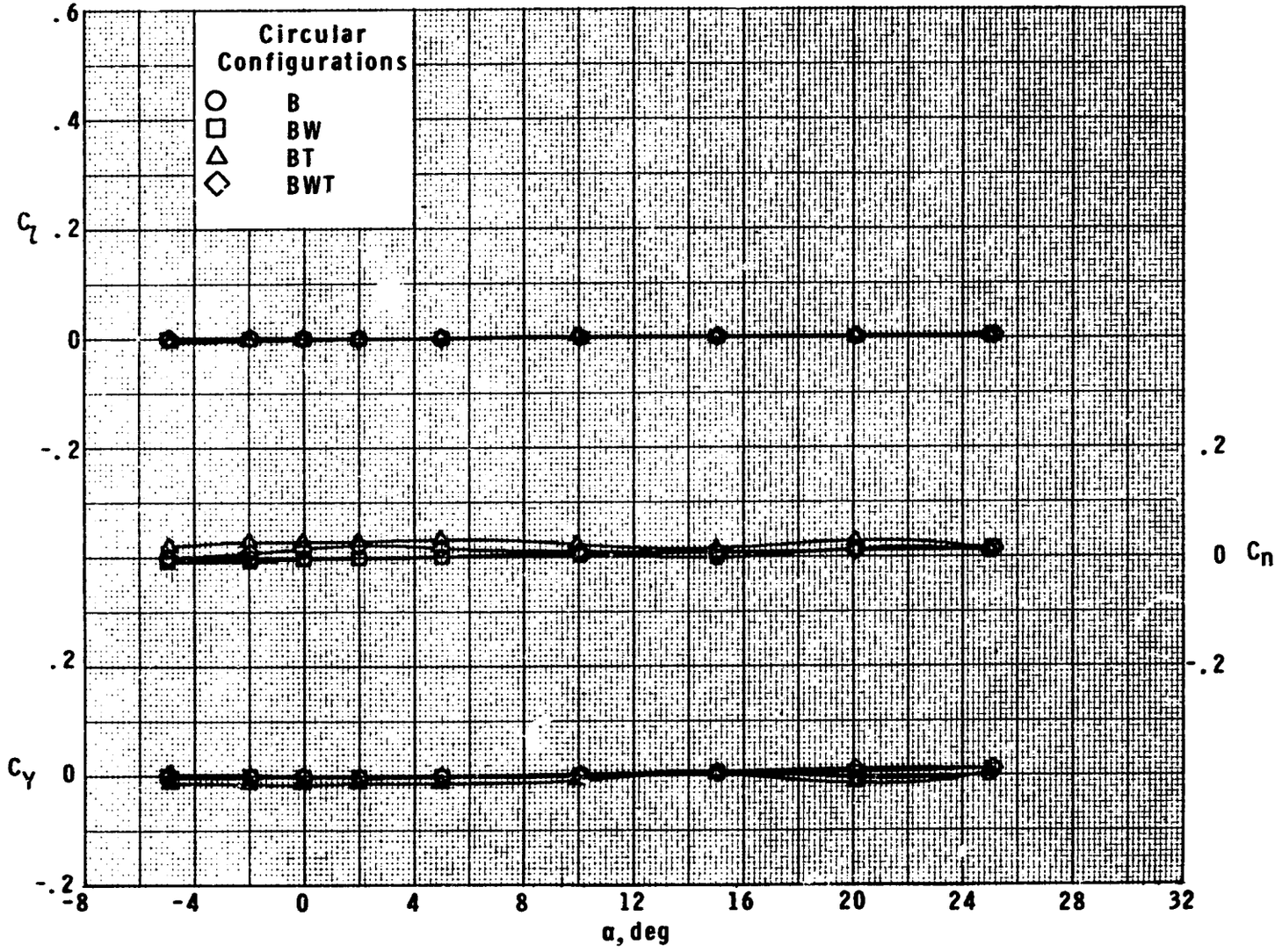

(d) M = 1.3.

Figure 6.- Continued.

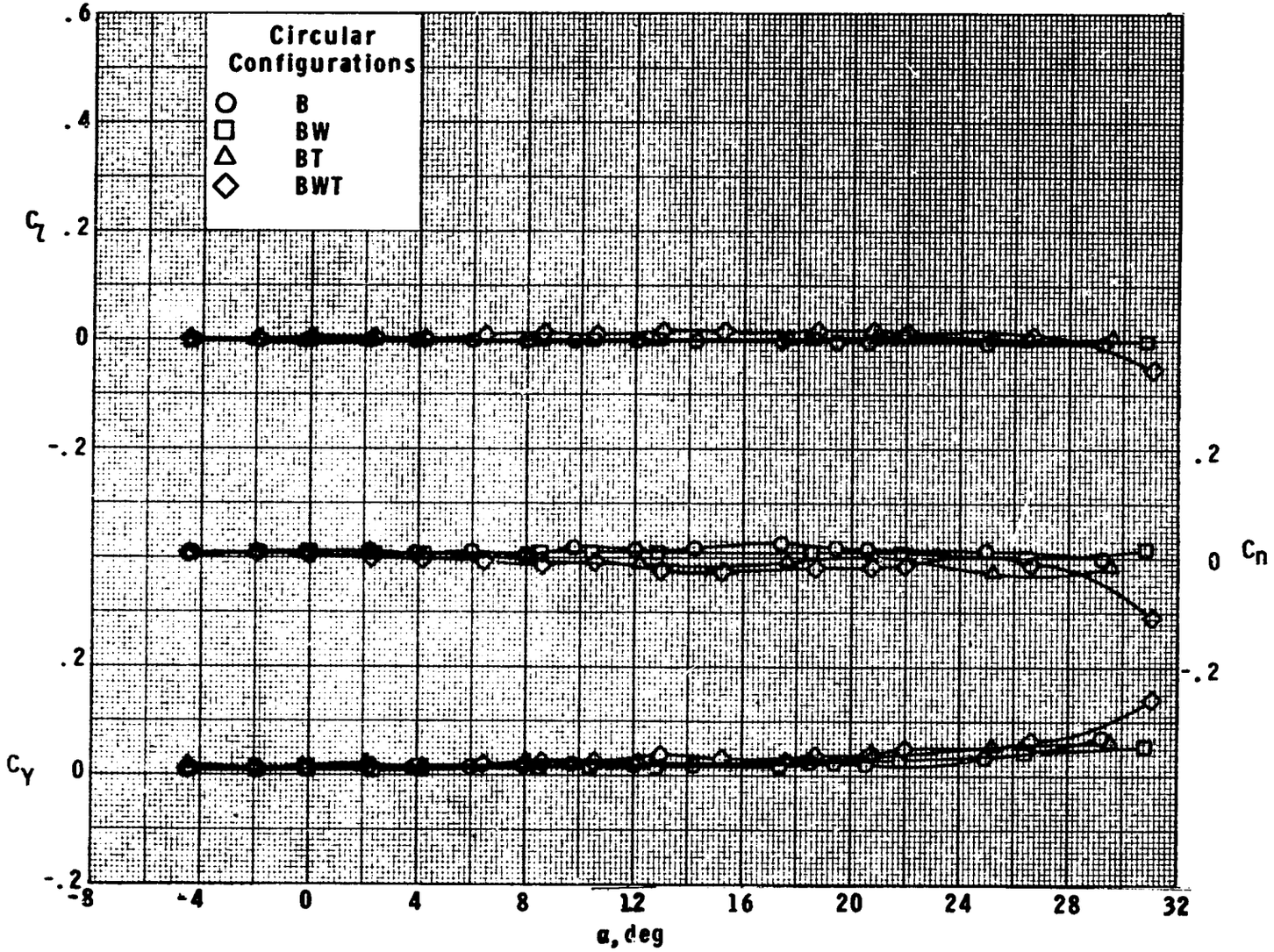

(e) M = 1.60.

Figure 6.- Continued.

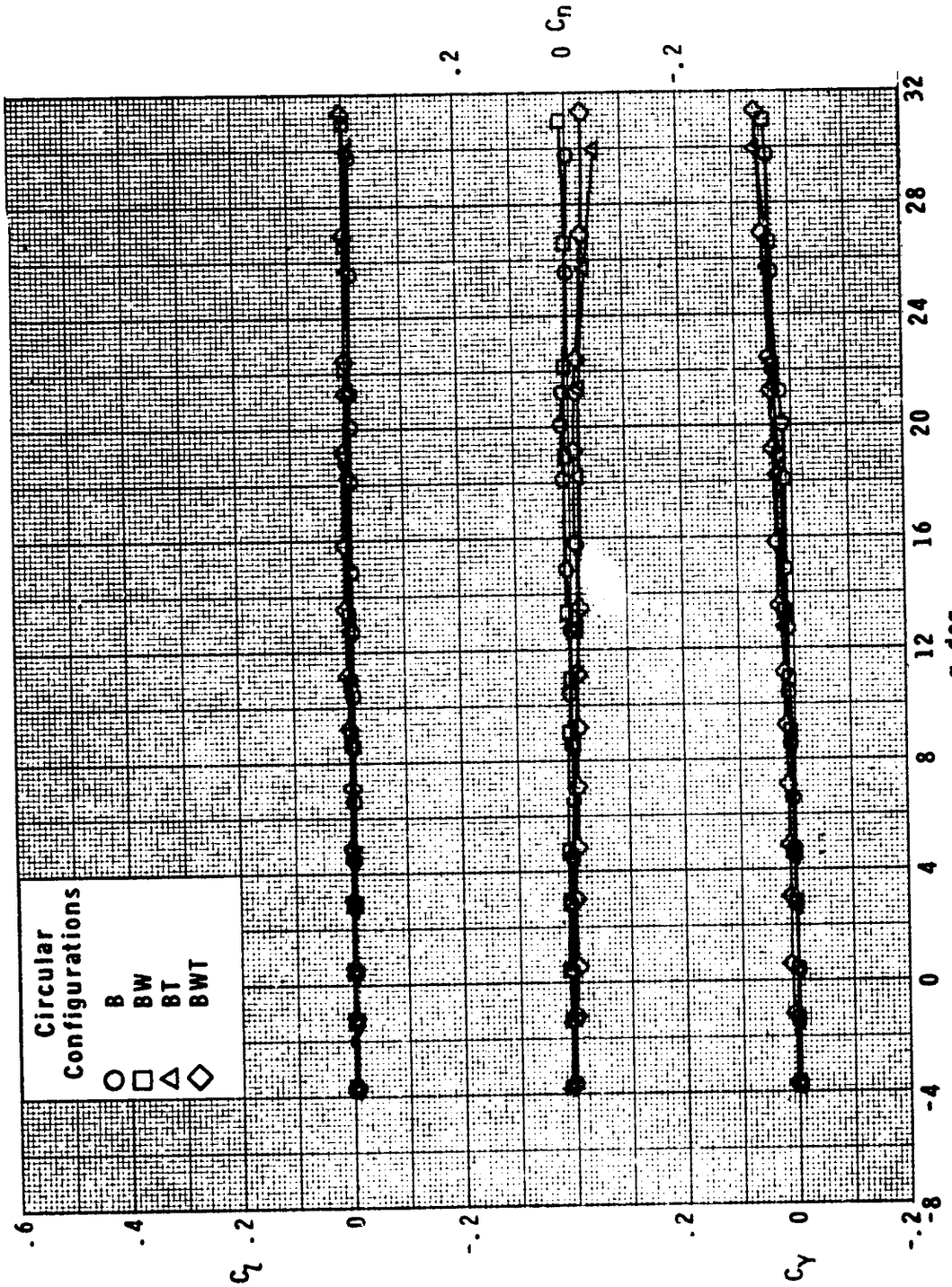

(f) M = 2.00.

Figure 6.- Continued.

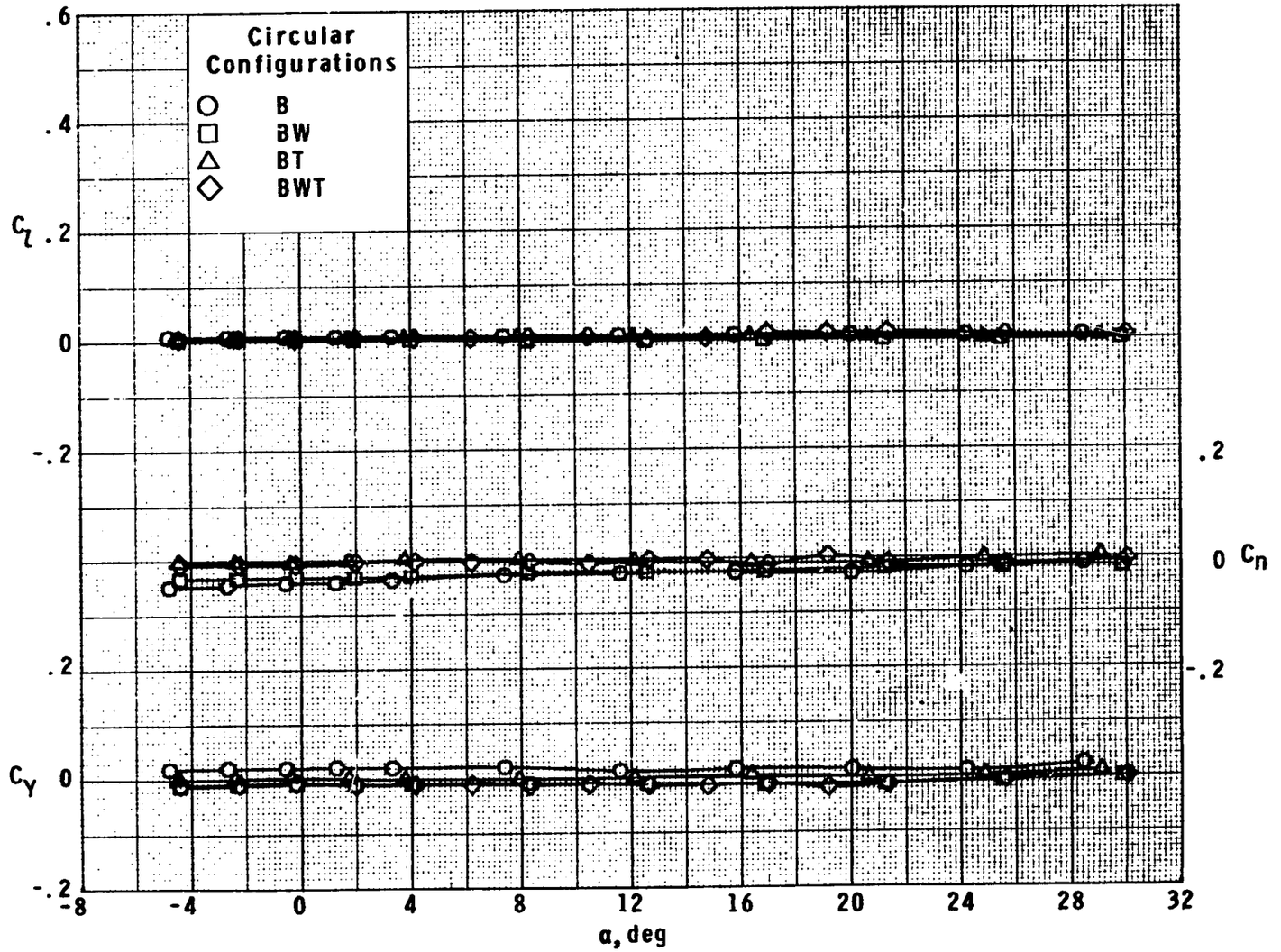

(g) M = 2.50.

Figure 6.- Continued.

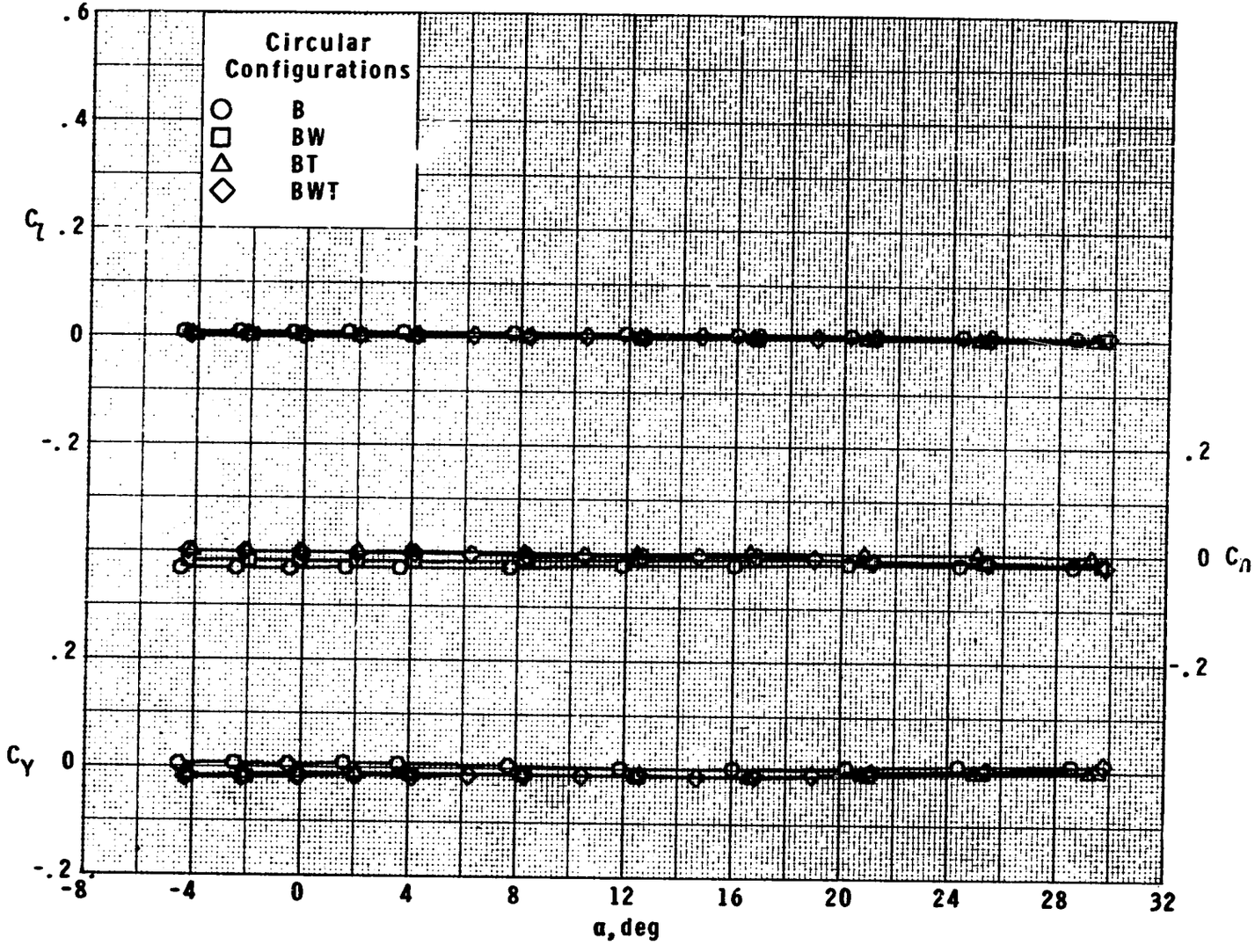

(h) M = 2.96.

Figure 6.- Continued.

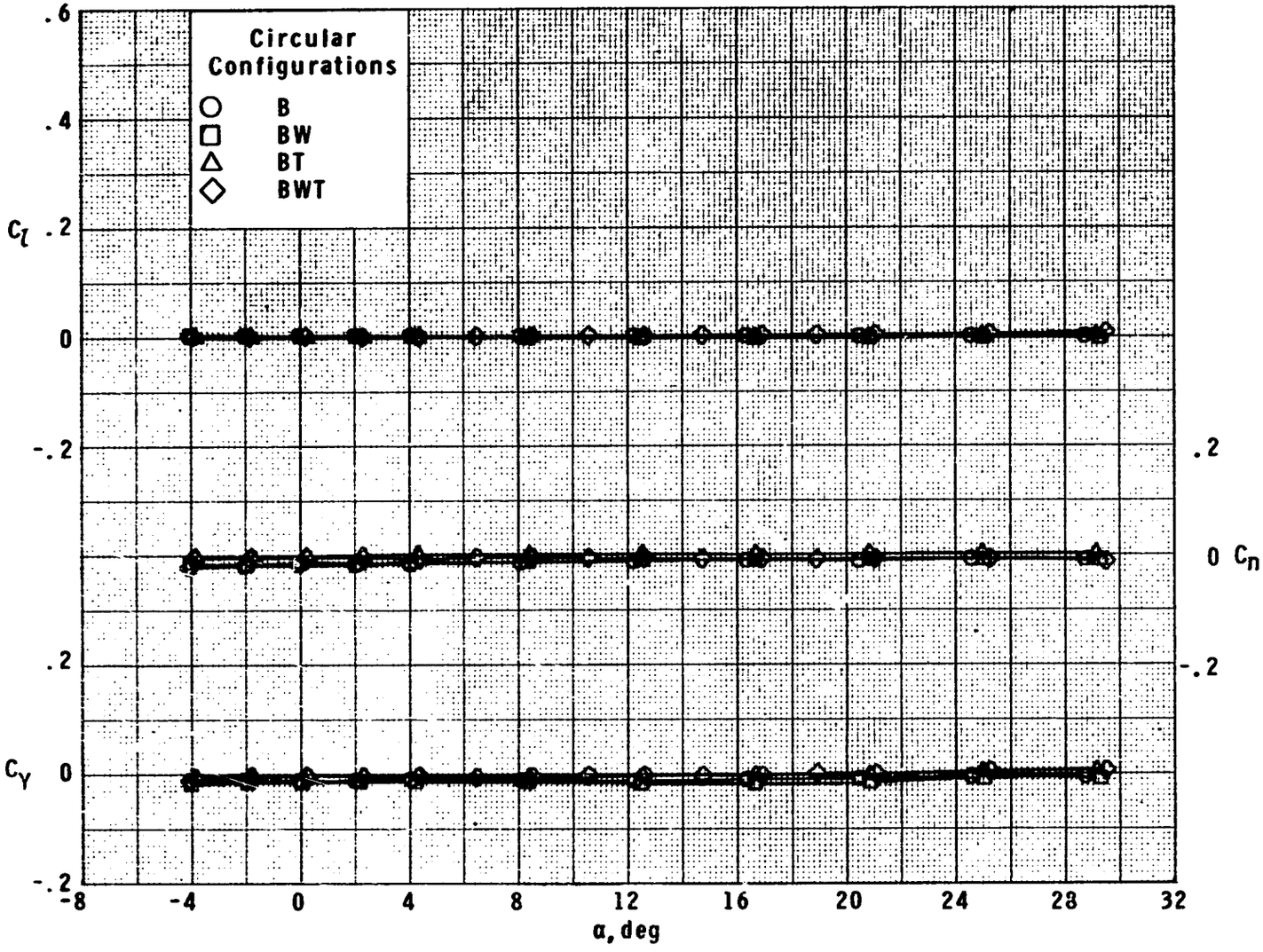

(i) M = 3.95.

Figure 6.- Continued.

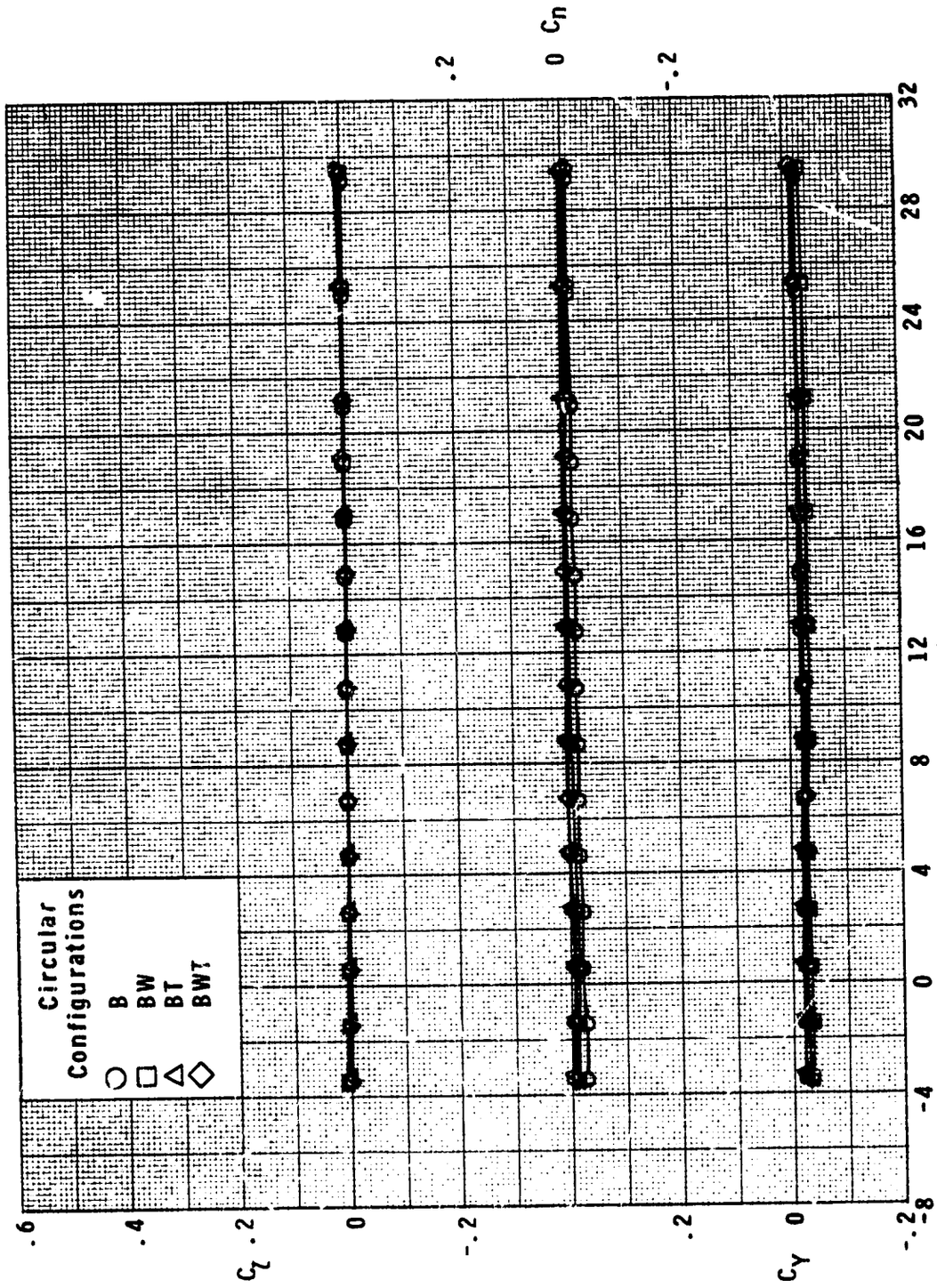

(j) M = 4.63.

Figure 6.- Concluded.

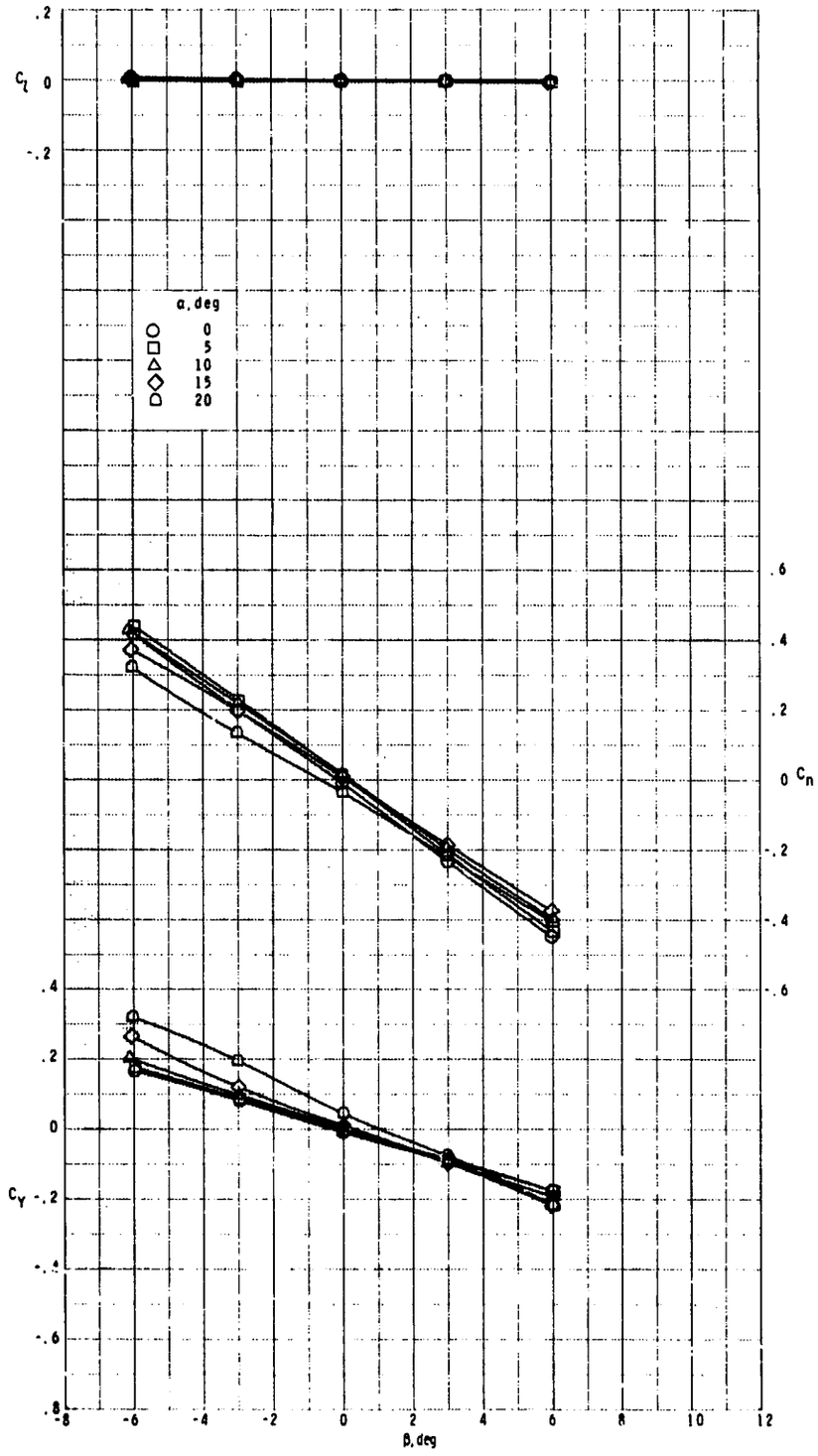

(a) M = 0.5.

Figure 7.- Effect of angle of attack on lateral aerodynamic characteristics of circular cross-section body with variation in angle of sideslip.

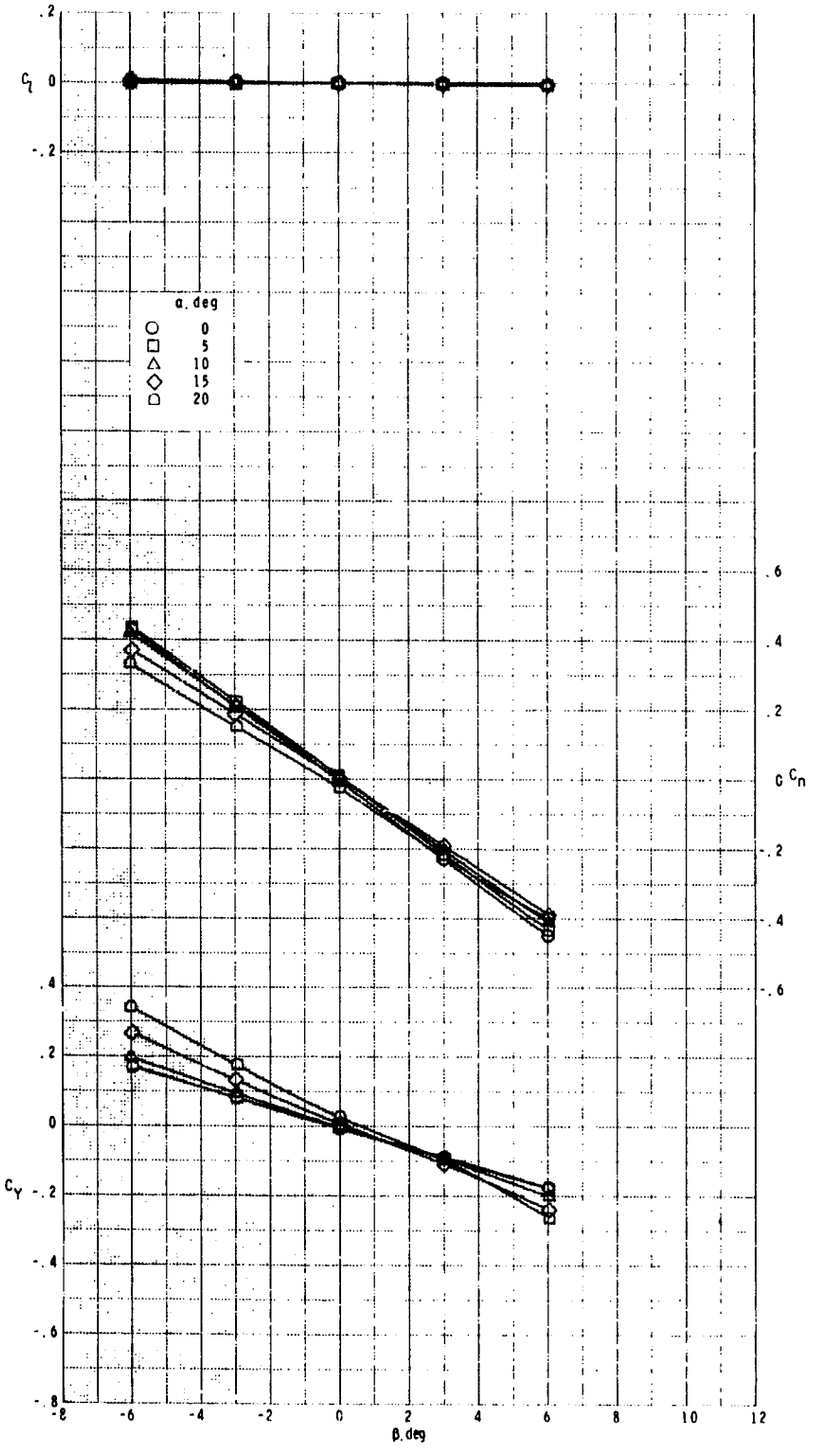

(b) M = 0.7.

Figure 7.- Continued.

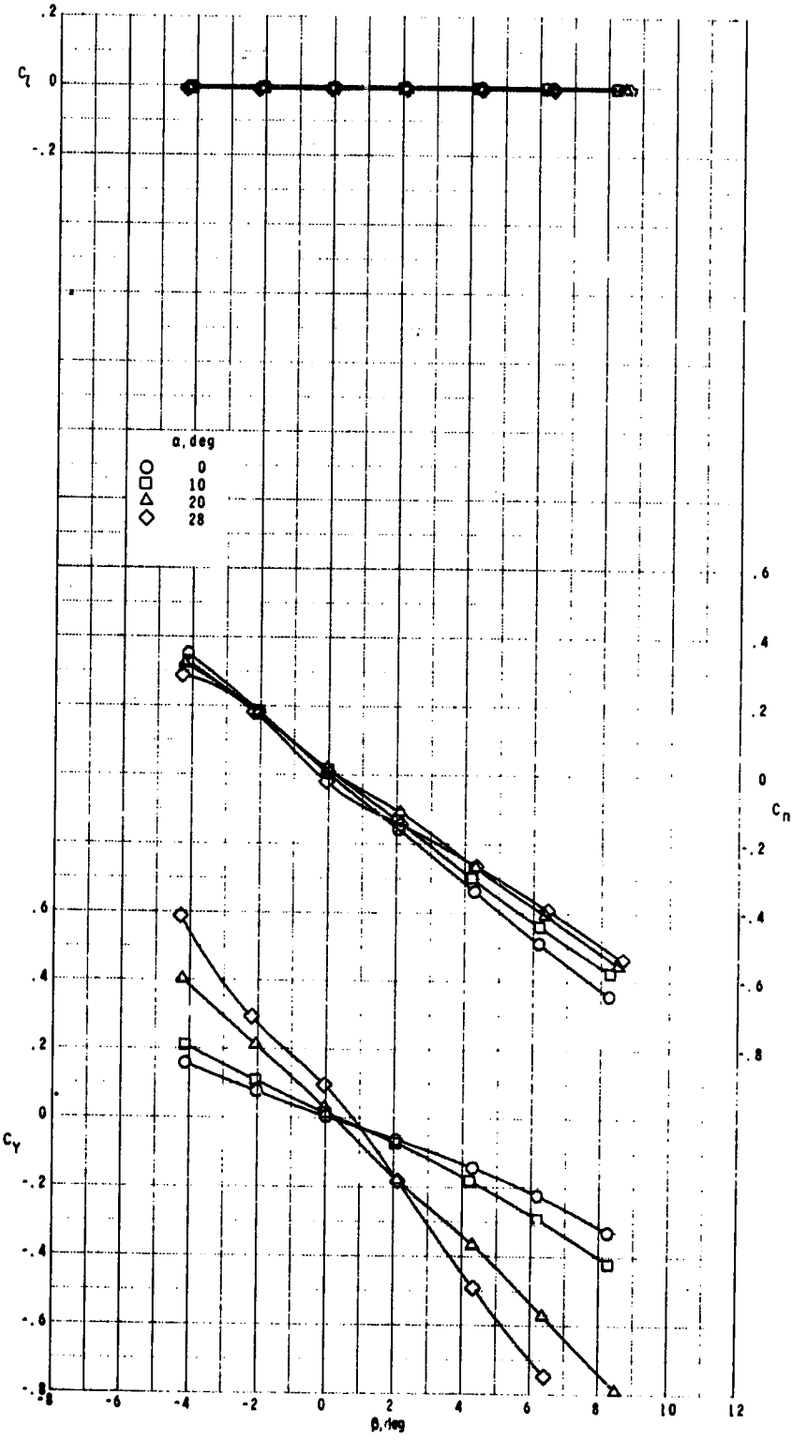

(c) M = 1.60.

Figure 7.- Continued.

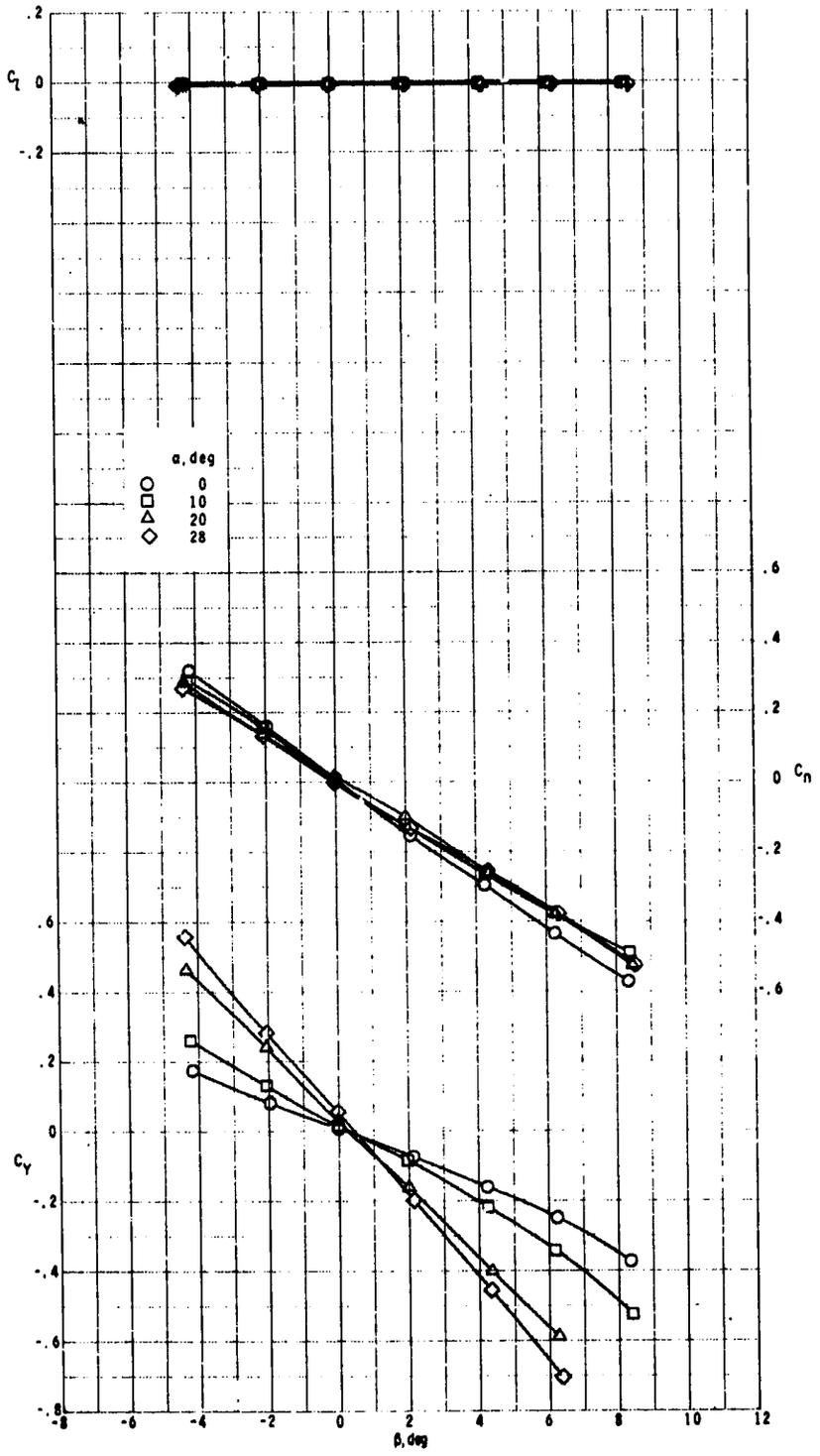

(d) M = 2.00.

Figure 7.- Continued.

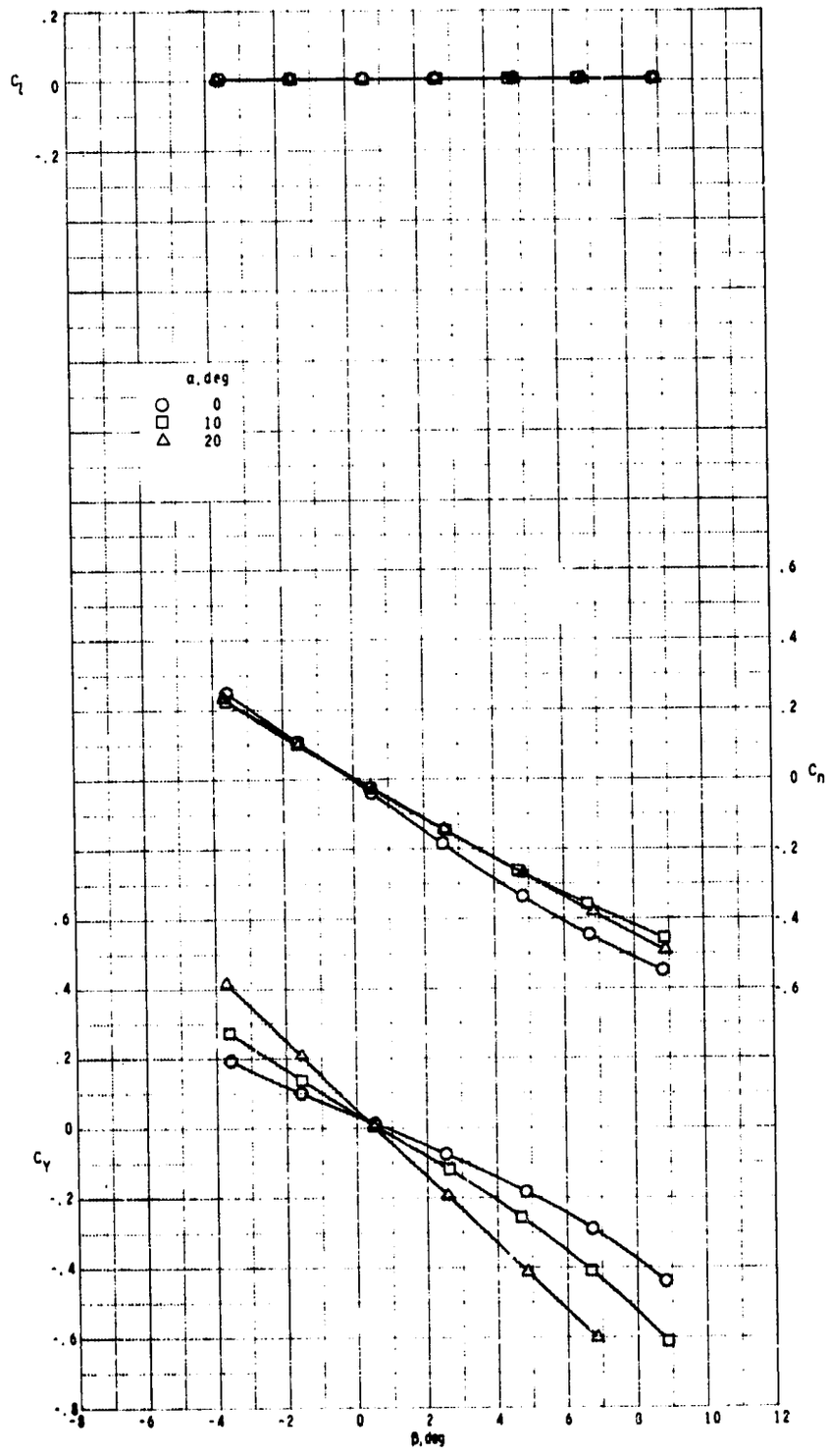

(e) M = 2.50.

Figure 7.- Continued.

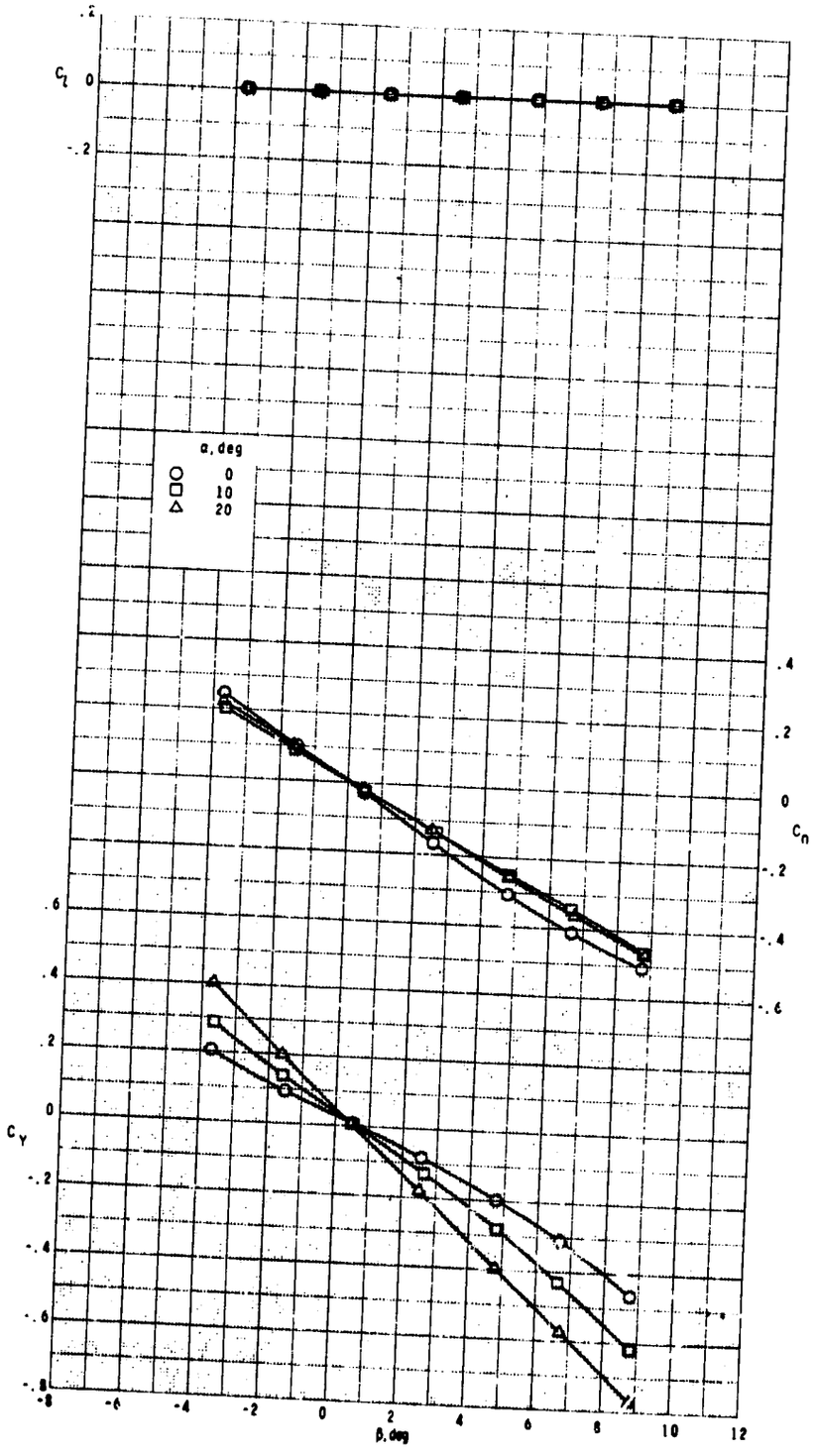

(f) M = 2.96.

Figure 7.- Continued.

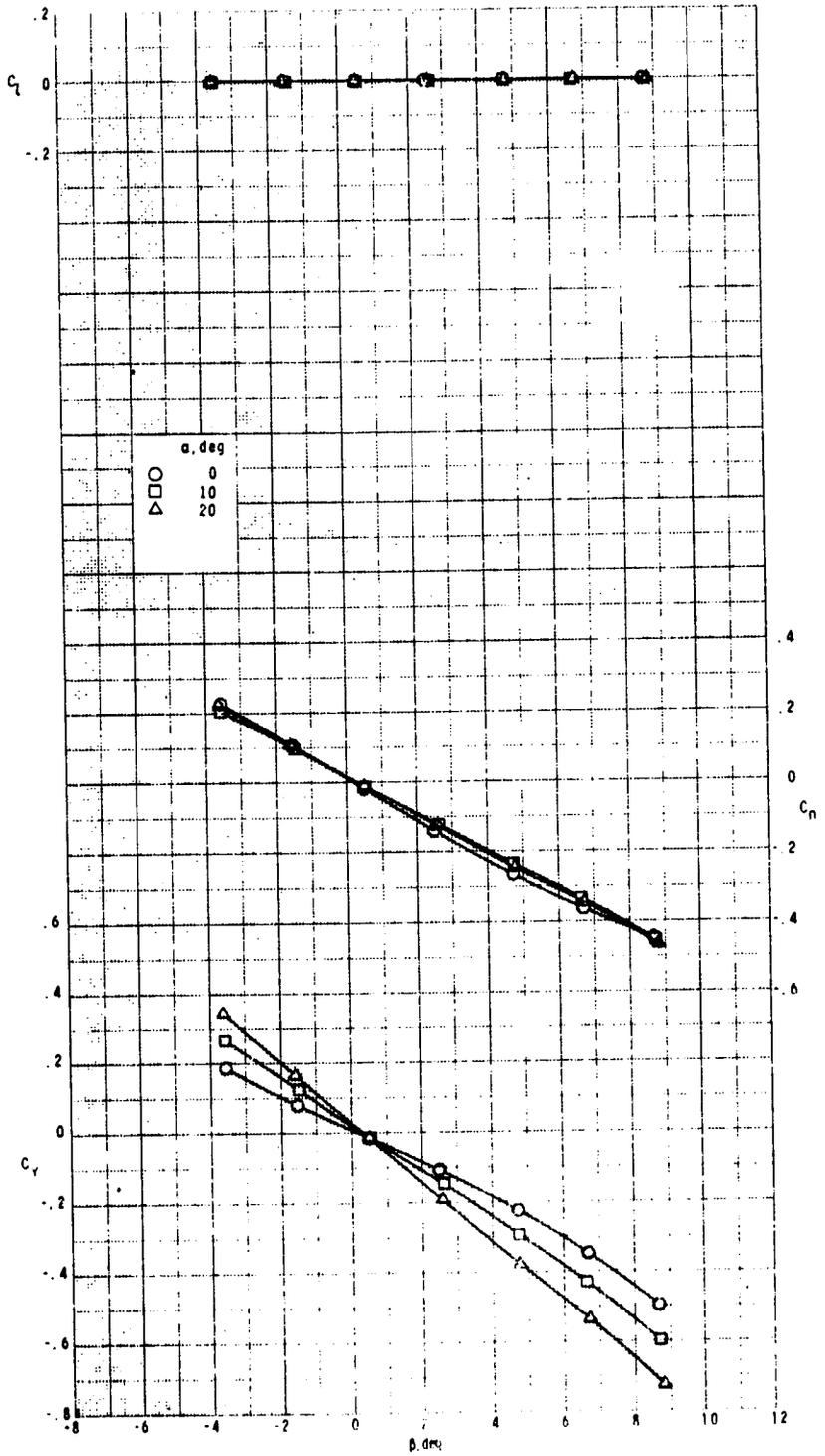

(c) $M = 2.05$.

Figure 7.- Continued.

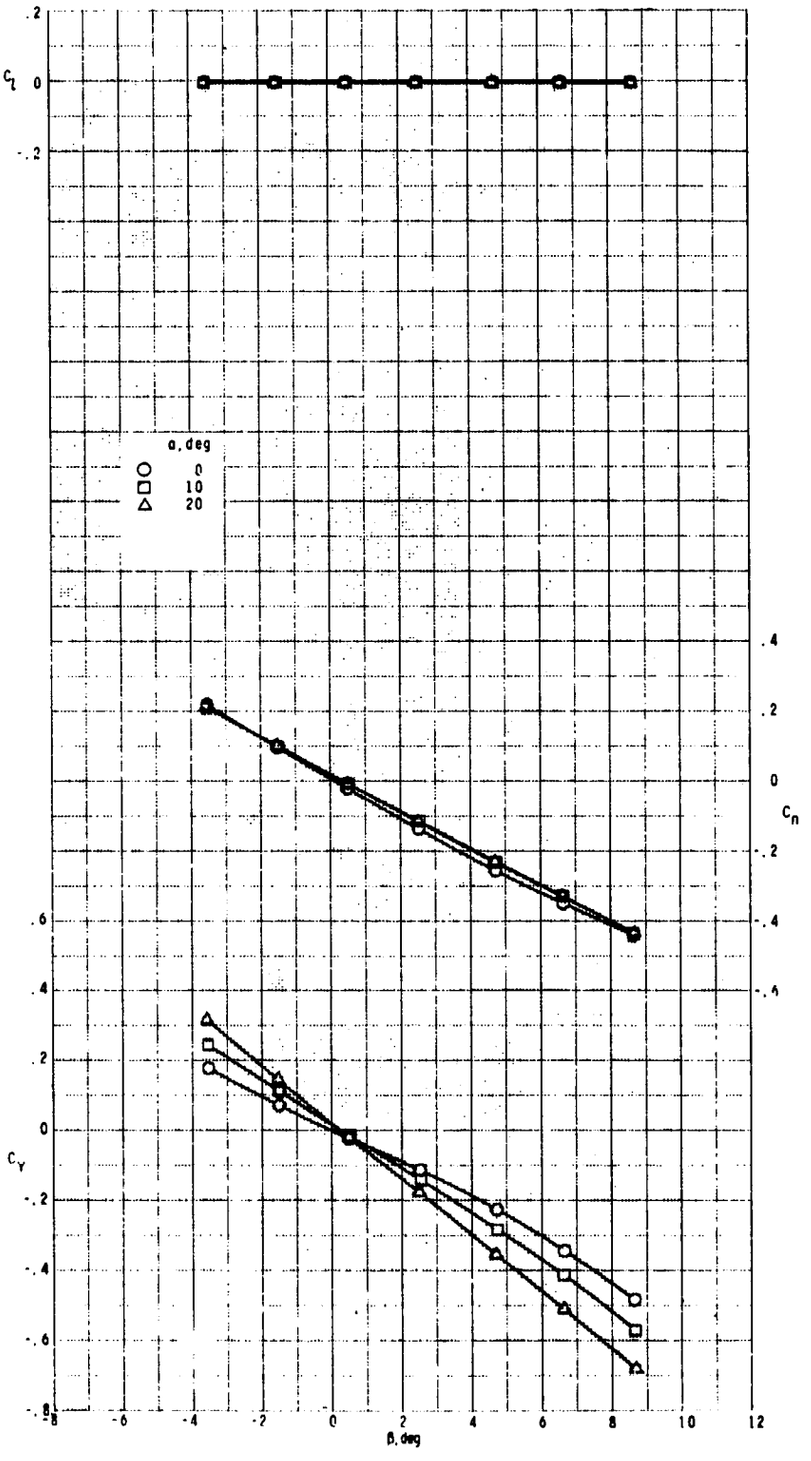

(h) M = 4.63.

Figure 7.- Concluded.

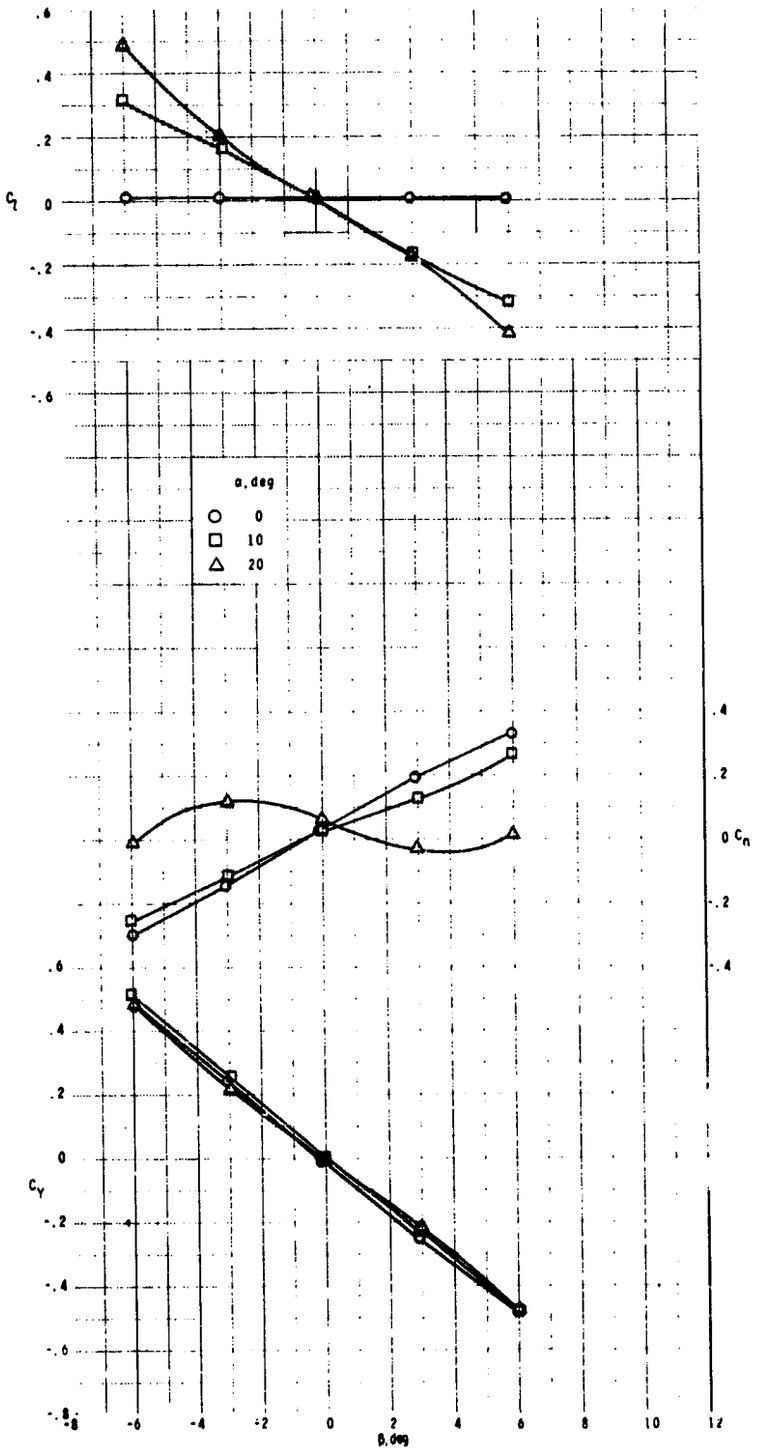

(a) M = 0.5.

Figure 8.- Effect of angle of attack on lateral aerodynamic characteristics of circular cross-section body-wing-tail configuration with variation in angle of sideslip.

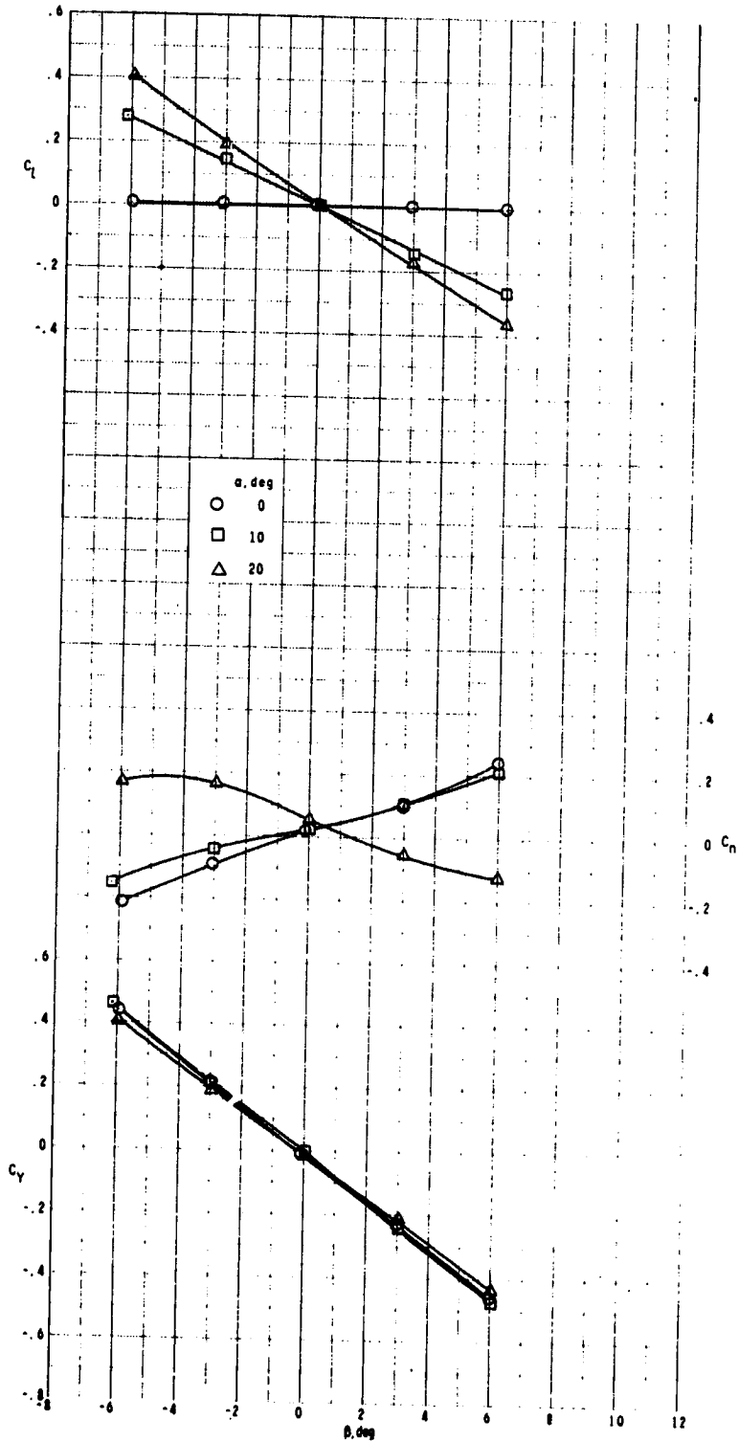

(b) M = 0.7.

Figure 8.- Continued.

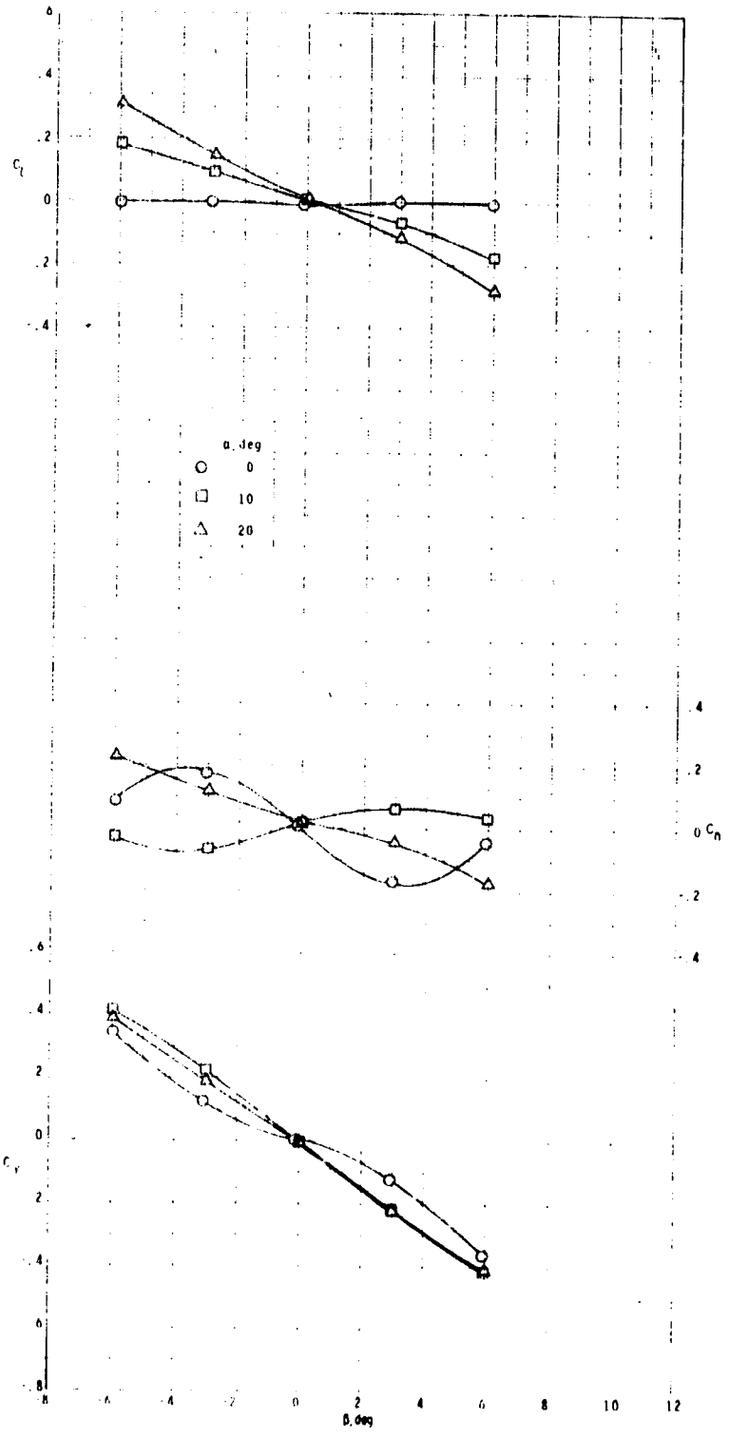

(c) M = 0.9.

Figure 3.- Continued.

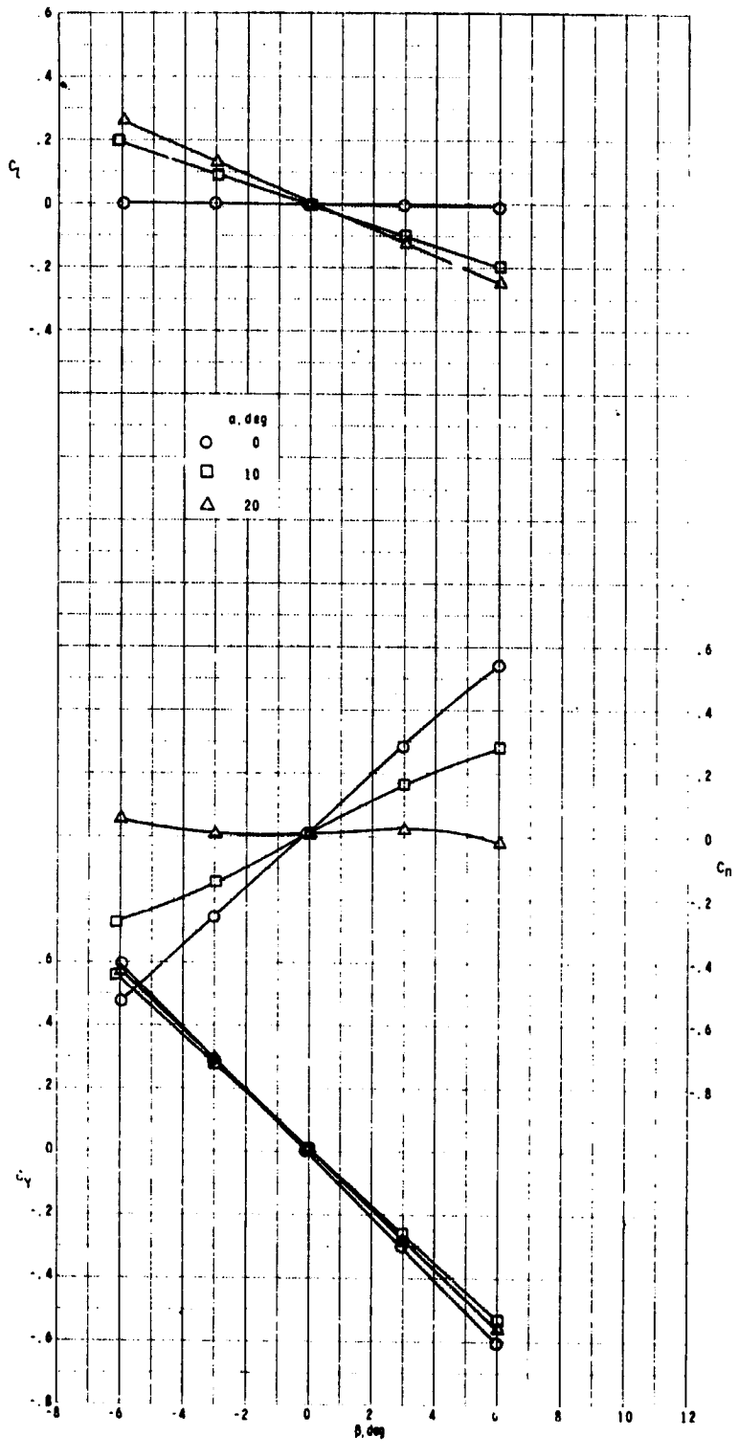

(d) M = 1.3.

Figure 8.- Continued.

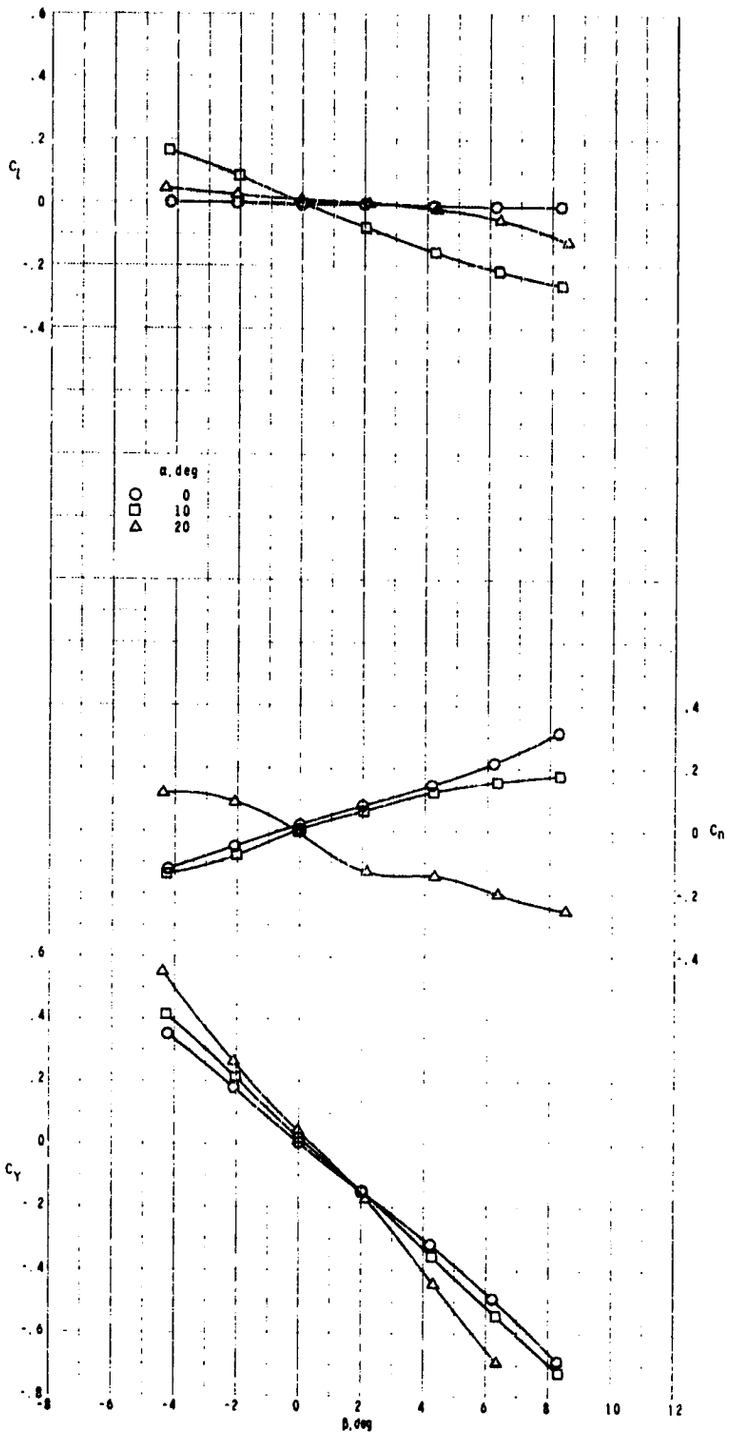

(e) M = 1.60.

Figure 8.- Continued.

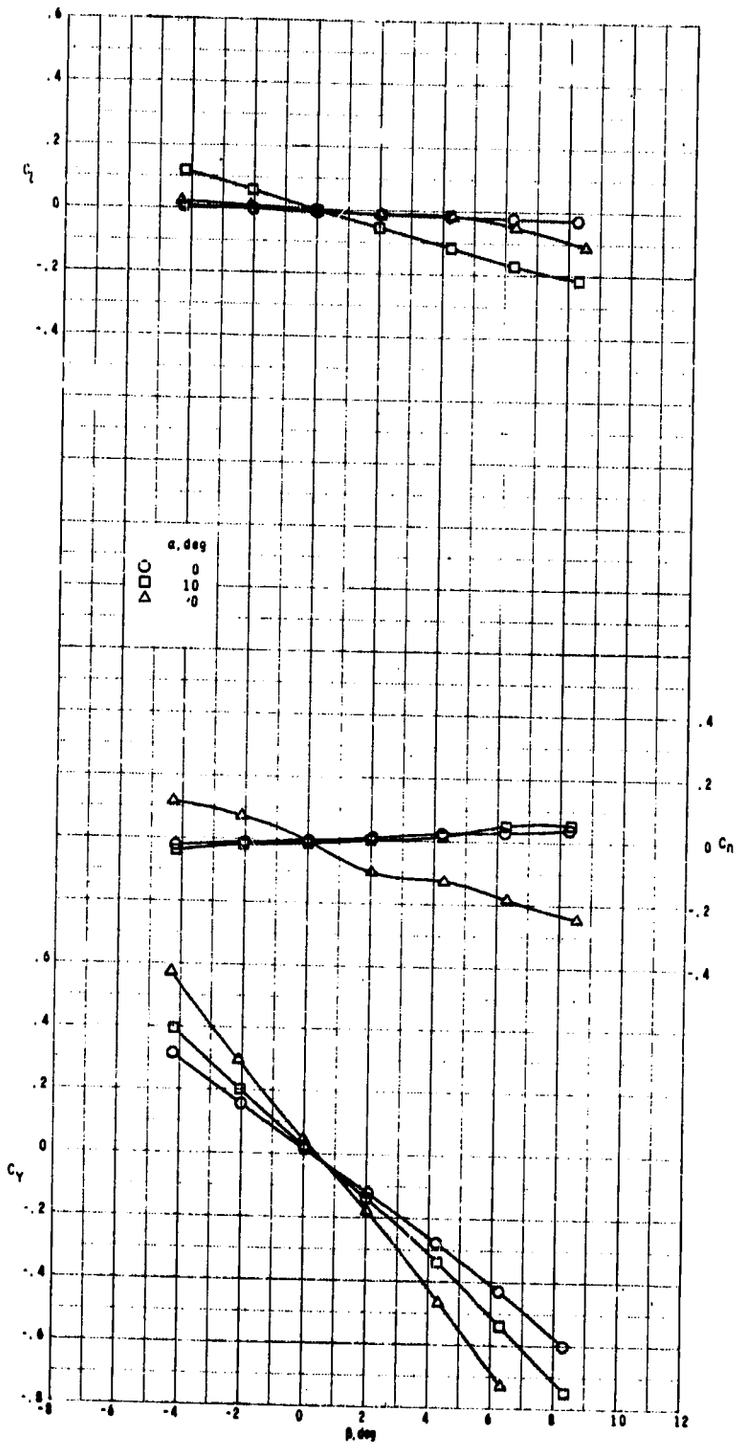

(f) M = 2.00.

Figure 8.- Continued.

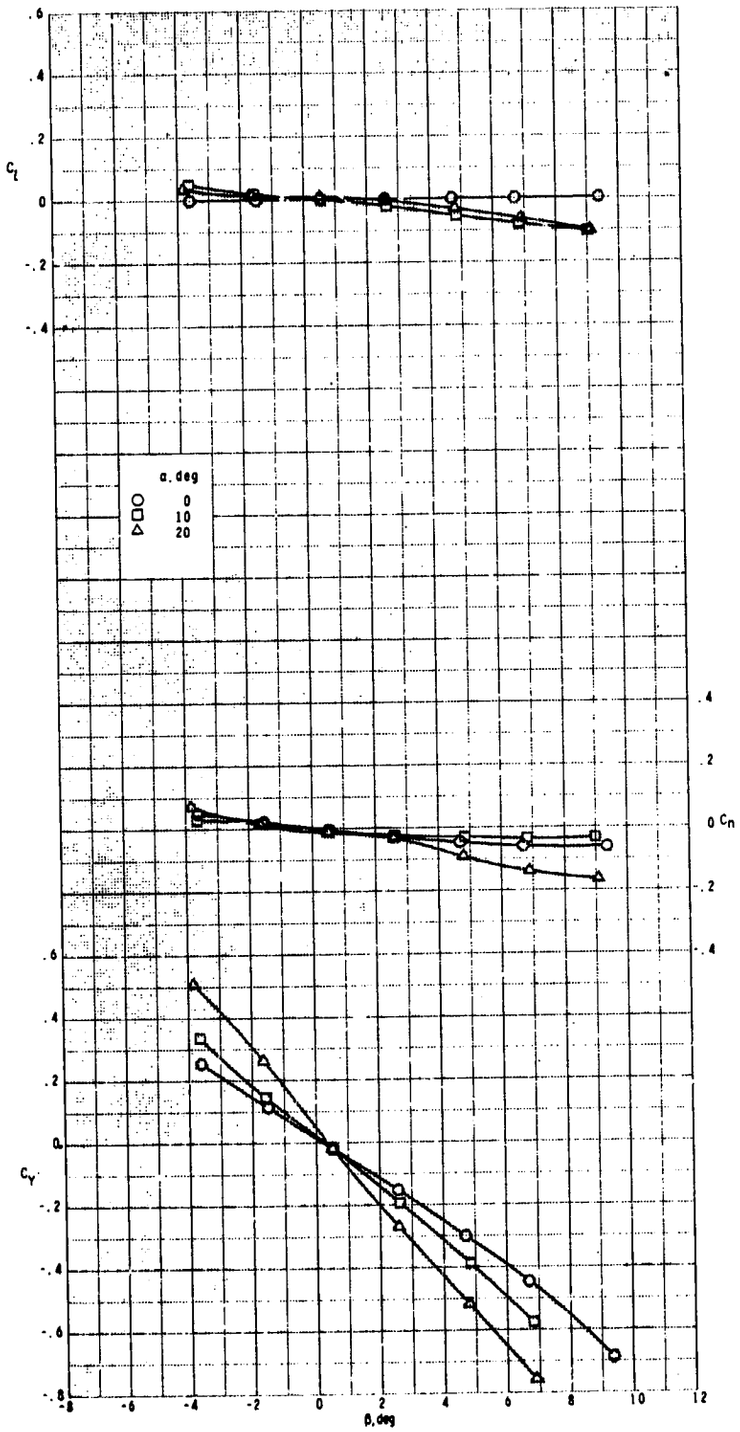

(g) M = 2.50.

Figure 8.- Continued.

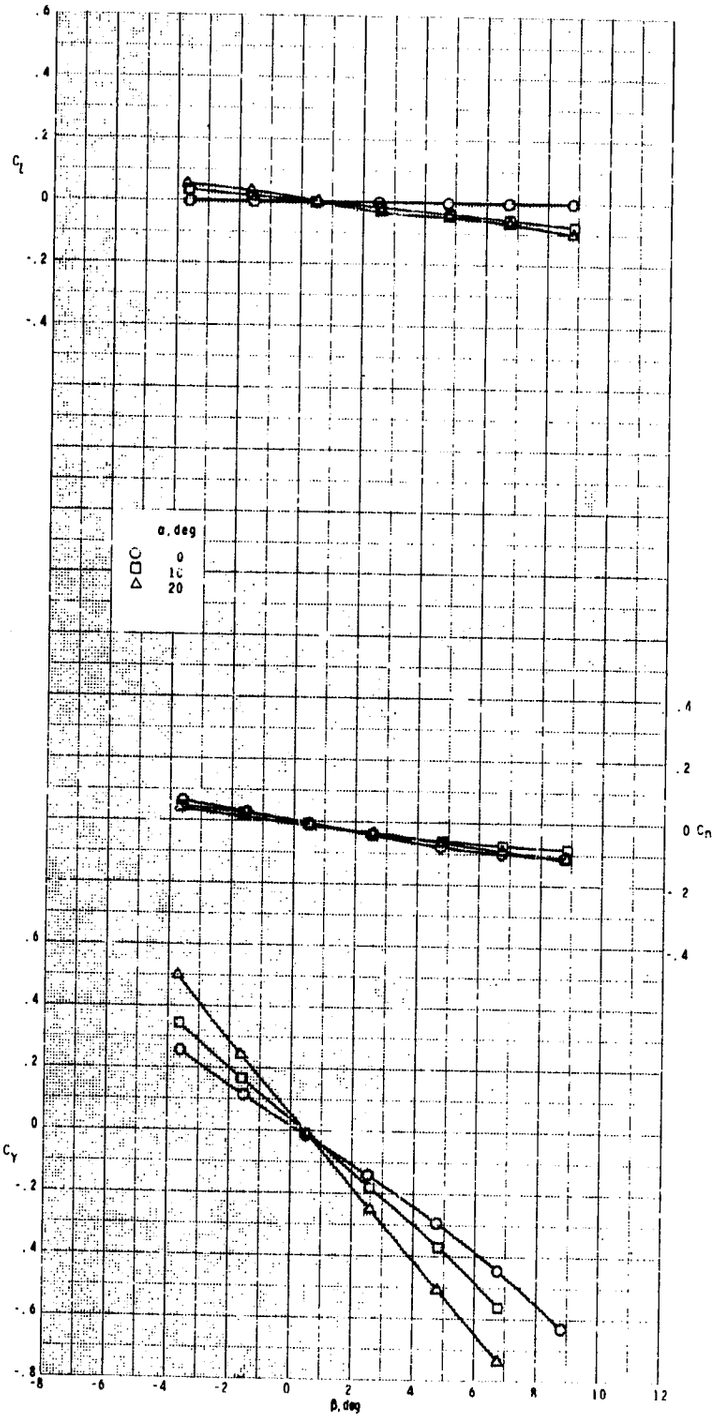

(h) M = 2.96.

Figure 8.- Continued.

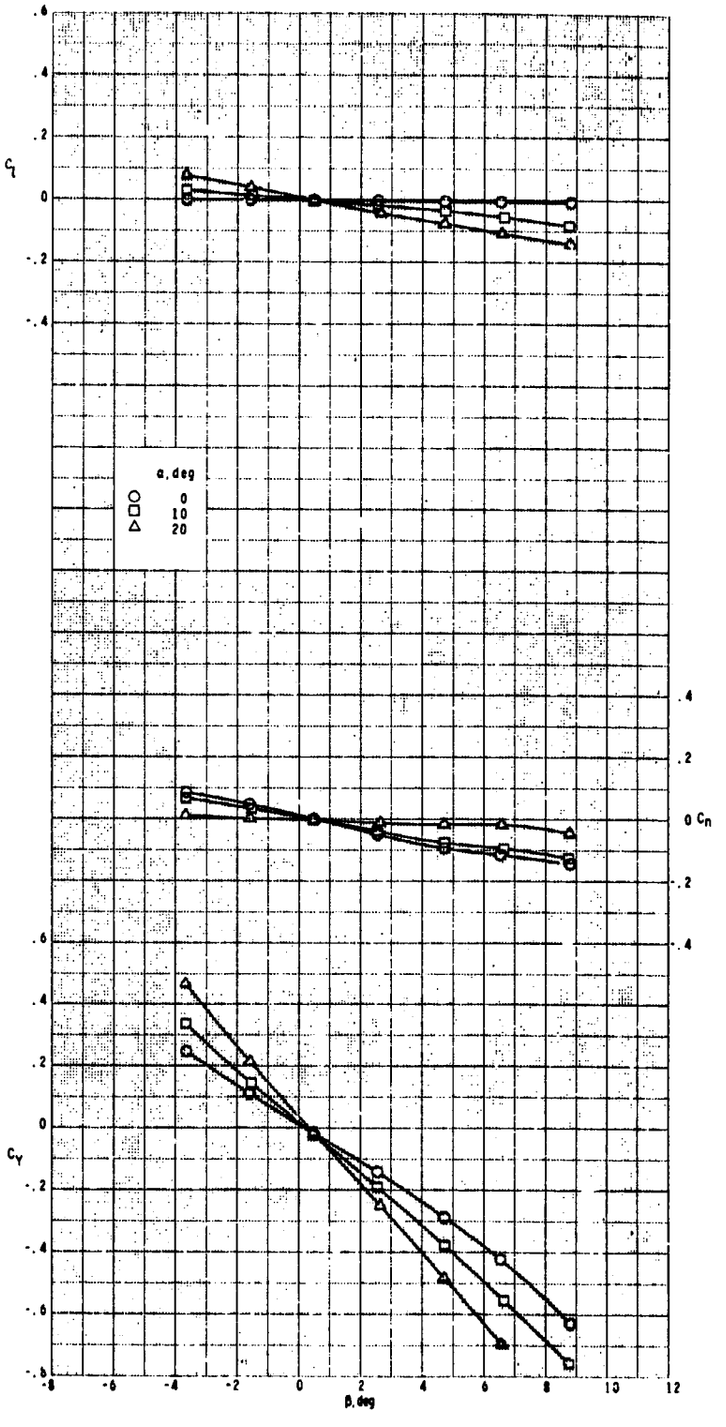

(i) M = 3.95.

Figure 8.- Continued.

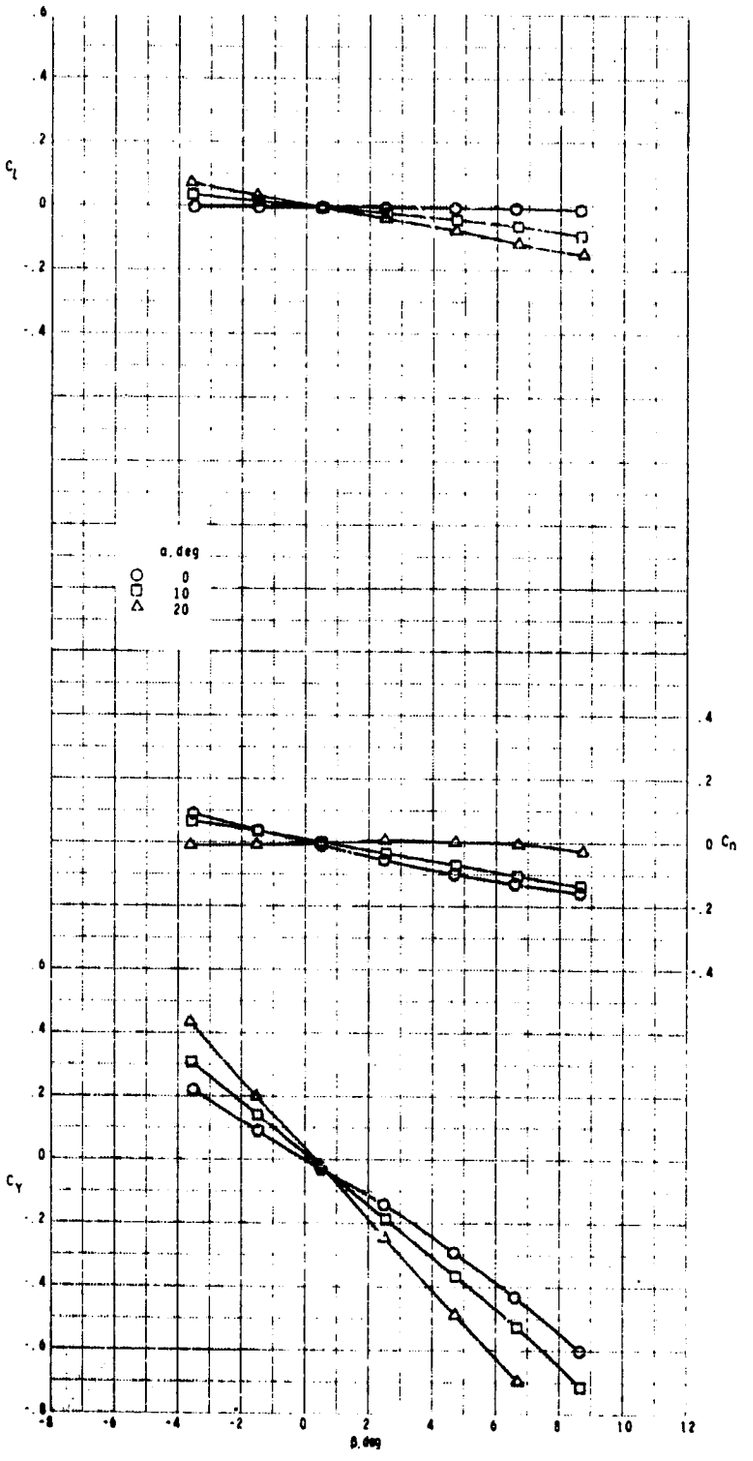

(j) M = 4.63.

Figure 8.- Concluded.

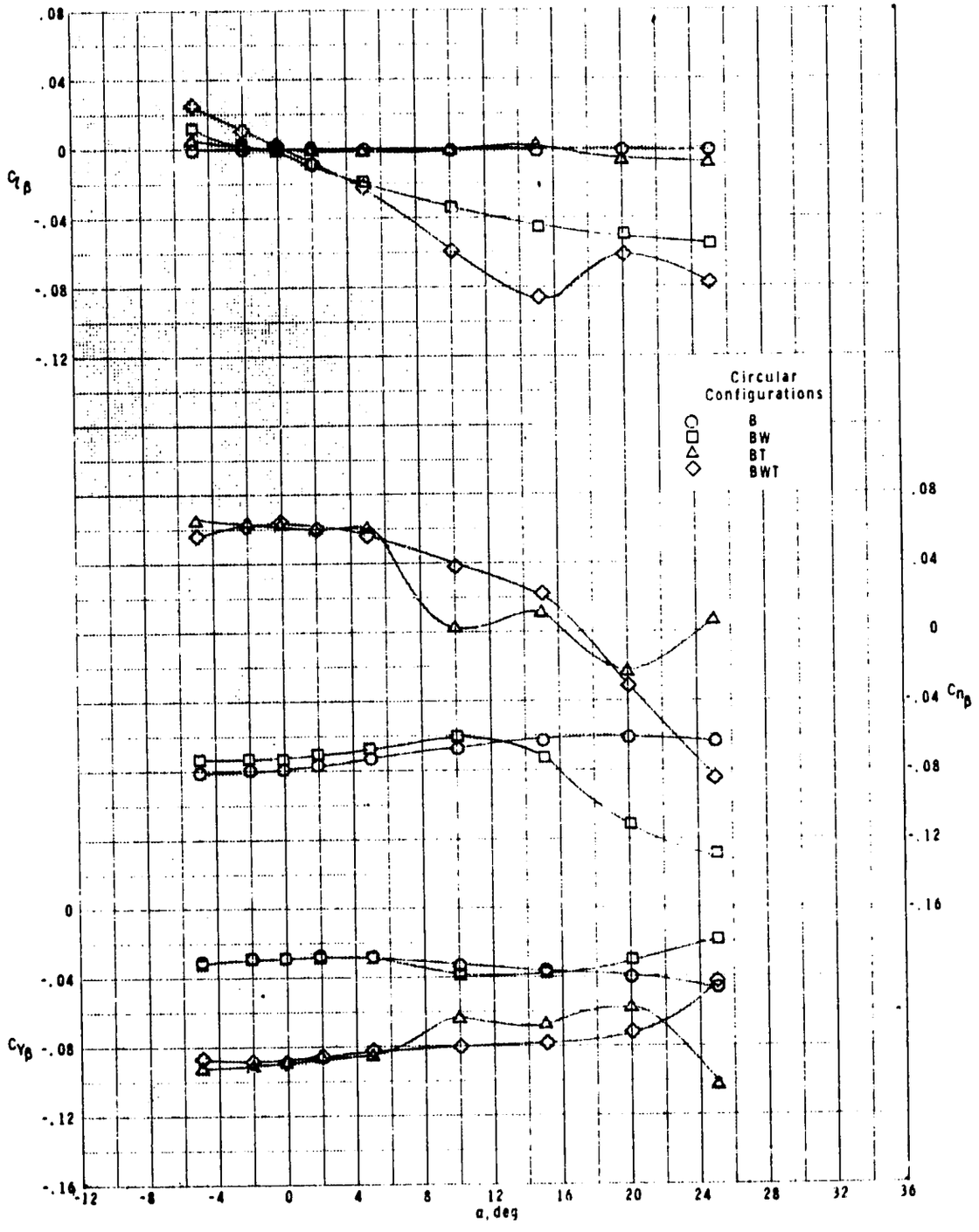

(a) M = 0.5.

Figure 9.- Effect of components on lateral-directional stability parameters of circular cross-section model with variation in angle of attack.

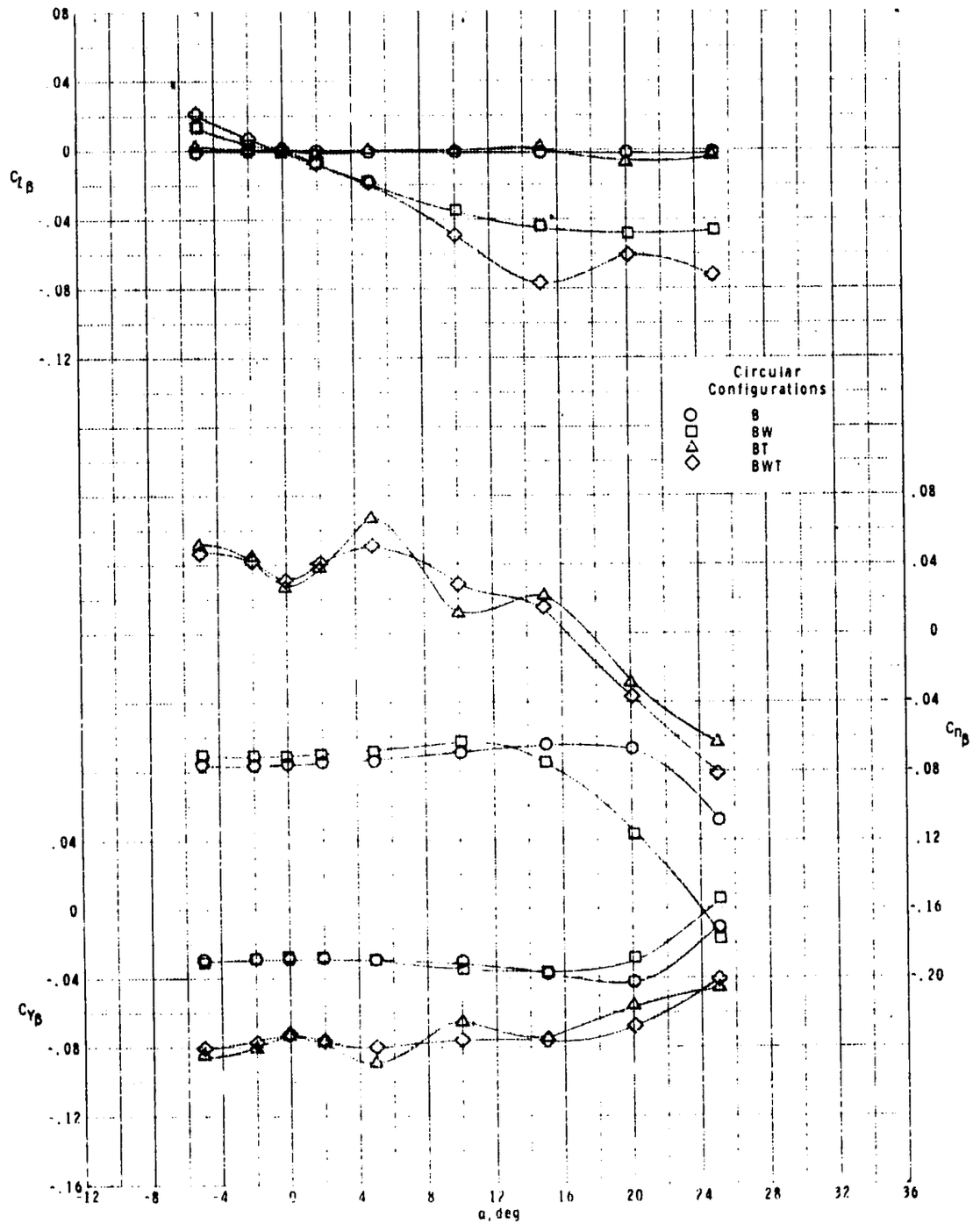

(b) M = 0.7.

Figure 9.- Continued.

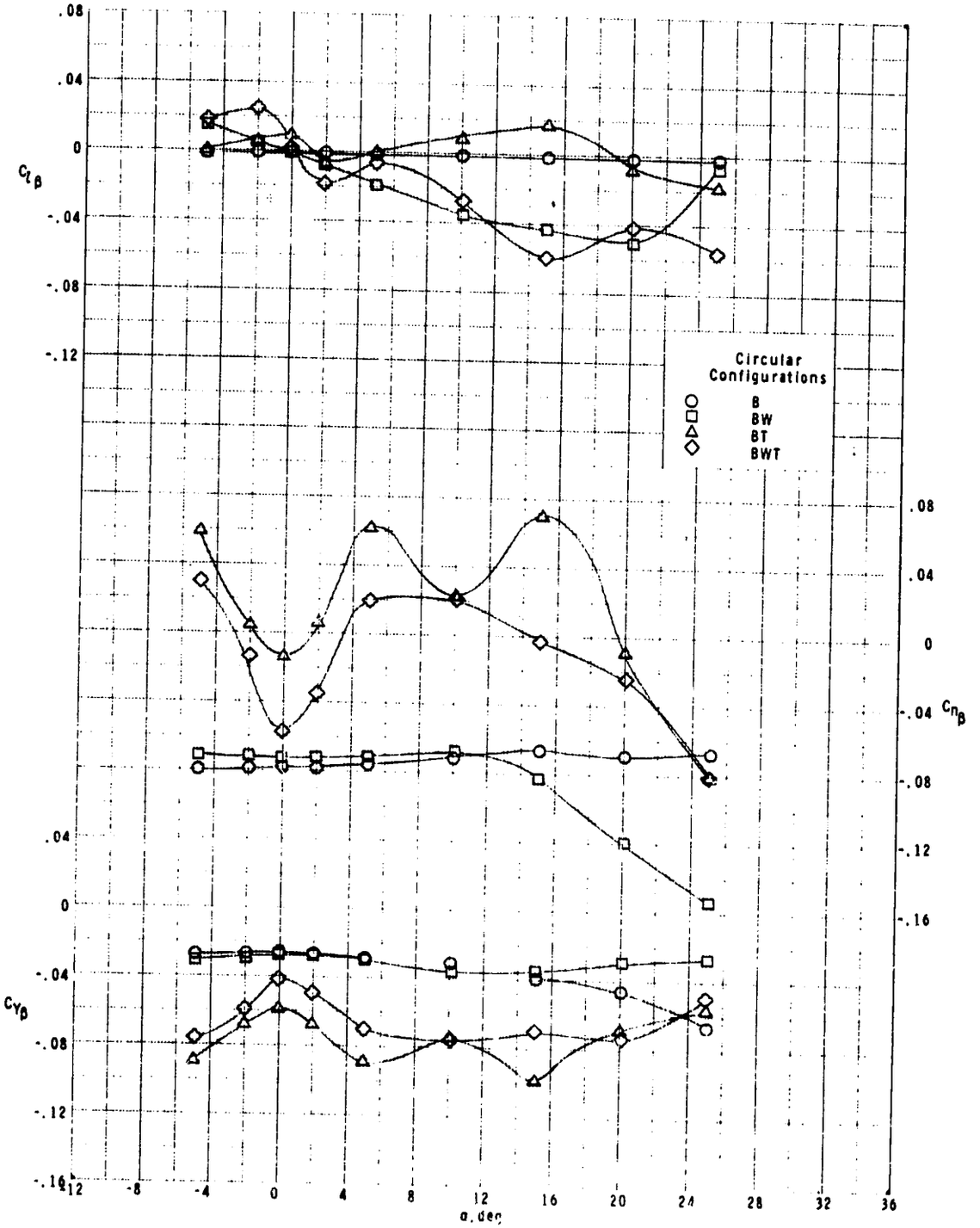

(c) M = 0.9.

Figure 9.- Continued.

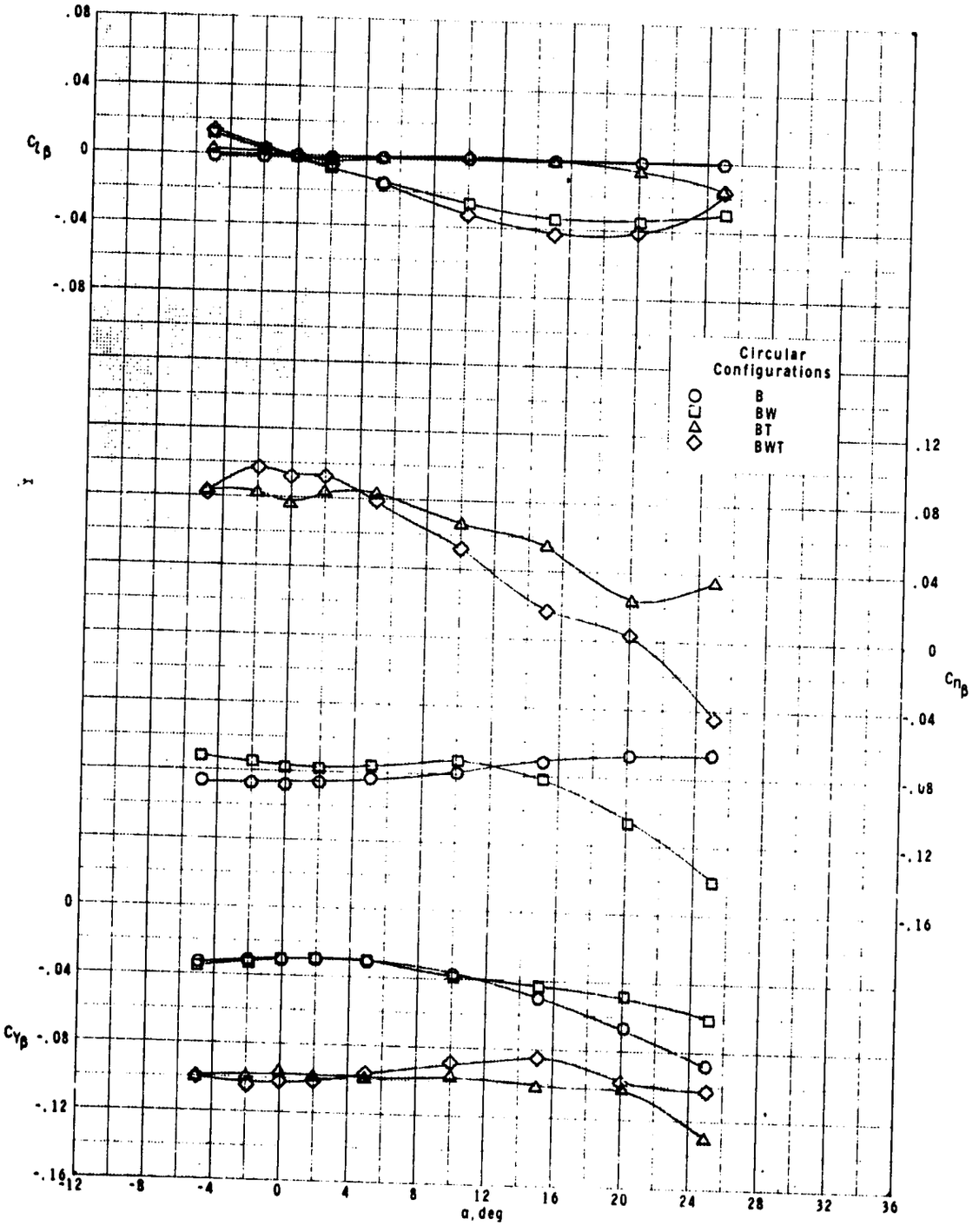

(d) M = 1.3.

Figure 9.- Continued.

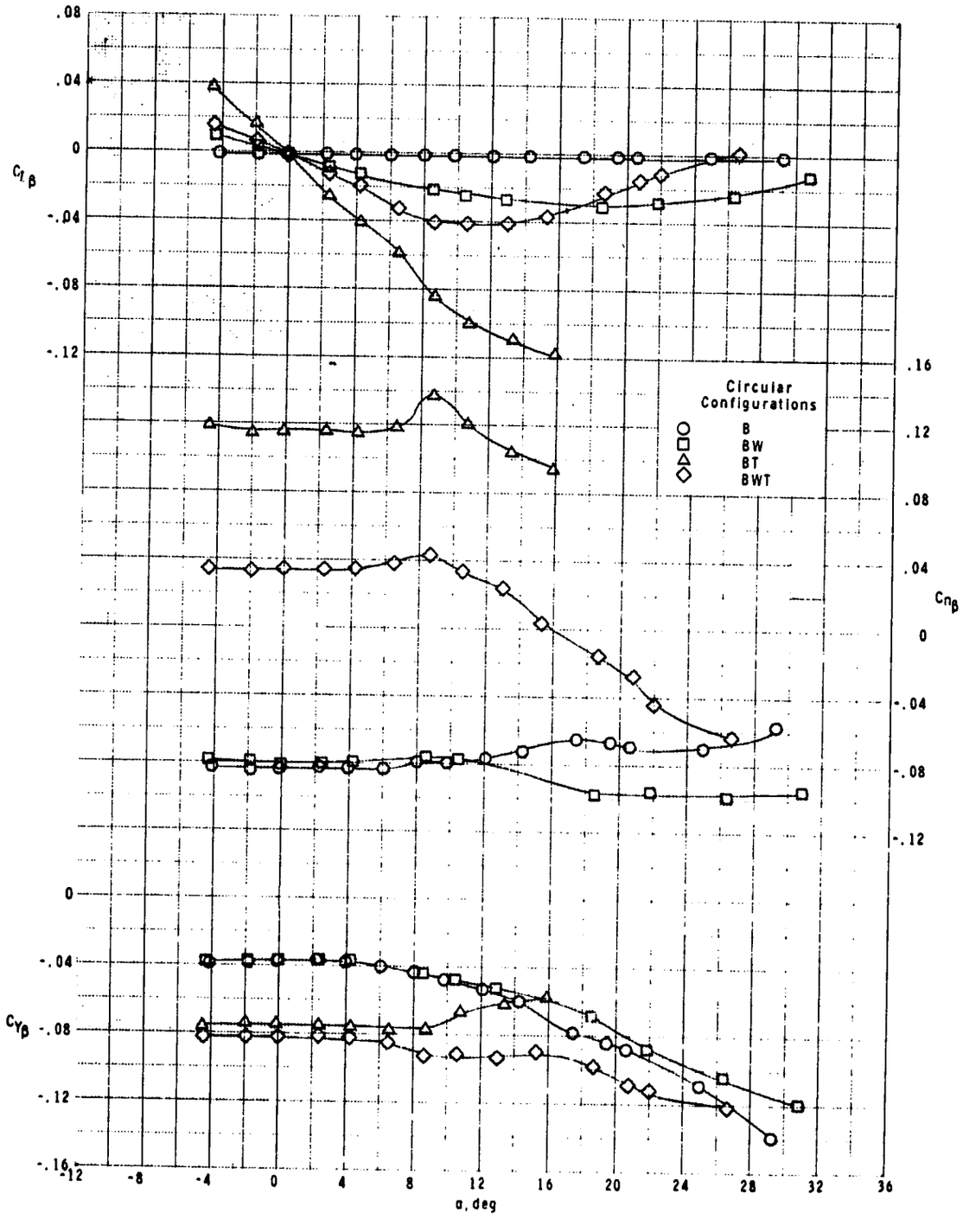

(e) M = 1.60.

Figure 9.- Continued.

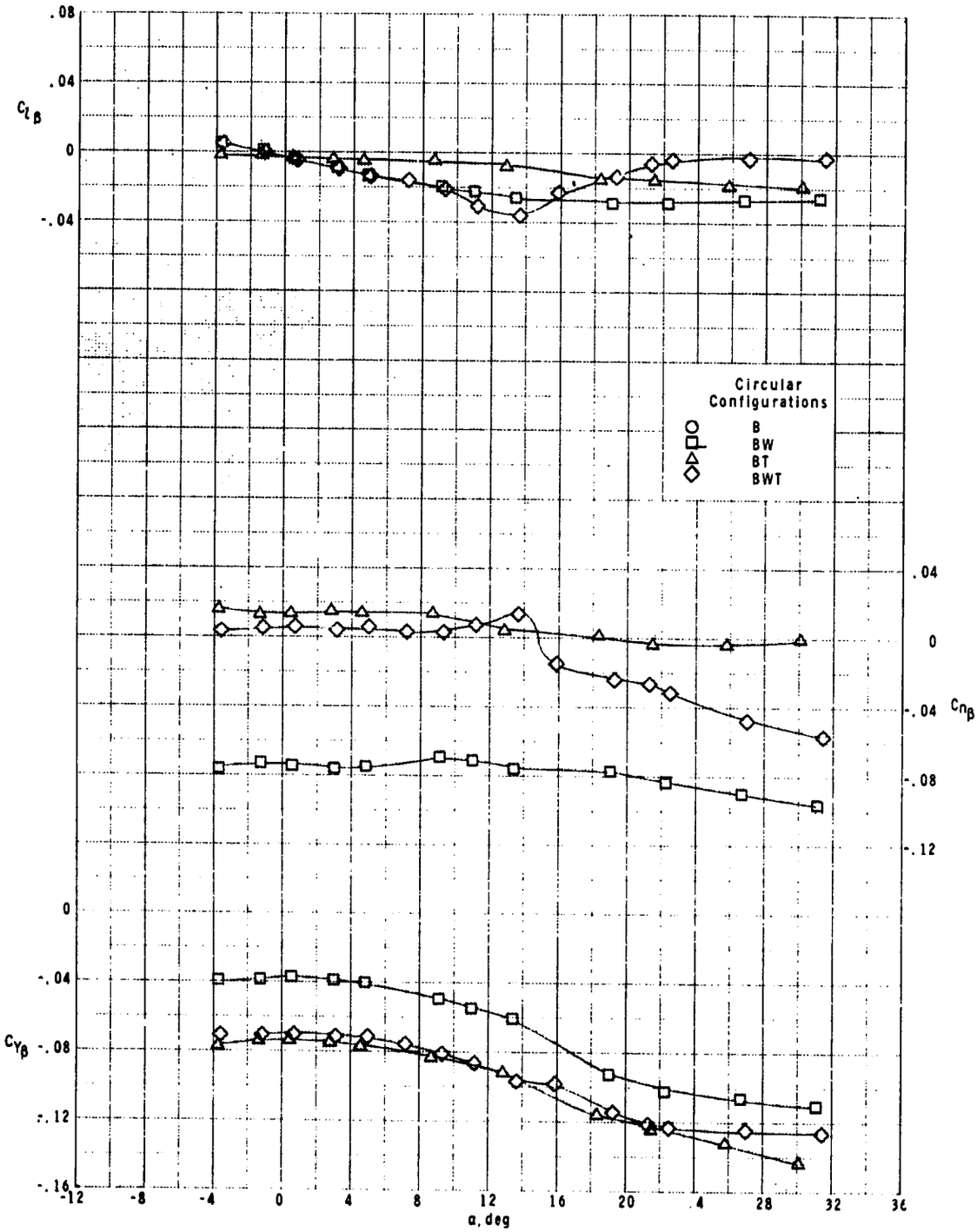

(f) M = 2.00.

Figure 9.- Continued.

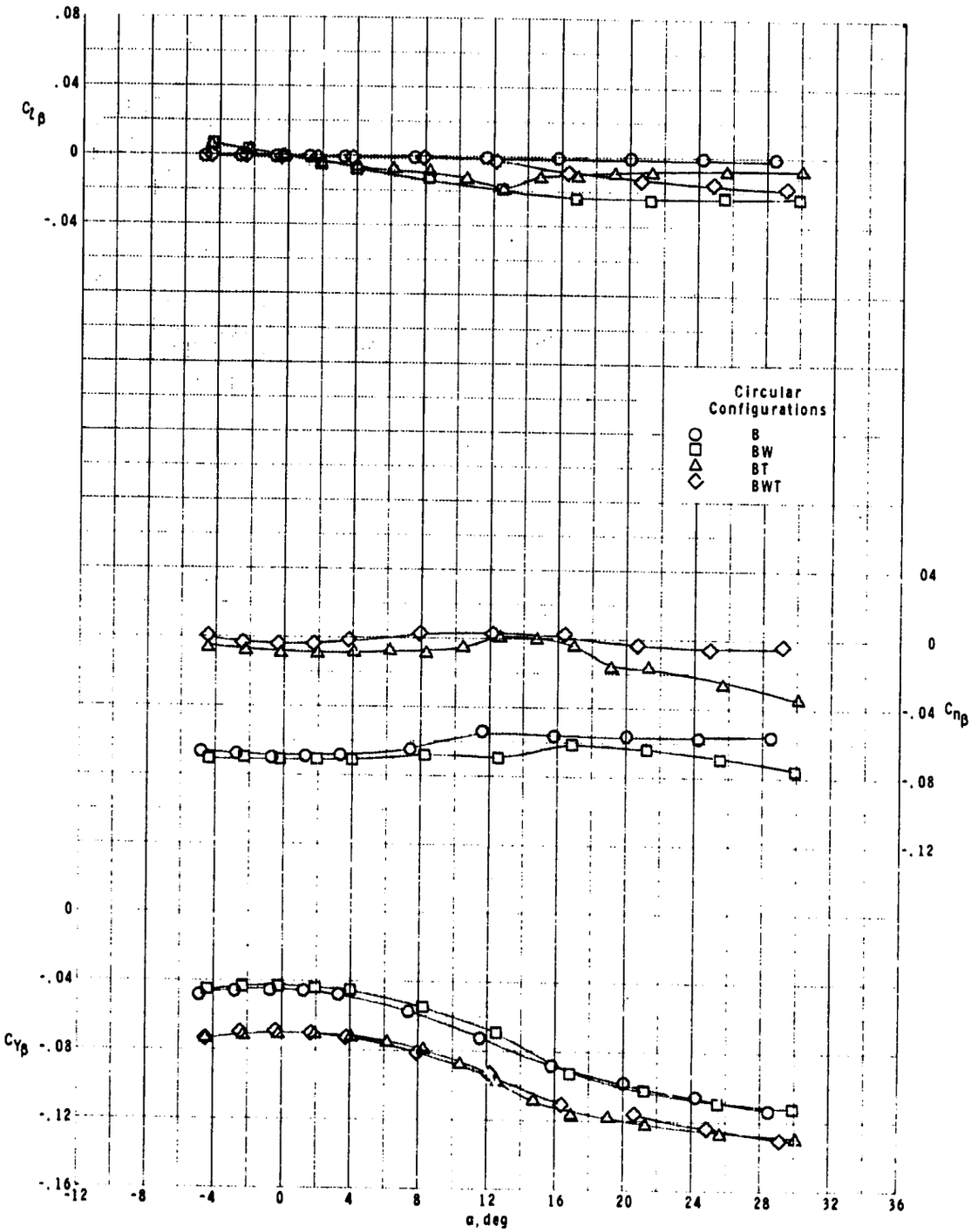

(g) M = 2.50.

Figure 9.- Continued.

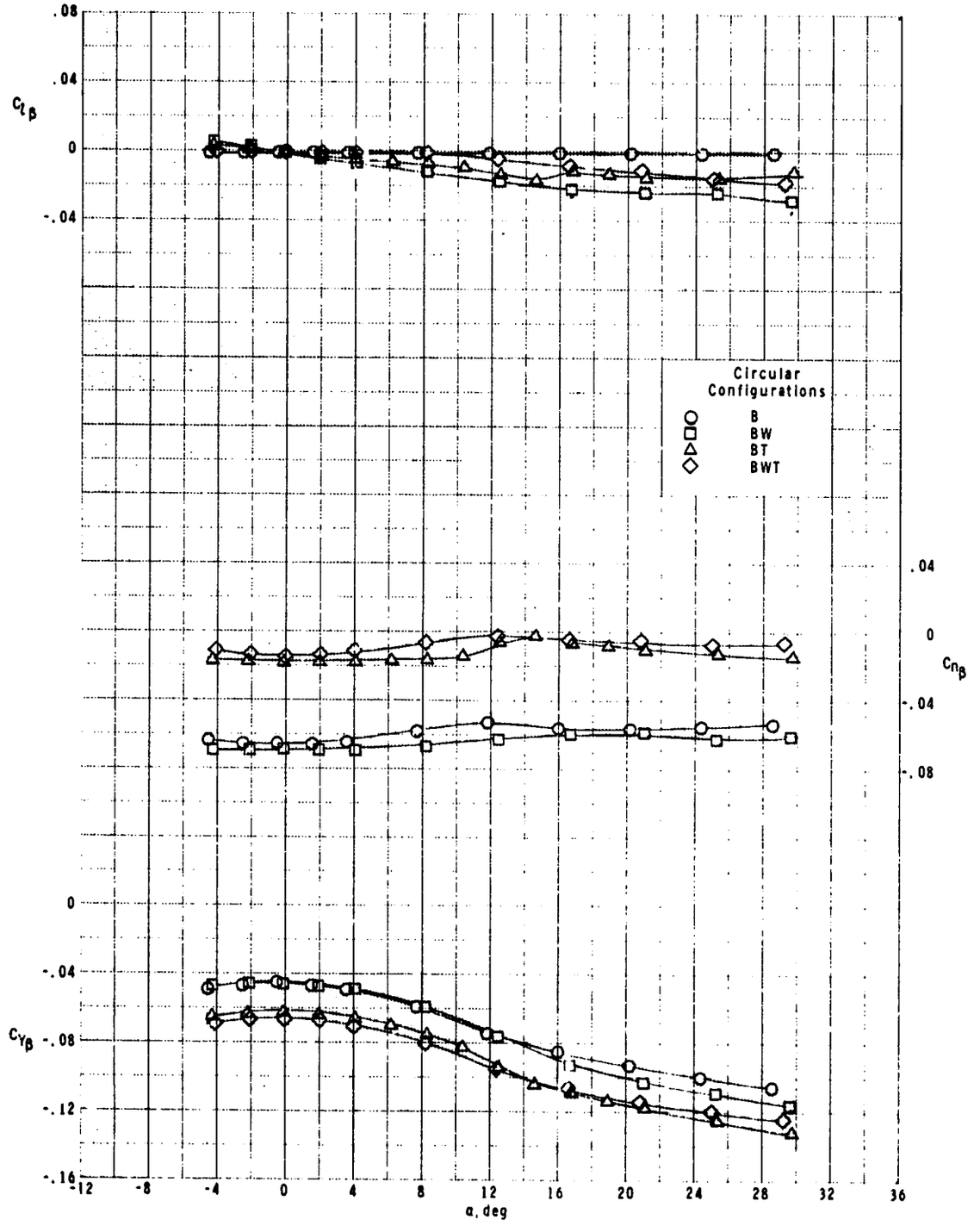

(h) M = 2.96.

Figure 9.- Continued.

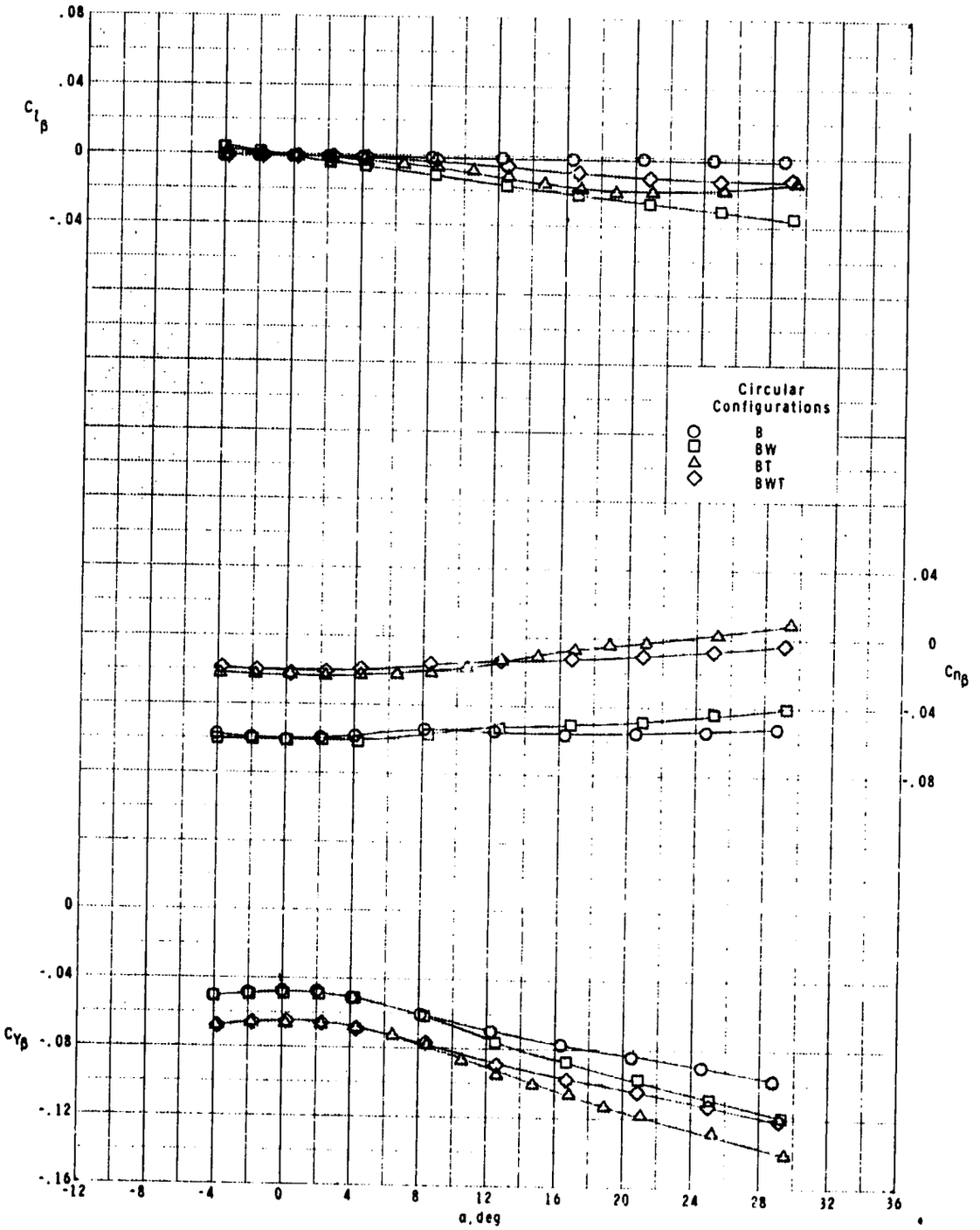

(i) M = 3.95.

Figure 9.- Continued.

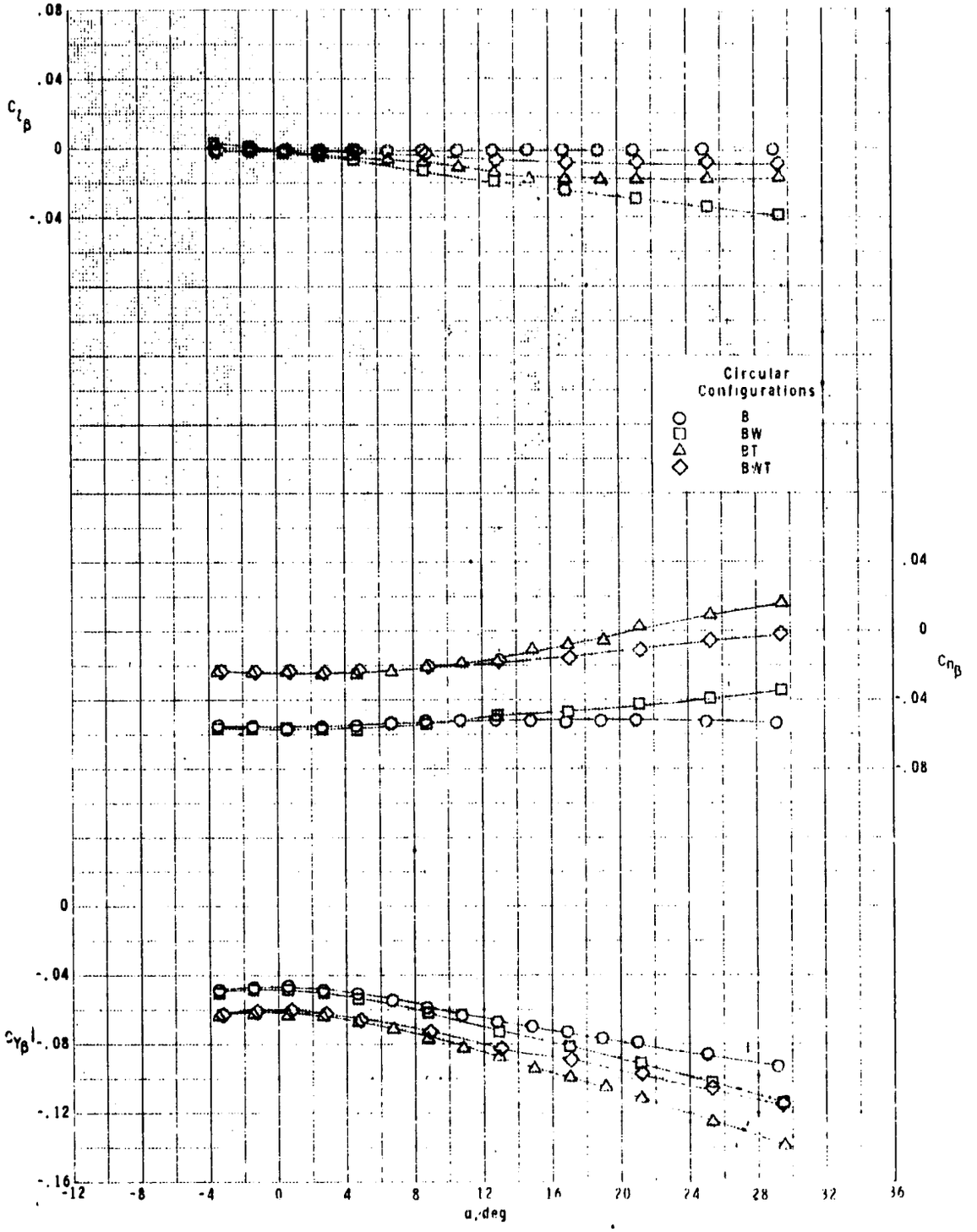

(j) M = 4.63.

Figure 9.- Concluded.

ORIGINAL PAGE IS
OF POOR QUALITY

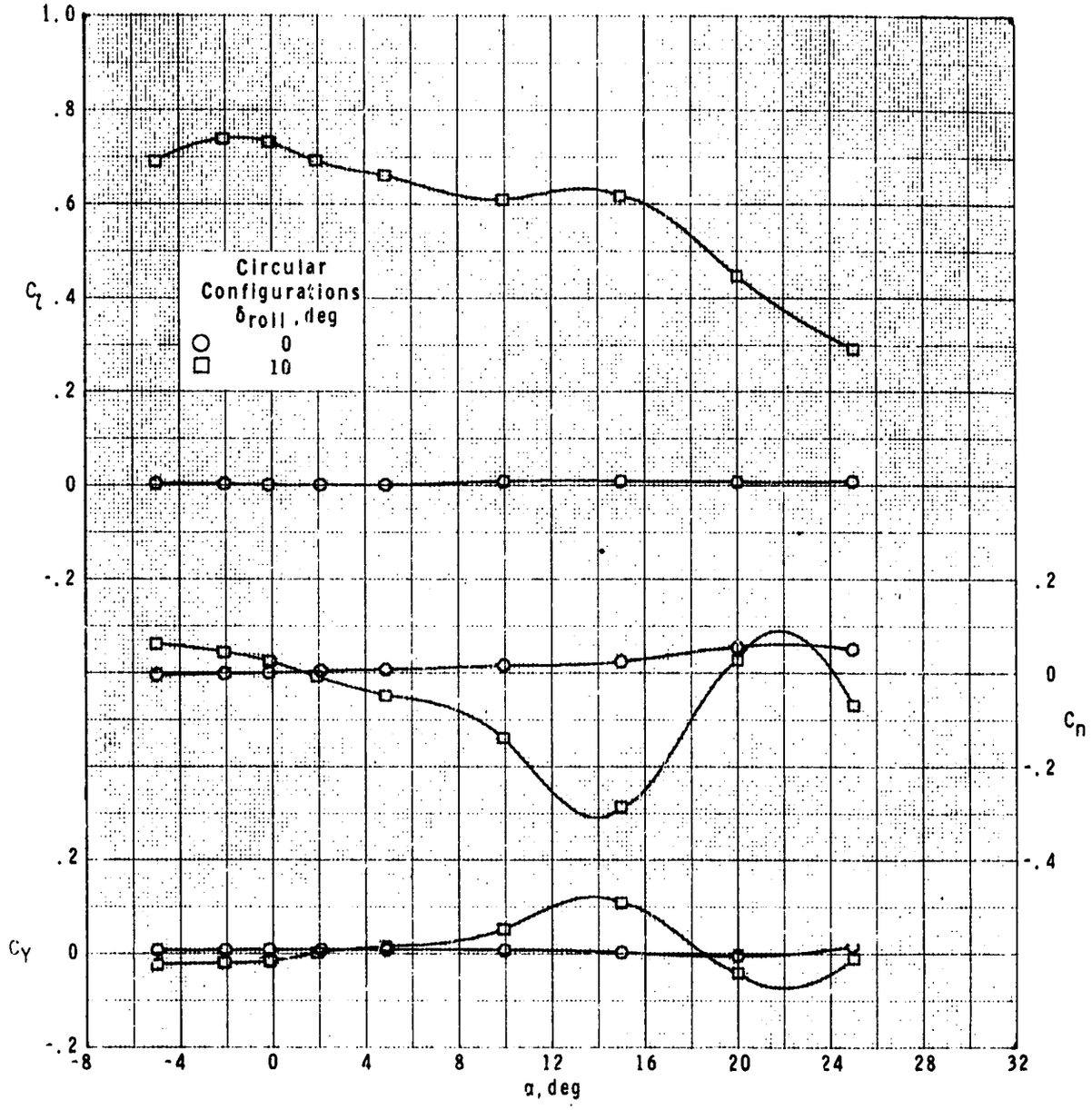

(a) M = 0.5.

Figure 10.- Roll-control effectiveness of circular cross-section body-wing-tail configuration with variation in angle of attack.

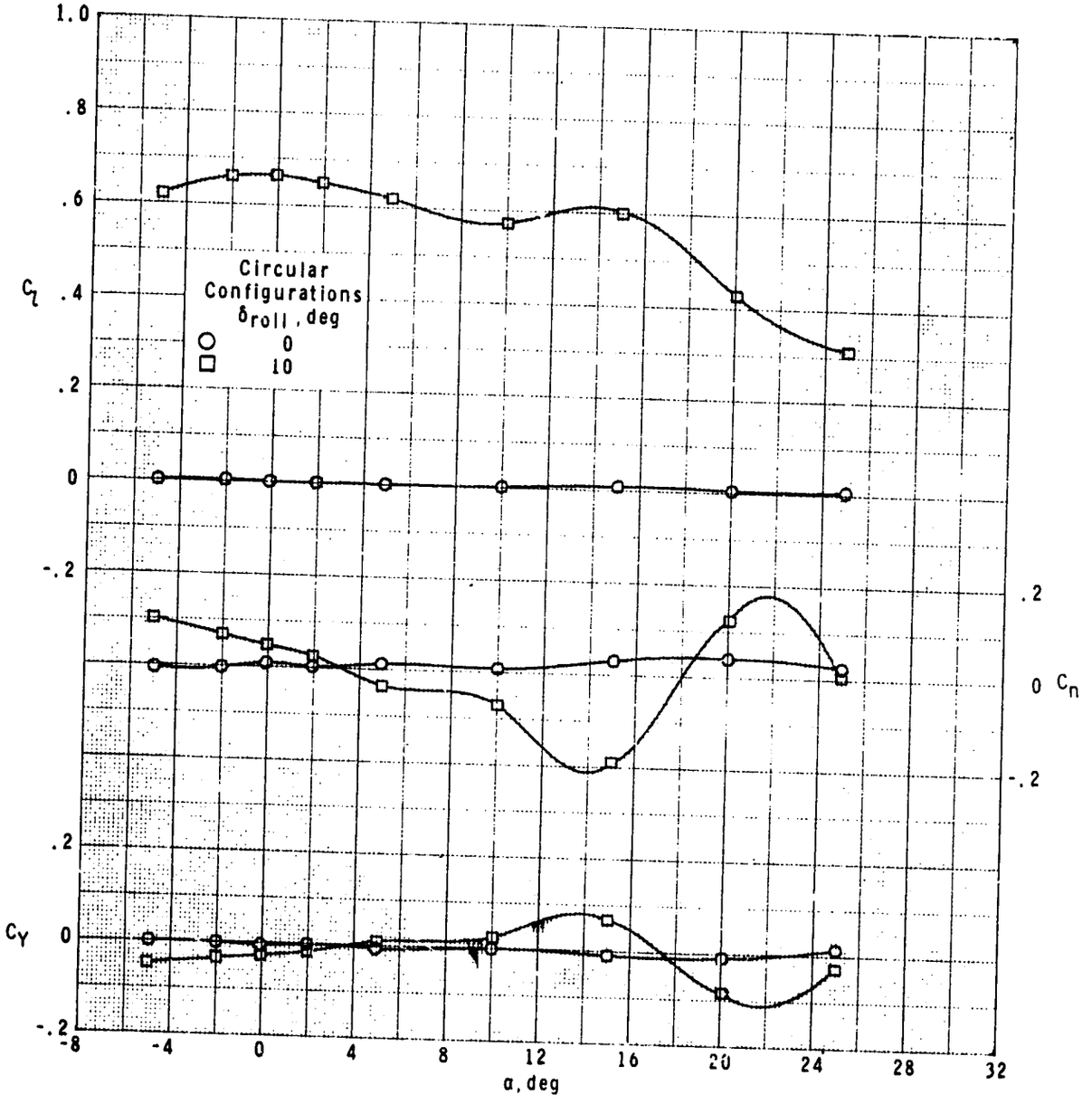

(b) M = 0.7.

Figure 10.- Continued.

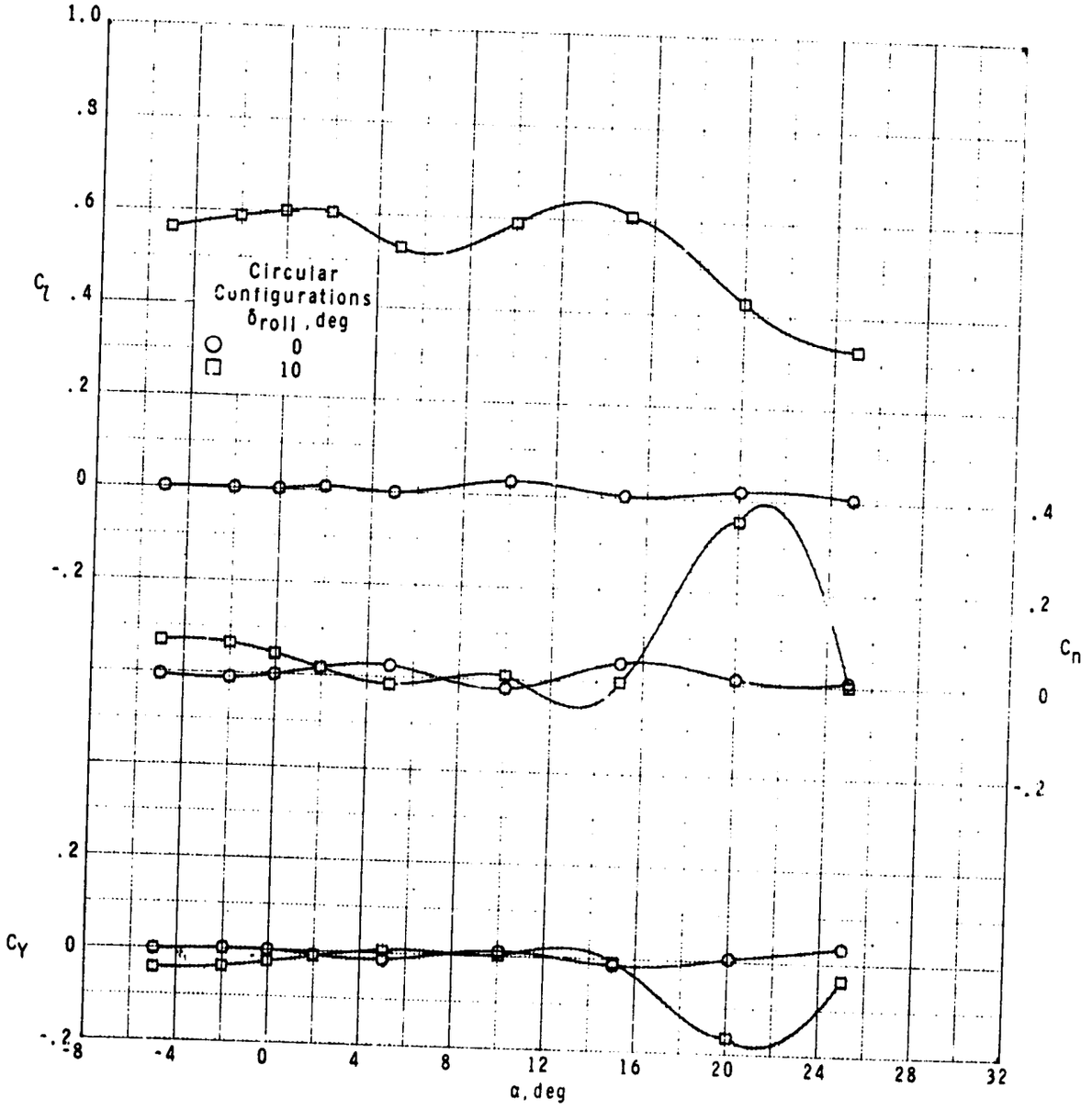

(c) M = 0.9.

Figure 10.- Continued.

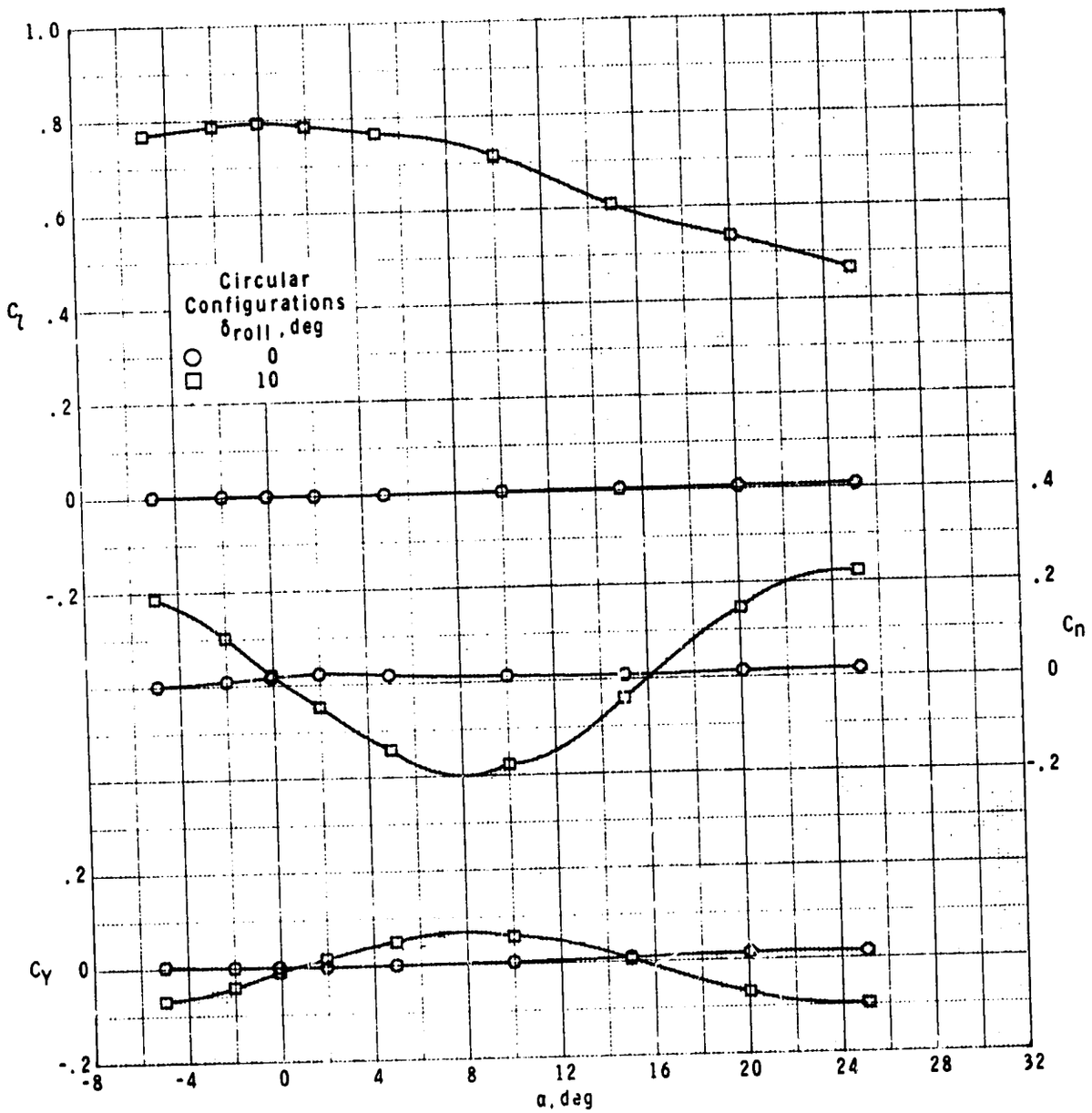

(d) M = 1.3.

Figure 10.- Continued.

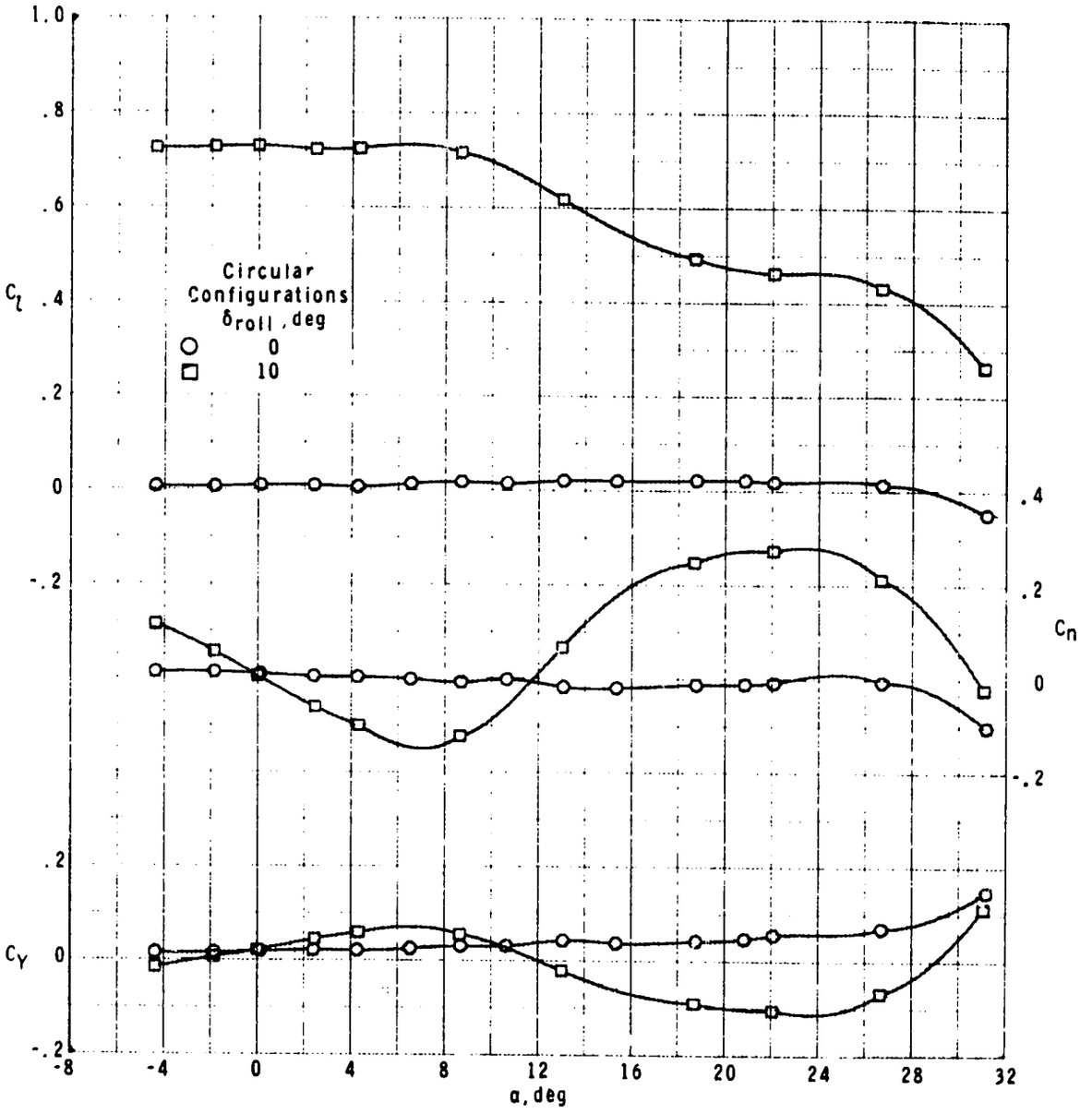

(e) M = 1.60.

Figure 10.- Continued.

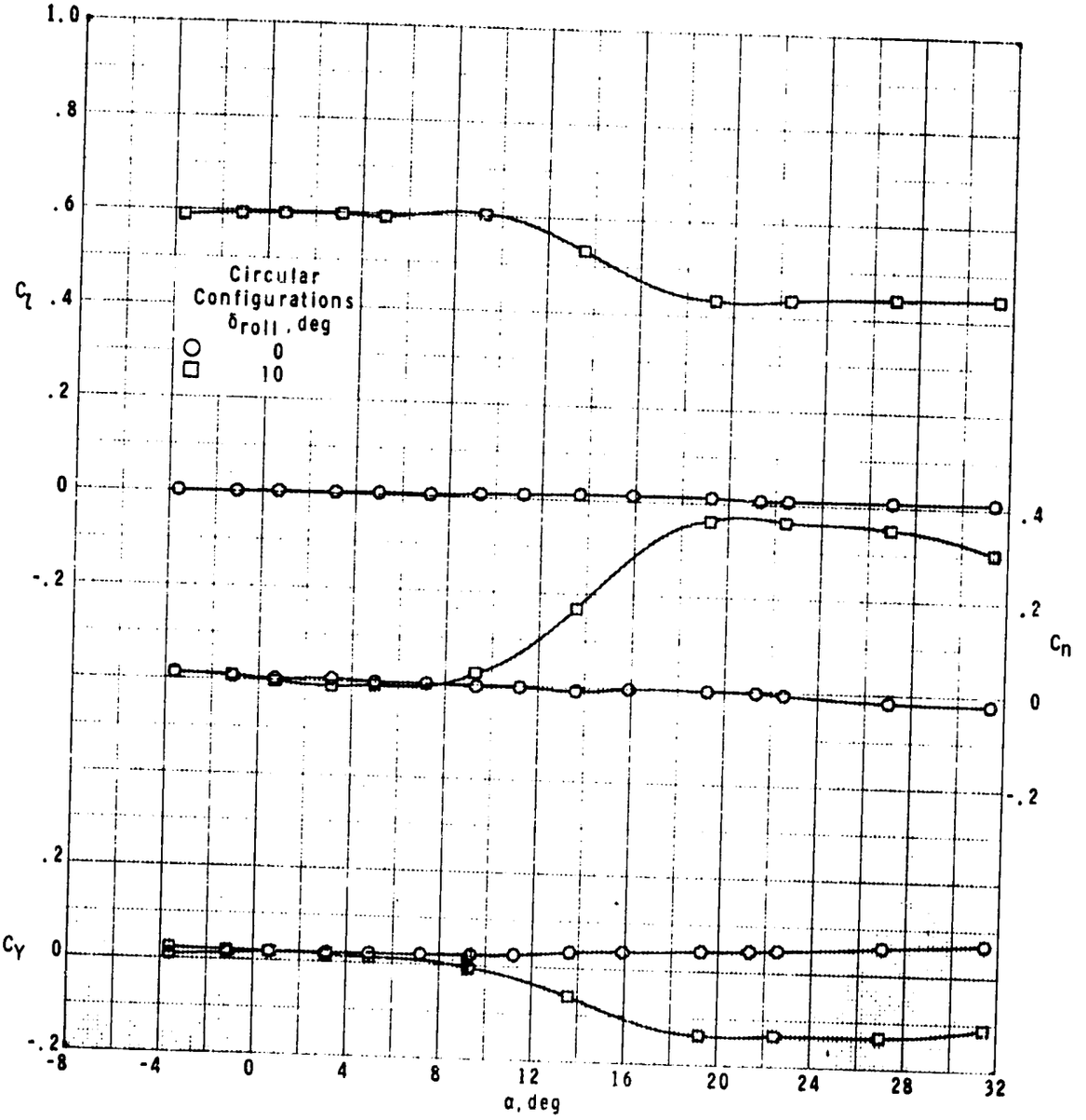

(f) M = 2.00.

Figure 10.- Continued.

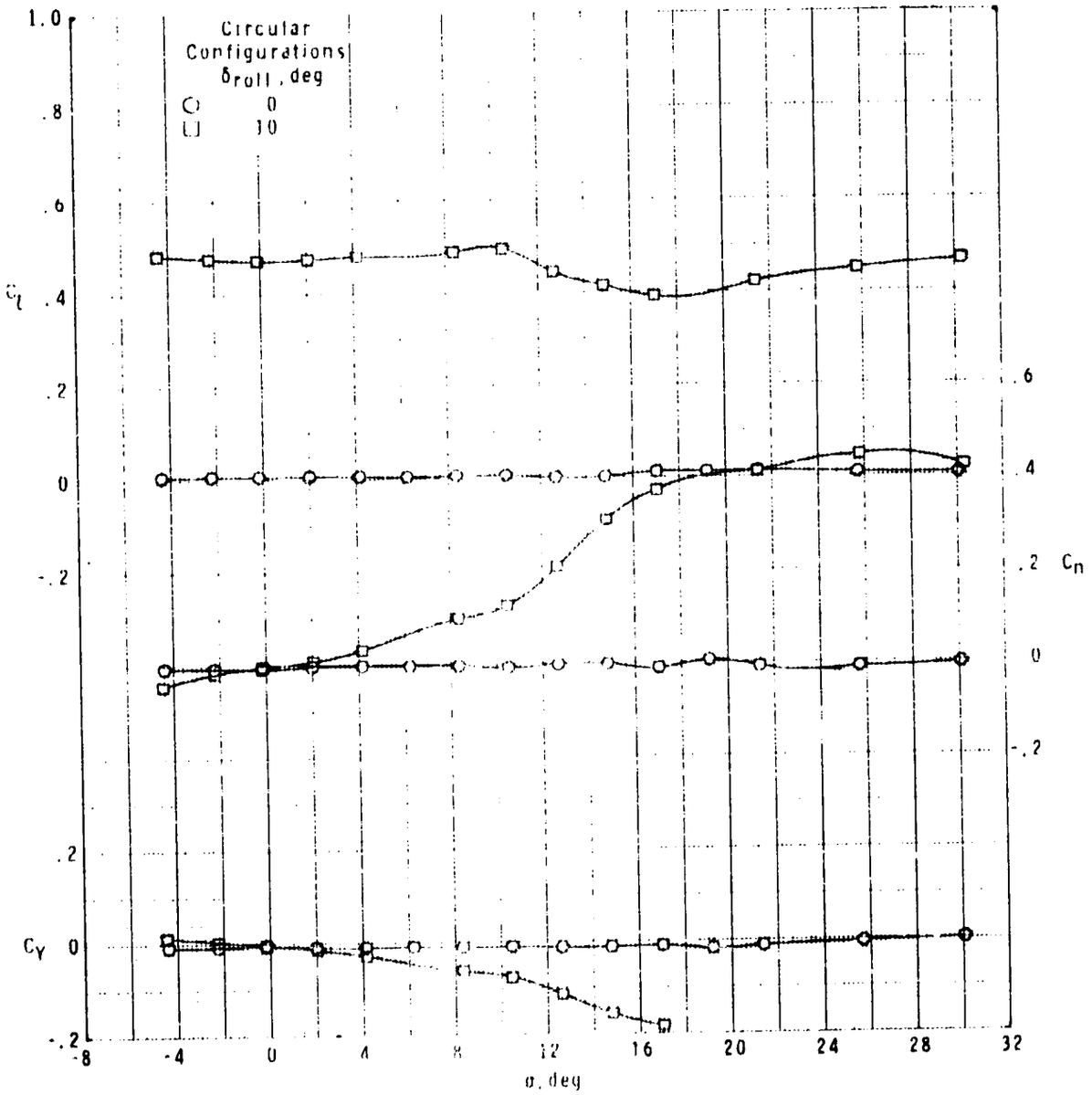
Circular
Configurations
δroll, deg
○ 0
□ 10
1.0
.8
.6
.4
.2
0
-.2
Cl
.2
0
-.2
CY
.6
.4
.2
0
-.2
Cn
-8
-4
0
4
8
12
16
20
24
28
32
α, deg

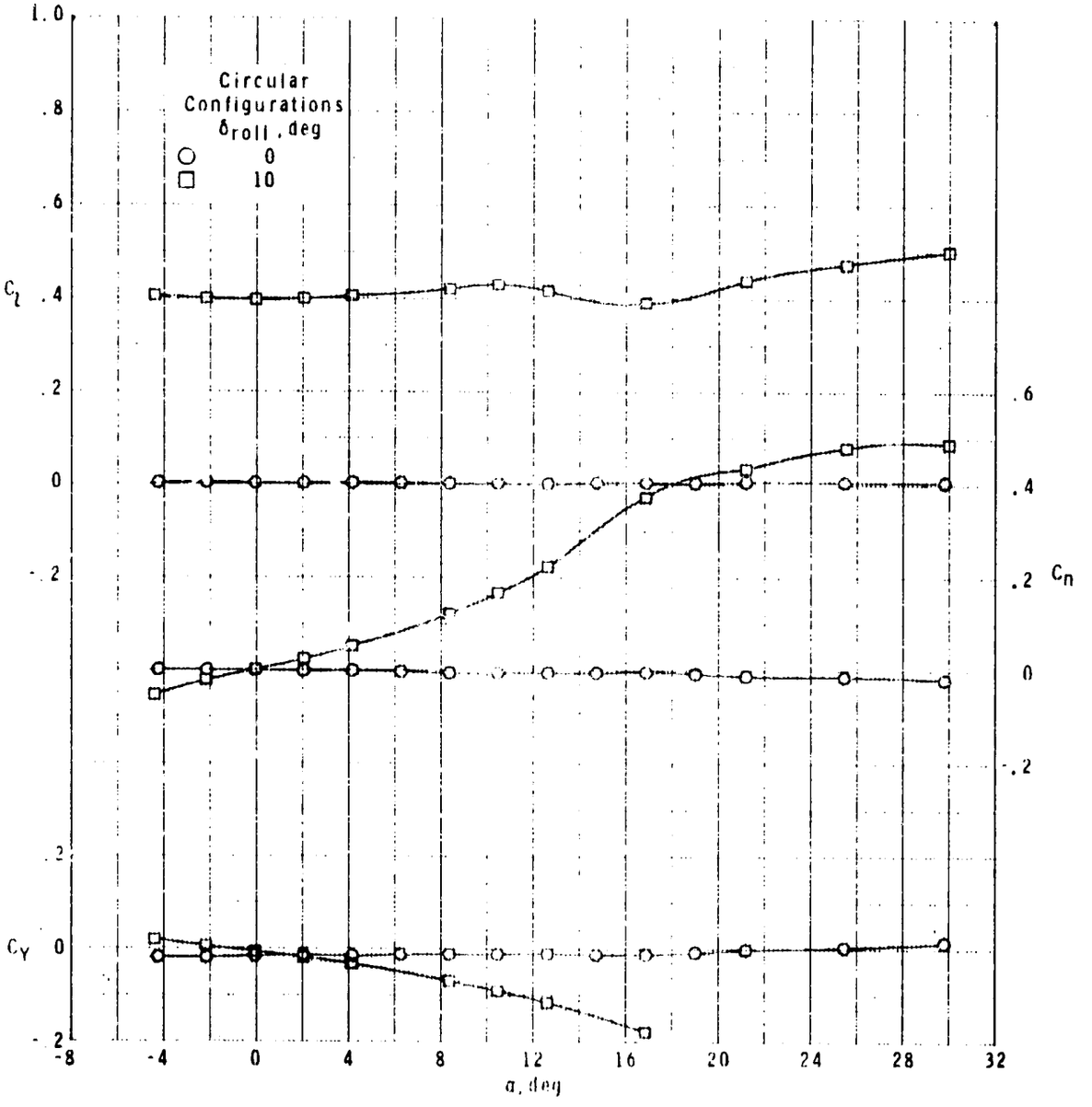

(b) [illegible]

Figure 10.- [illegible]

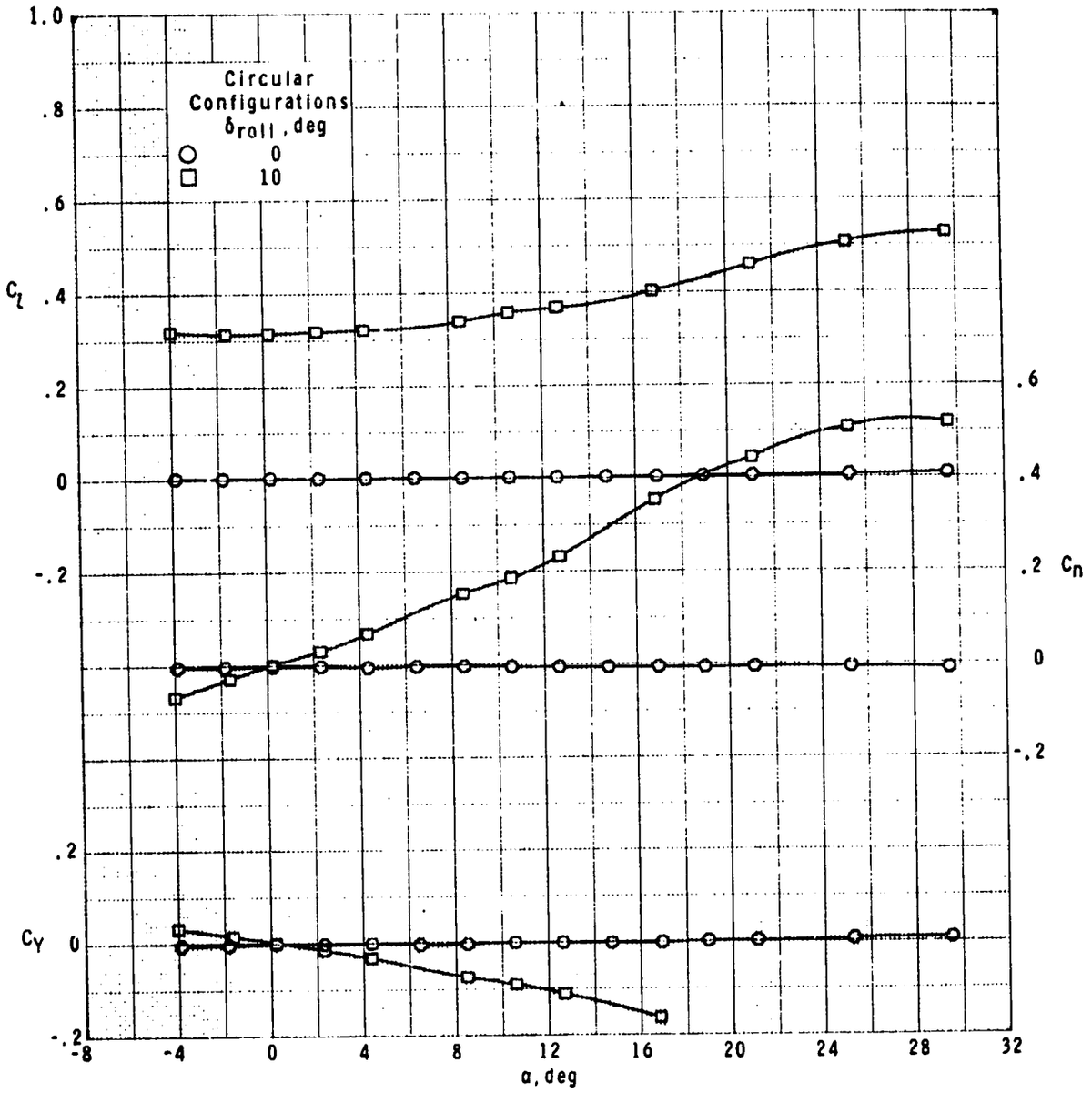

(i) M = 3.95.

Figure 10.- Continued.

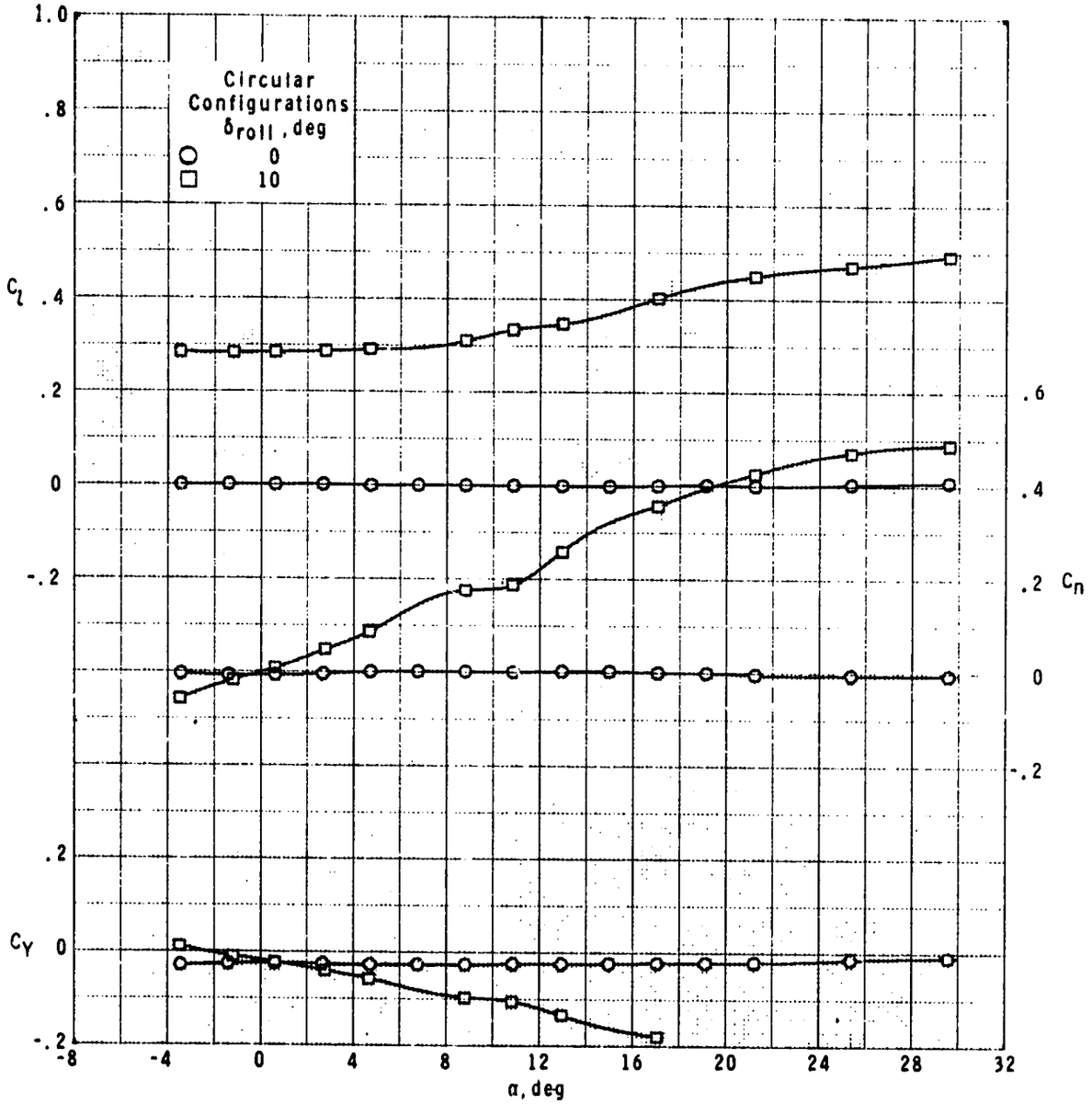

(j) $M = 4.63$.

Figure 10.- Concluded.

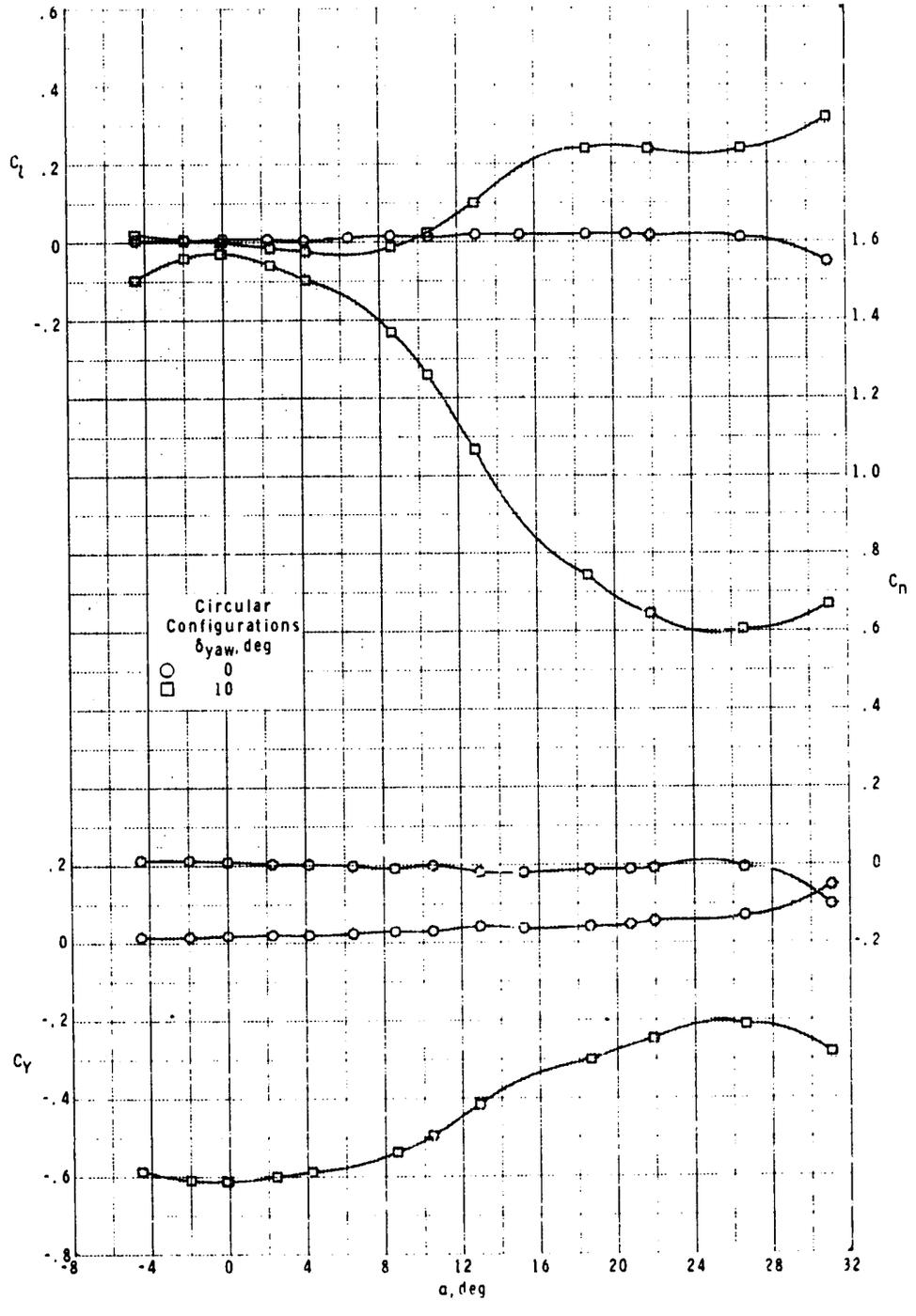

(a) $\Gamma = 1.6°$.

Figure 11.- Yaw-control effectiveness of circular cross-sectional ty-wing-tail configurations with variation in angle of attack.

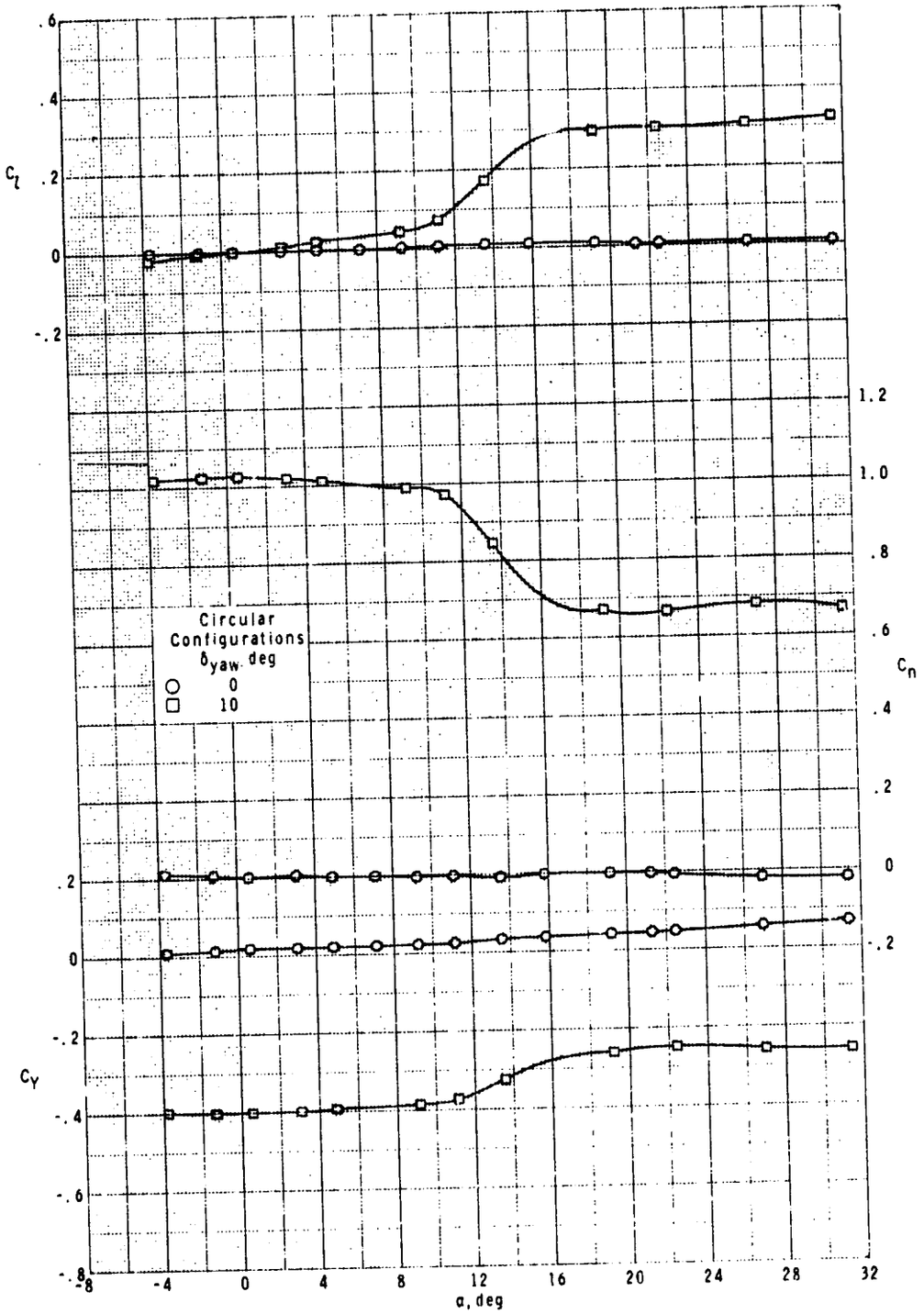

(b) M = 2.00.

Figure 11.- Continued.

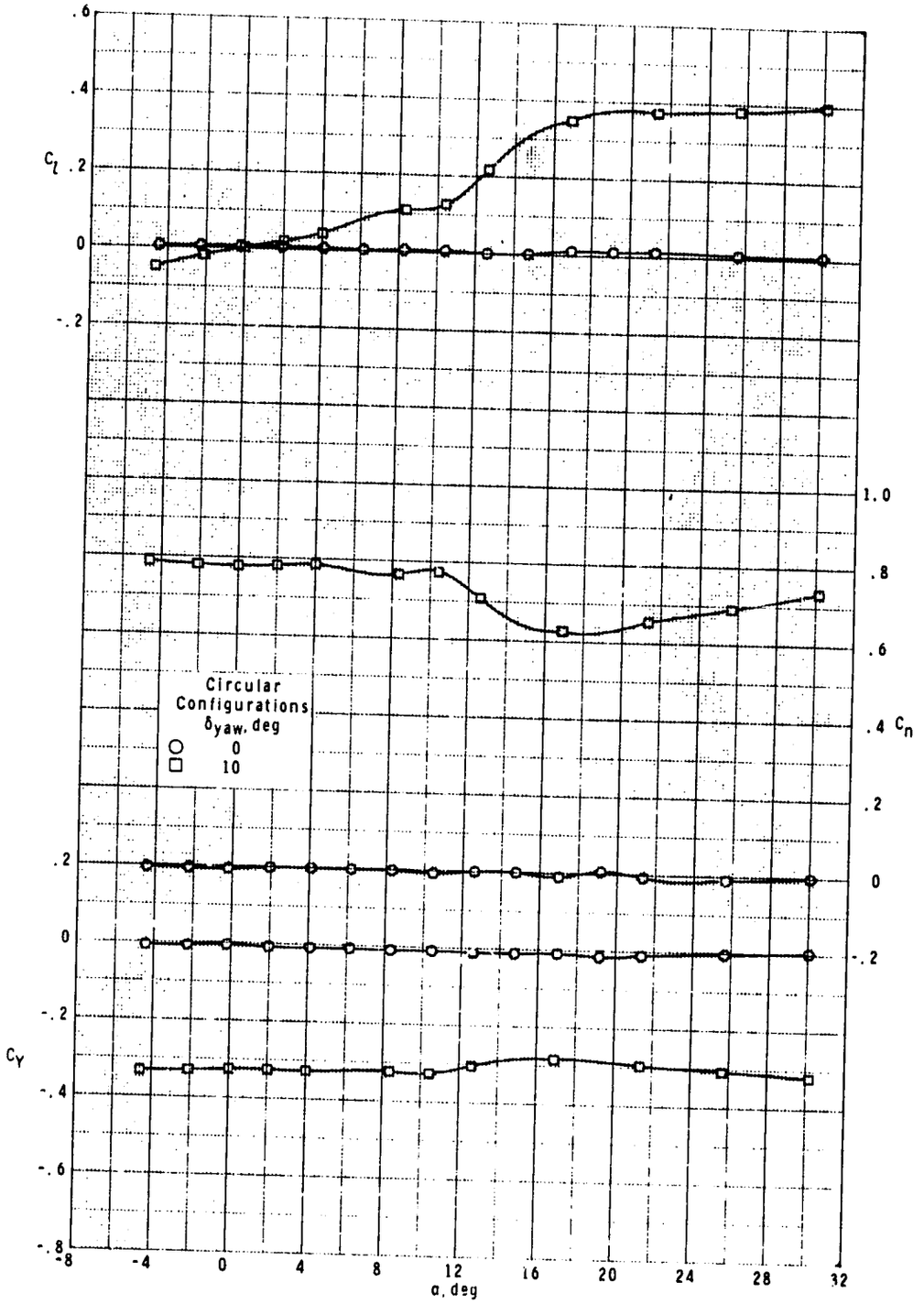

(c) M = 2.50.

Figure 11.- Continued.

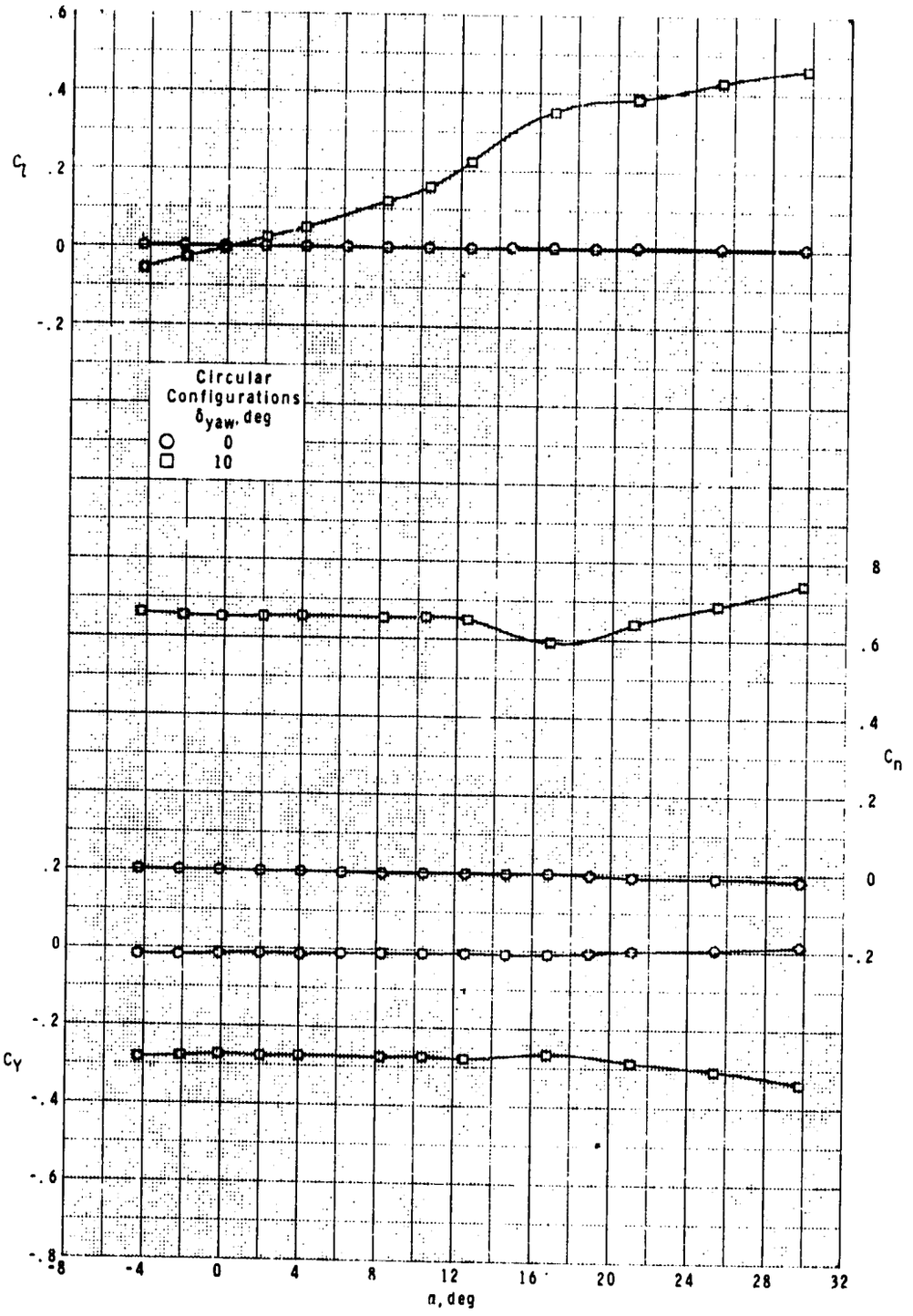

(d) M = 2.96.

Figure 11.- Continued.

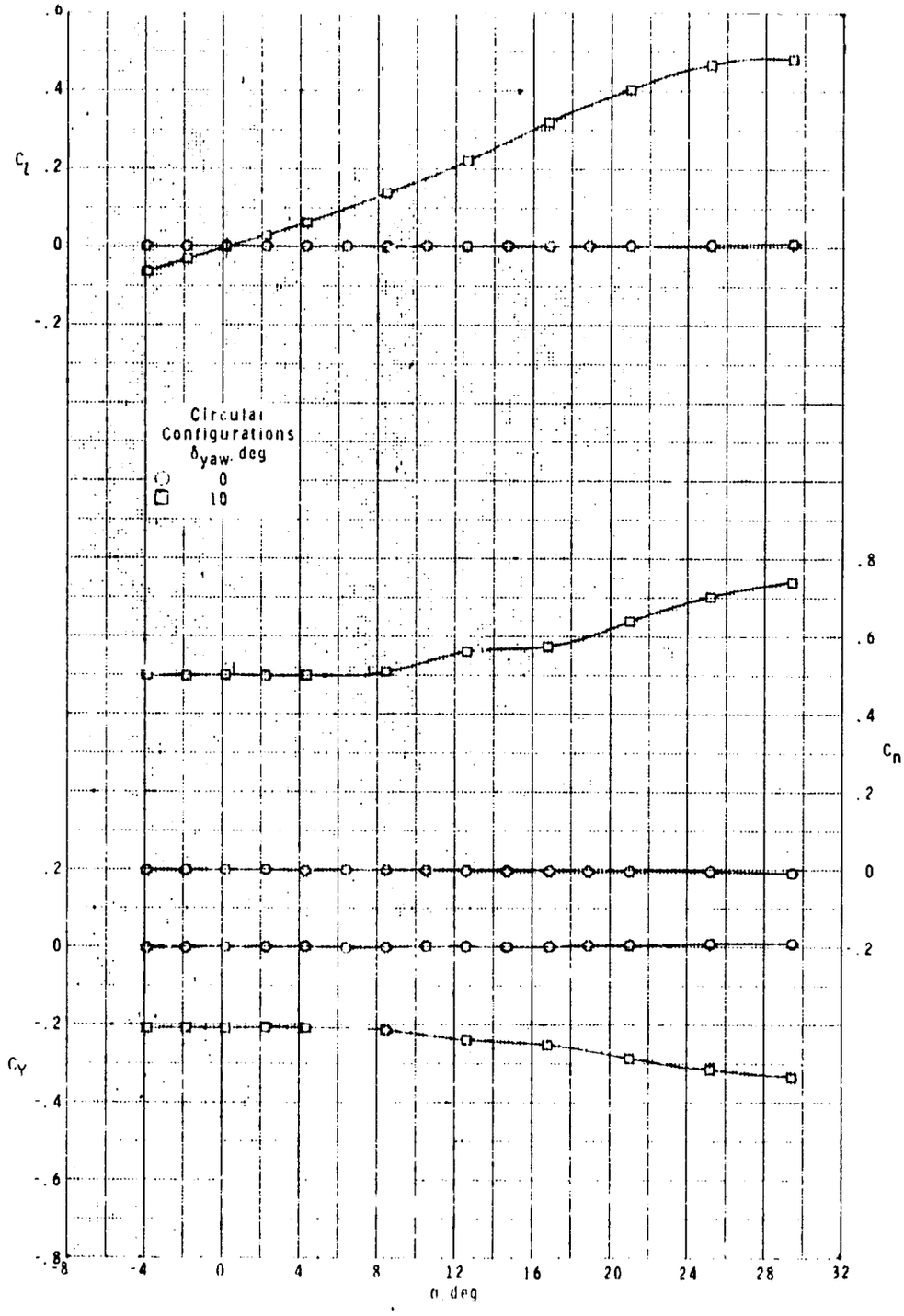

(c) M = 0.95.

Figure 11. - Continued.

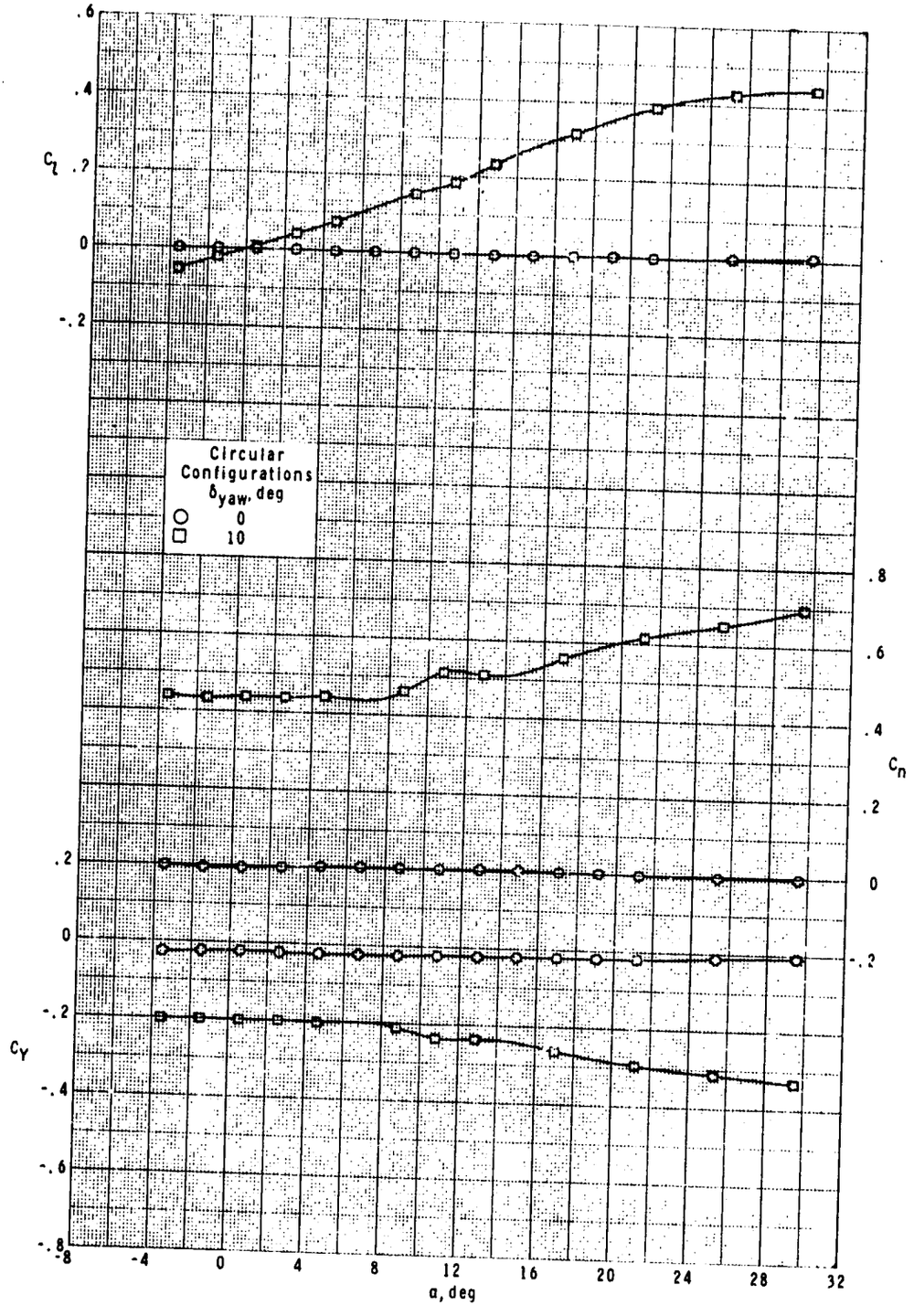

(f) M = 4.63.

Figure 11.- Concluded.

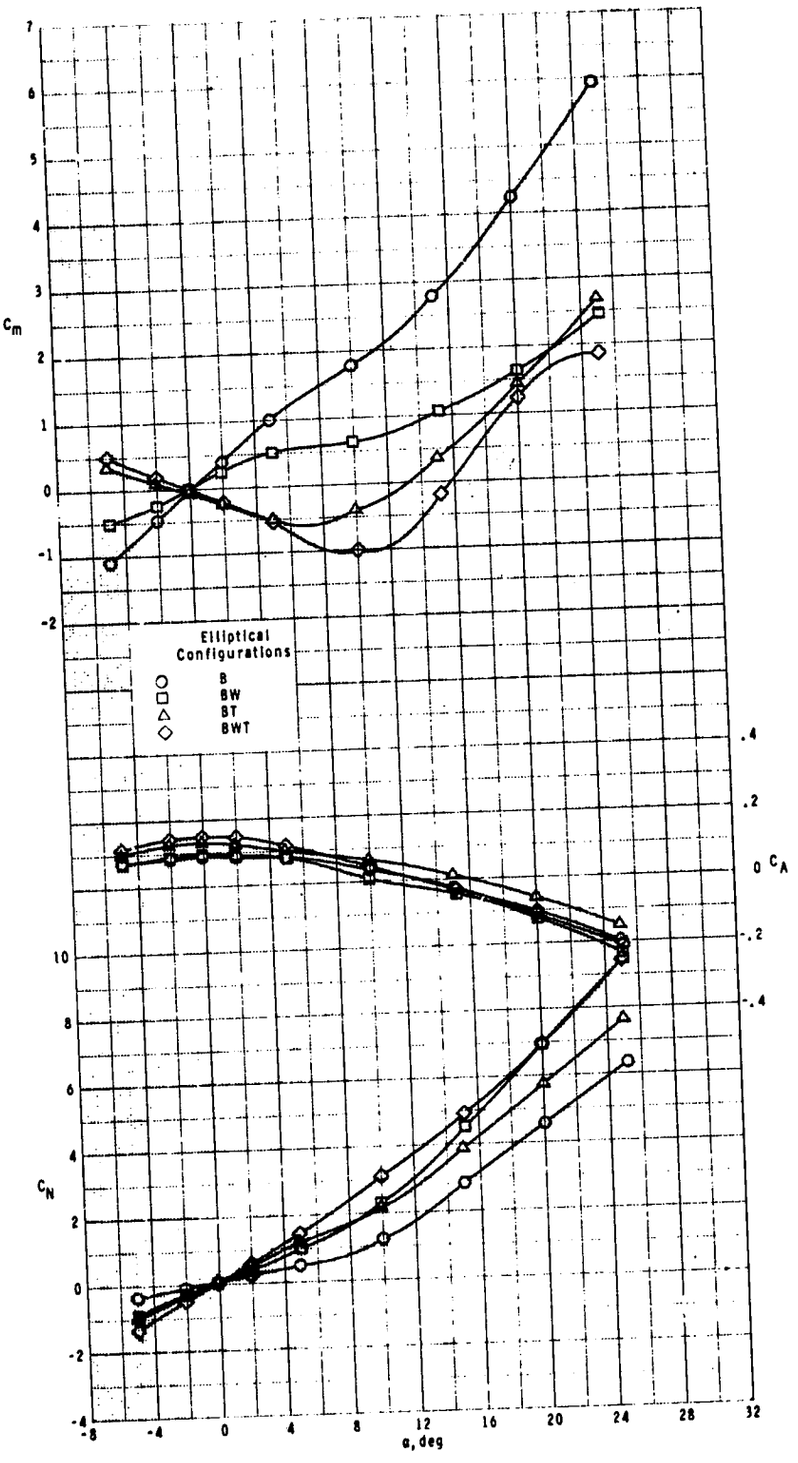

(a) M = 0.5.

Figure 12.- Effect of components on longitudinal aerodynamic characteristics of elliptical cross-section model with variation in angle of attack.

C.2

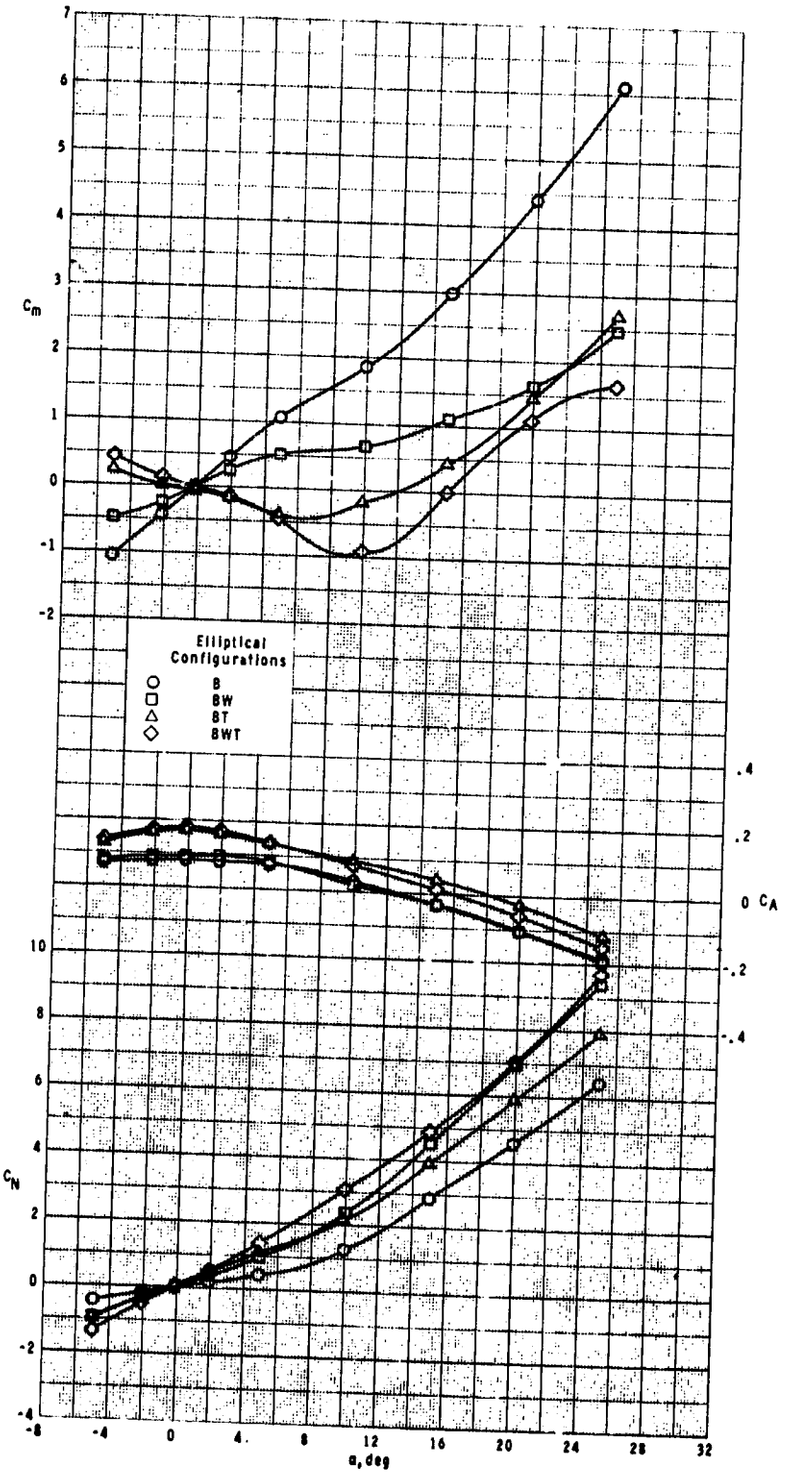

(b) M = 0.7.

Figure 12.- Continued.

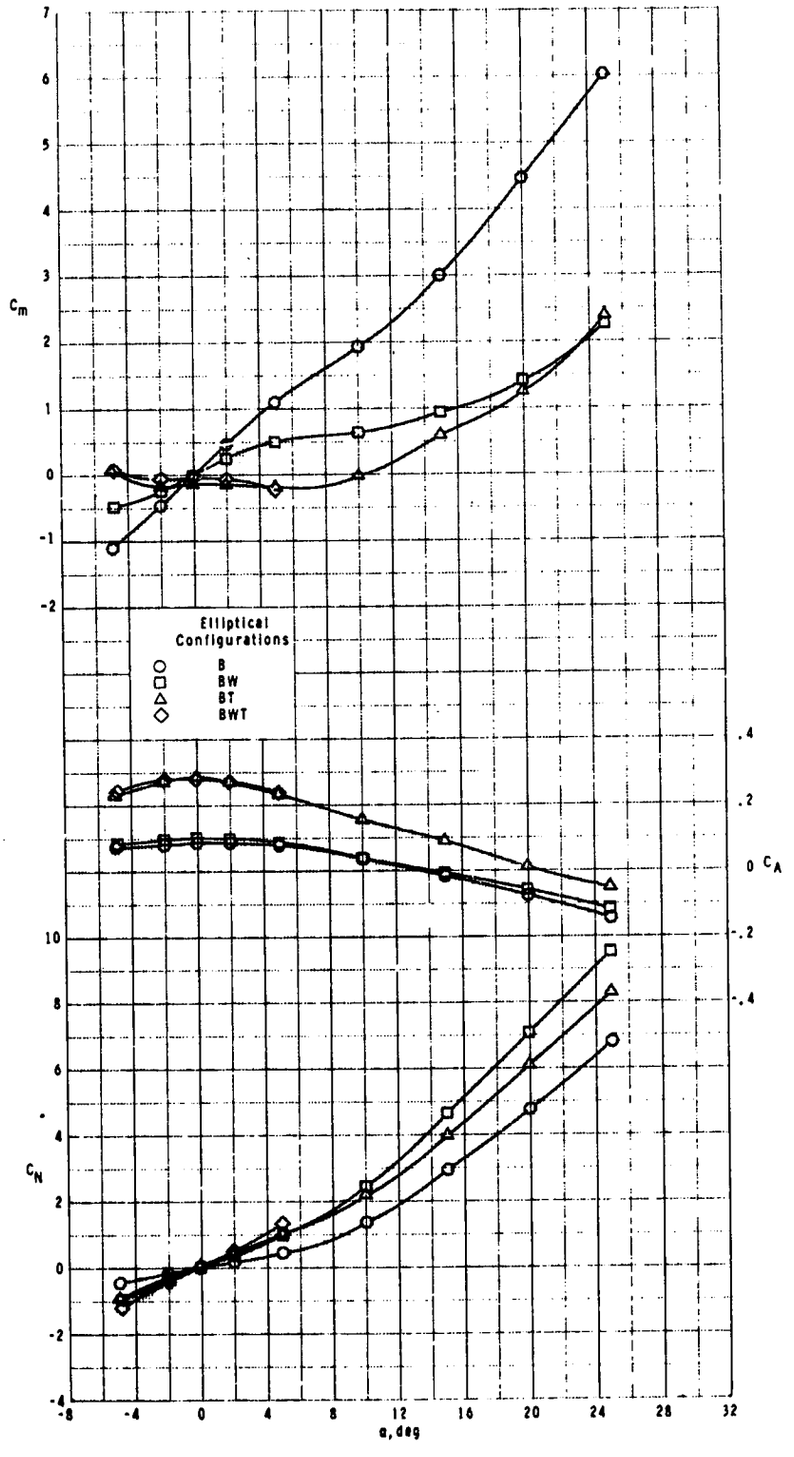

(c) M = 0.9.

Figure 12.- Continued.

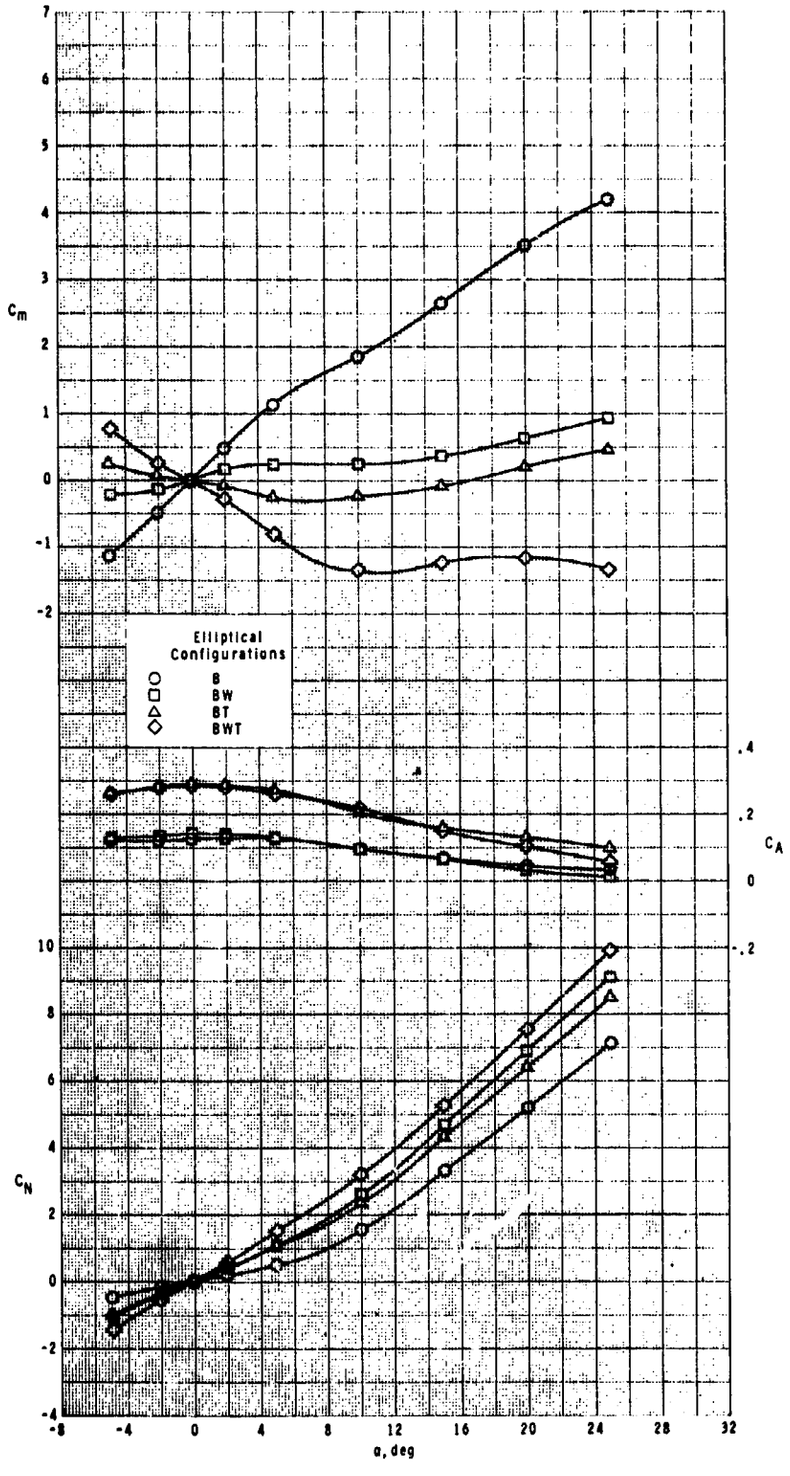

(d) M = 1.3.

Figure 12.- Continued.

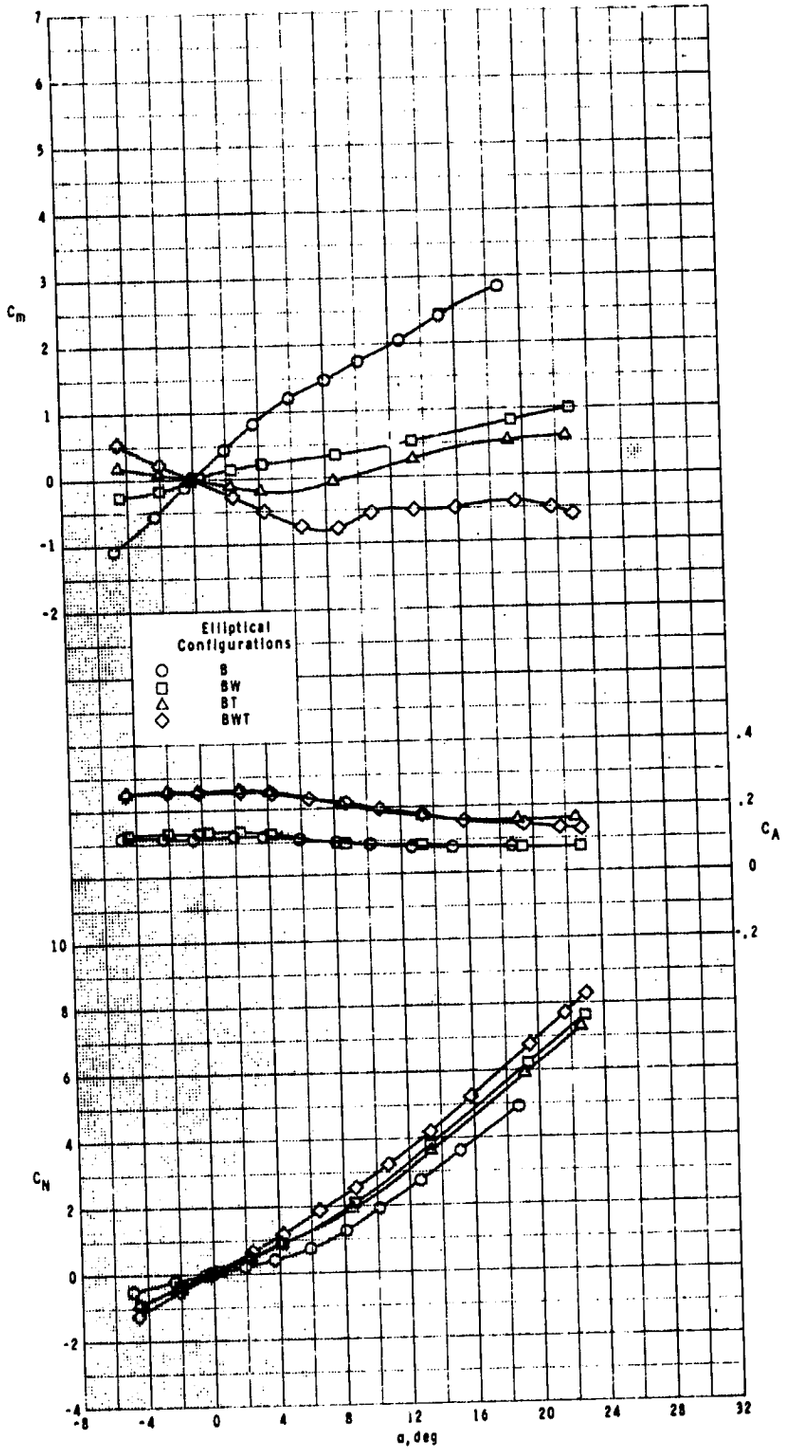

(e) M = 1.60.

Figure 12.- Continued.

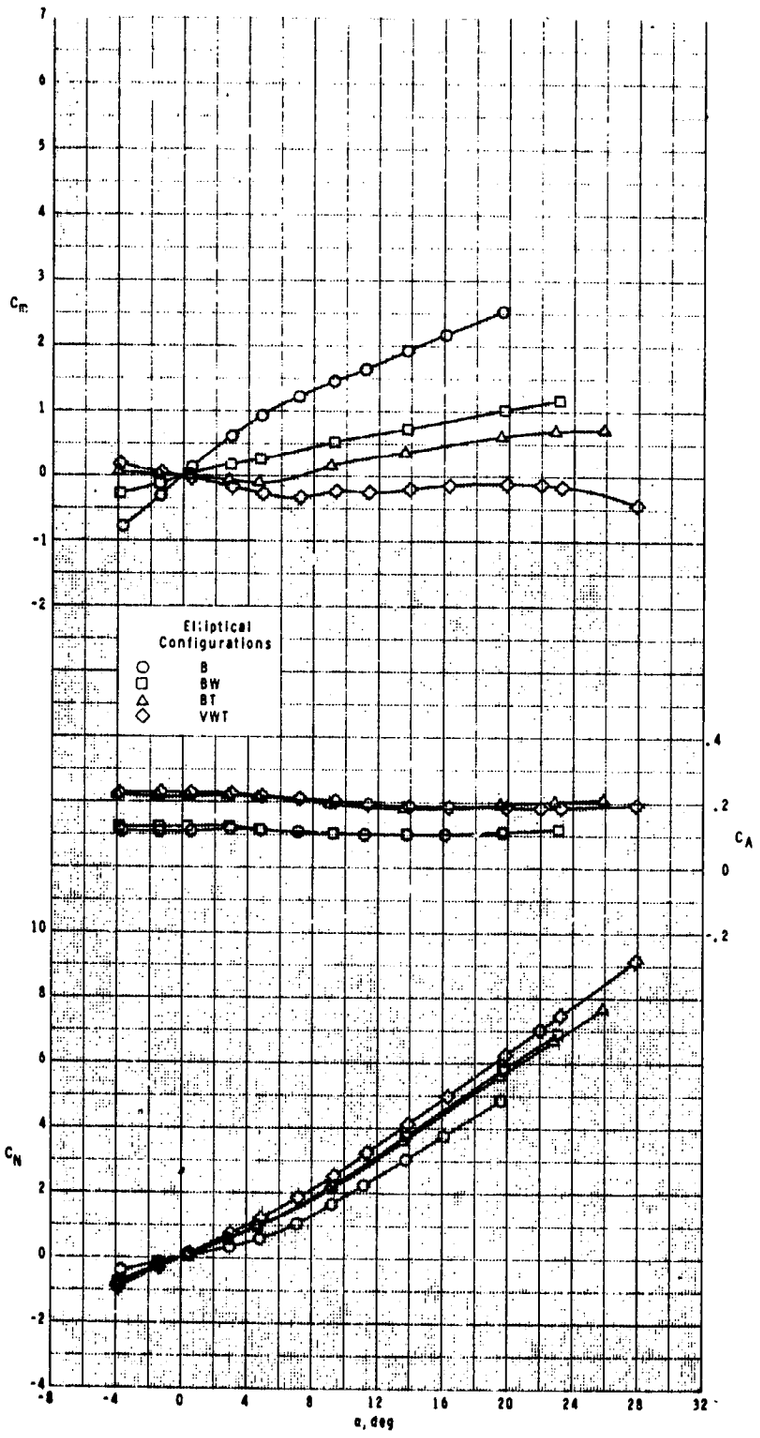

(f) M = 2.00.

Figure 12.- Continued.

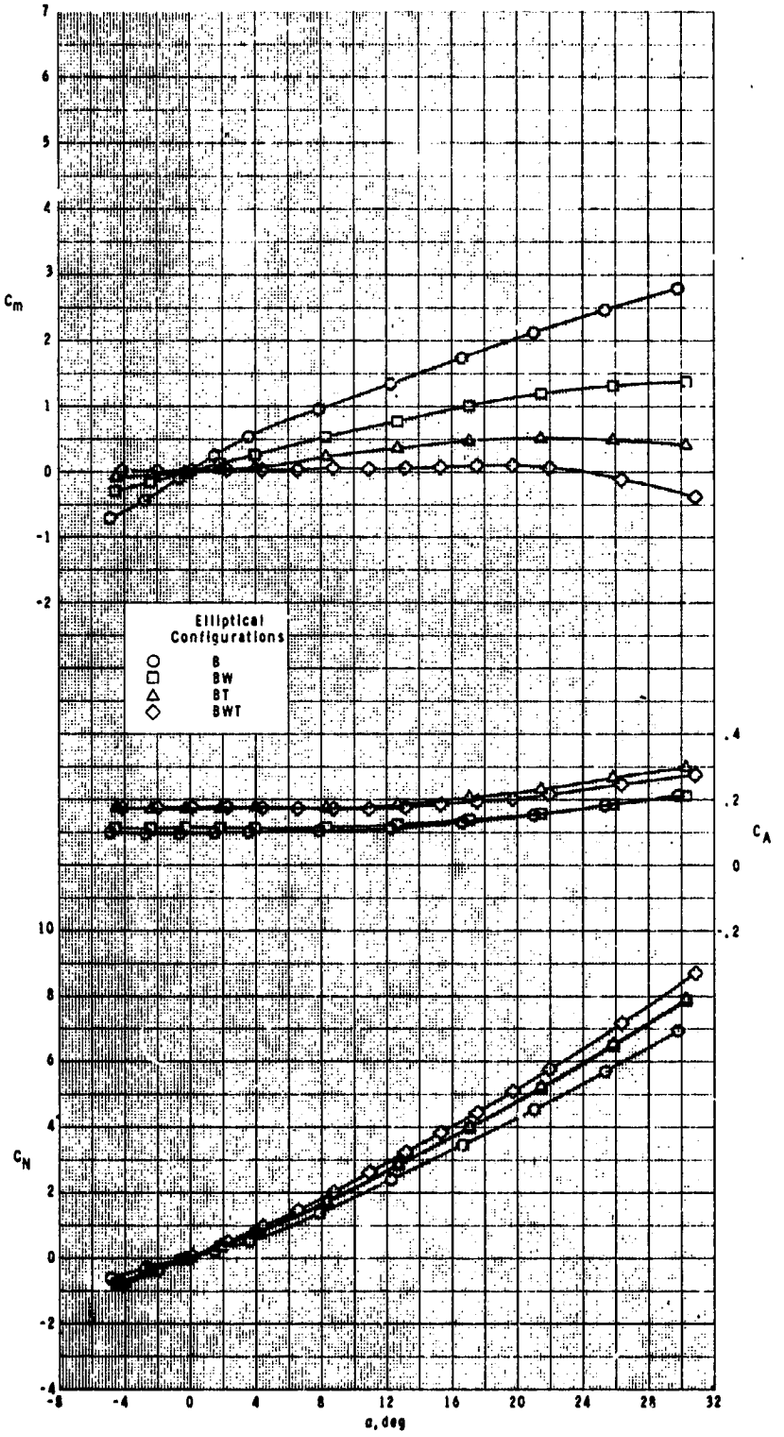

(g) M = 2.96.

Figure 12.- Continued.

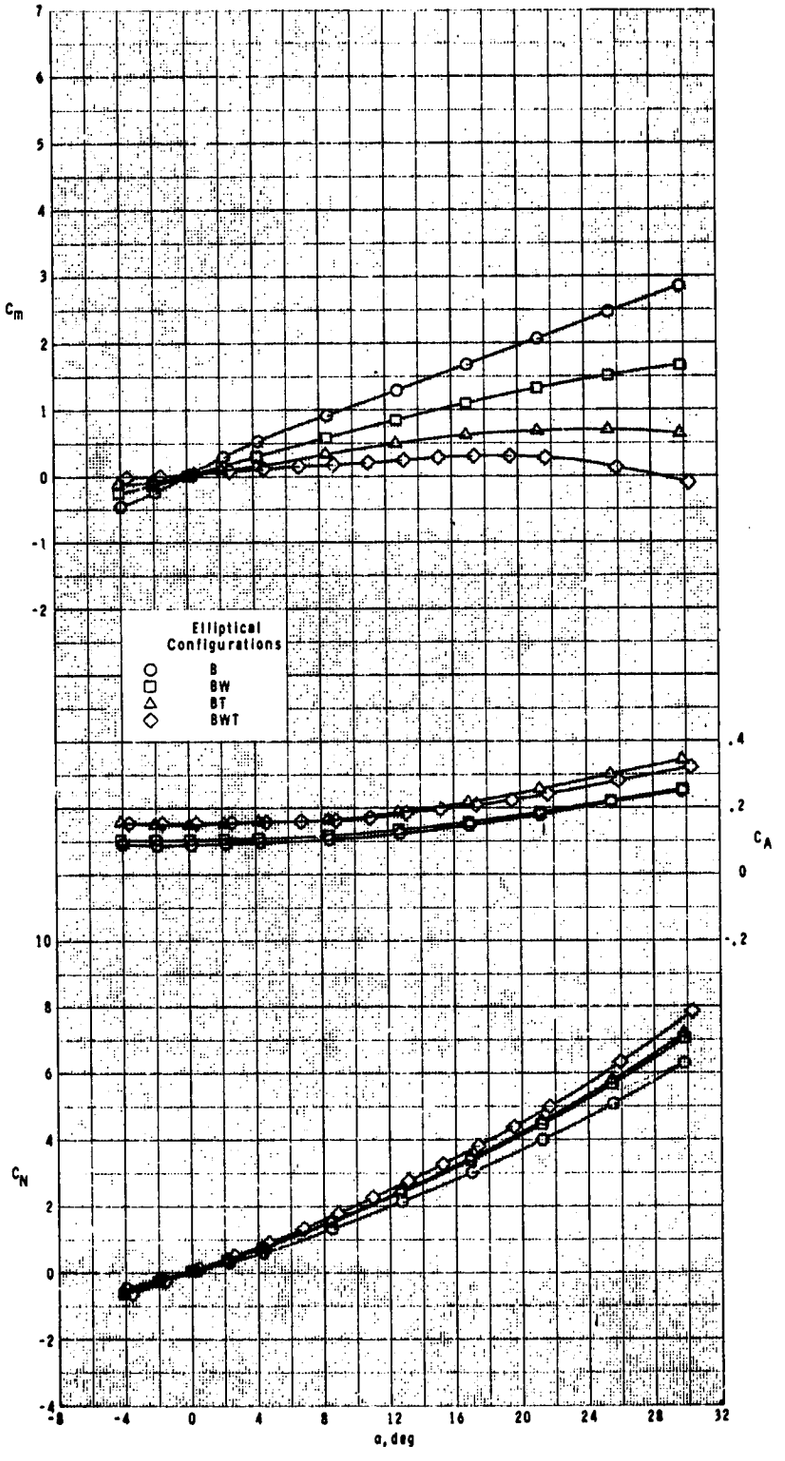

(h) M = 3.95.

Figure 12.- Continued.

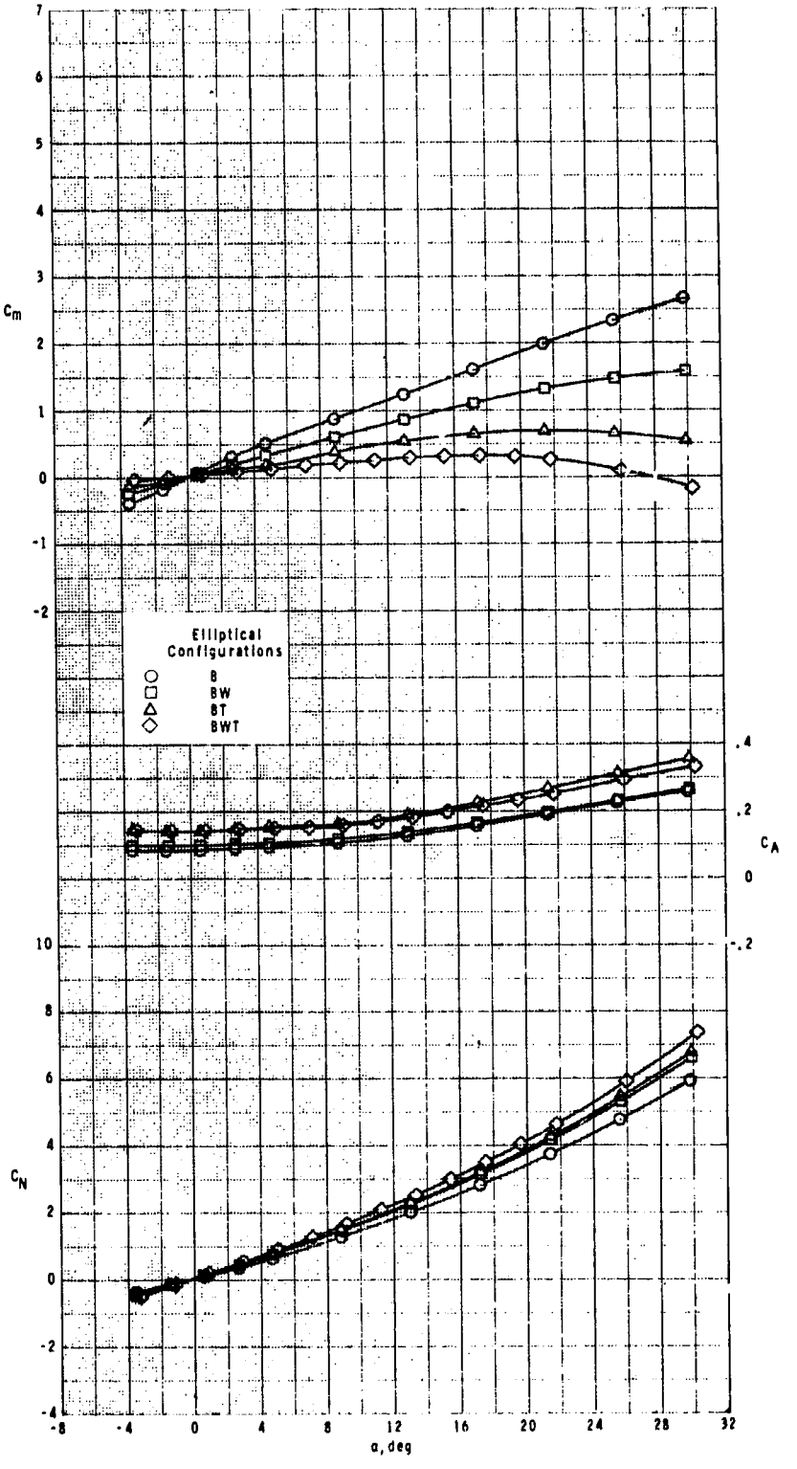

(i) M = 4.63.

Figure 12.- Concluded.

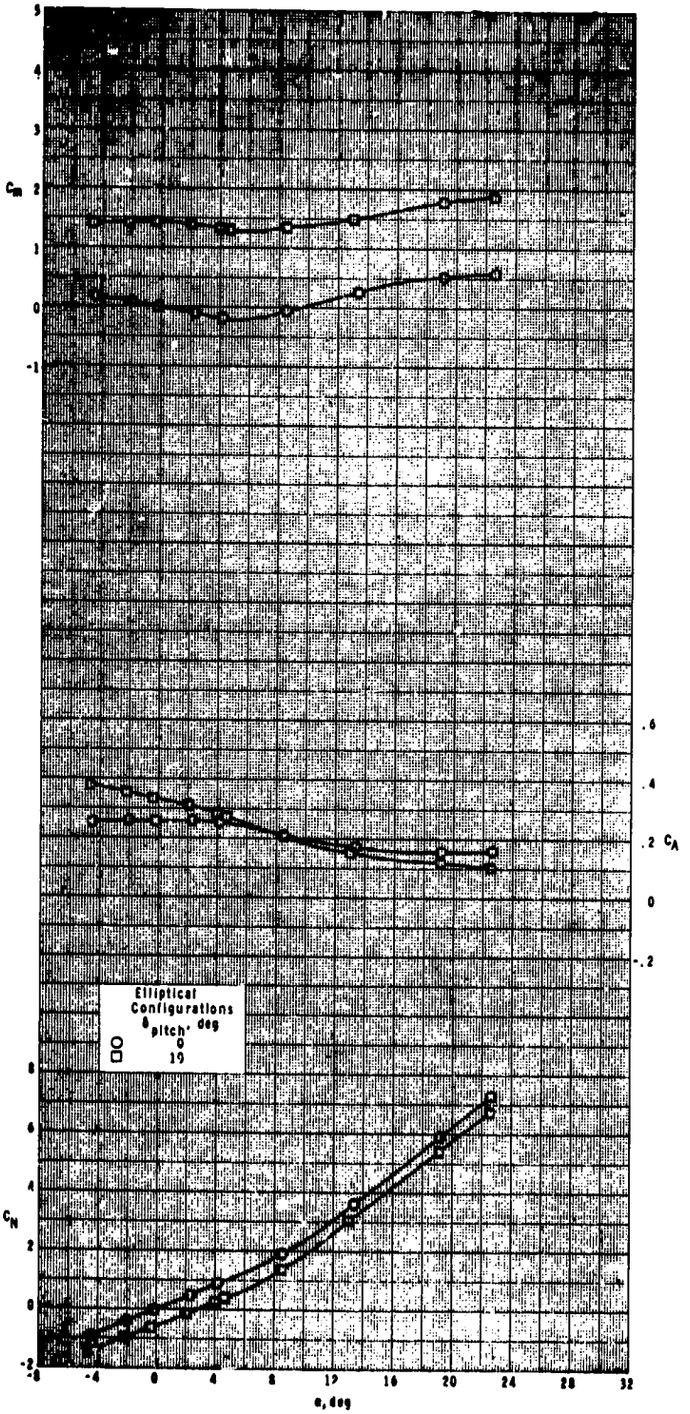

(a) M = 1.60.

Figure 13.- Pitch-control effectiveness of elliptical cross-section body-tail configuration with variation in angle of attack.

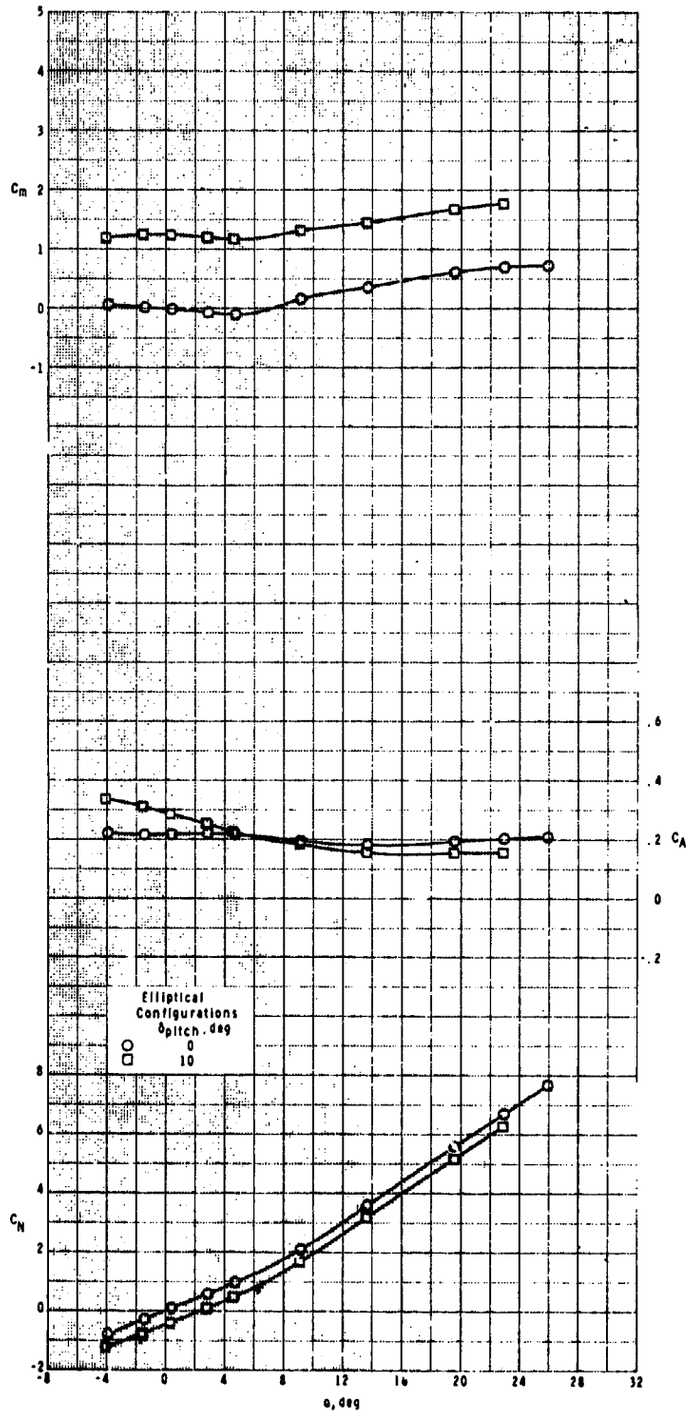

(b) M = 2.00.

Figure 13.- Continued.

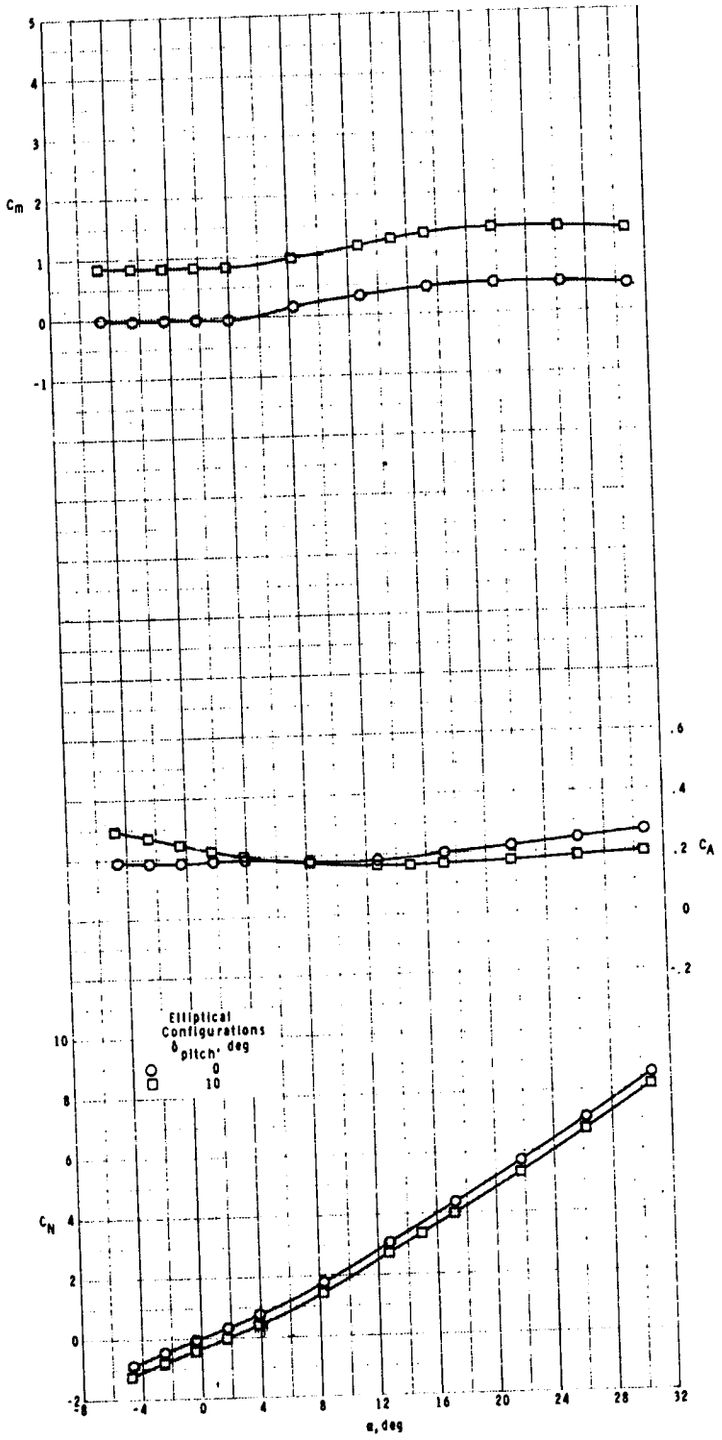

(c) M = 2.50.

Figure 13.- Continued.

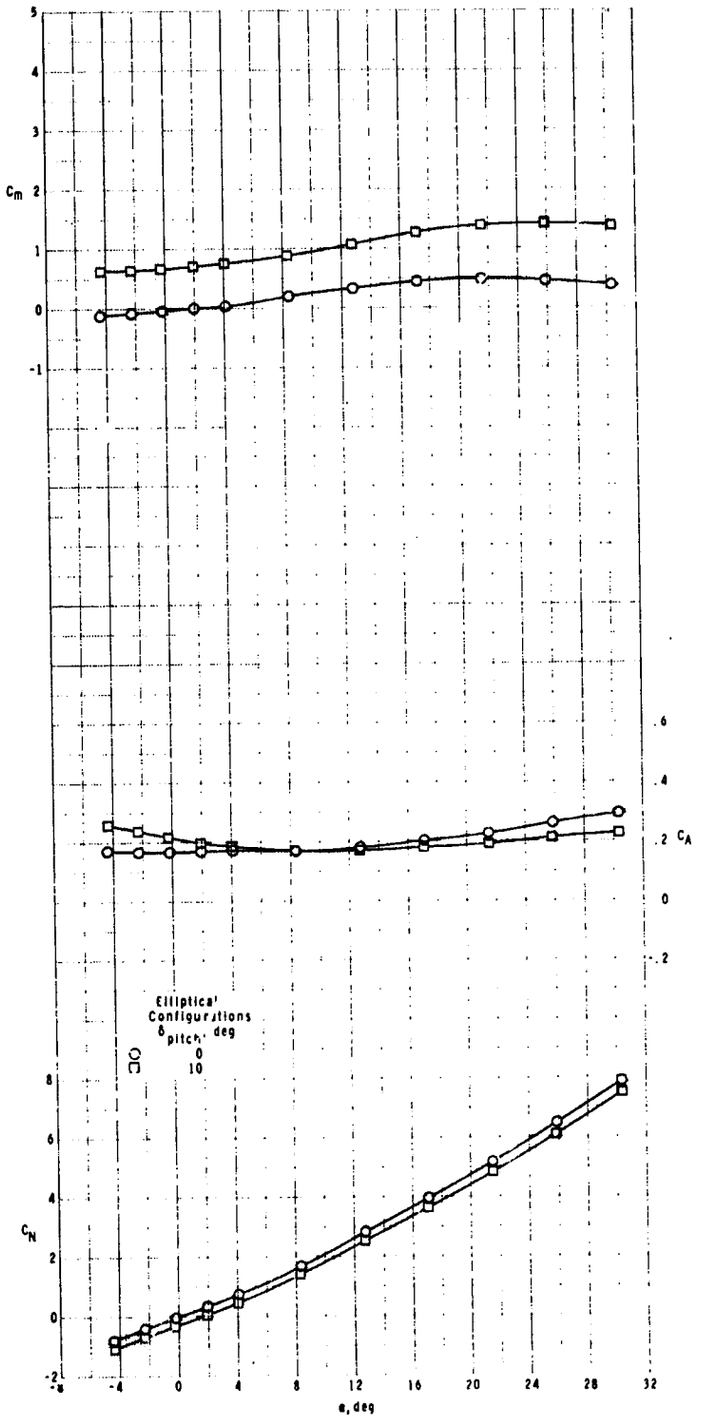

(d) M = 2.96.

Figure 13.- Continued.

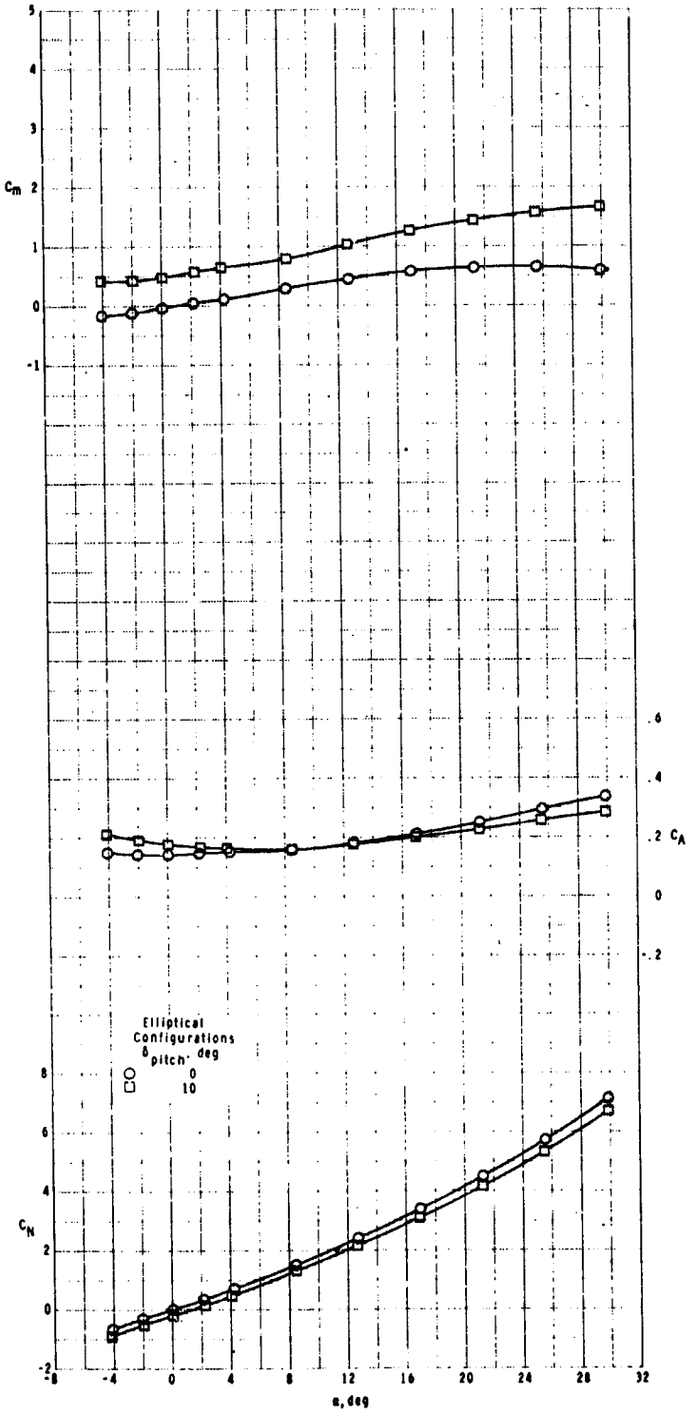

(e) M = 3.95.

Figure 13.- Continued.

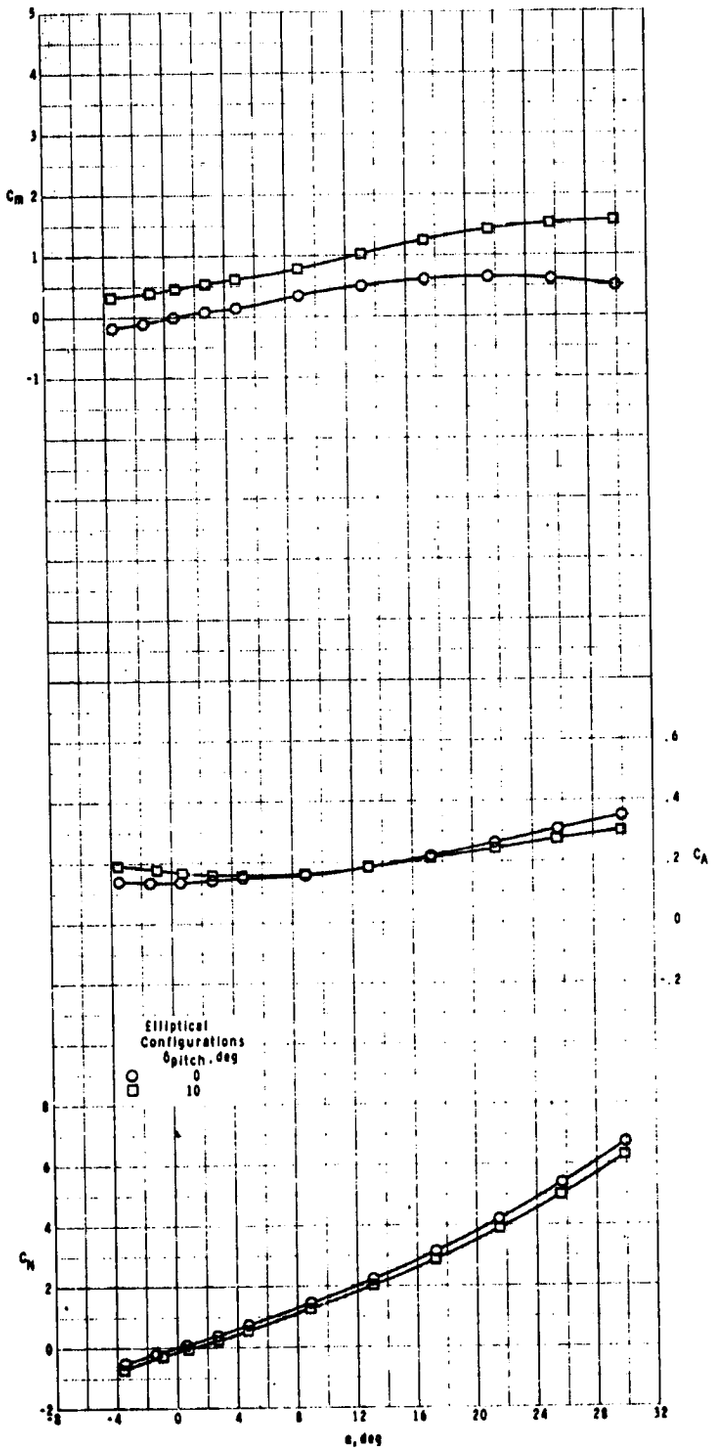

(f) M = 4.63.

Figure 13.- Concluded.

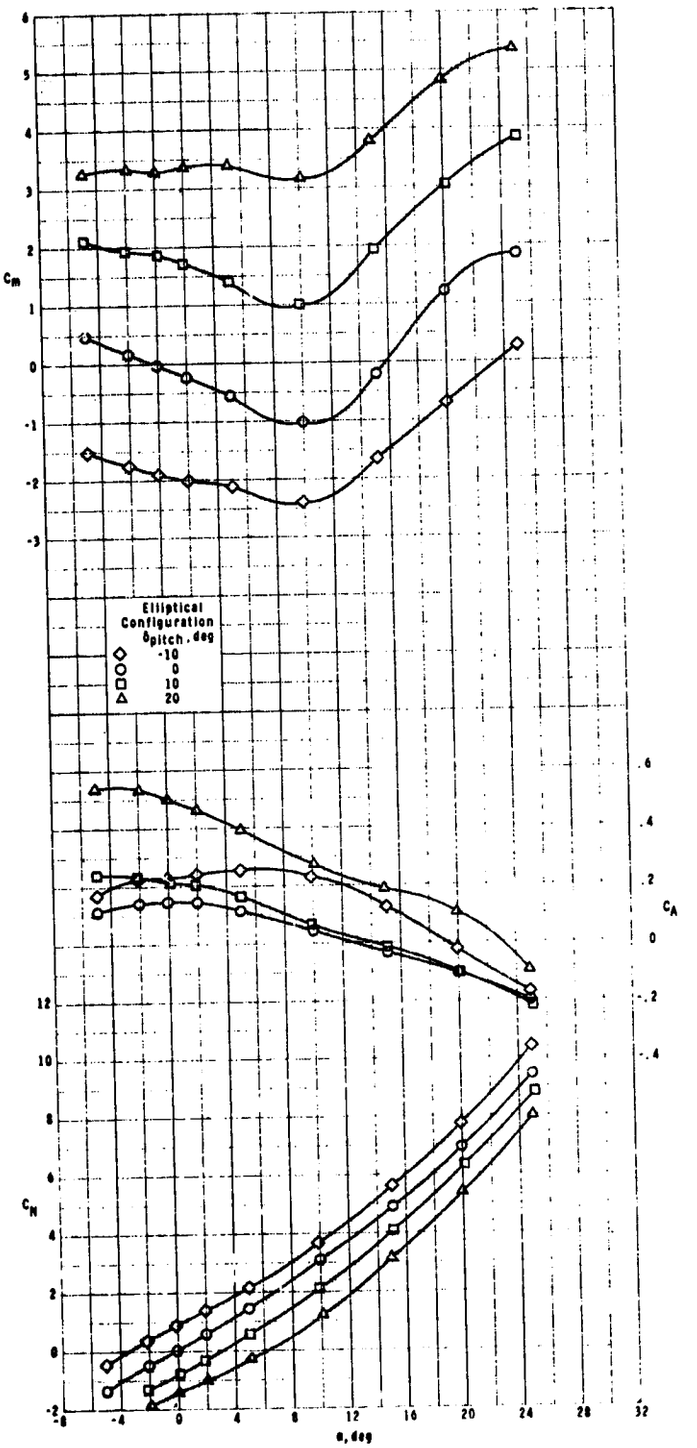

(a) M = 0.5.

Figure 14.- Pitch-control effectiveness of elliptical cross-section body-wing-tail configuration with variation in angle of attack.

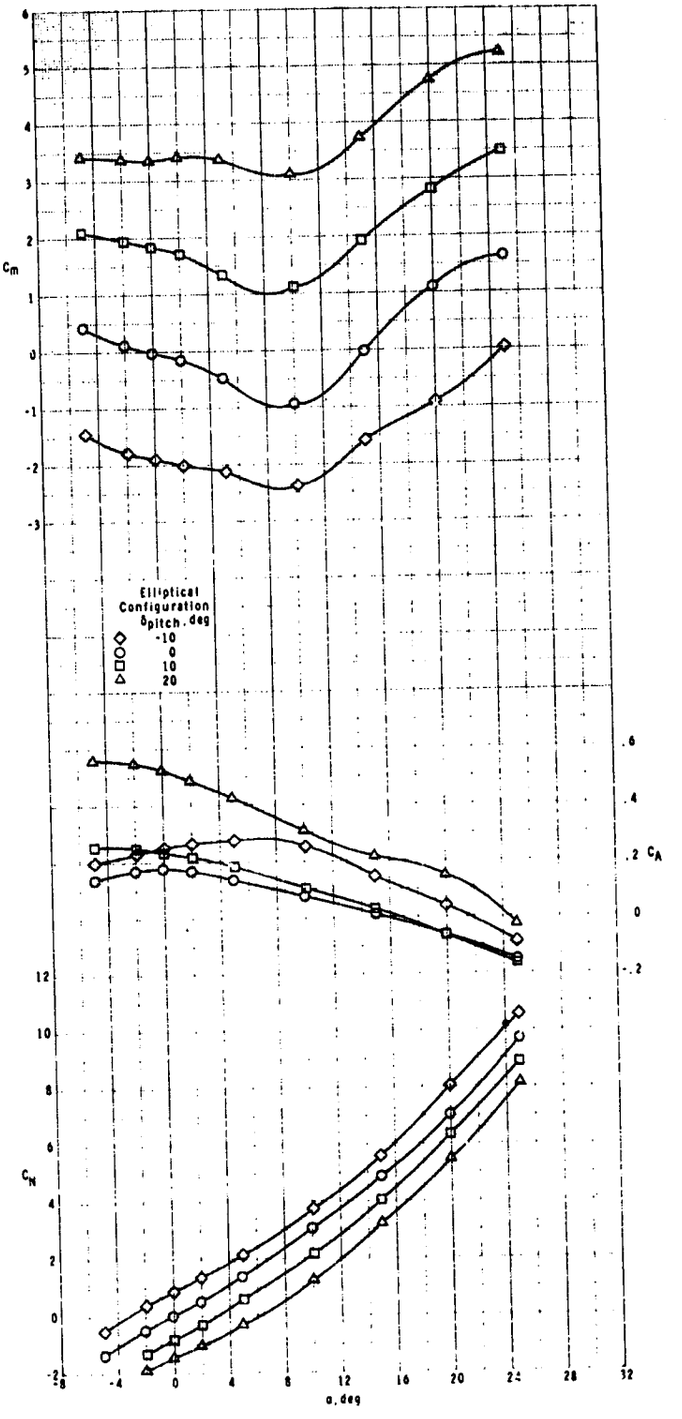

(b) M = 0.7.

Figure 14.- Continued.

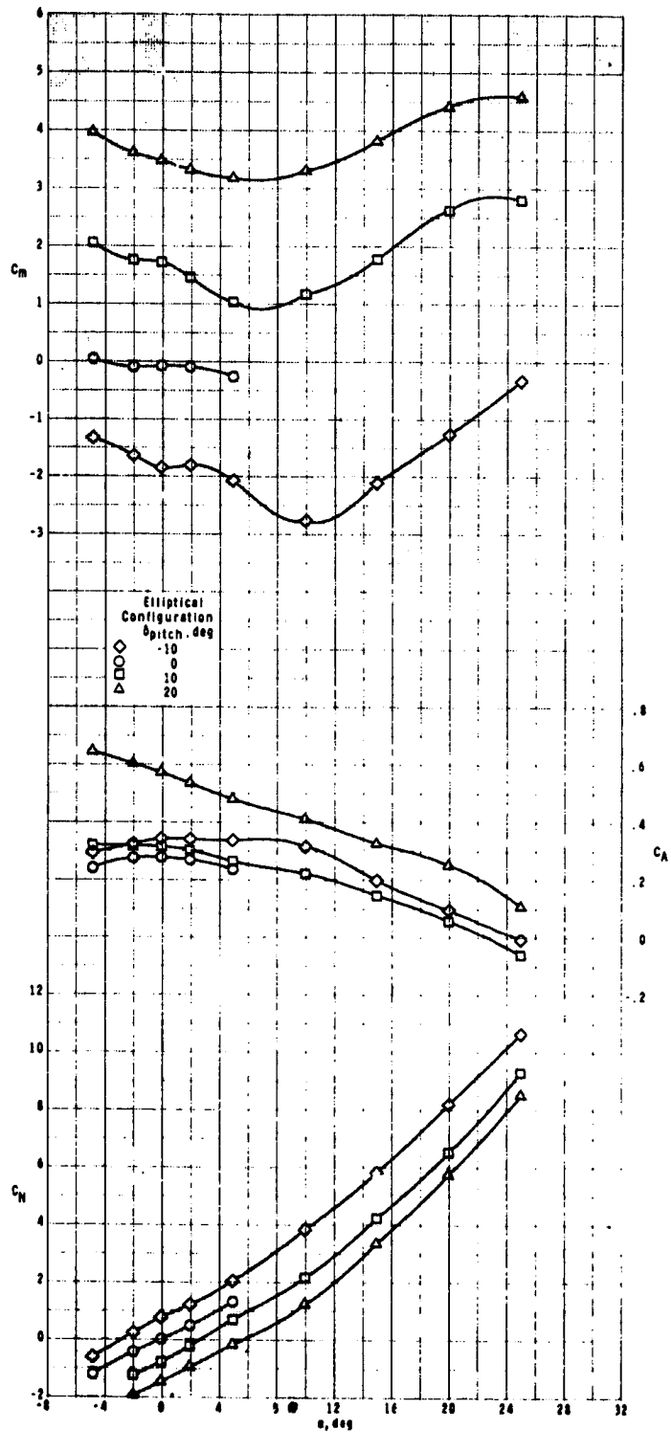

(c) M = 0.9.

Figure 14.- Continued.

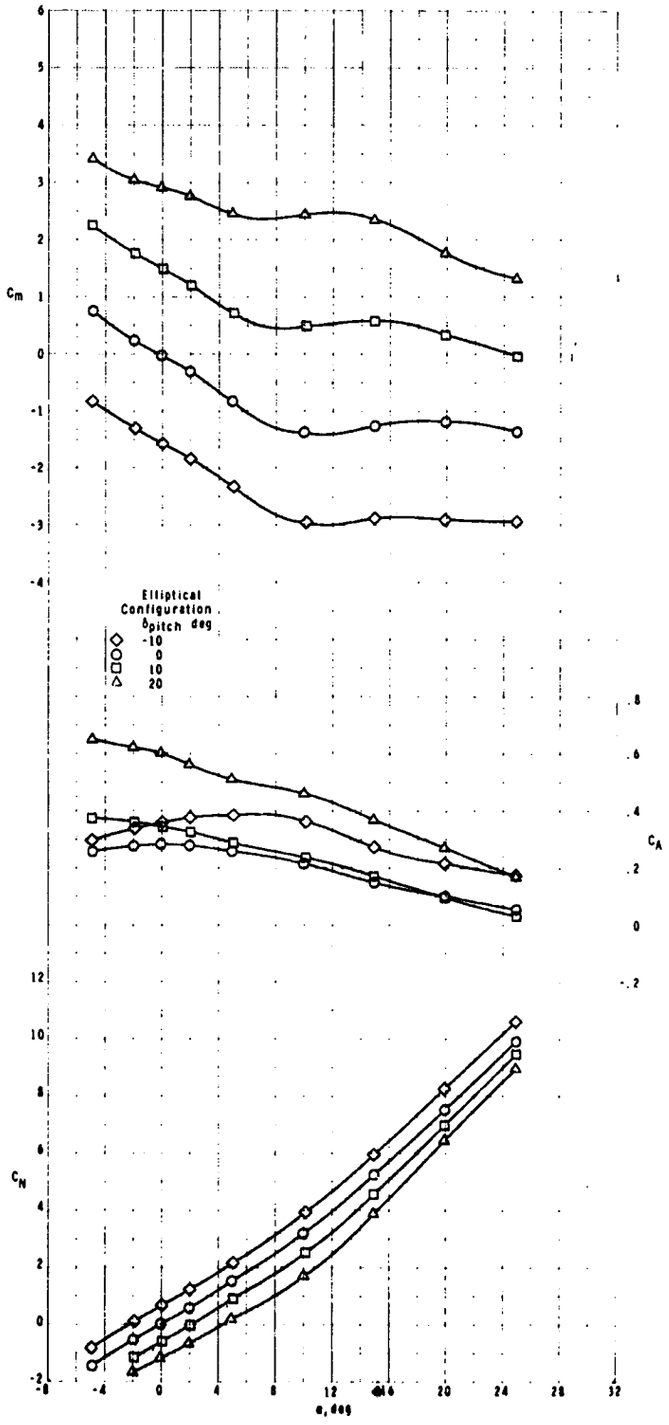

(d) M = 1.3.

Figure 14.- Continued.

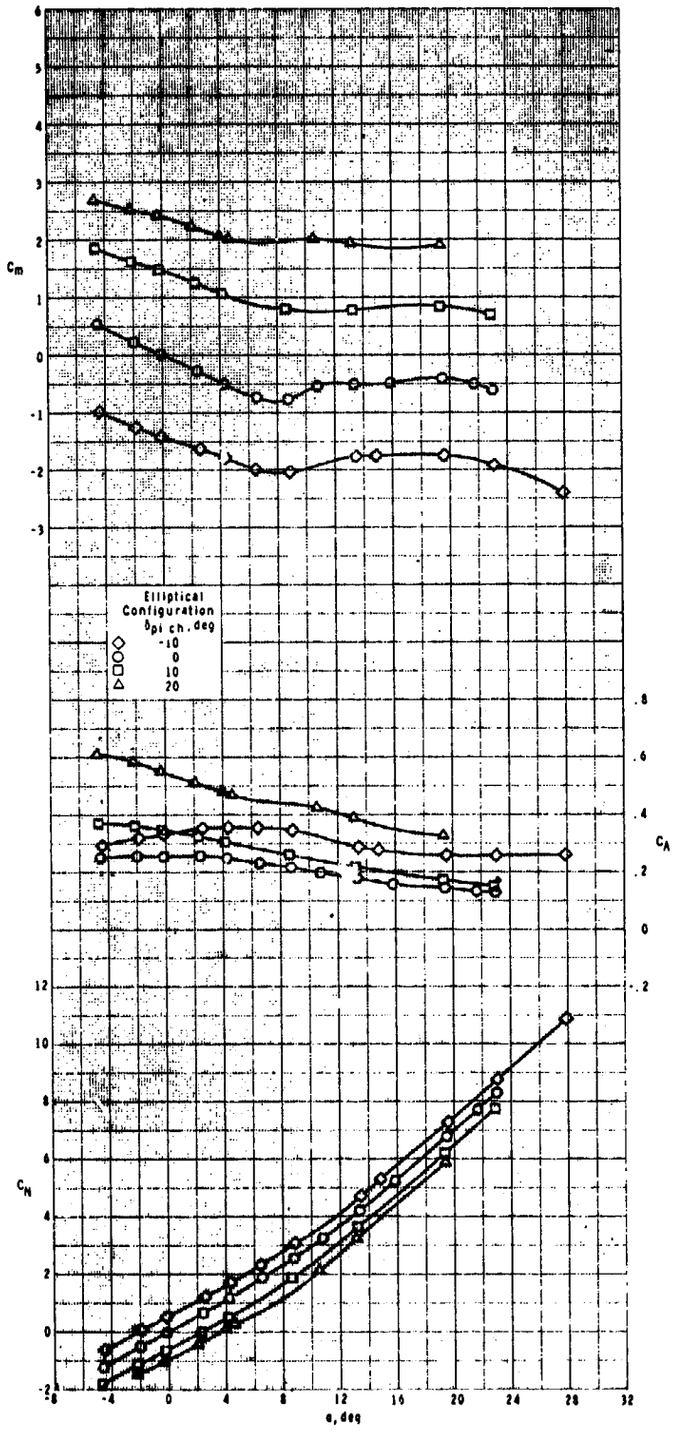

(e) M = 1.60.

Figure 14.- Continued.

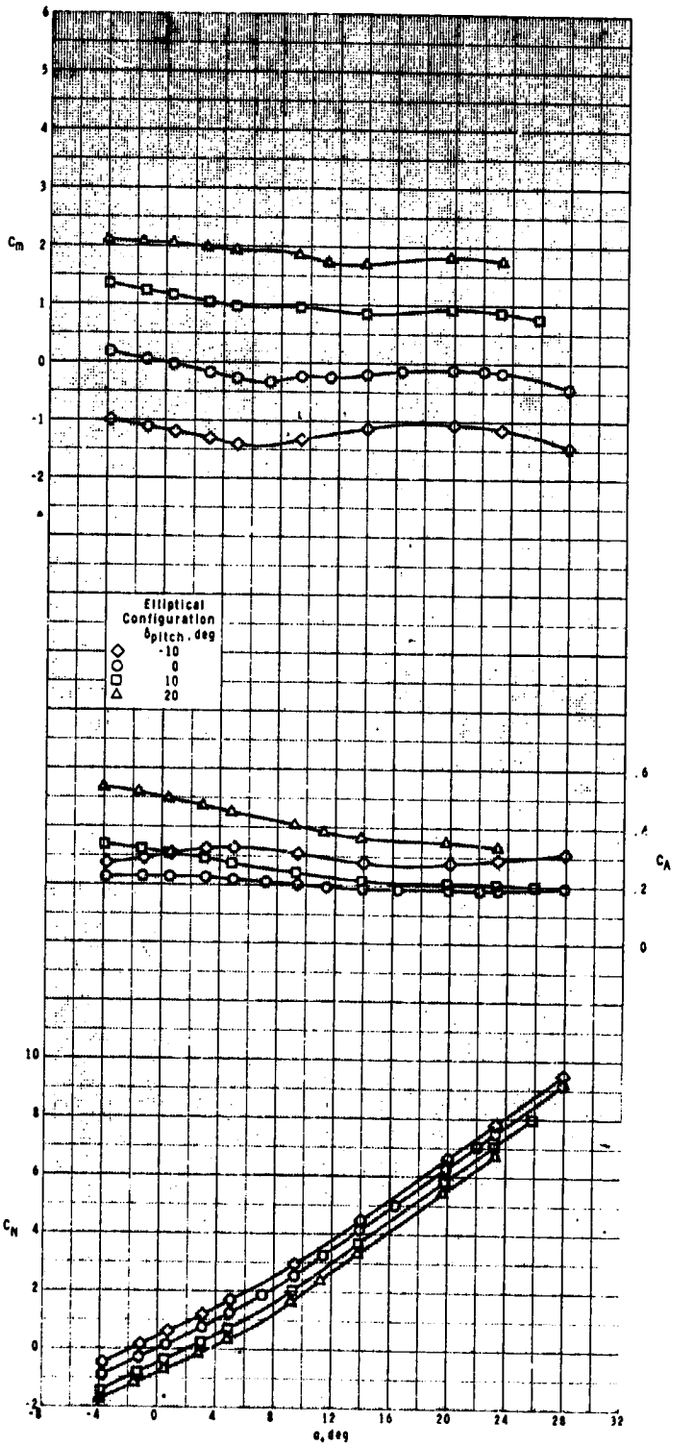

(f) M = 2.00.

Figure 14.- Continued.

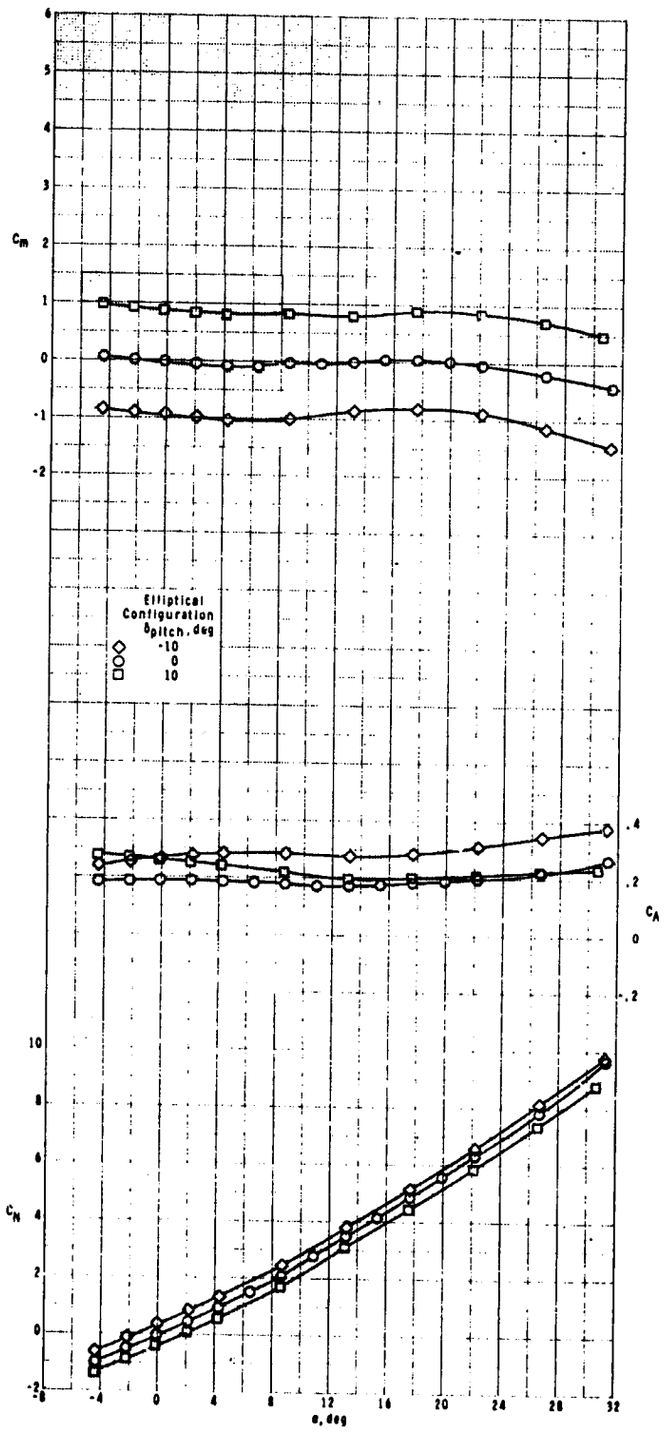

(g) M = 2.50.

Figure 14.- Continued.

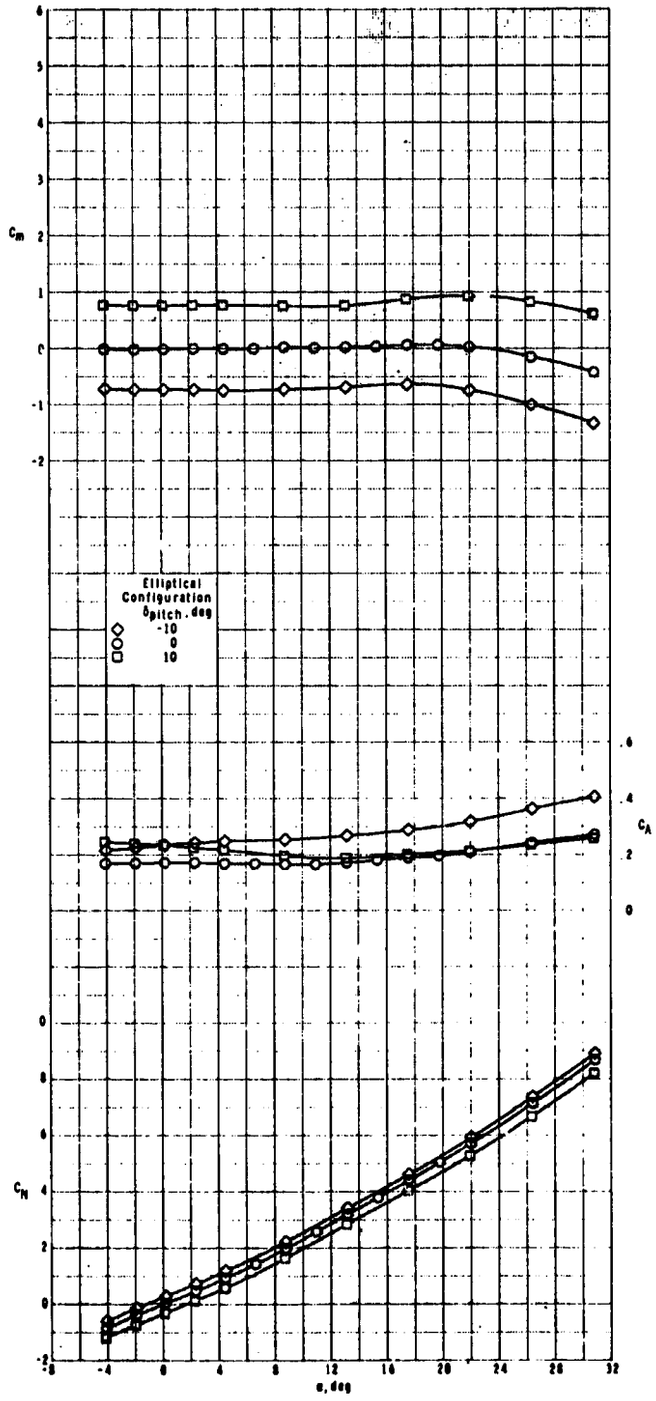

(h) M = 2.96.

Figure 14.- Continued.

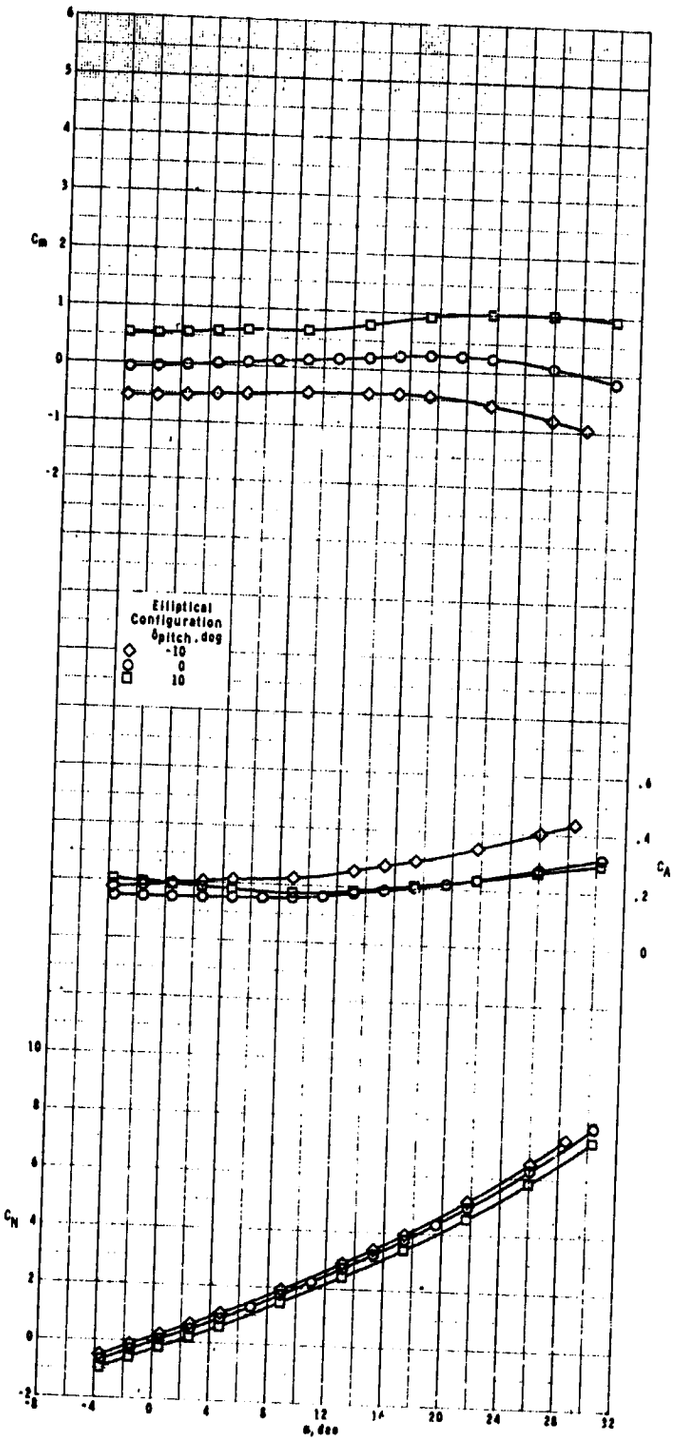

(i) M = 3.95.

Figure 14.- Continued.

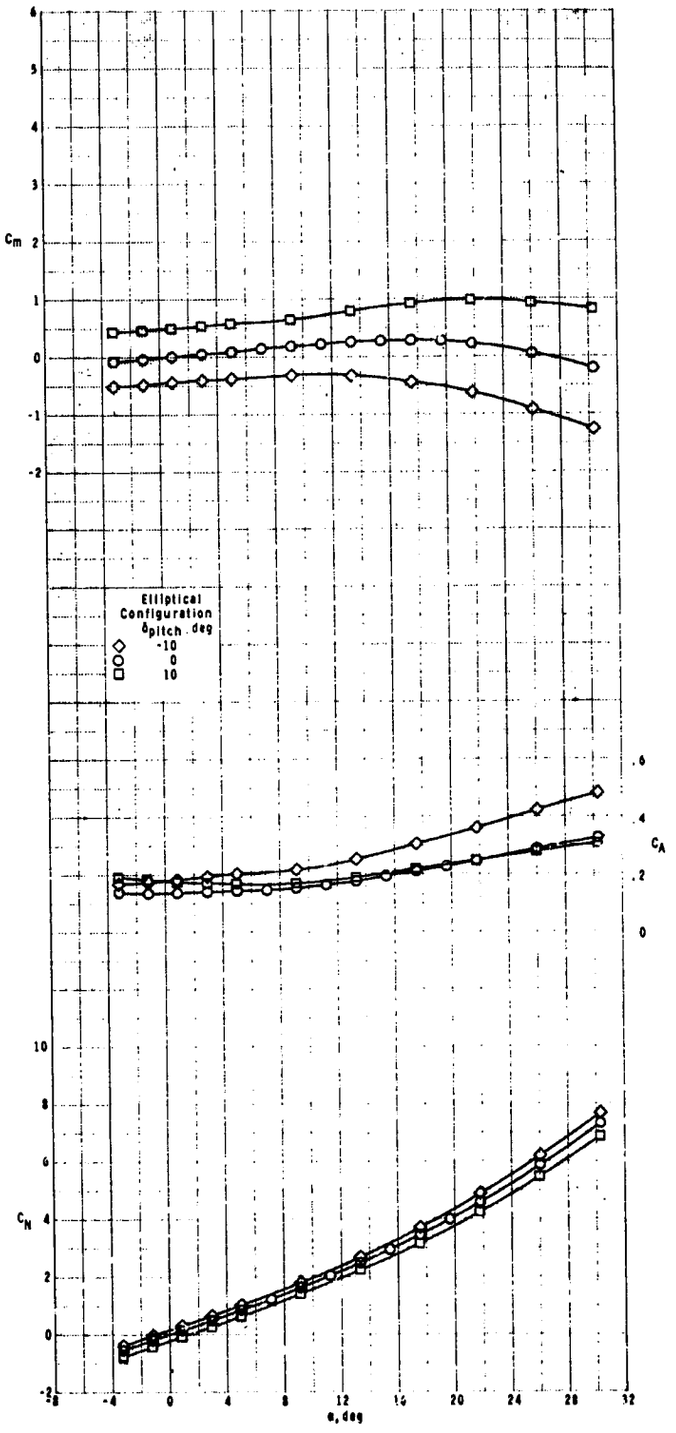

(j) M = 4.63.

Figure 14.- Concluded.

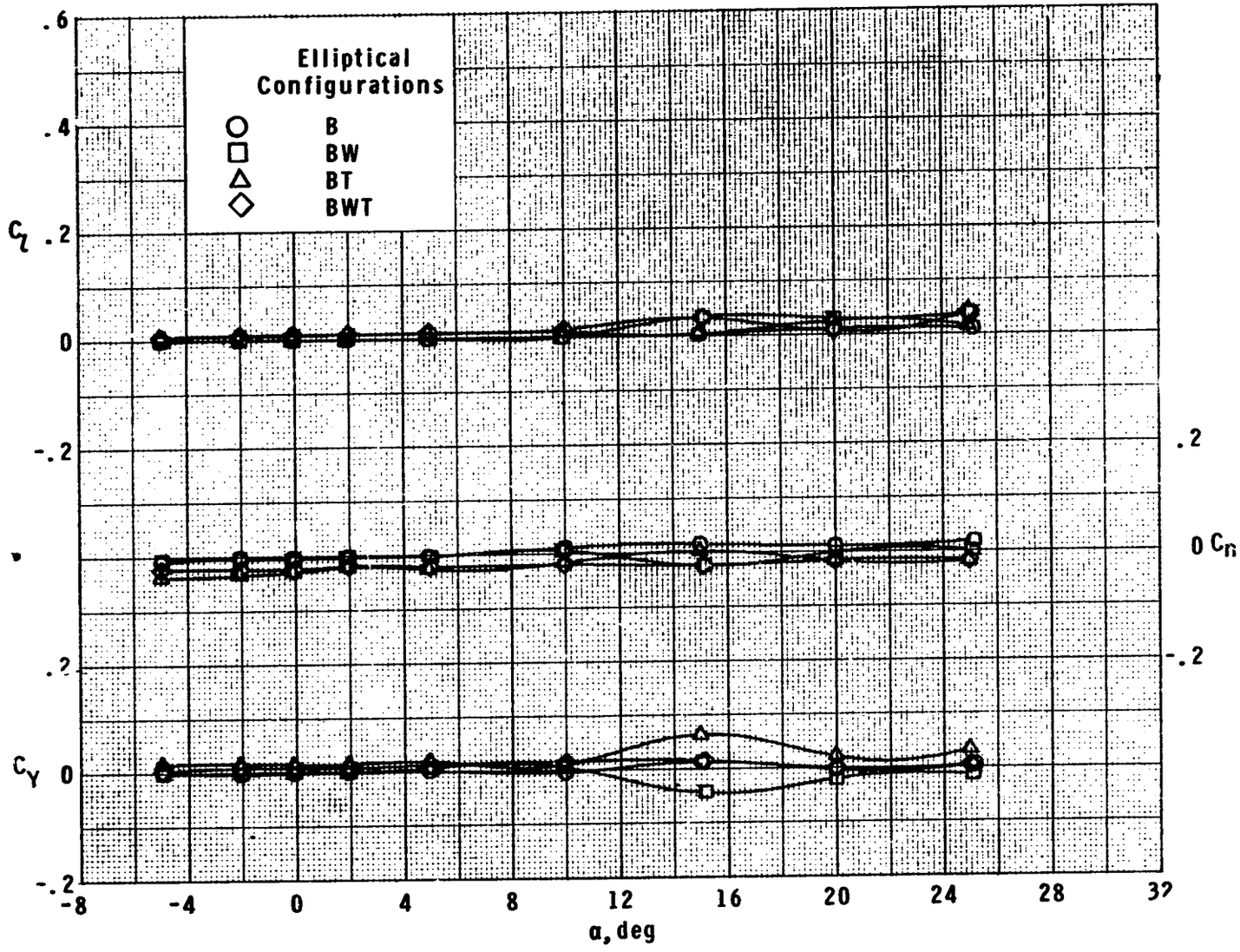

(a) M = 0.5.

Figure 15.- Effect of components on lateral aerodynamic characteristics of elliptical cross-section model with variation in angle of attack.

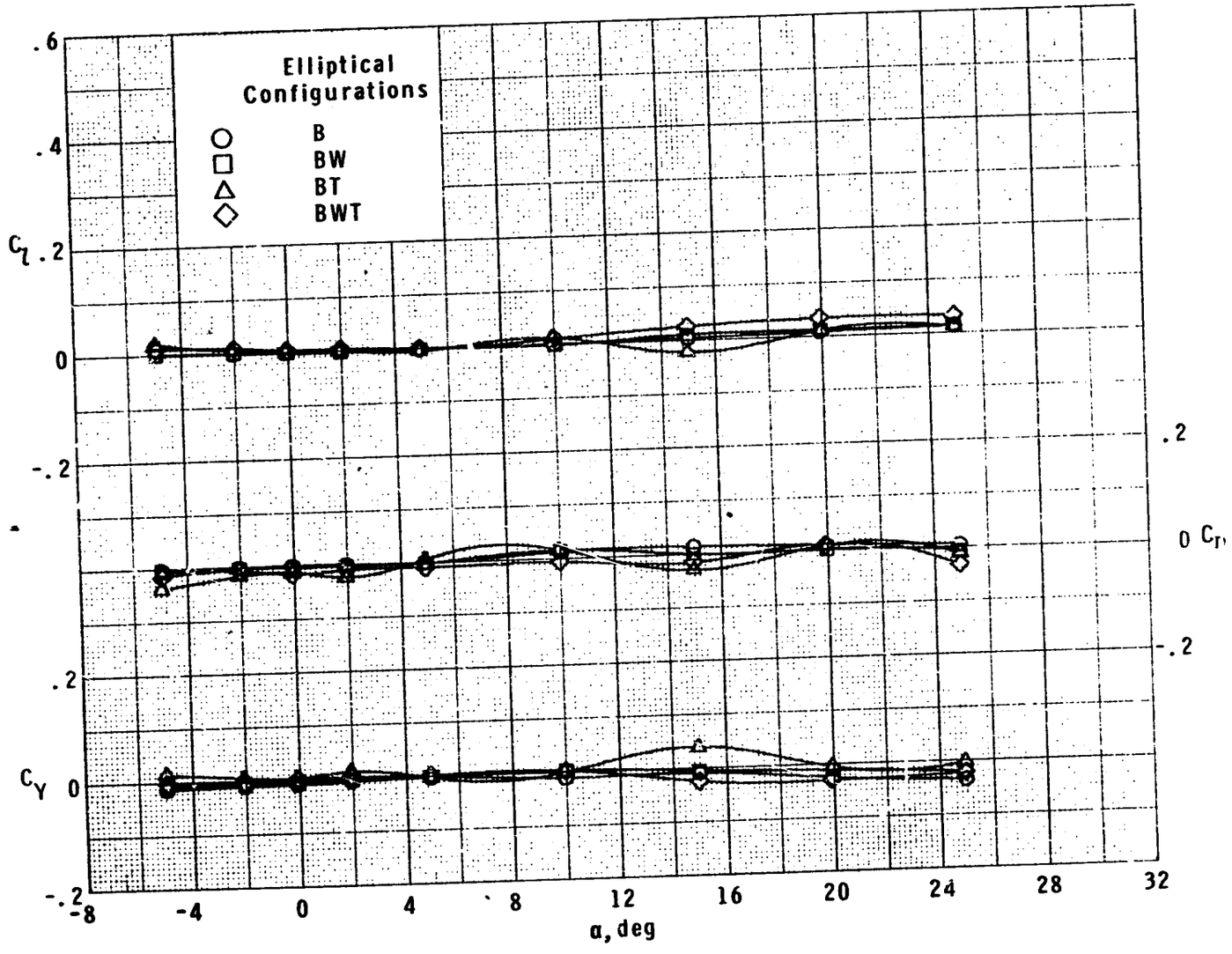

(b) M = 0.7.

Figure 15.- Continued.

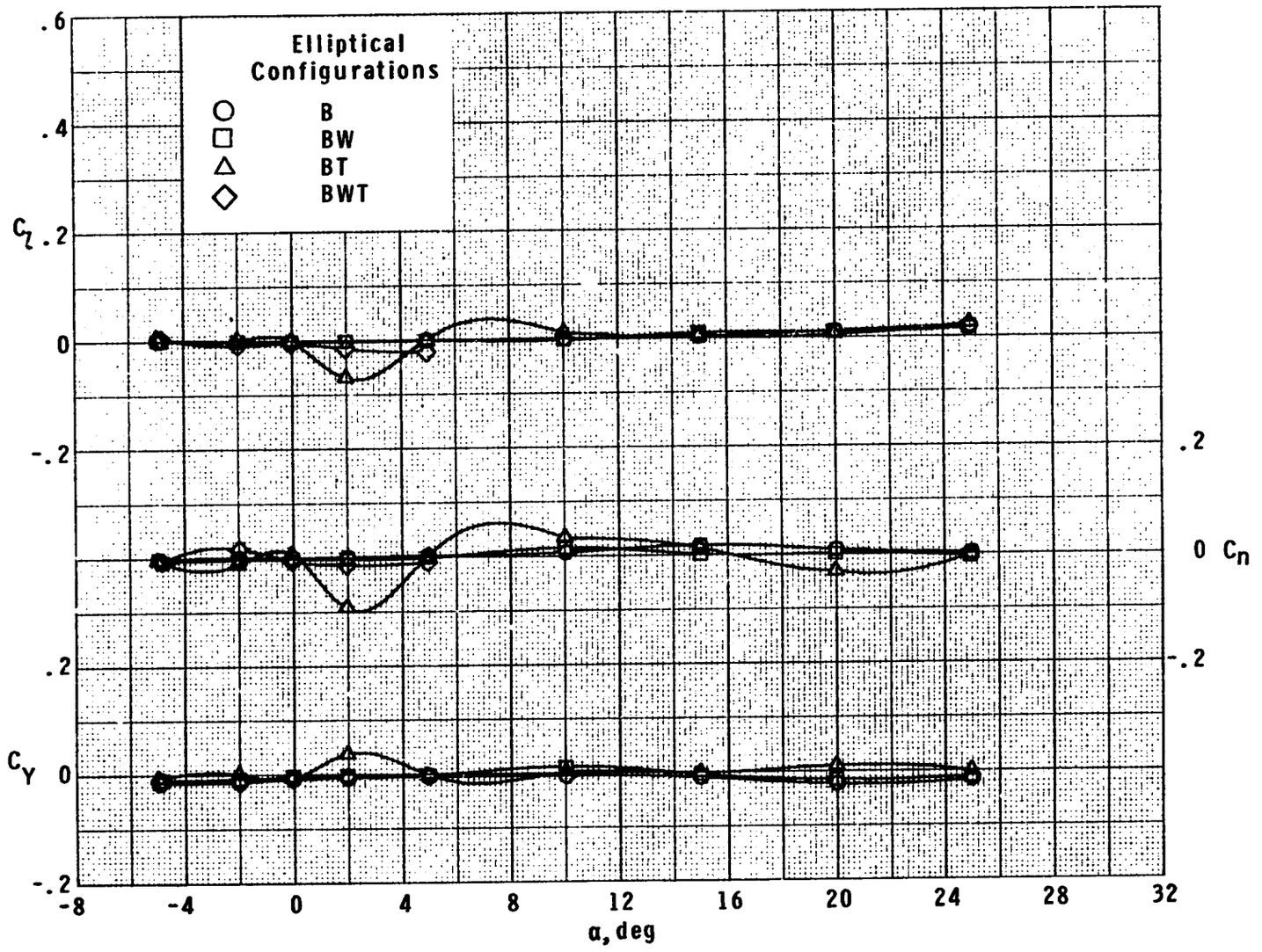

(c) M = 0.9.

Figure 15.- Continued.

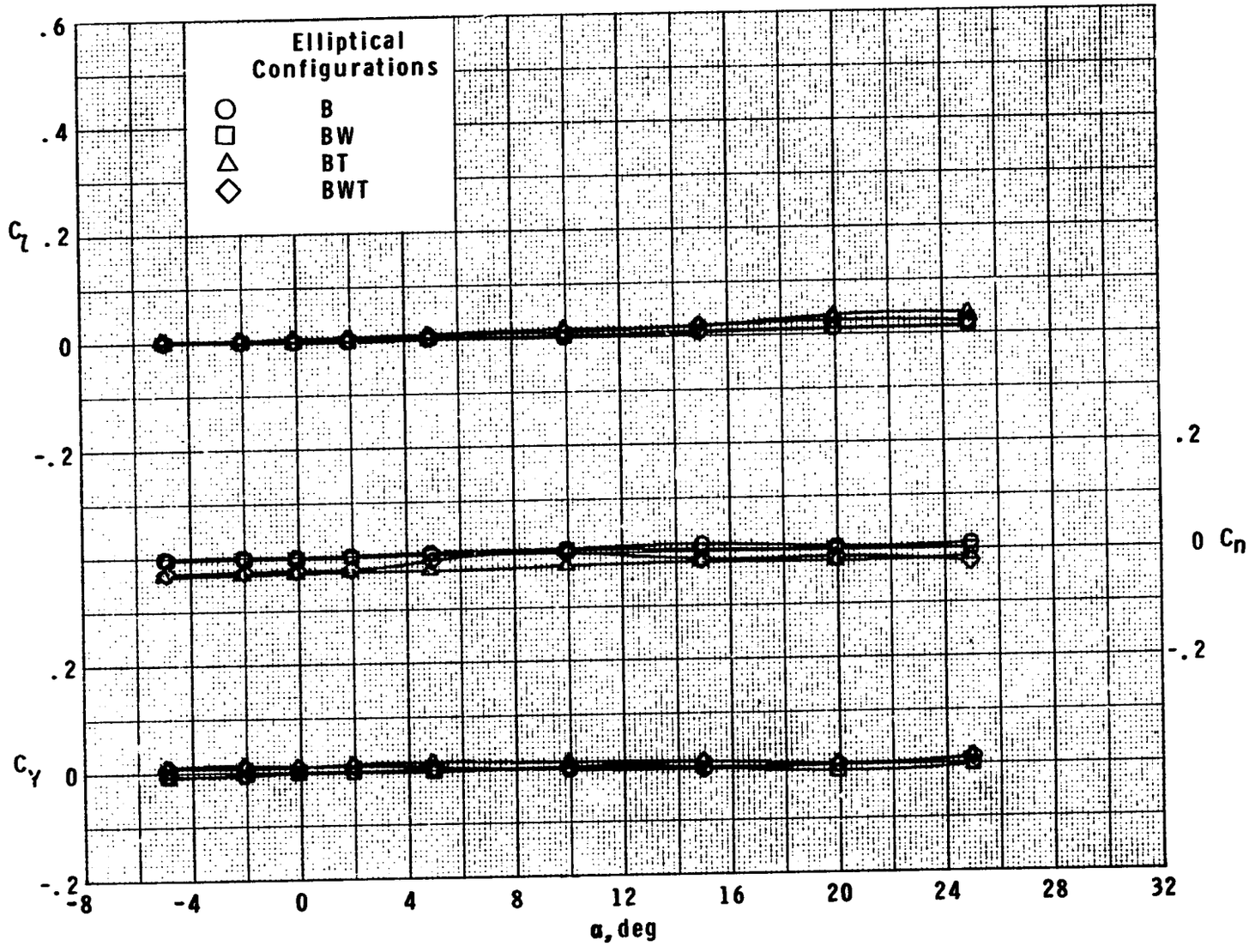

(d) M = 1.3.

Figure 15.- Continued.

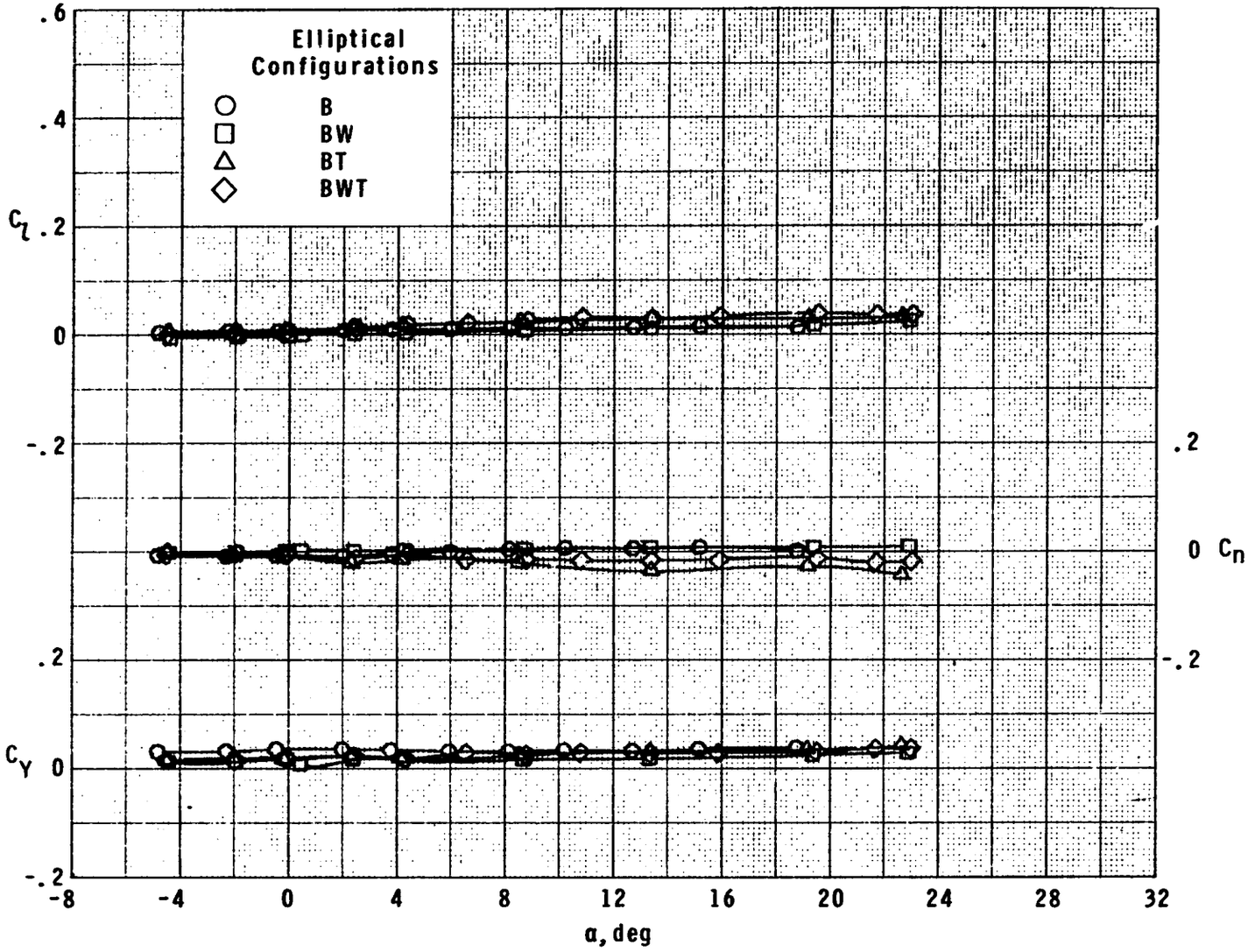

(e) M = 1.60.

Figure 15.- Continued.

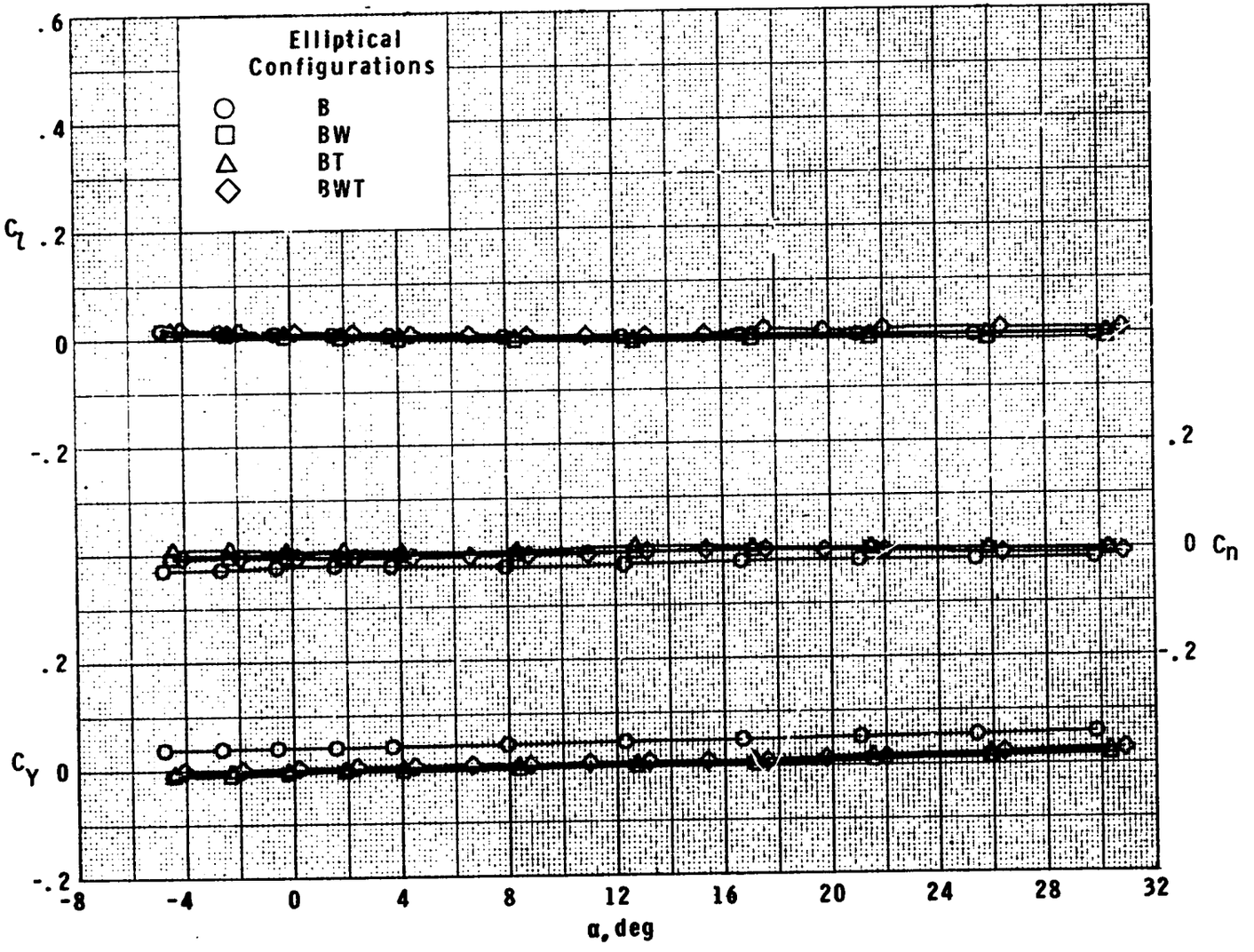

(f) M = 2.96.

Figure 15.- Continued.

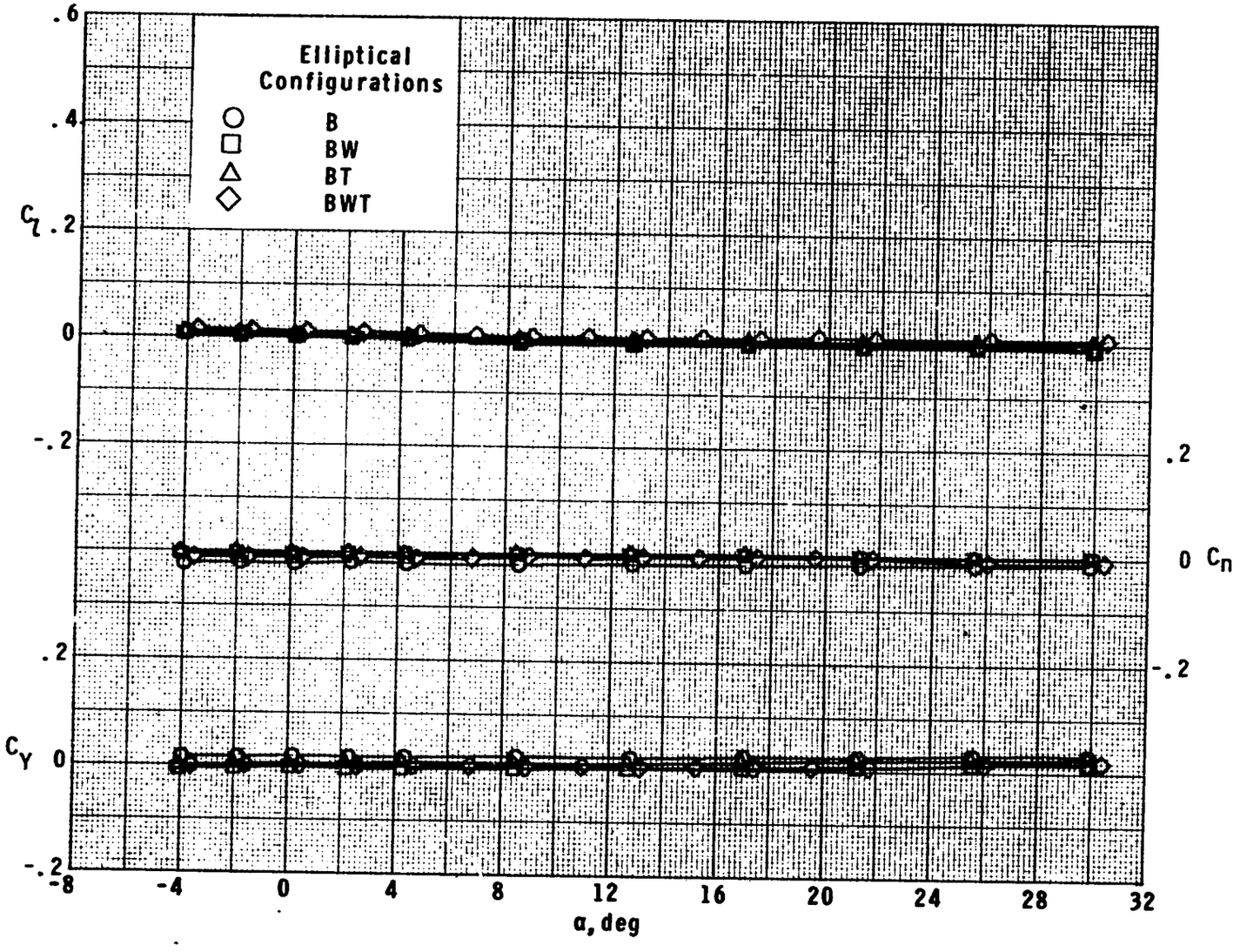

(g) M = 3.95.

Figure 15.- Continued.

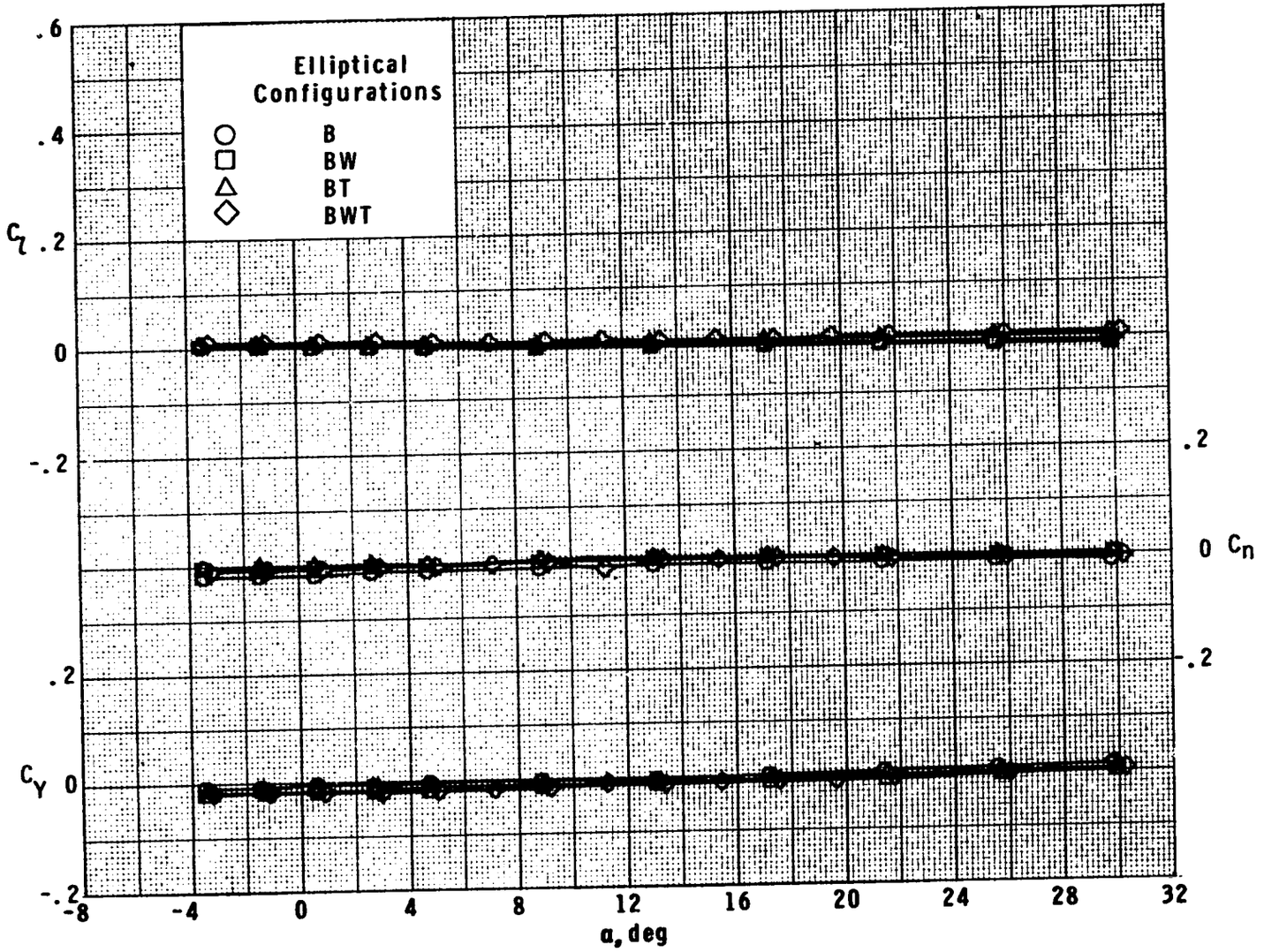

(h) M = 4.63.

Figure 15.- Concluded.

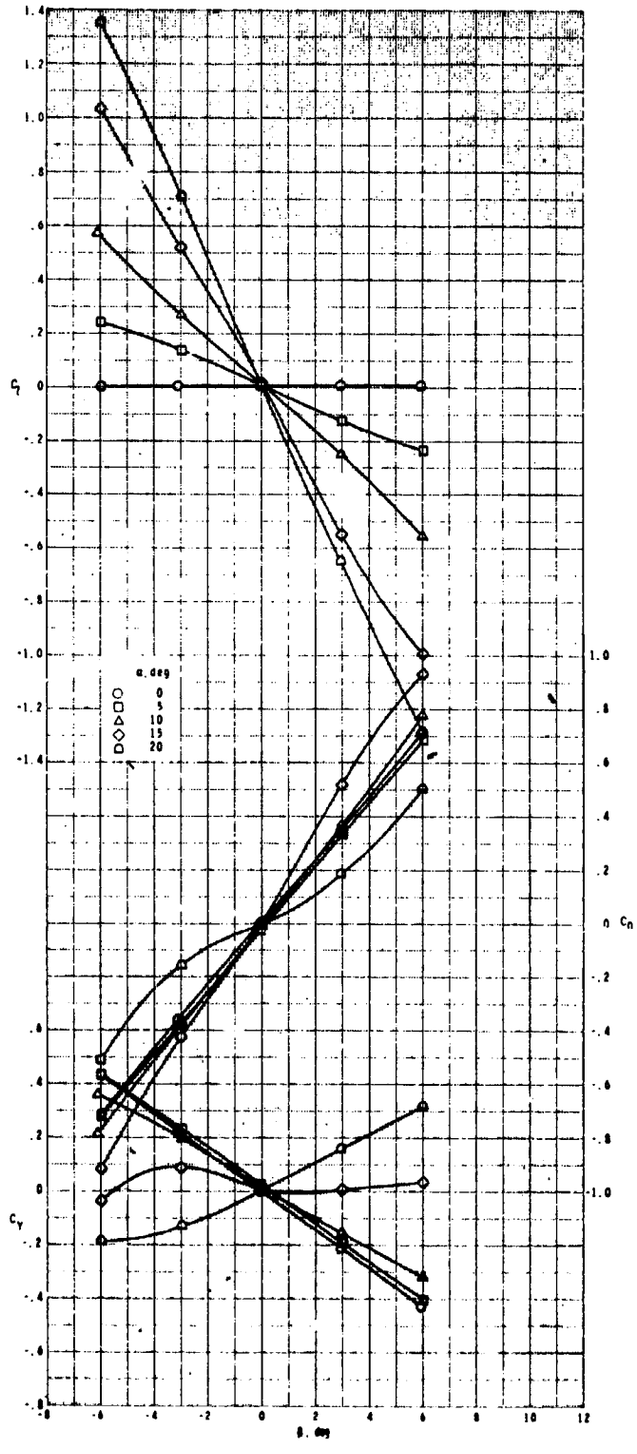

(a) M = 0.5.

Figure 16.- Effect of angle of attack on lateral aerodynamic characteristics of elliptical cross-section body-wing-tail configuration with variation in angle of sideslip.

ORIGINAL PAGE IS
OF POOR QUALITY

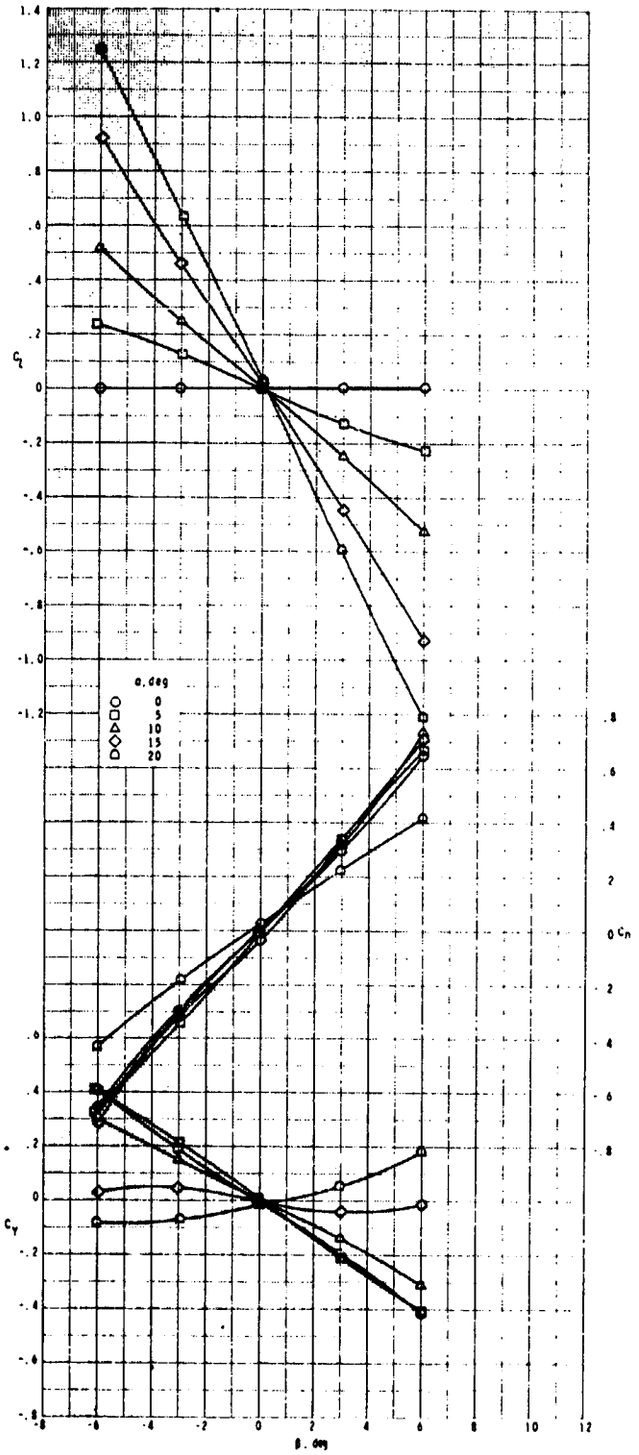

(b) M = 0.7.

Figure 16.- Continued.

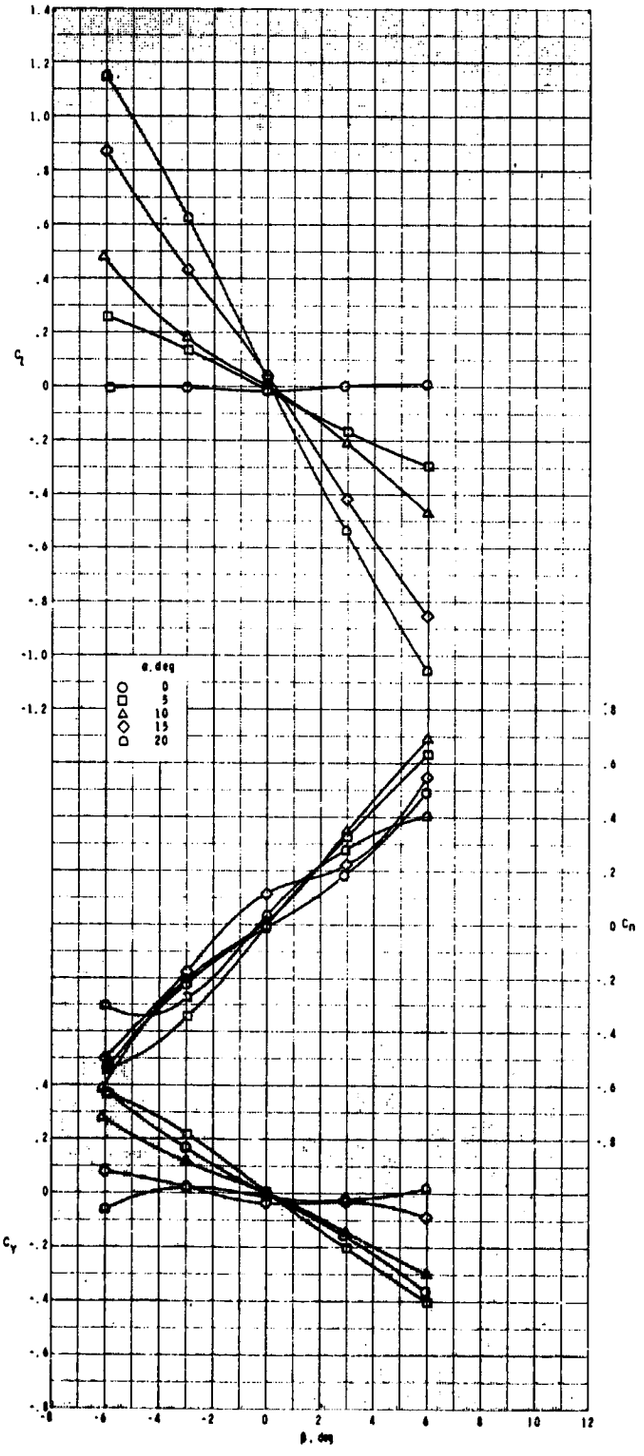

(c) M = 0.9.

Figure 16.- Continued.

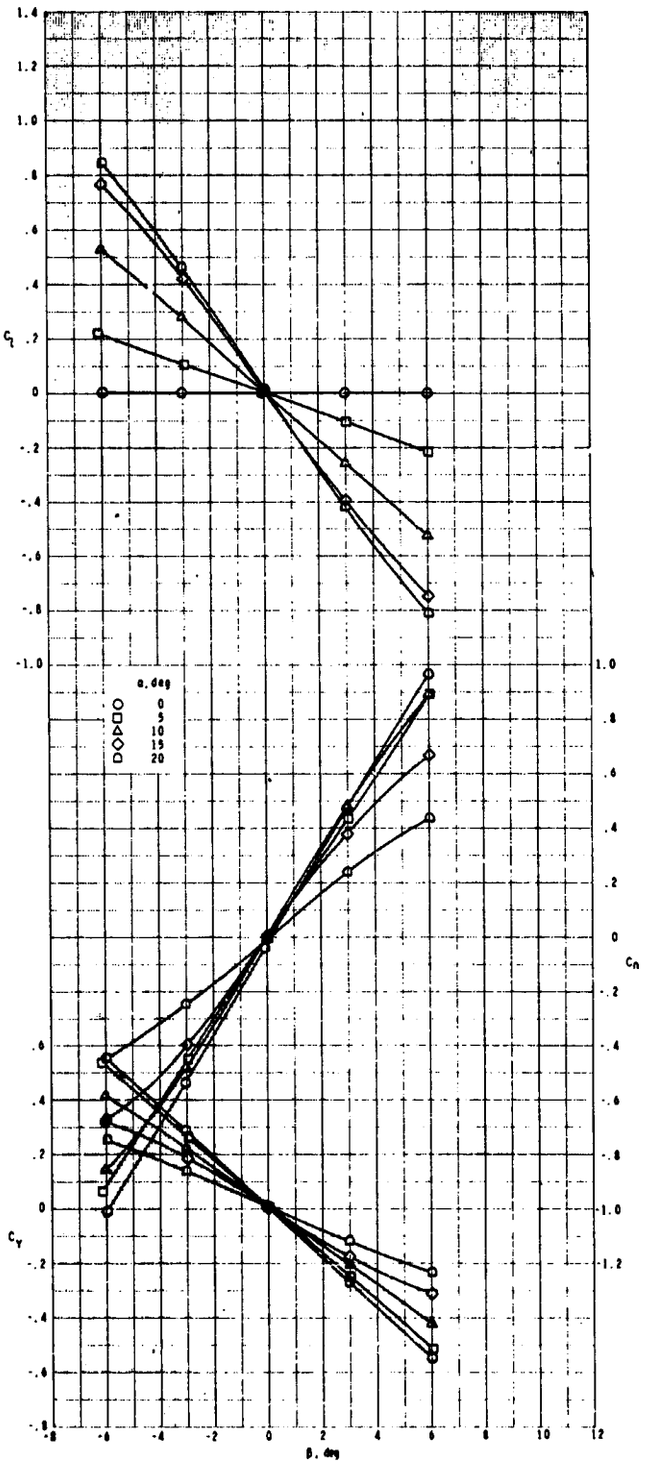

(d) M = 1.3.

Figure 16.- Continued.

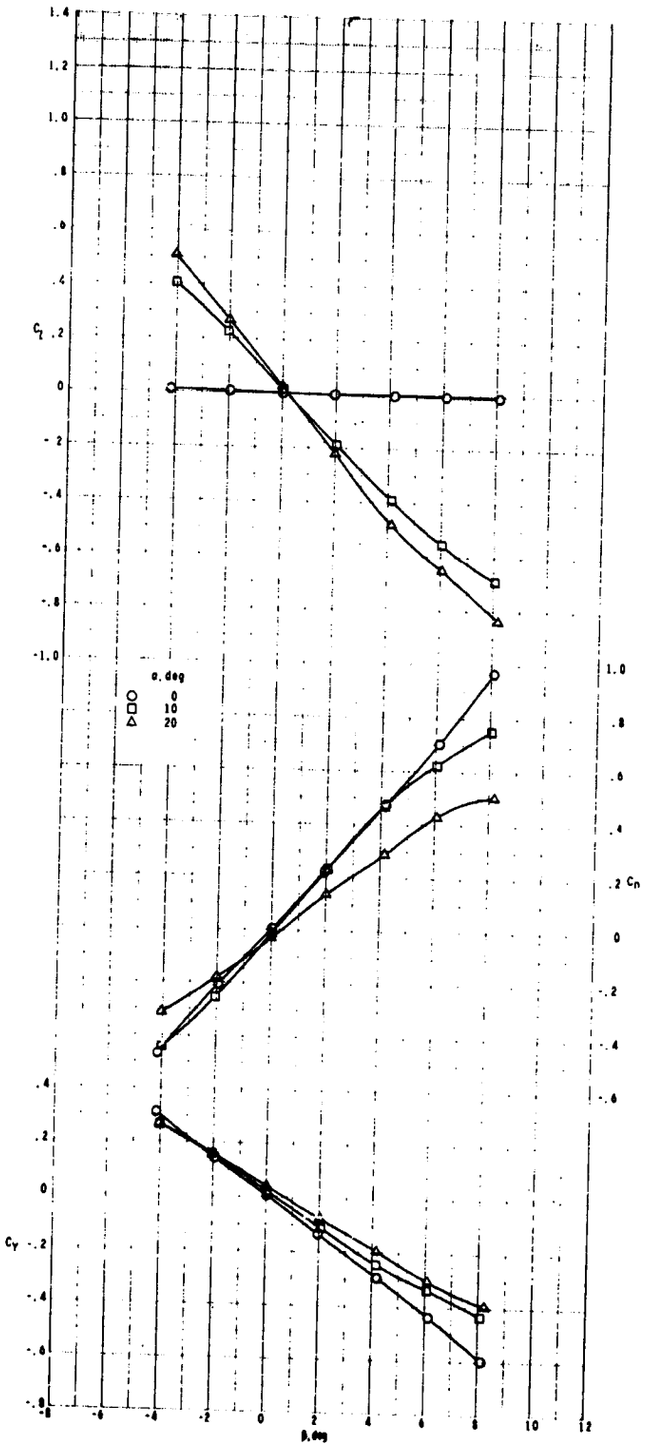

(e) M = 1.60.

Figure 16.- Continued.

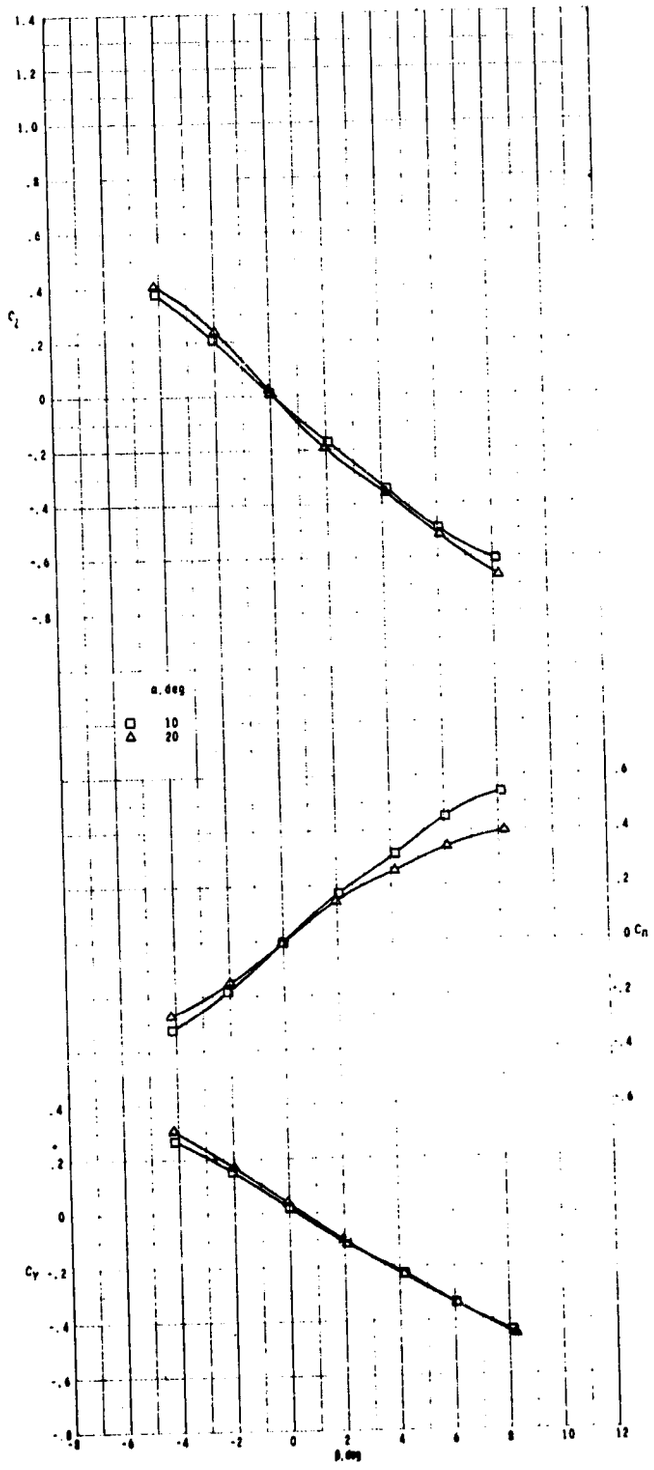

(f) M = 2.00.

Figure 16.- Continued.

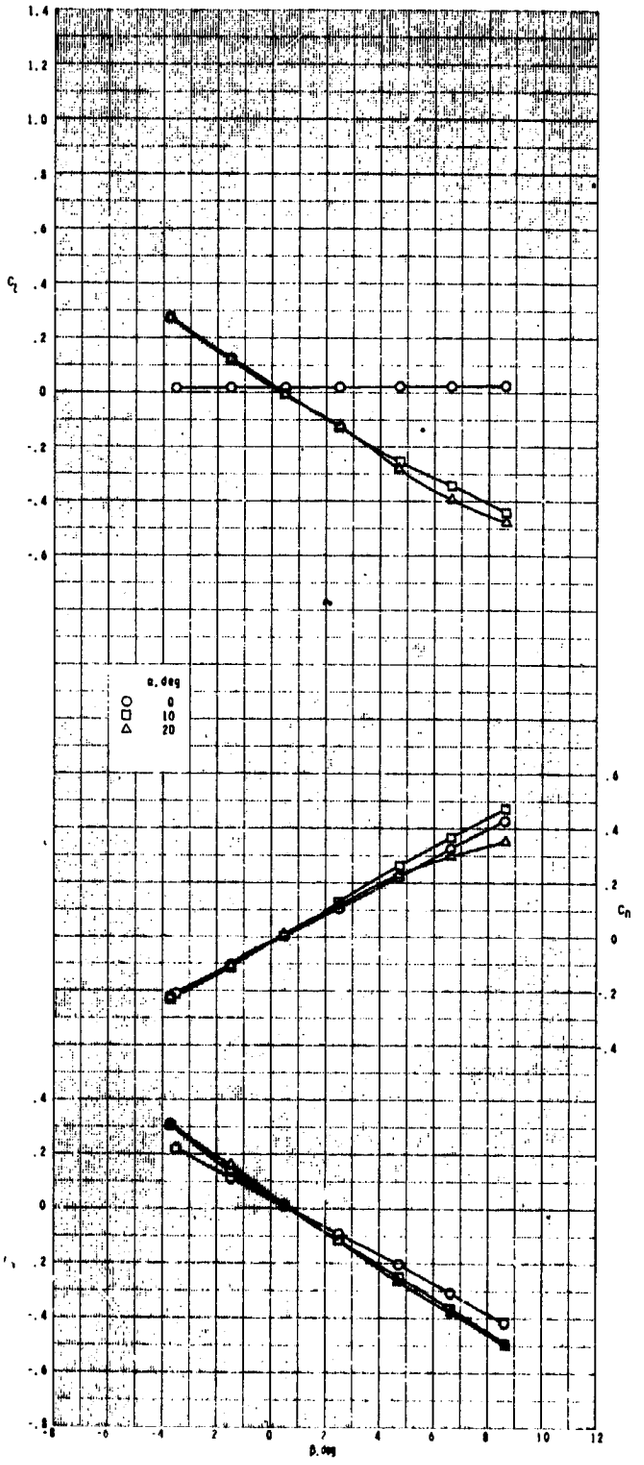

(g) M = 2.50.

Figure 16.- Continued.

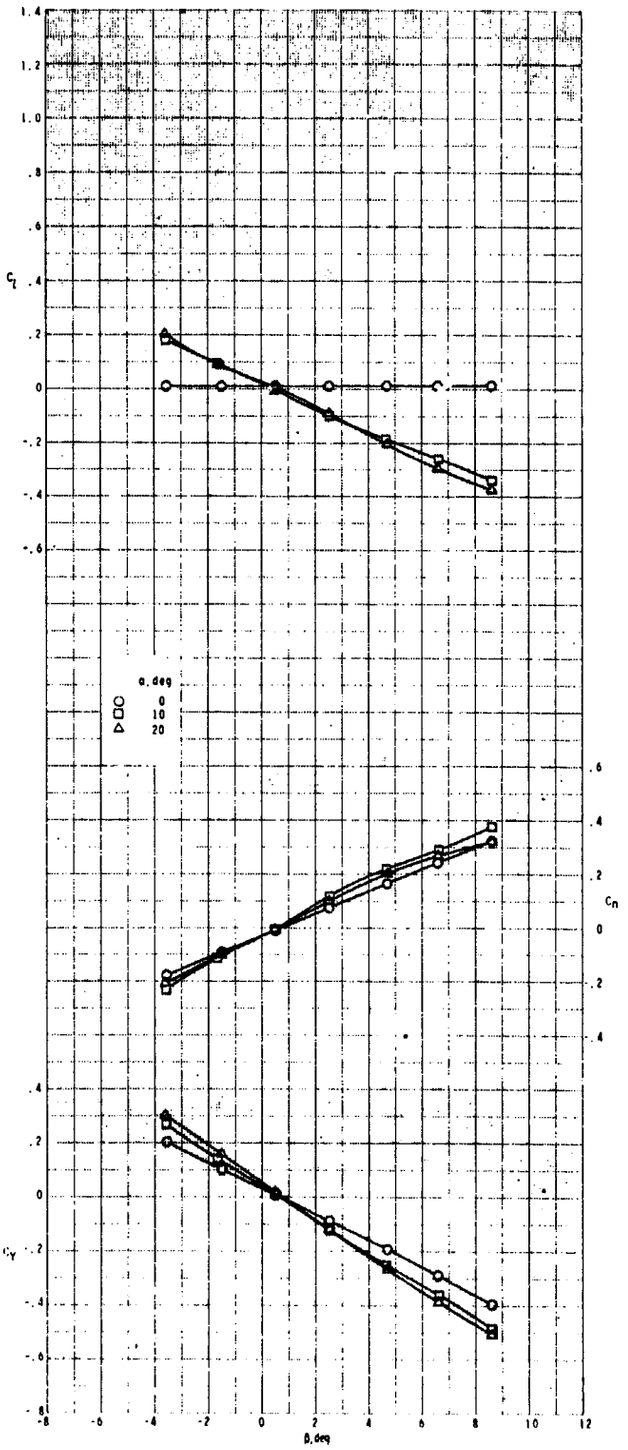

(h) M = 2.96.

Figure 16.- Continued.

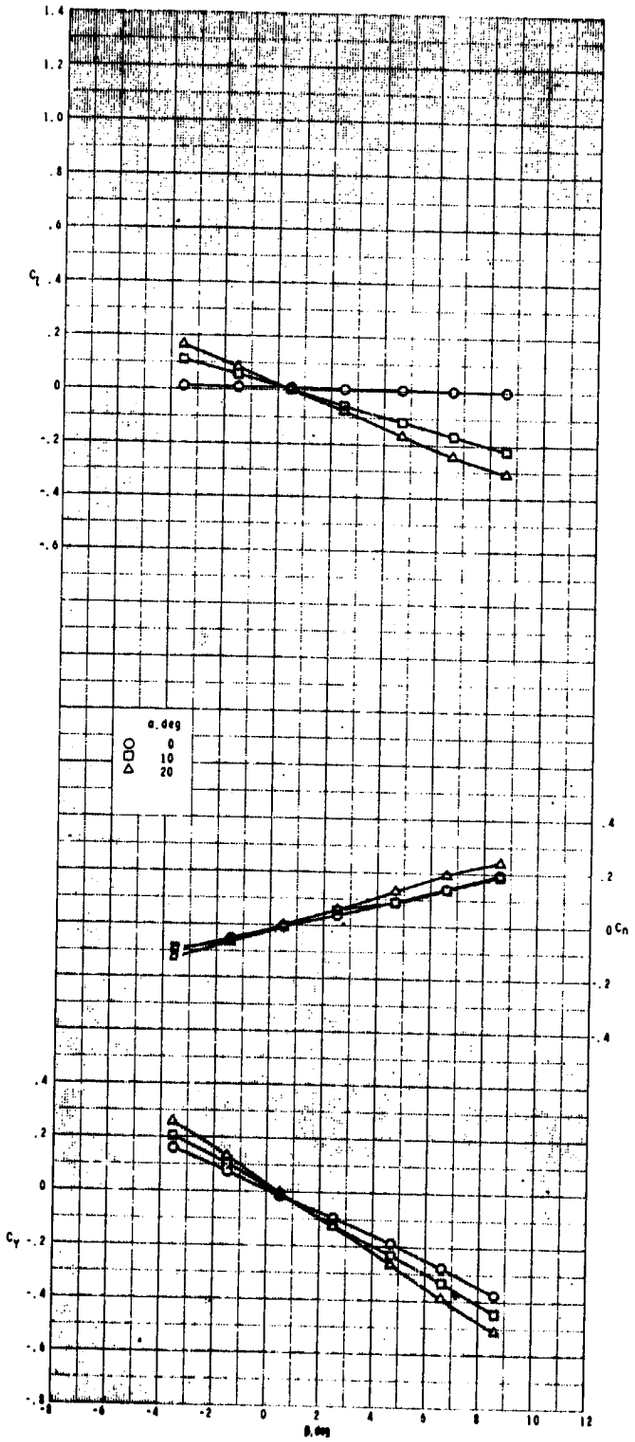

(i) M = 3.95.

Figure 16.- Continued.

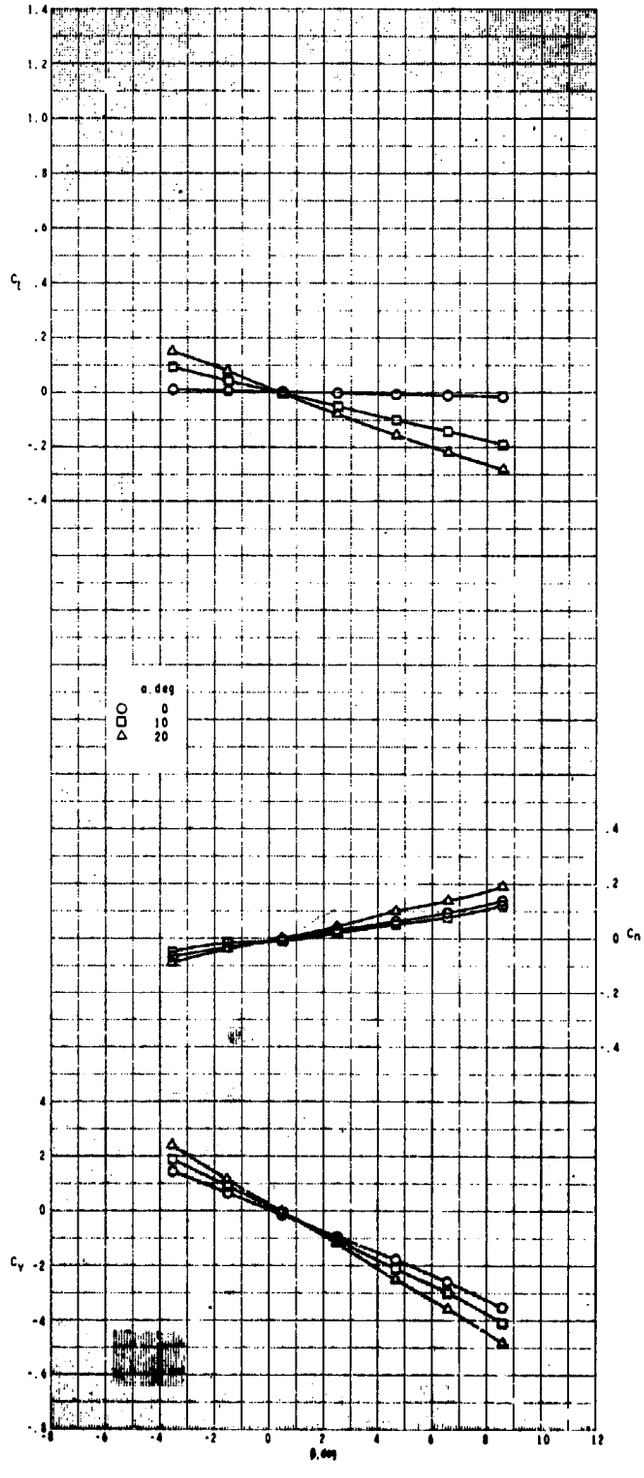

(j) M = 4.63.

Figure 16.- Concluded.

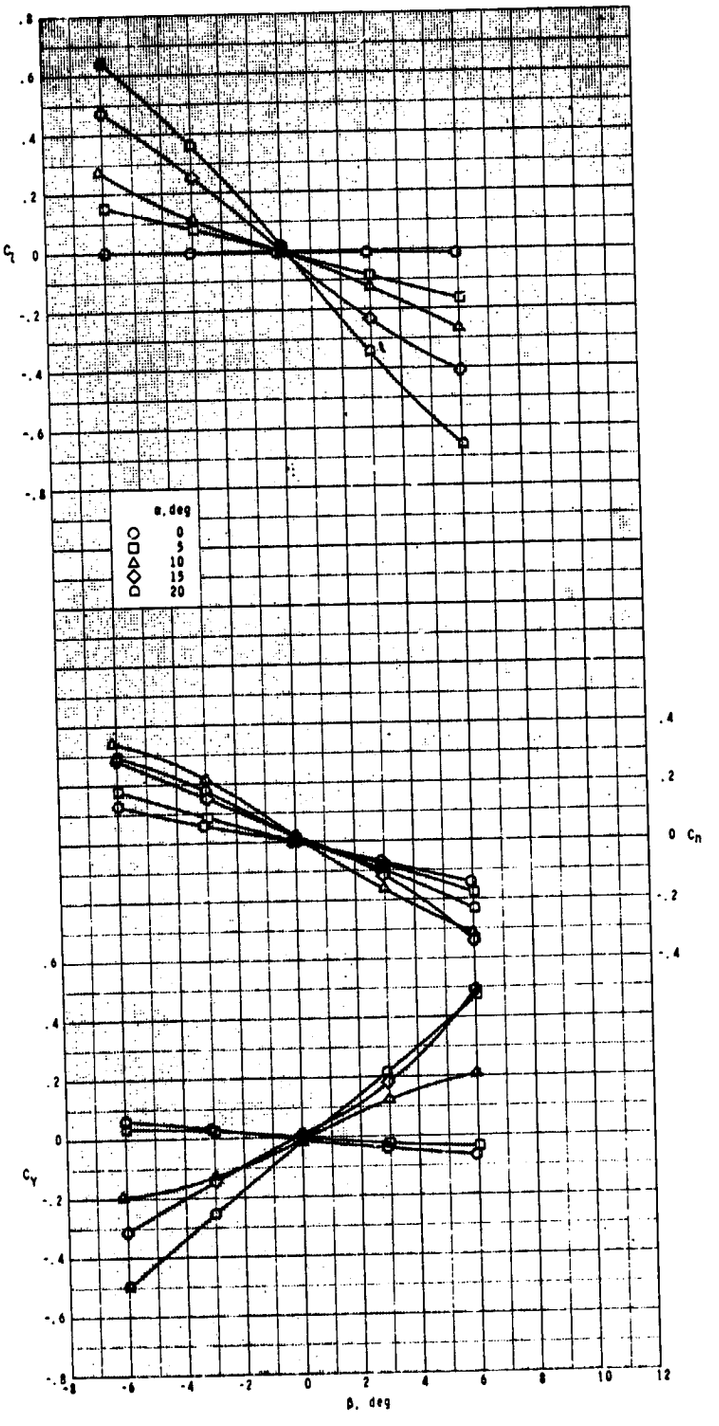

(a) M = 0.5.

Figure 17.- Effect of angle of attack on lateral aerodynamic characteristics of elliptical cross-section body-wing-tail configuration with angle of sideslip.

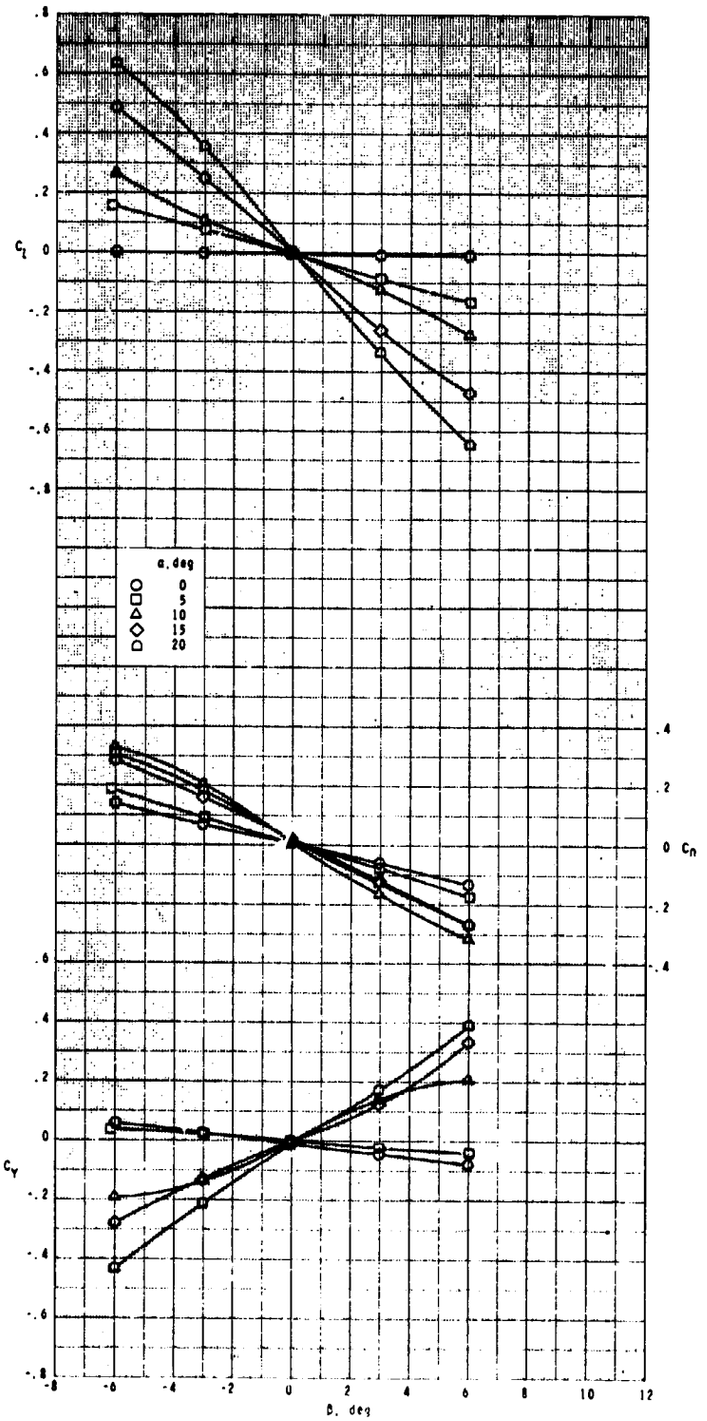

(b) M = 0.7.

Figure 17.- Continued.

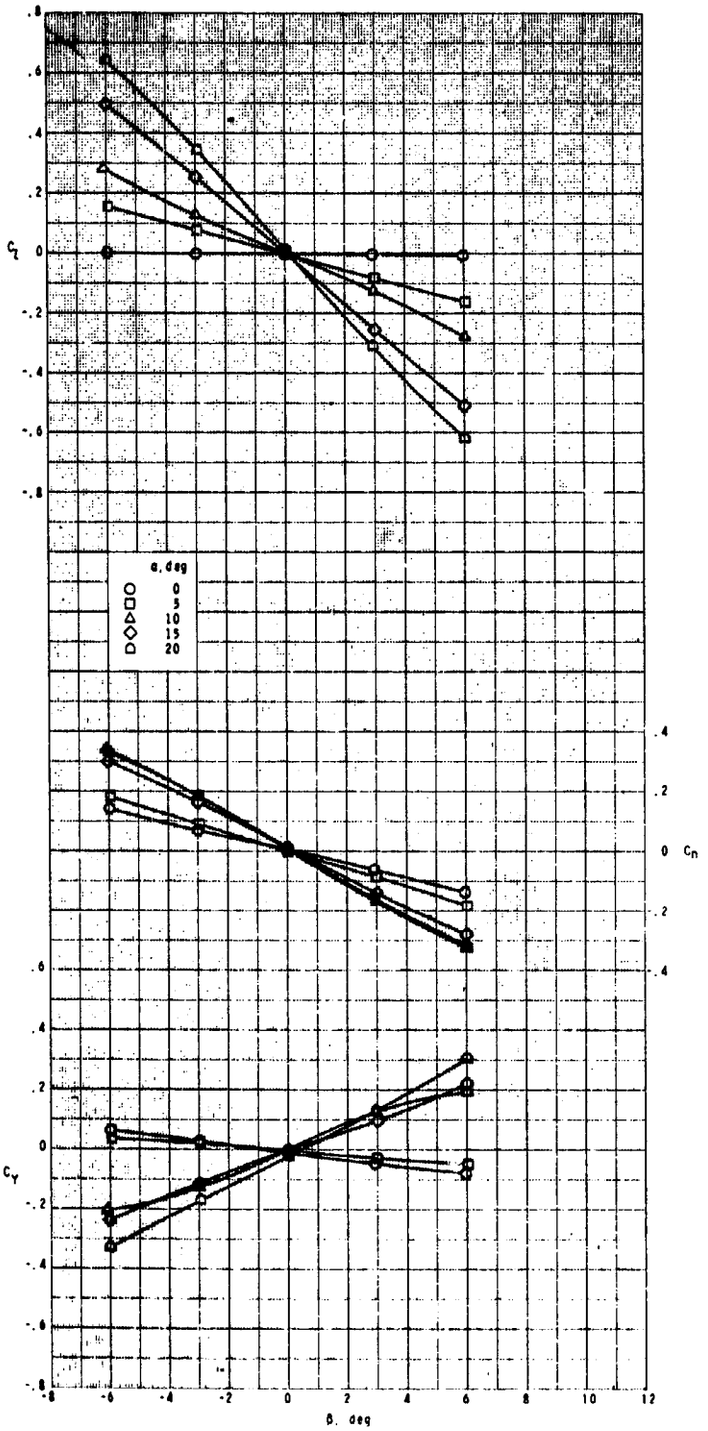

(c) M = 0.9.

Figure 17.- Continued.

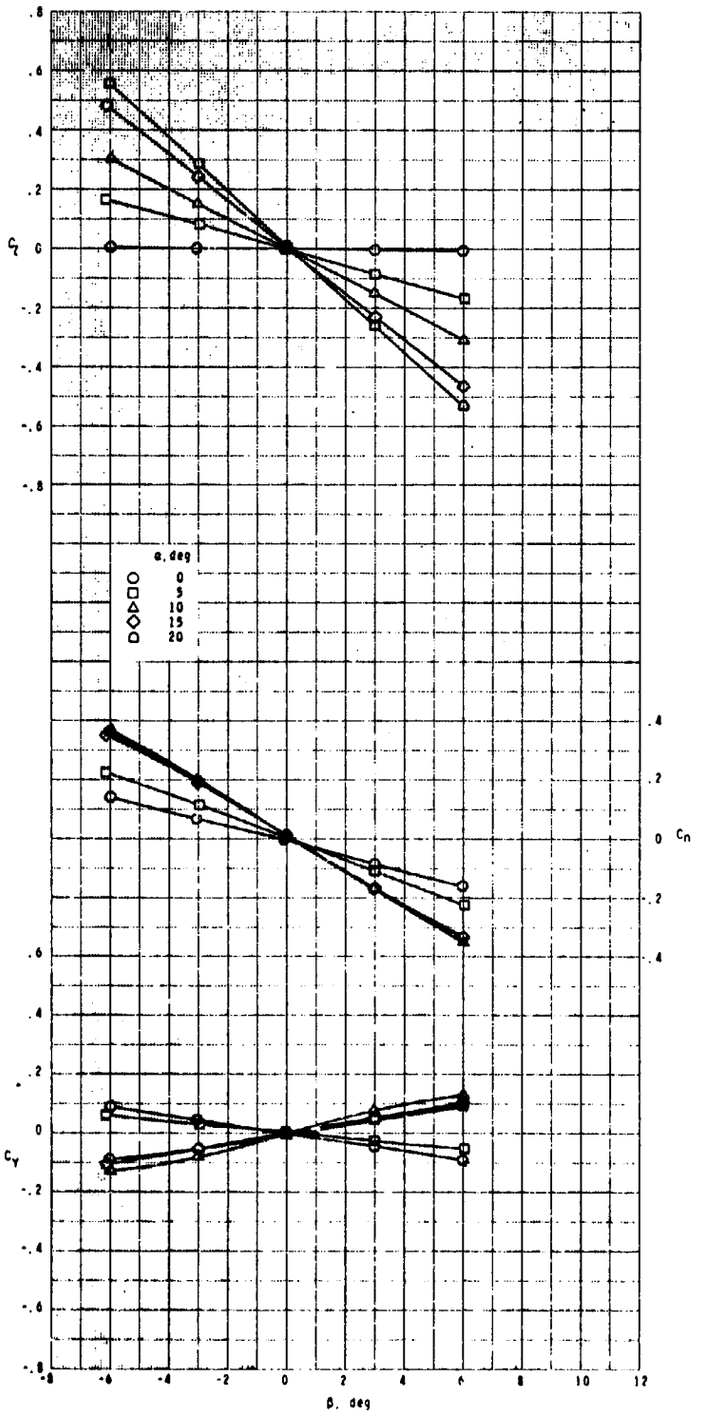

(d) M = 1.3.

Figure 17.- Continued.

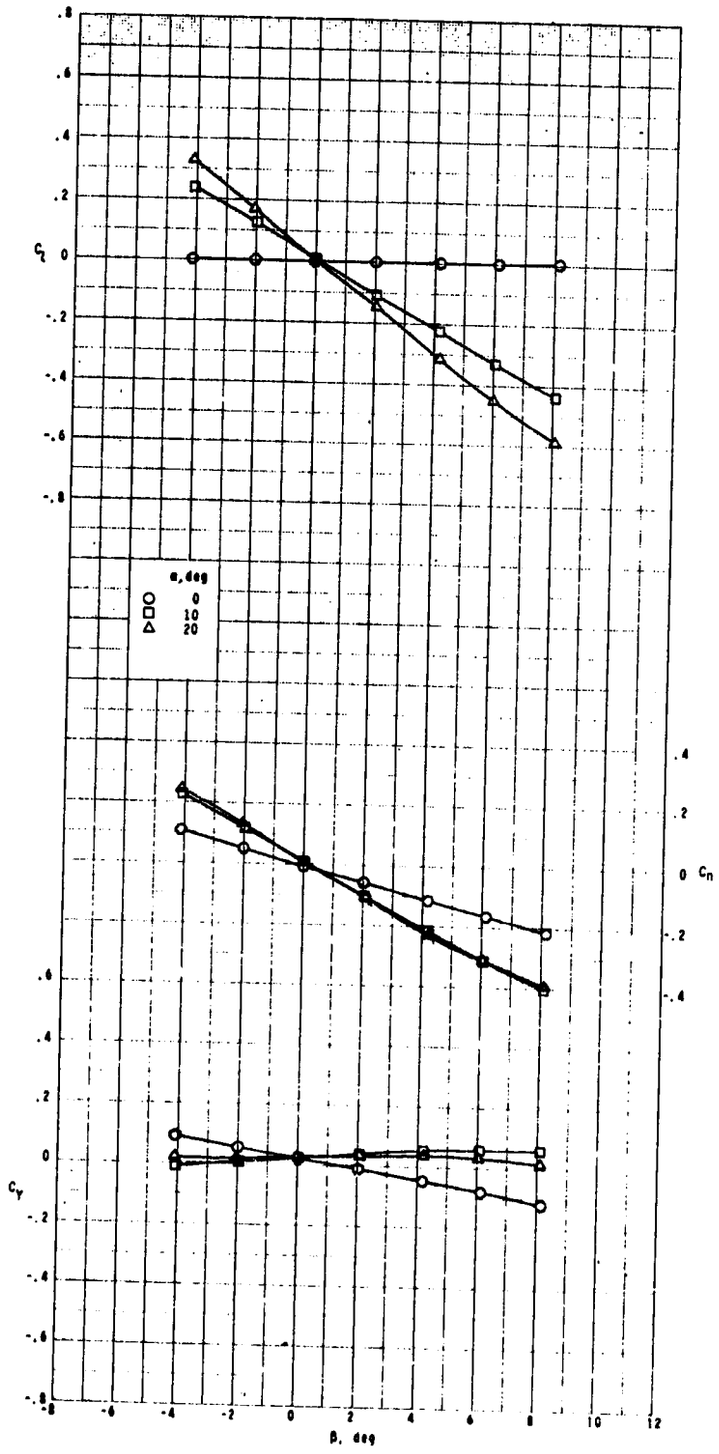

(e) M = 1.60.

Figure 17.- Continued.

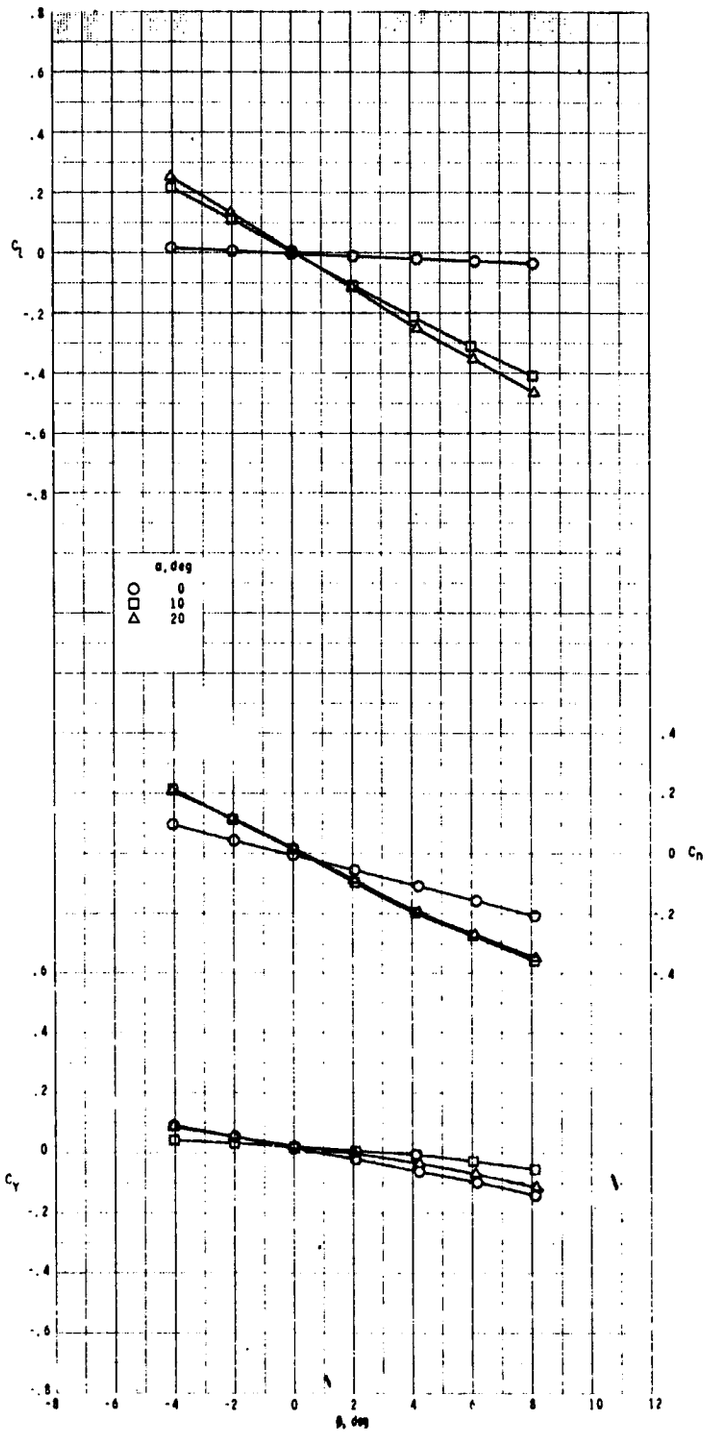

(f) M = 2.00.

Figure 17.- Continued.

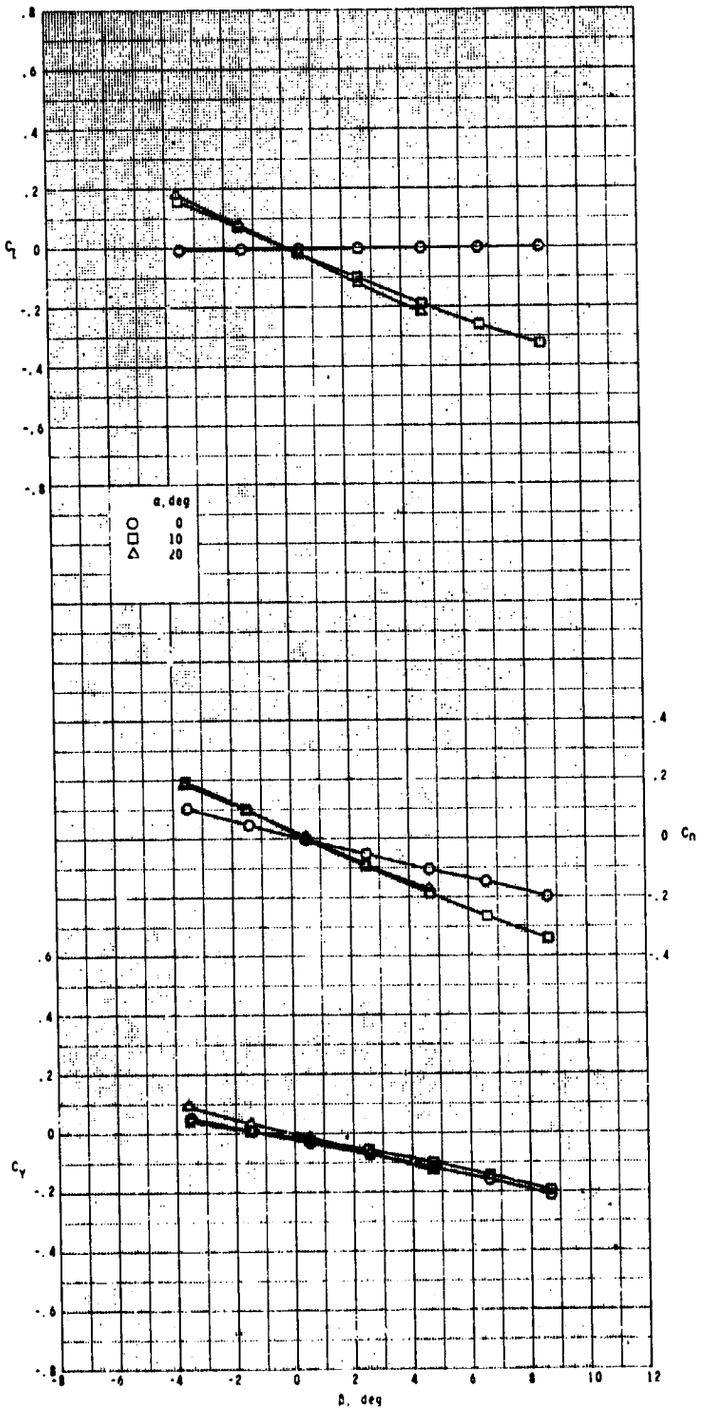

(g) M = 2.50.

Figure 17.- Continued.

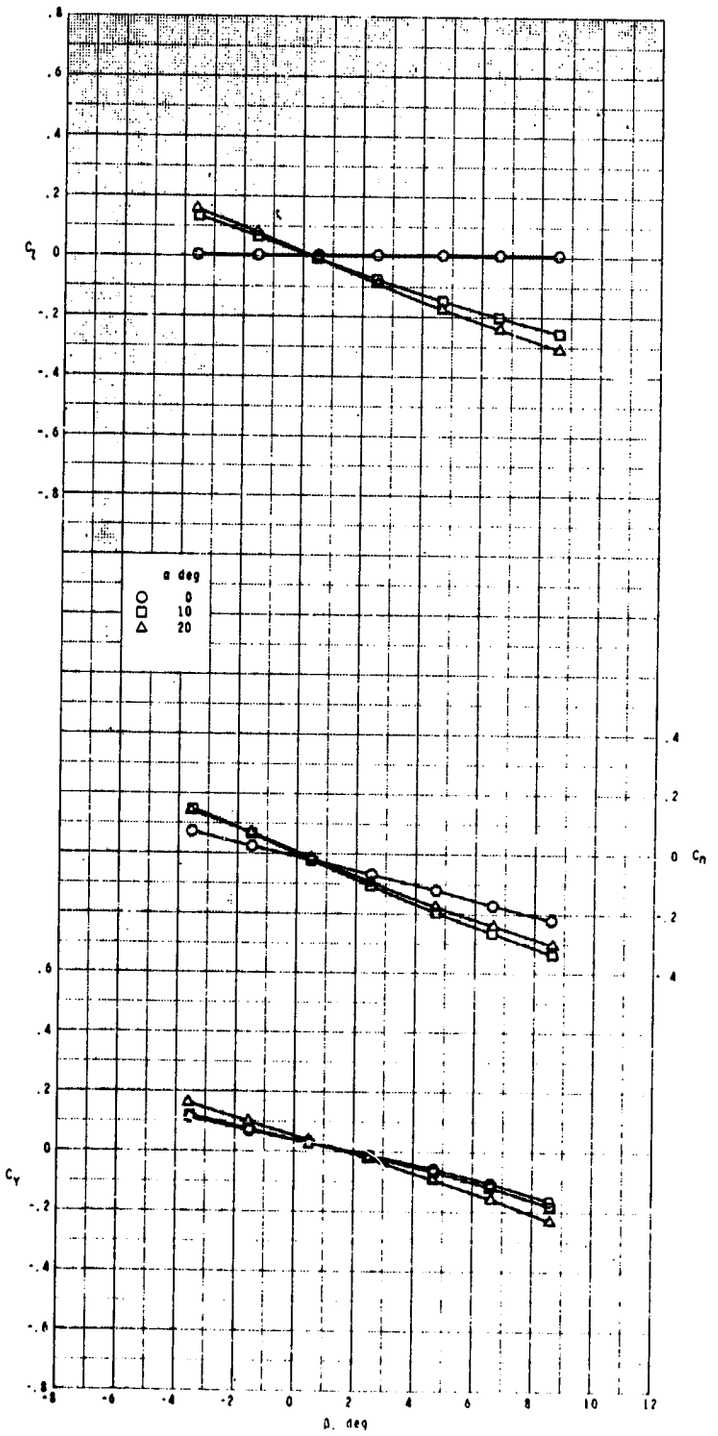

(h) M = 2.96.

Figure 17.- Continued.

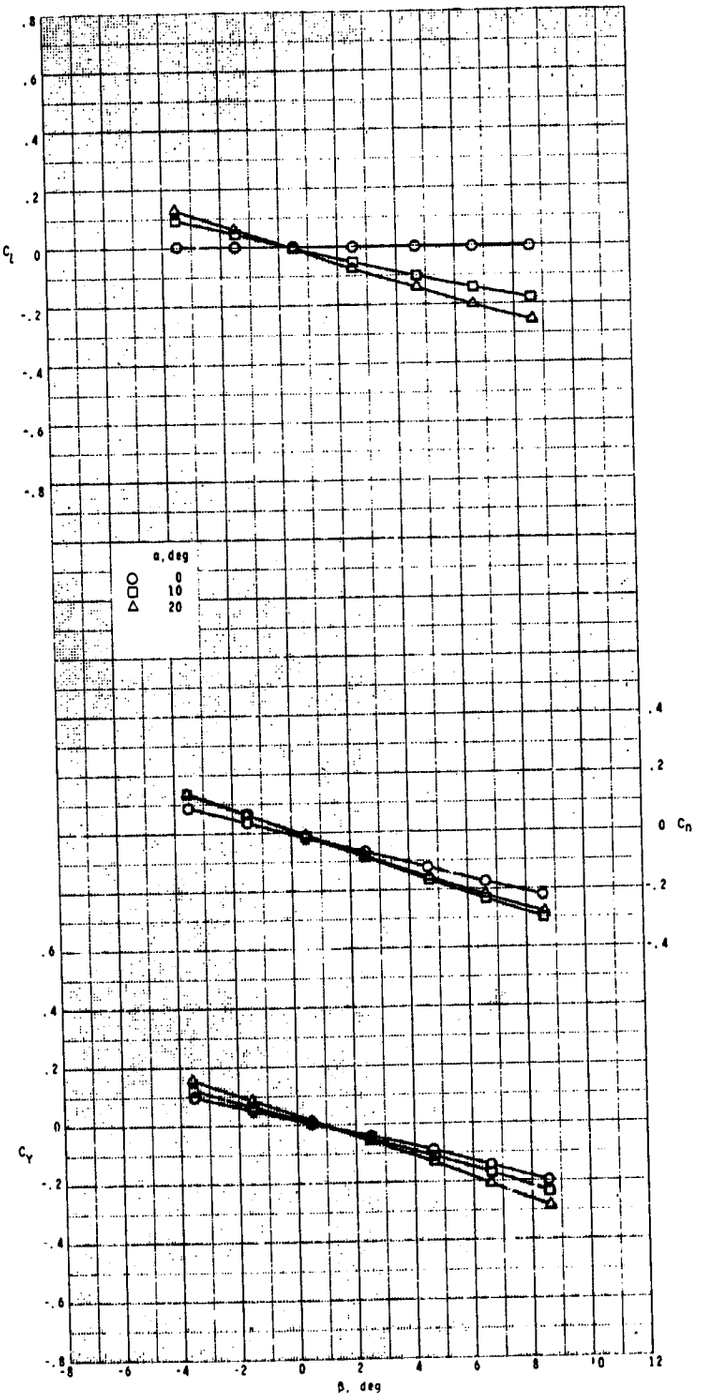

(i) M = 3.95.

Figure 17.- Continued.

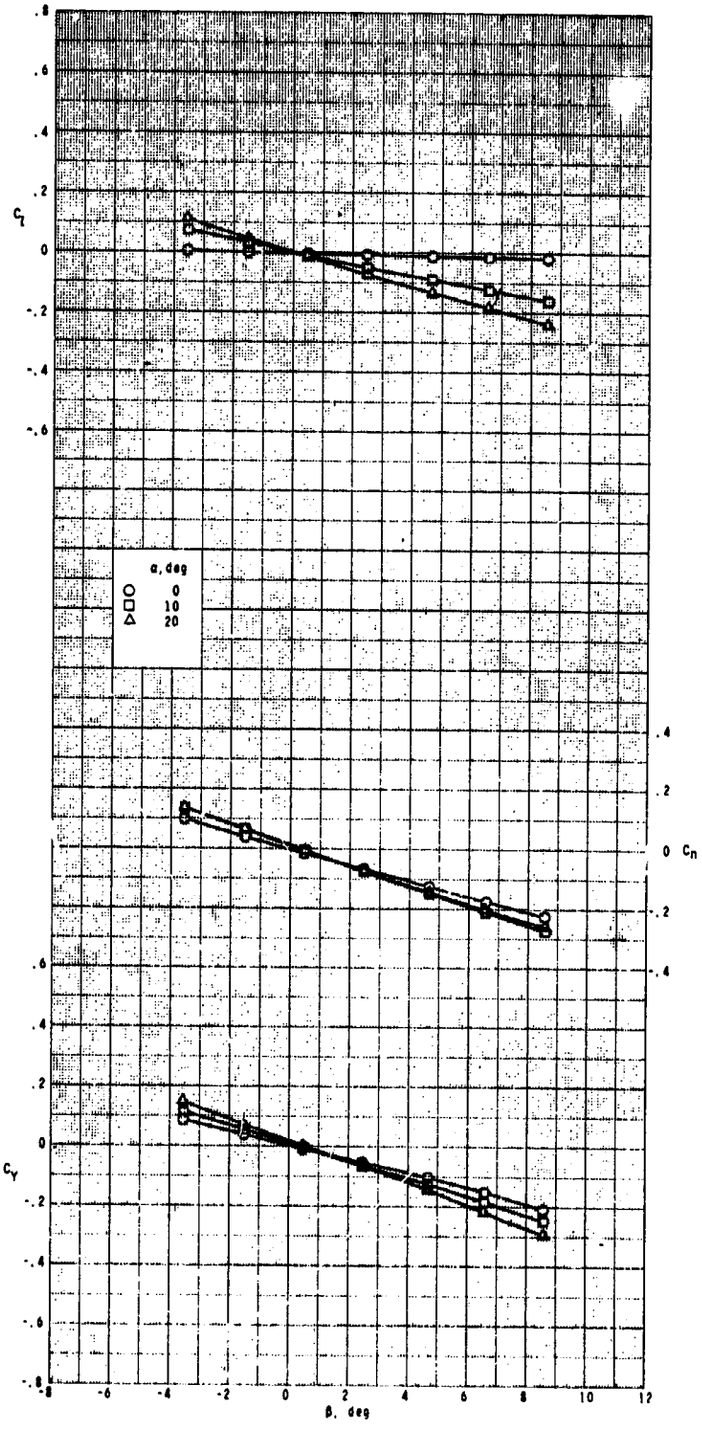

(j) M = 4.63.

Figure 17.- Concluded.

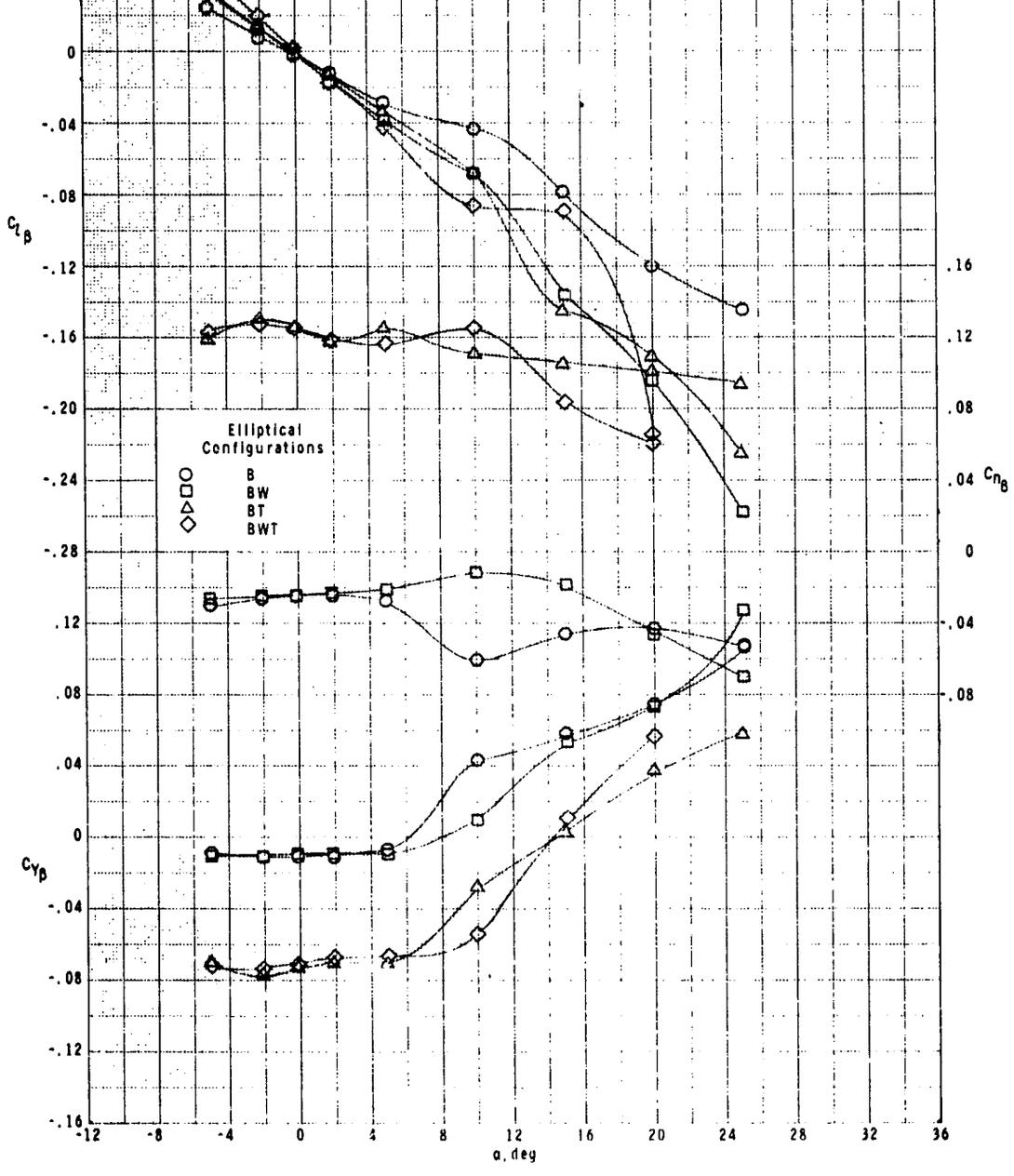

(a) M = 0.5.

Figure 18.- Effect of components on lateral-directional stability parameters of elliptical cross-section model with variation in angle of attack.

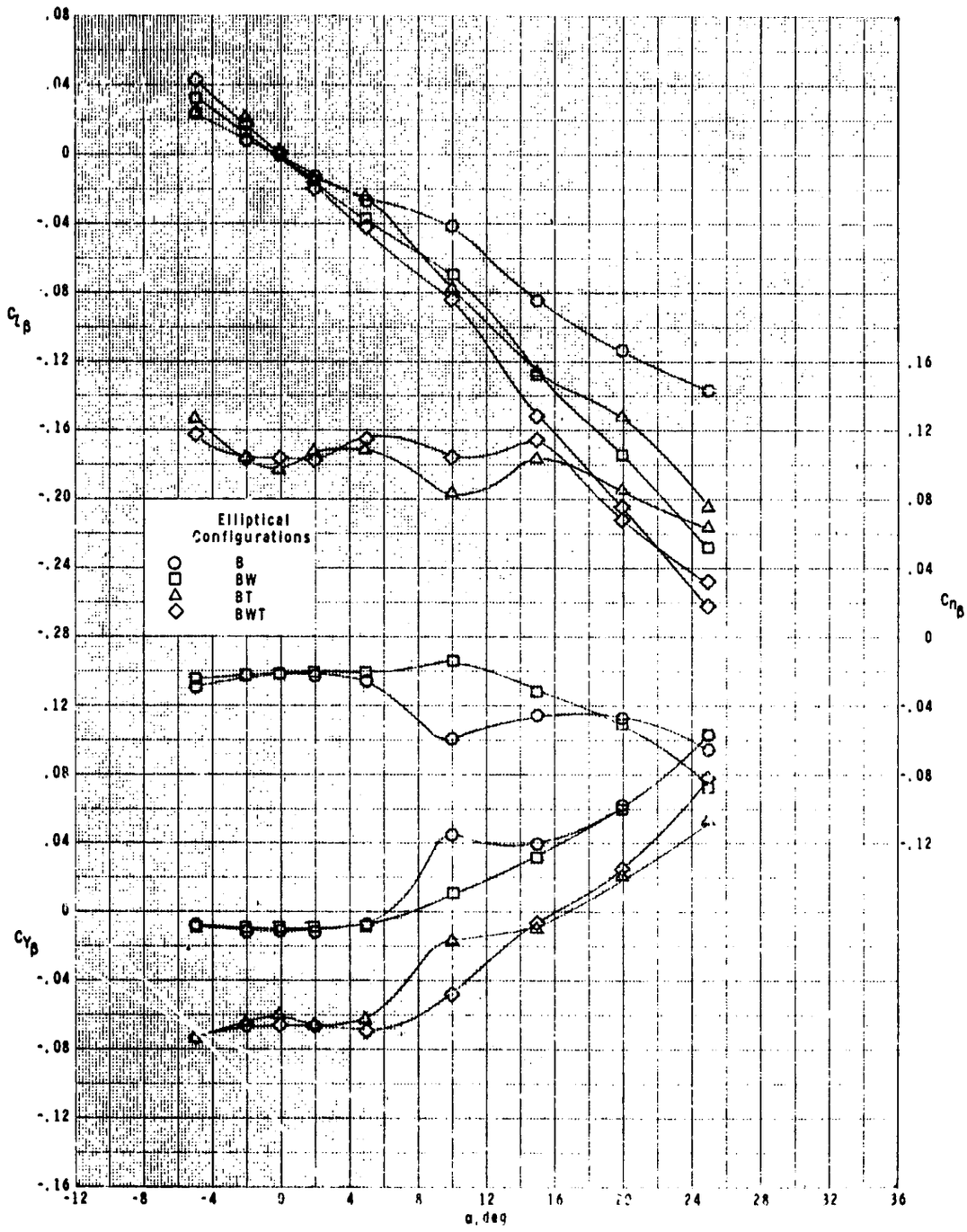

(b) M = 0.7.

Figure 18.- Continued.

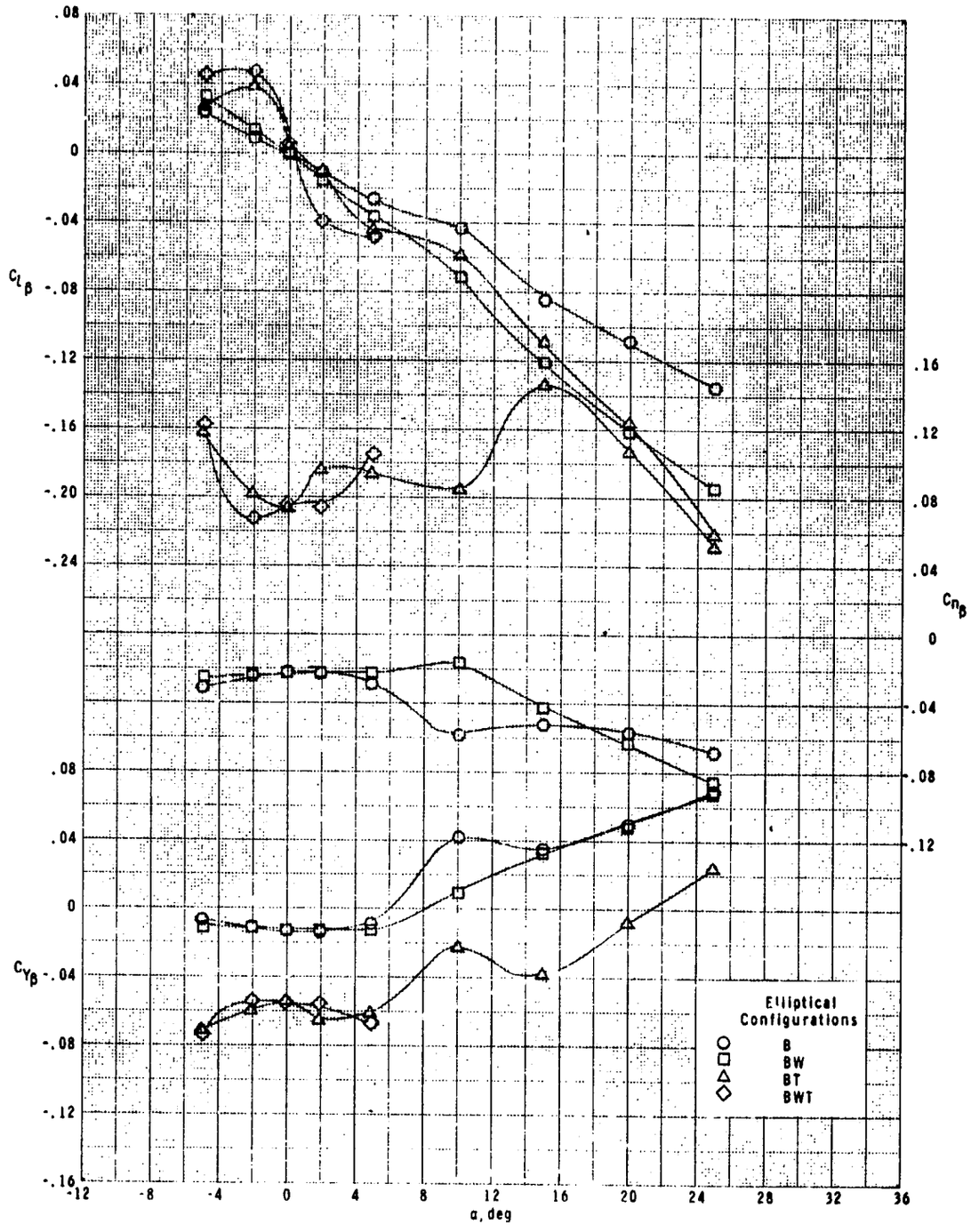

(e) M = 0.9.

Figure 18.- Continued.

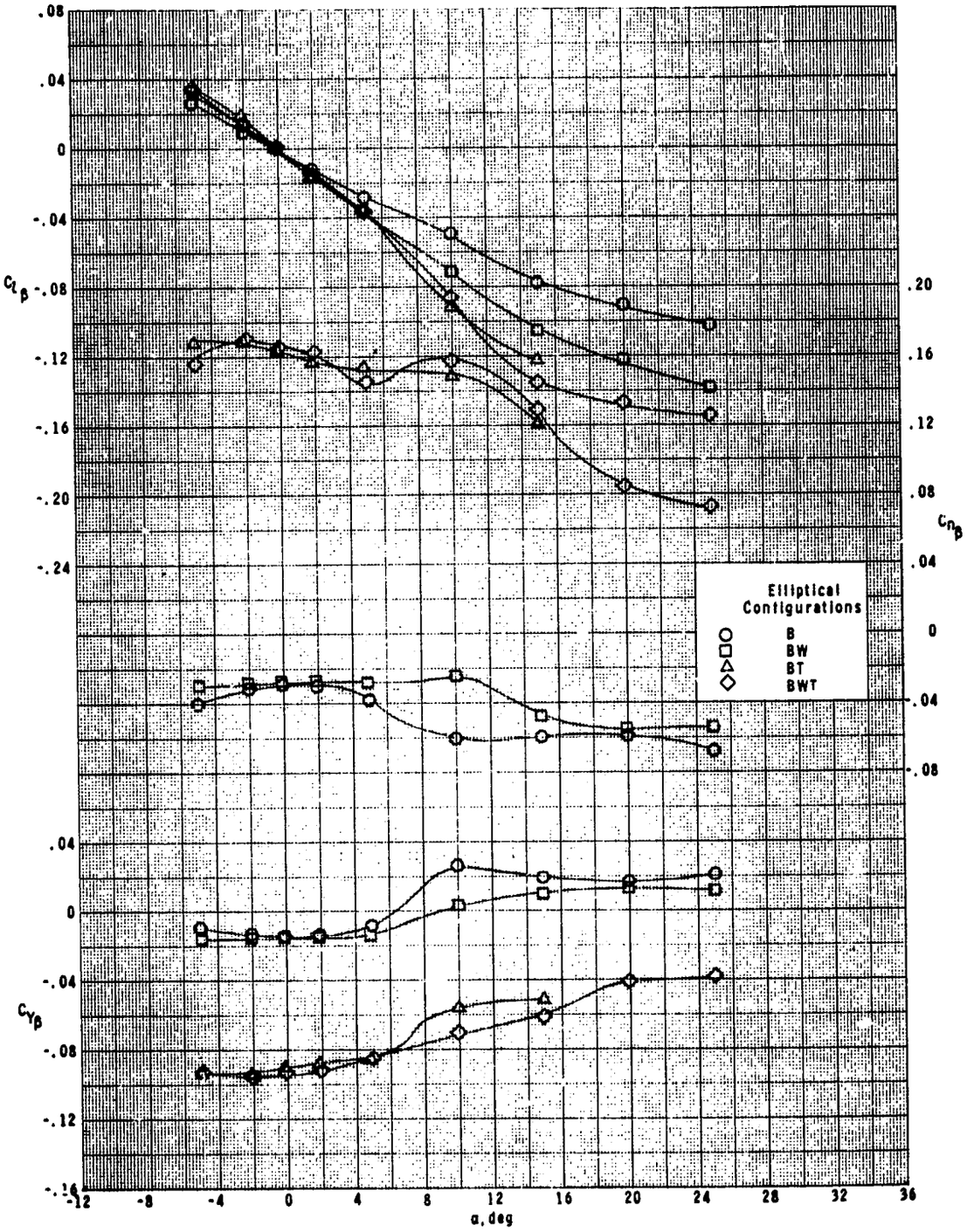

(d) M = 1.3.

Figure 18.- Continued.

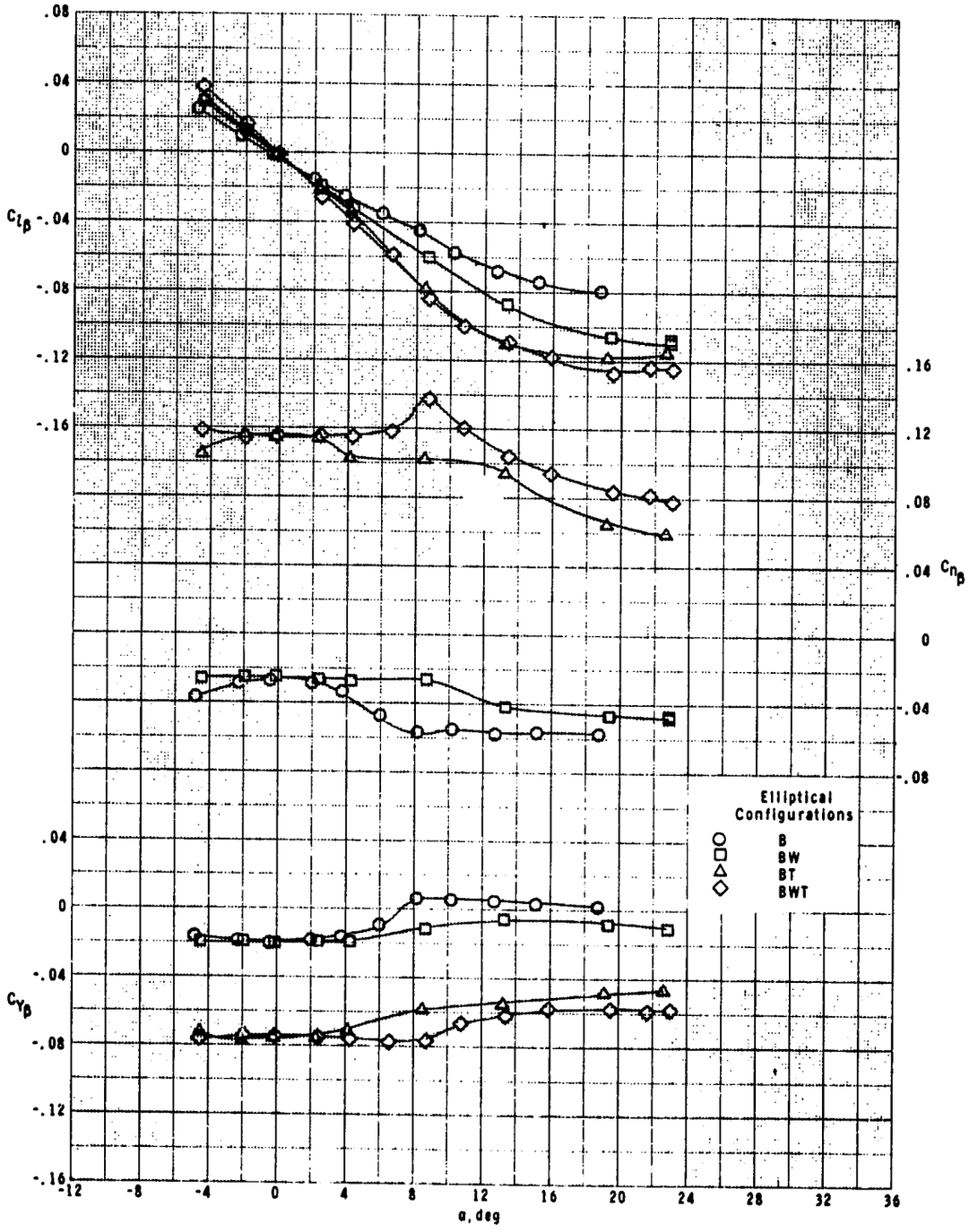

(e) M = 1.60.

Figure 18.- Continued.

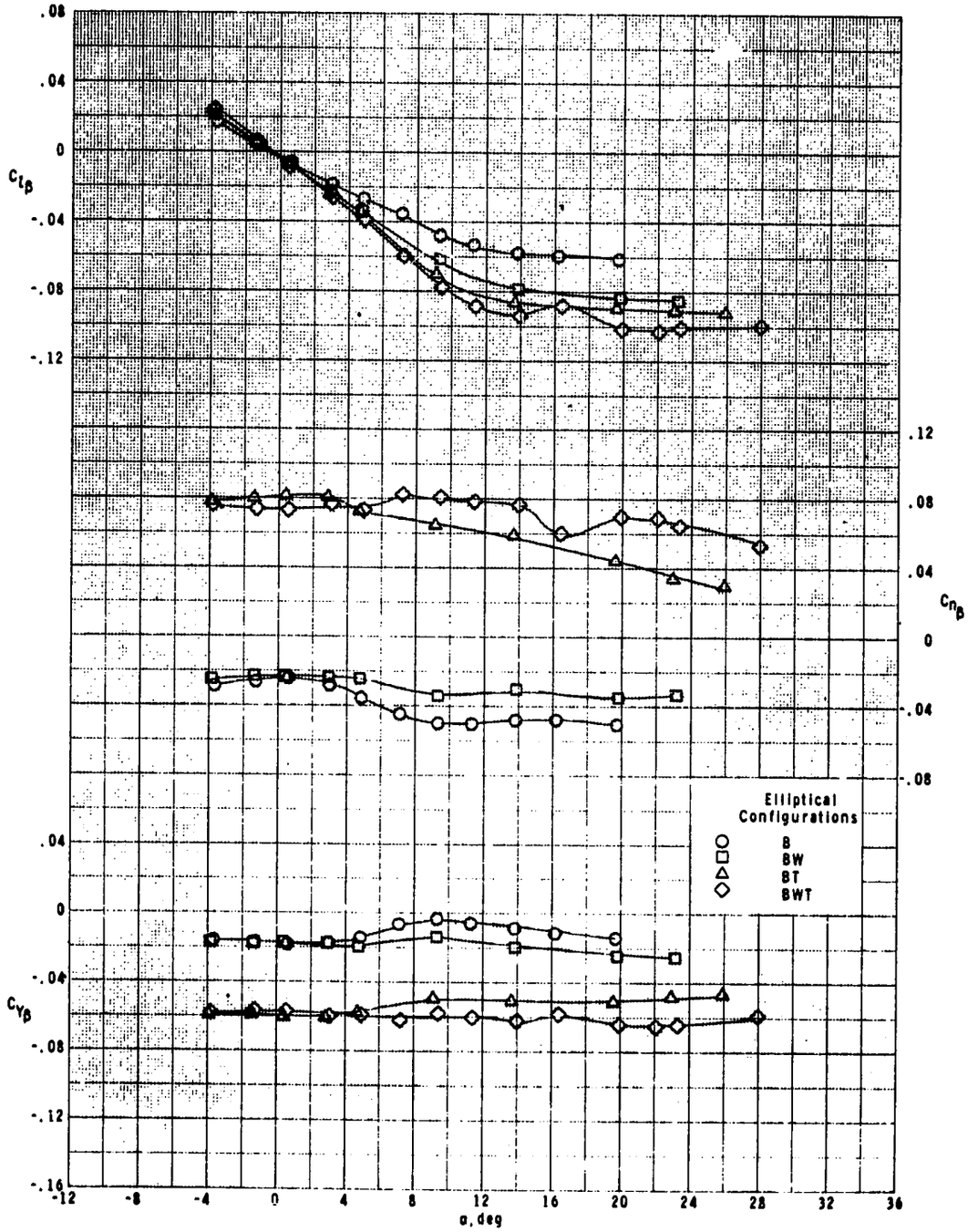

(f) M = 2.00.

Figure 18.- Continued.

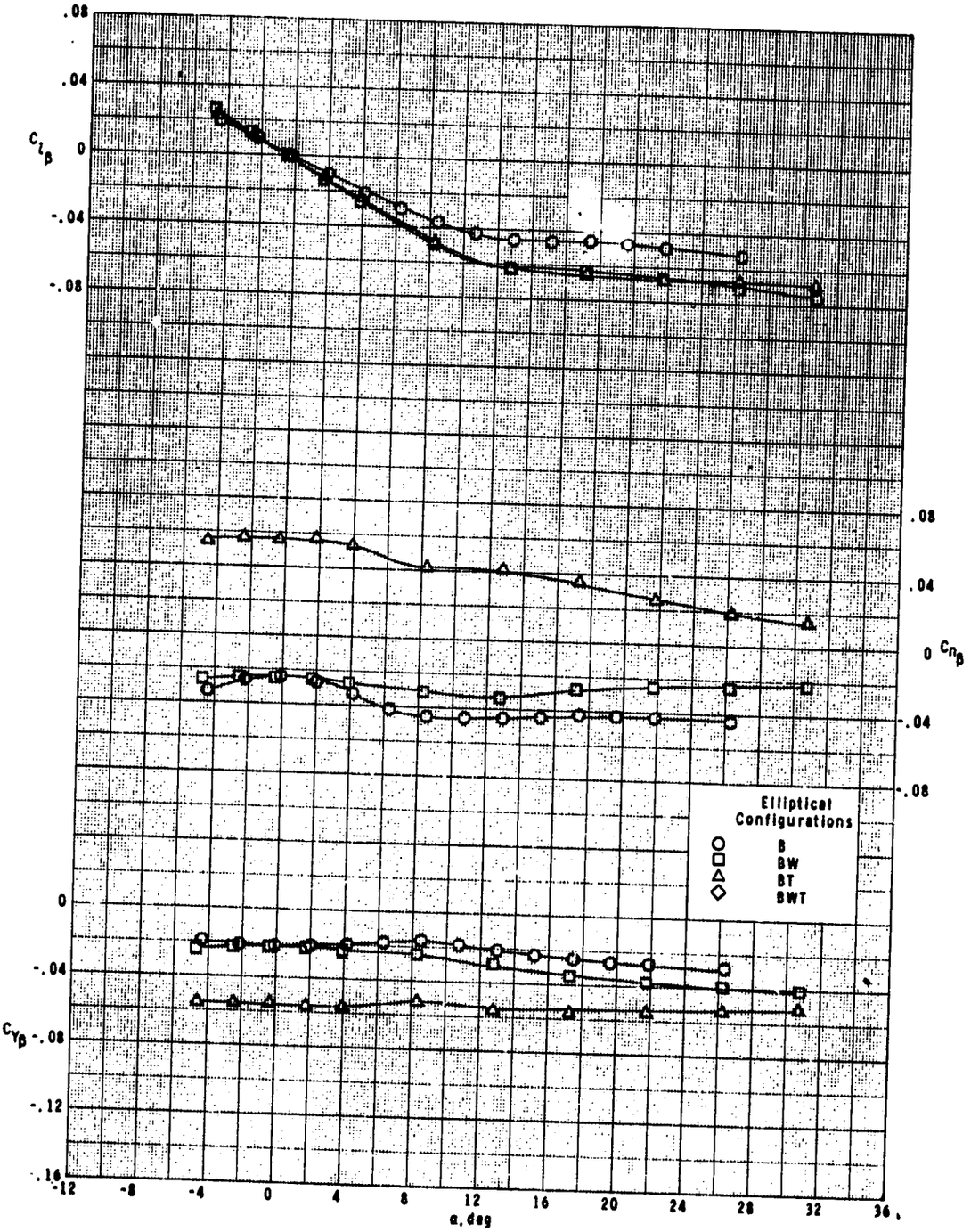

(g) M = 2.50.

Figure 18.- Continued.

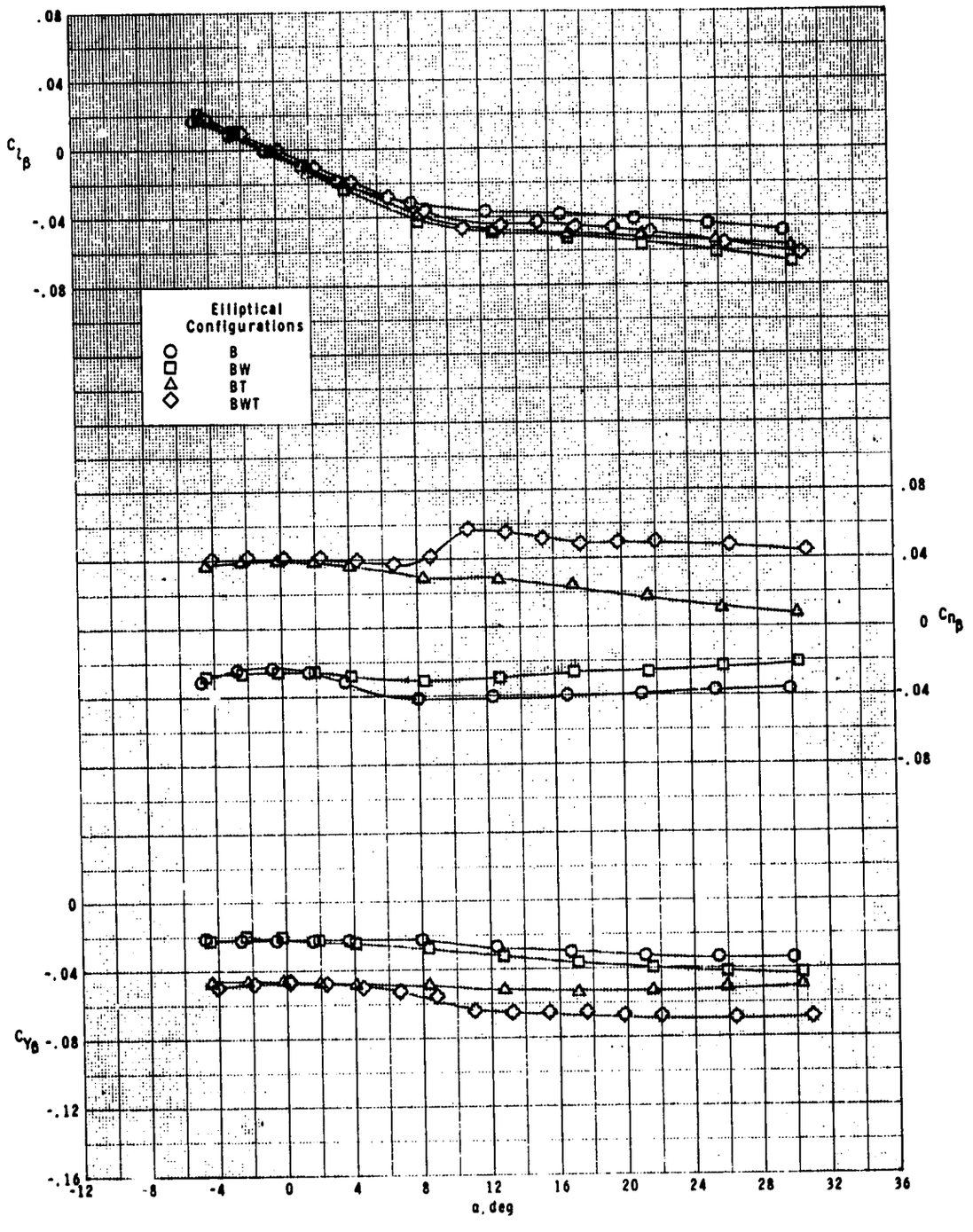

(h) M = 2.96.

Figure 18.- Continued.

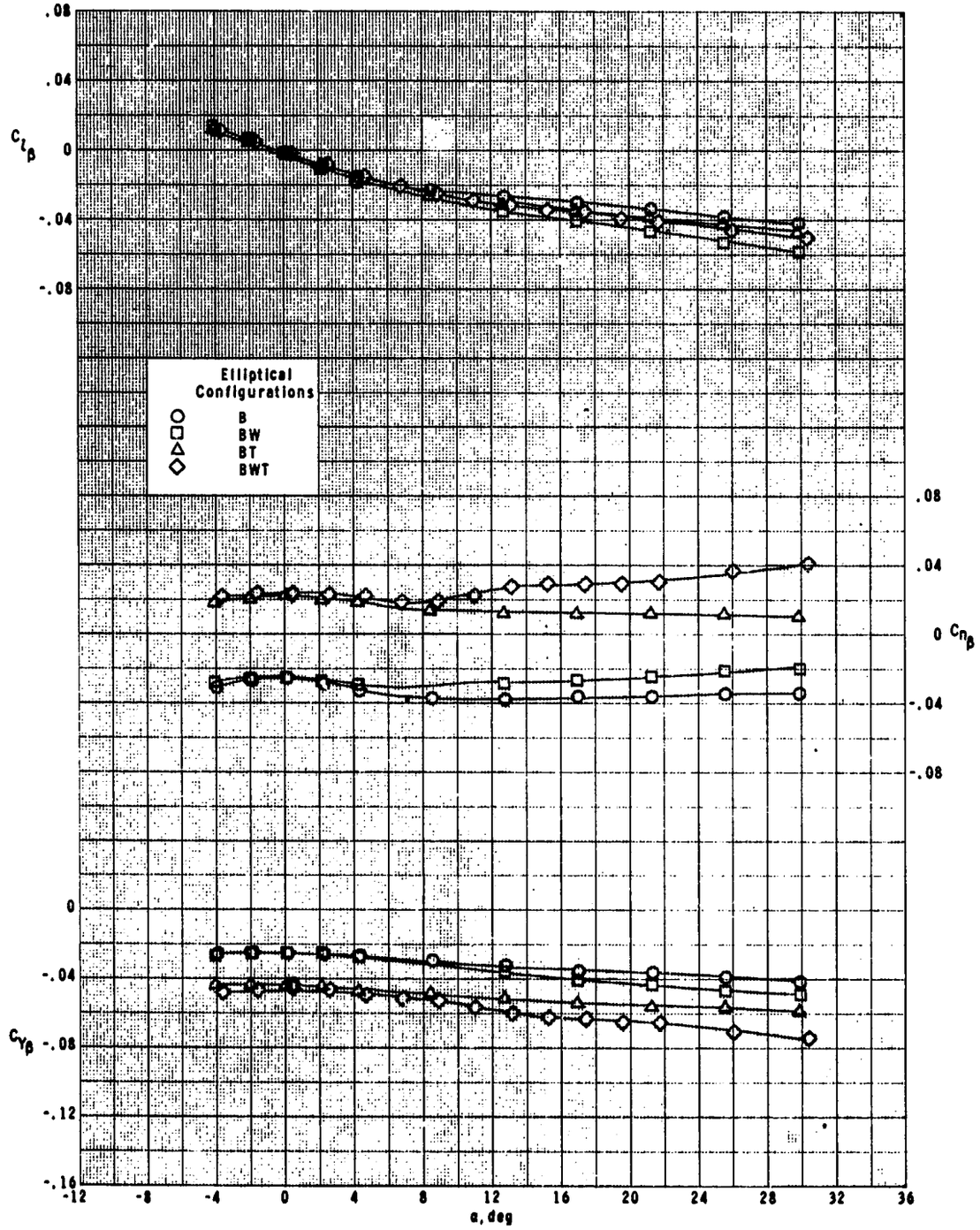

(i) M = 3.95.

Figure 18.- Continued.

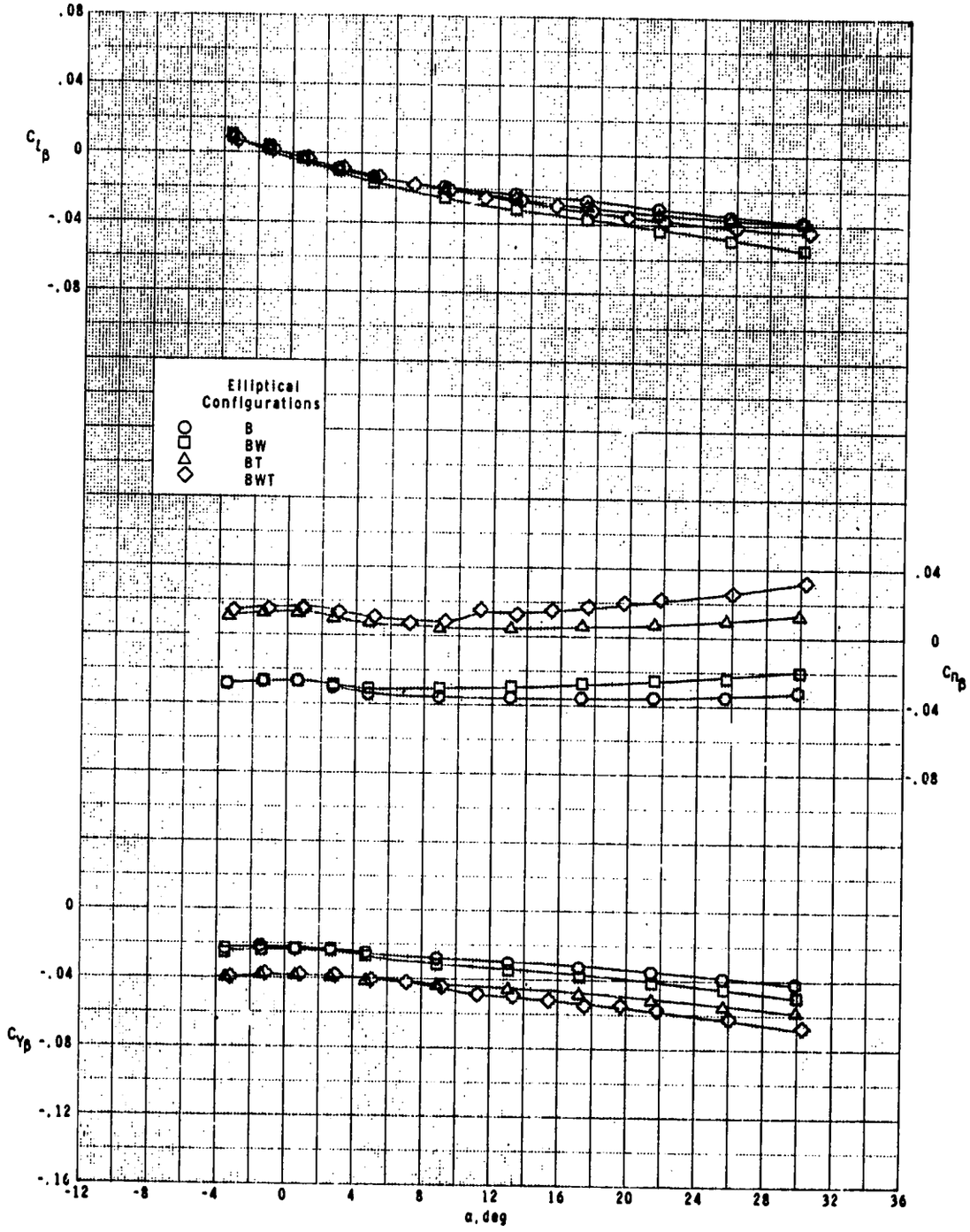

(j) M = 4.63.

Figure 18.- Concluded.

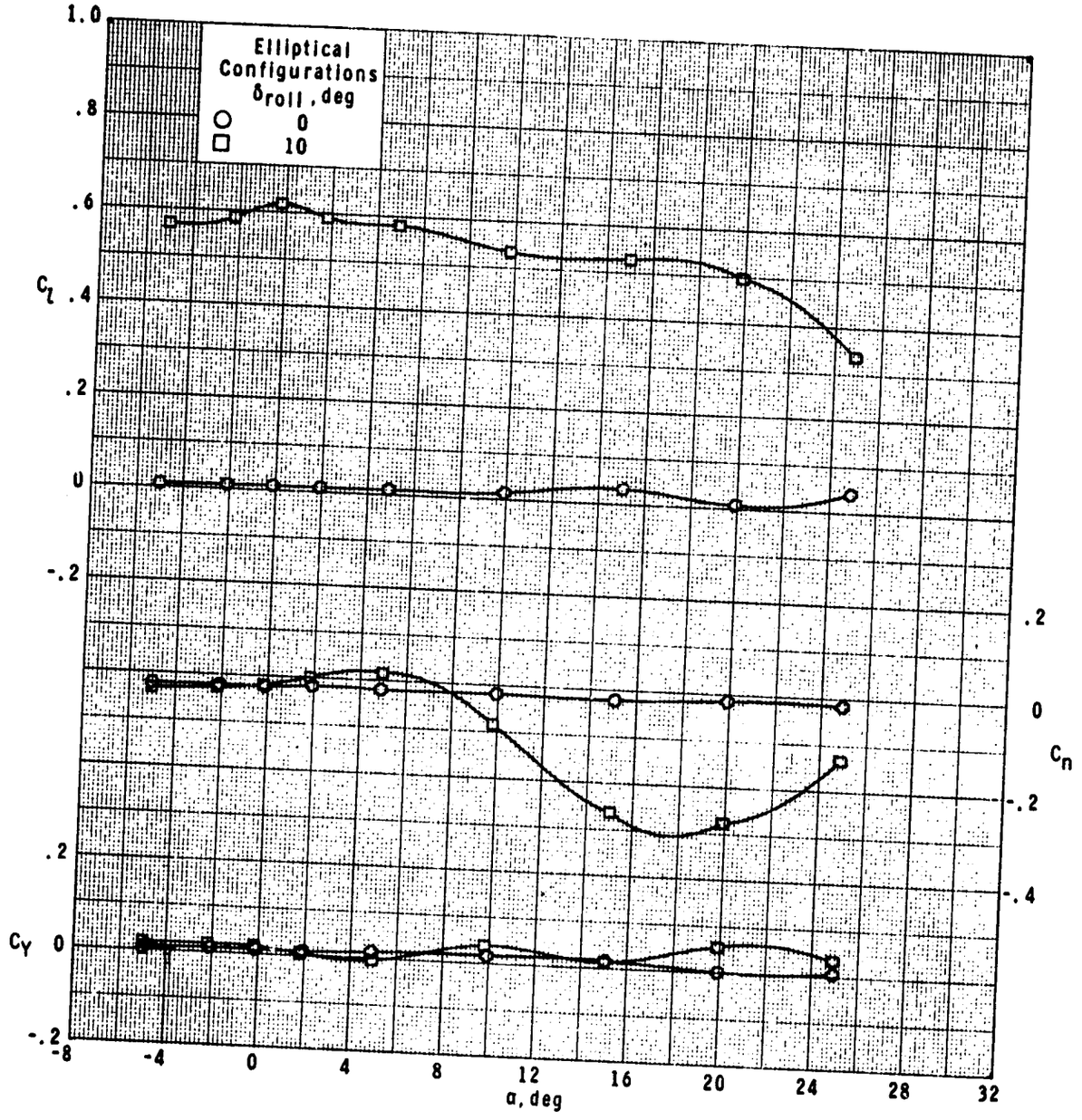

(a) M = 0.5.

Figure 19.- Roll-control effectiveness of elliptical cross-section body-wing-tail configuration with variation in angle of attack.

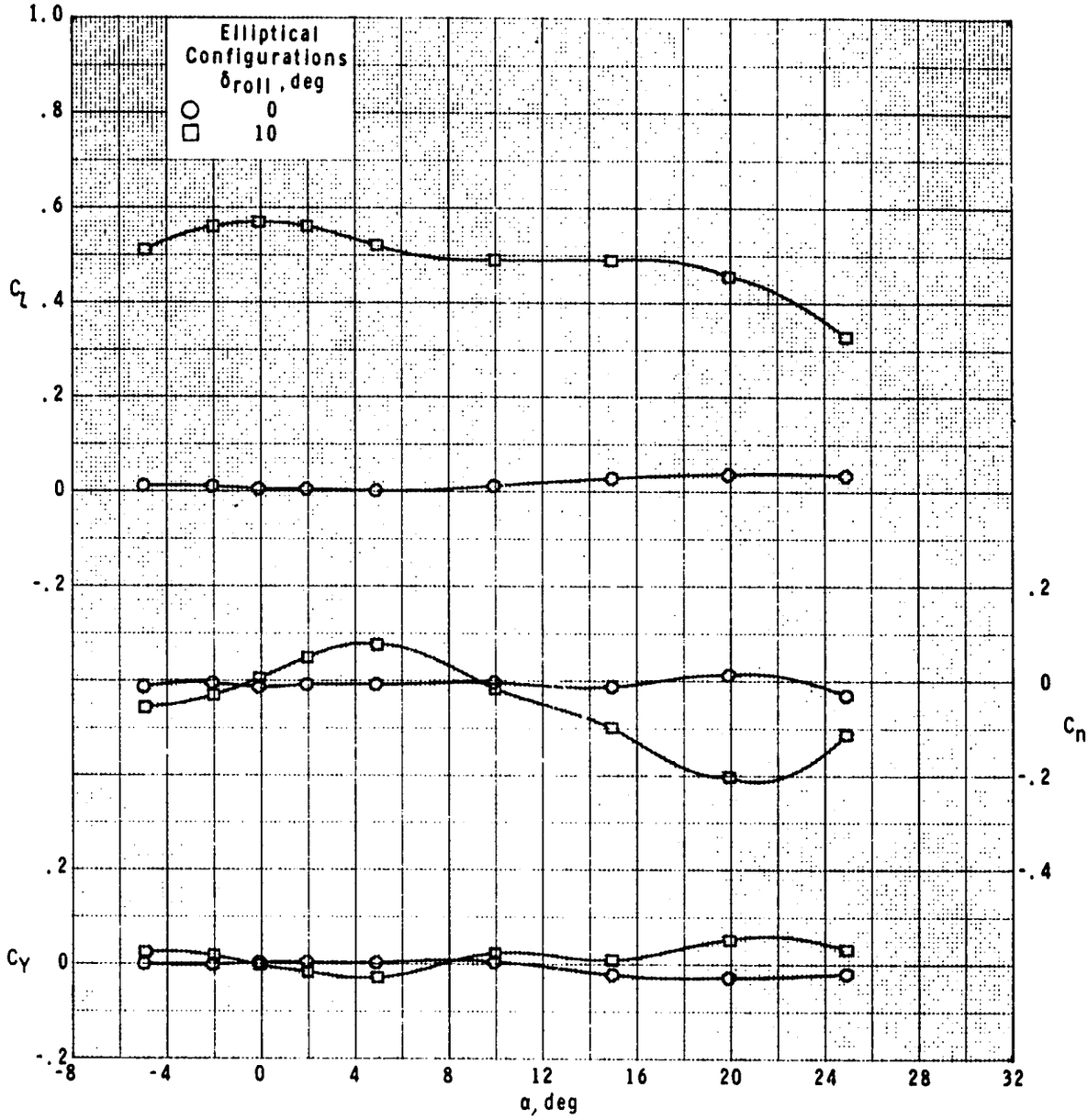

(b) M = 0.7.

Figure 19.- Continued.

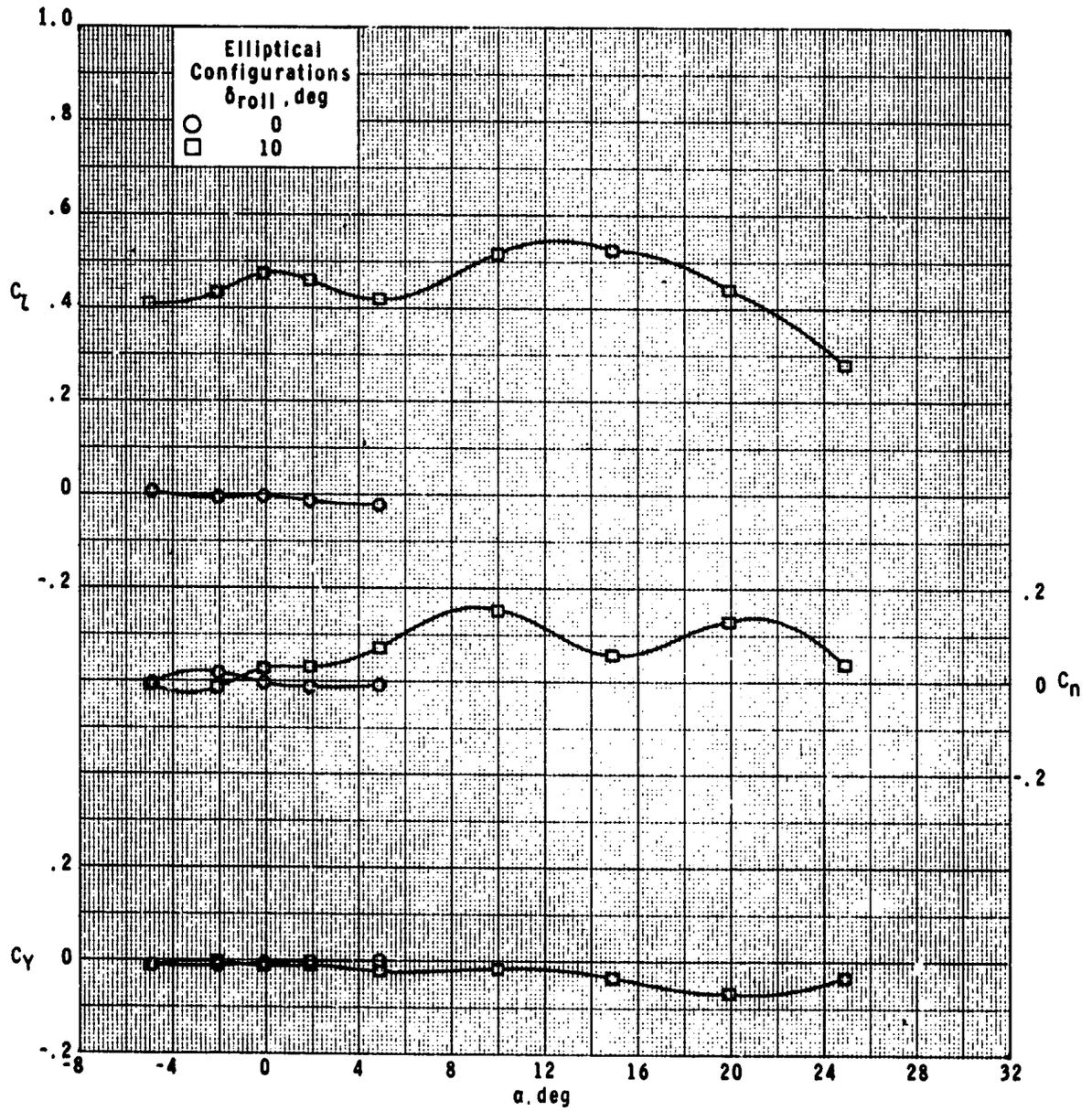

(c) M = 0.9.

Figure 19.- Continued.

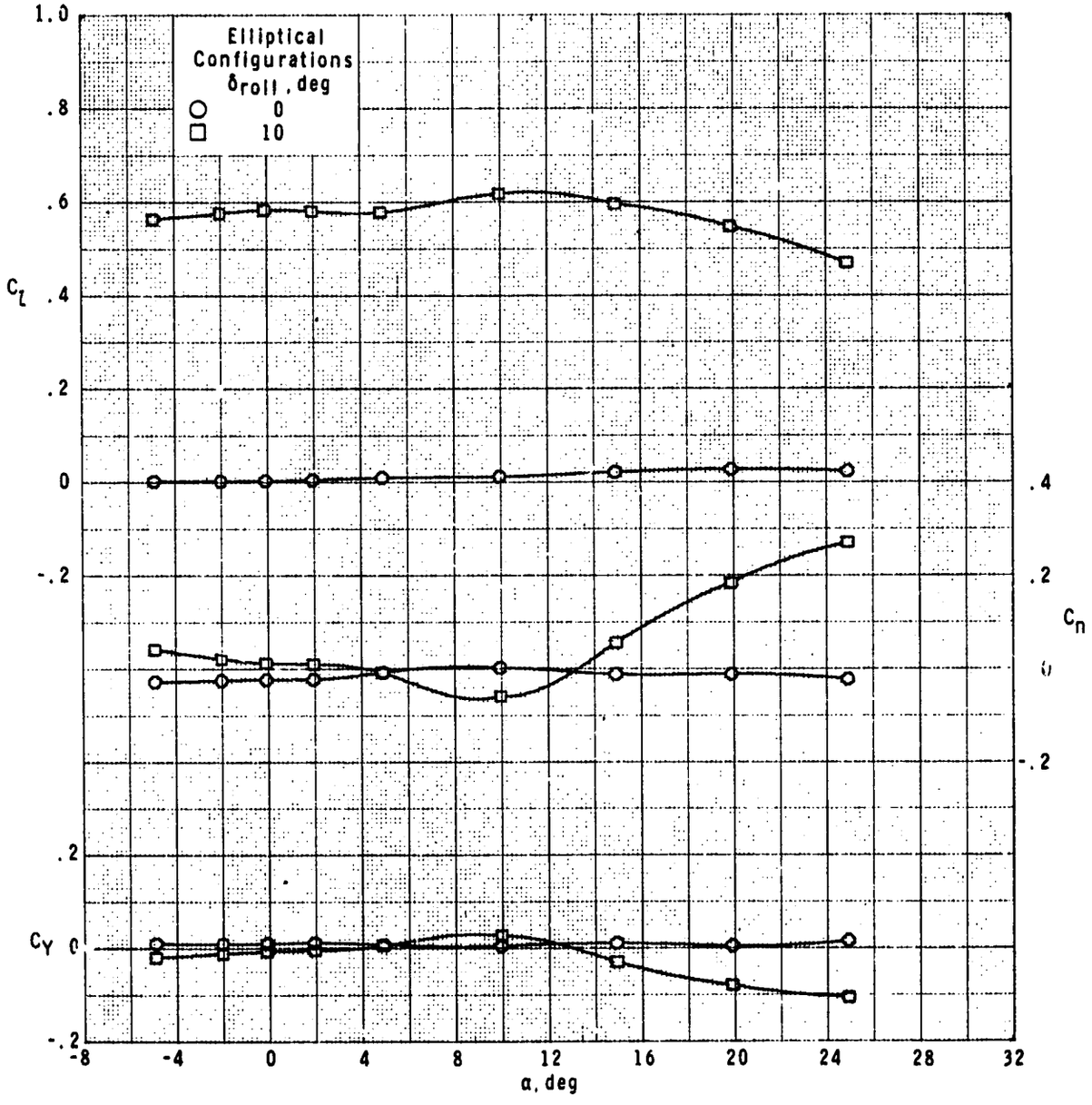

(d) M = 1.3.

Figure 19.- Continued.

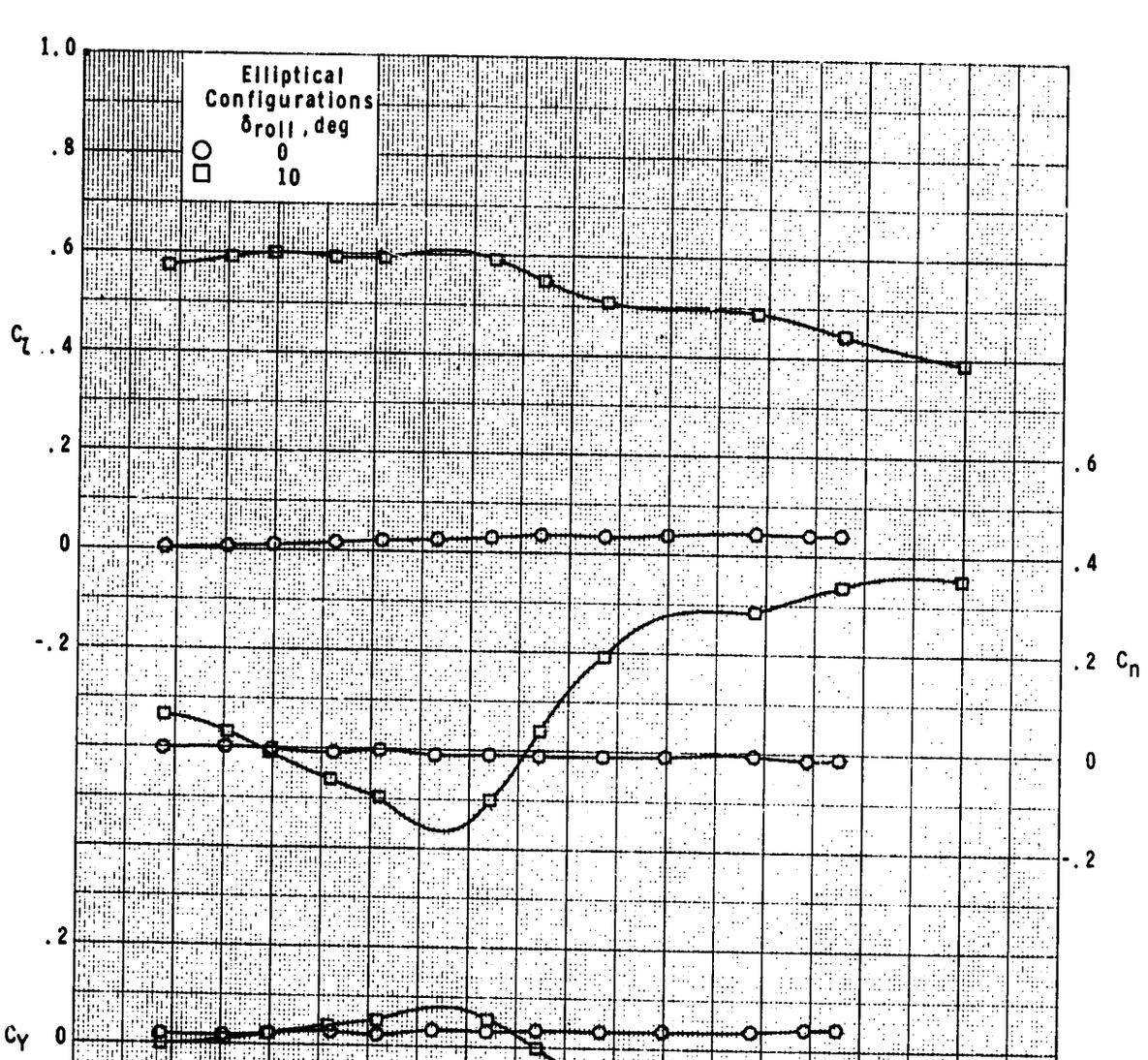

(e) M = 1.60.

Figure 19.- Continued.

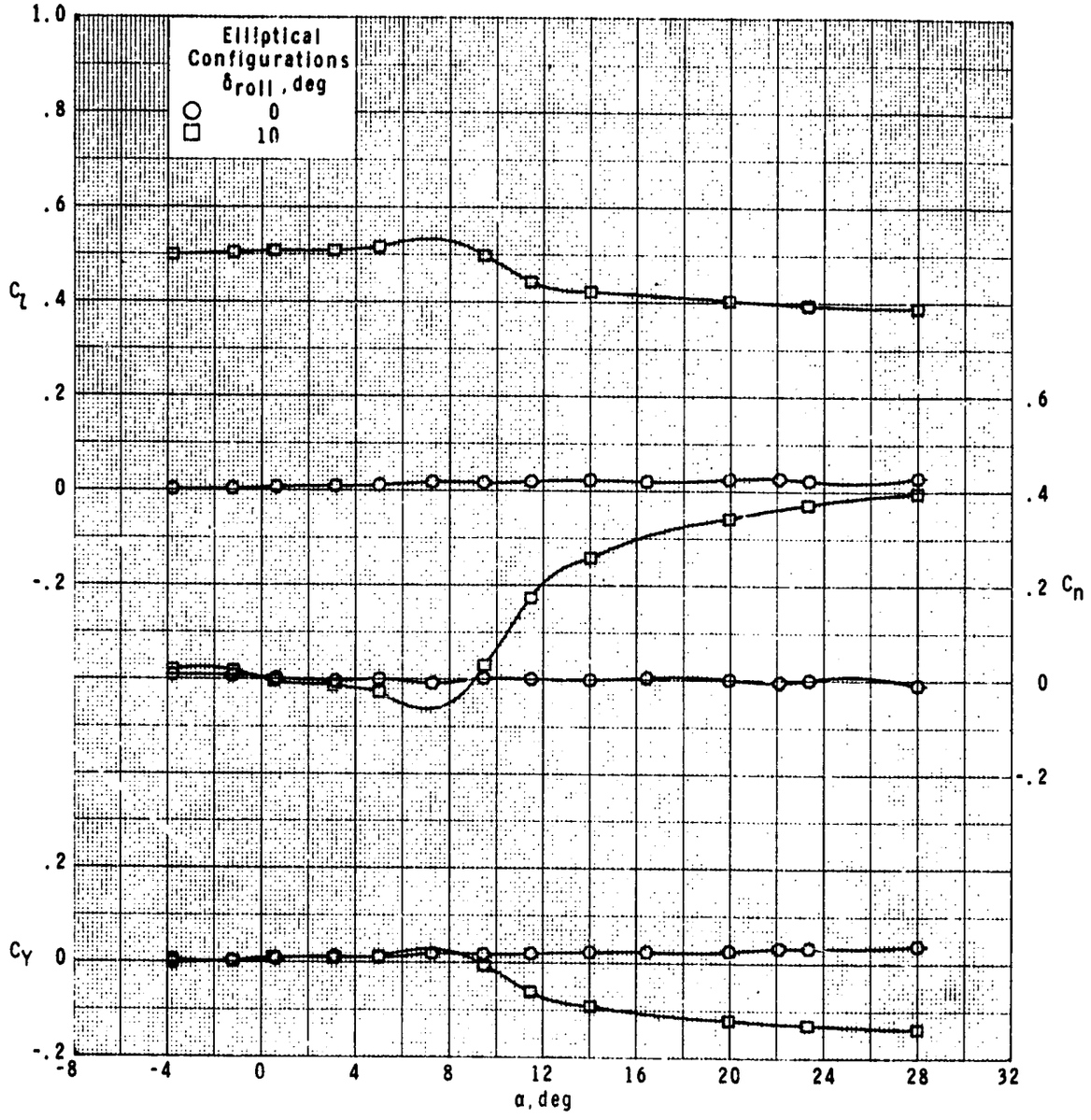

(f) M = 2.00.

Figure 19.- Continued.

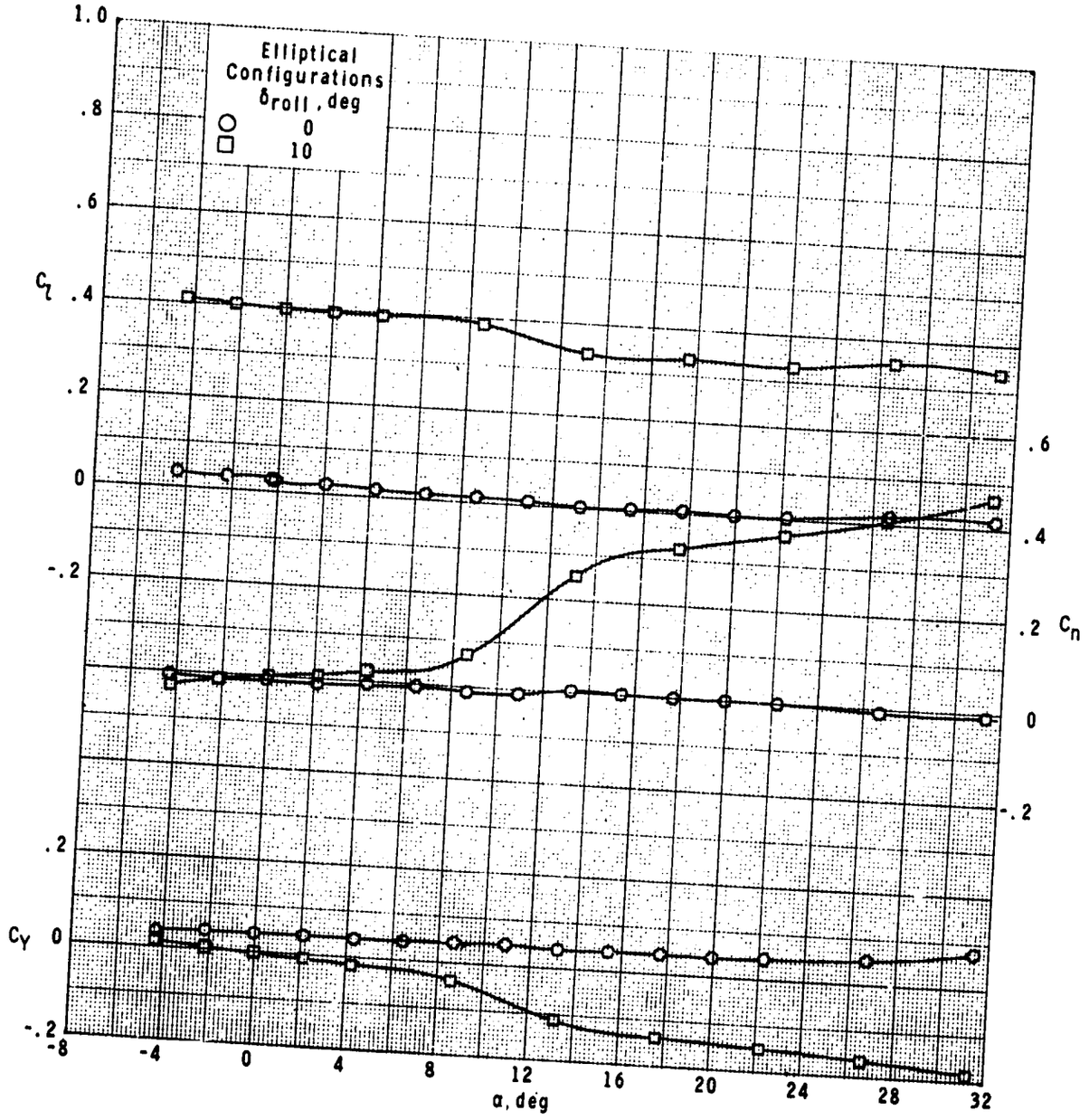

(g) M = 2.50.

Figure 19.- Continued.

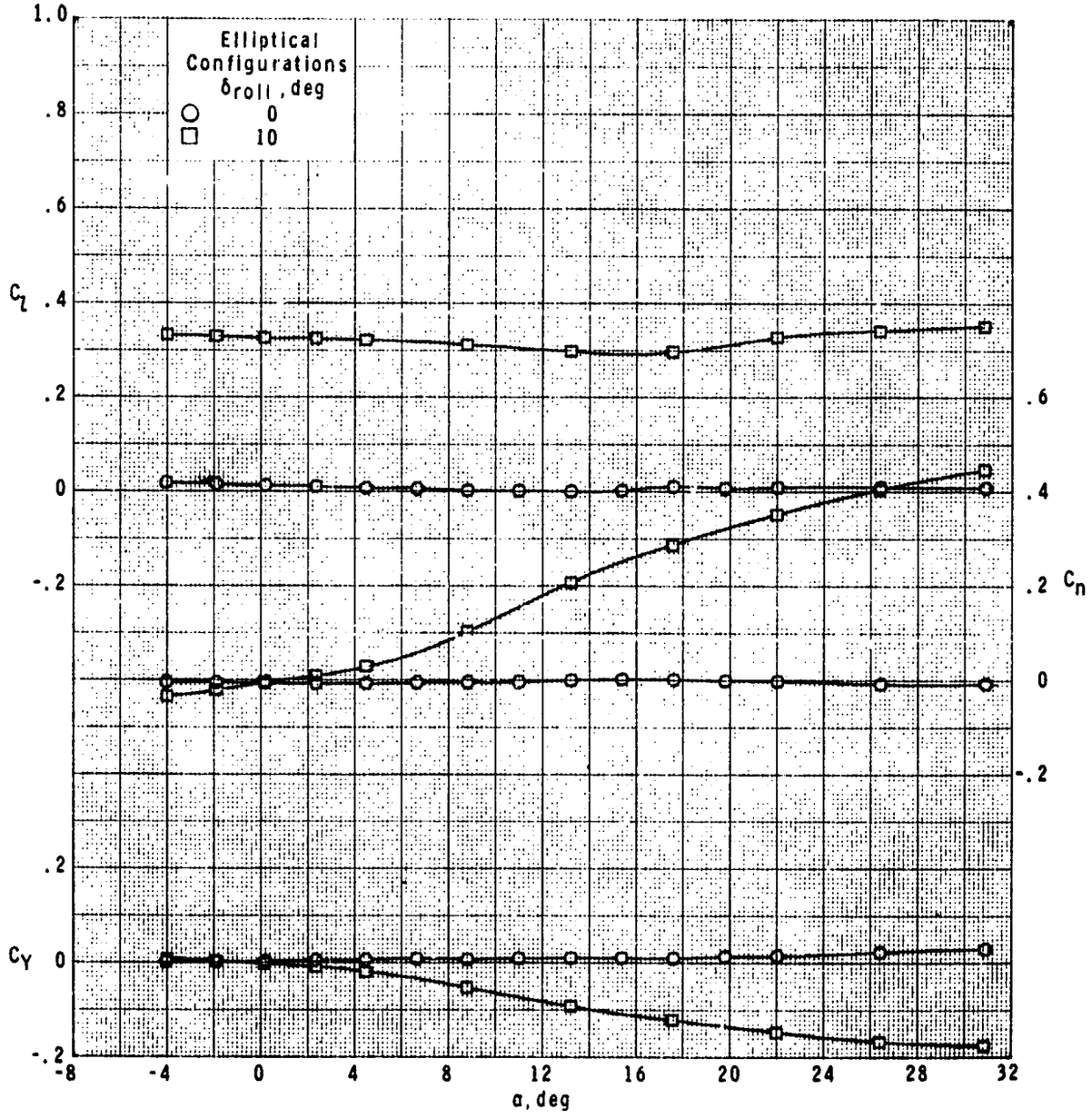

(h) M = 2.96.

Figure 19.- Continued.

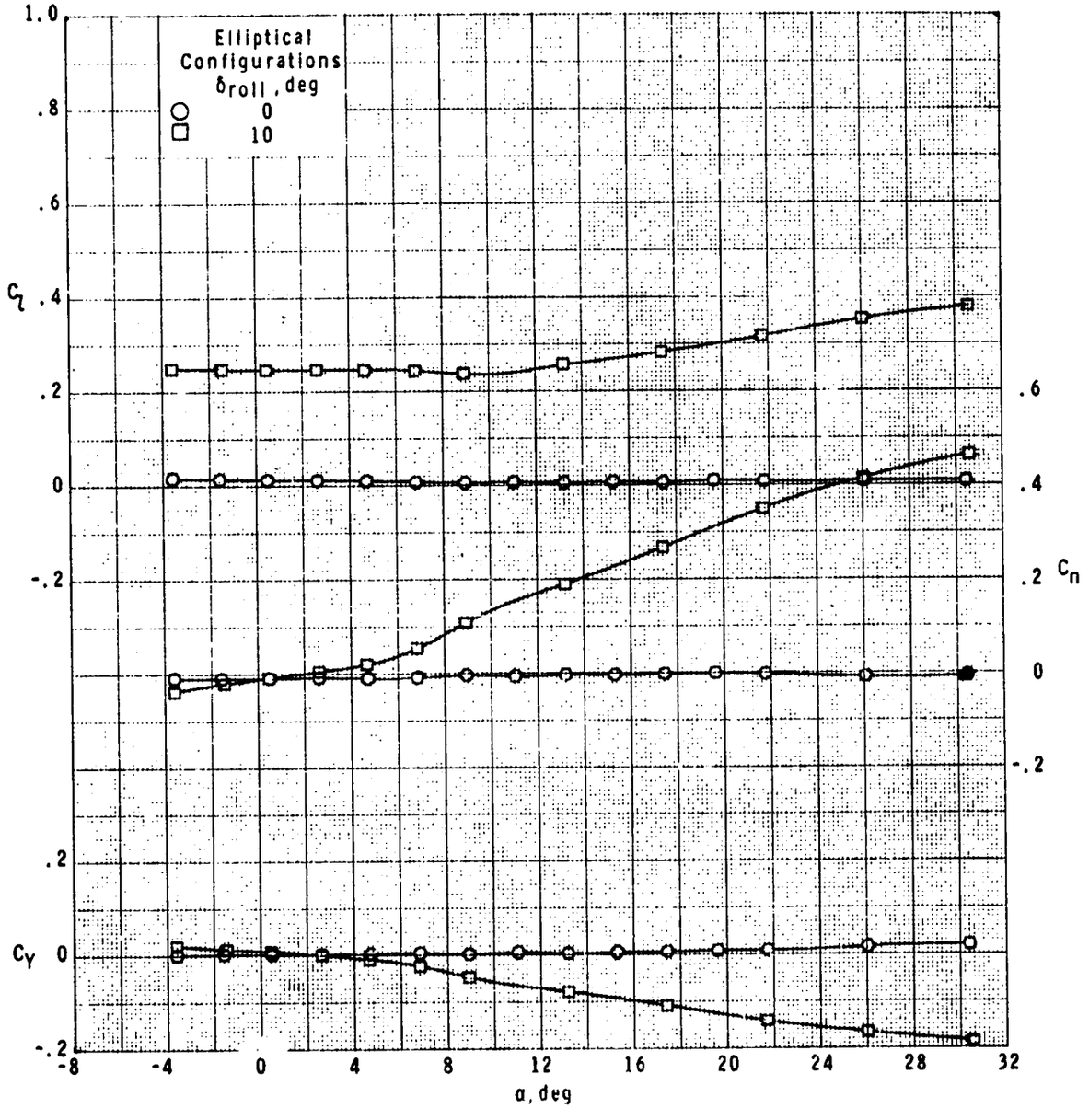

(i) M = 3.95.

Figure 19.- Continued.

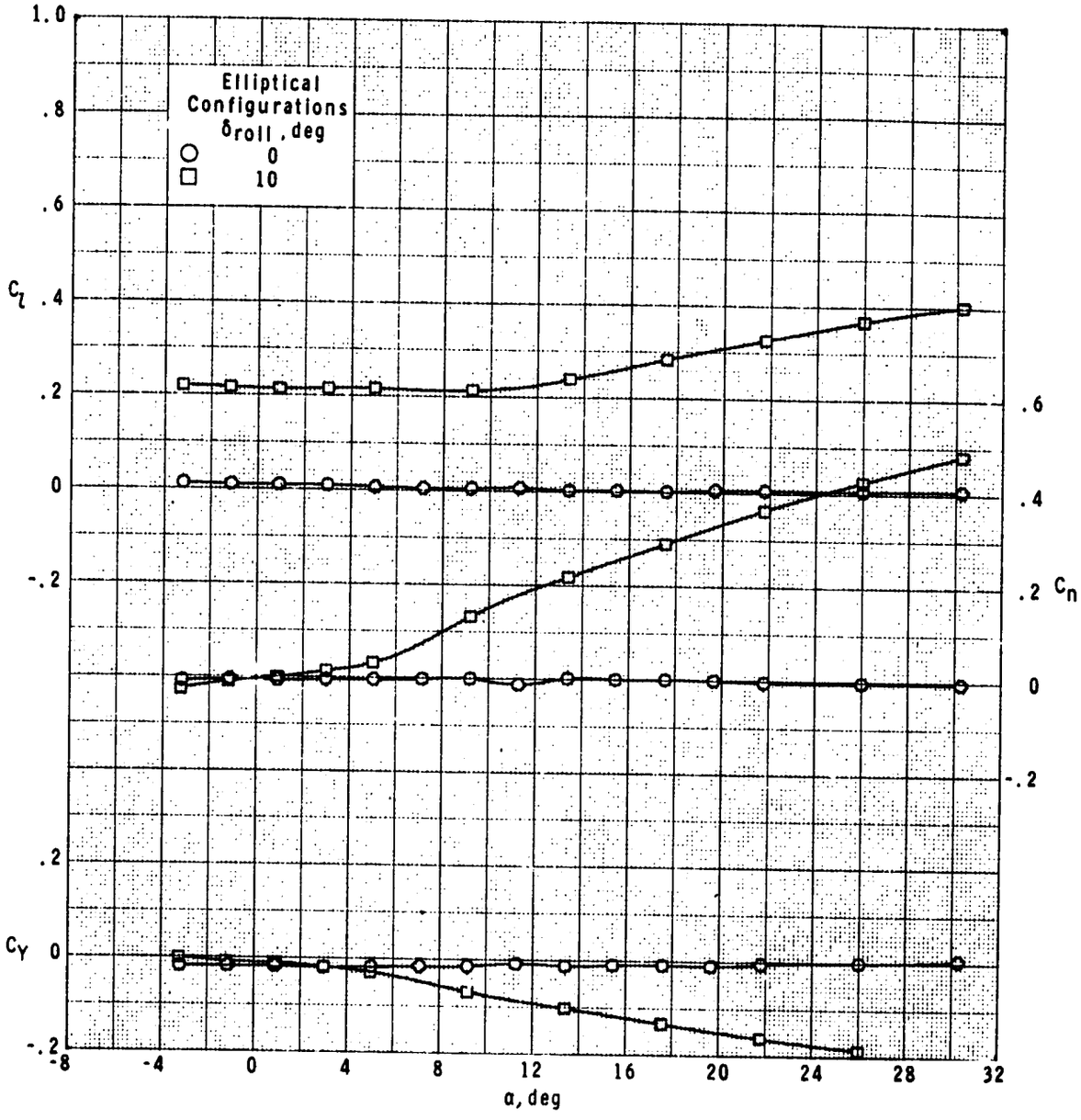

(j) M = 4.63.

Figure 19.- Concluded.

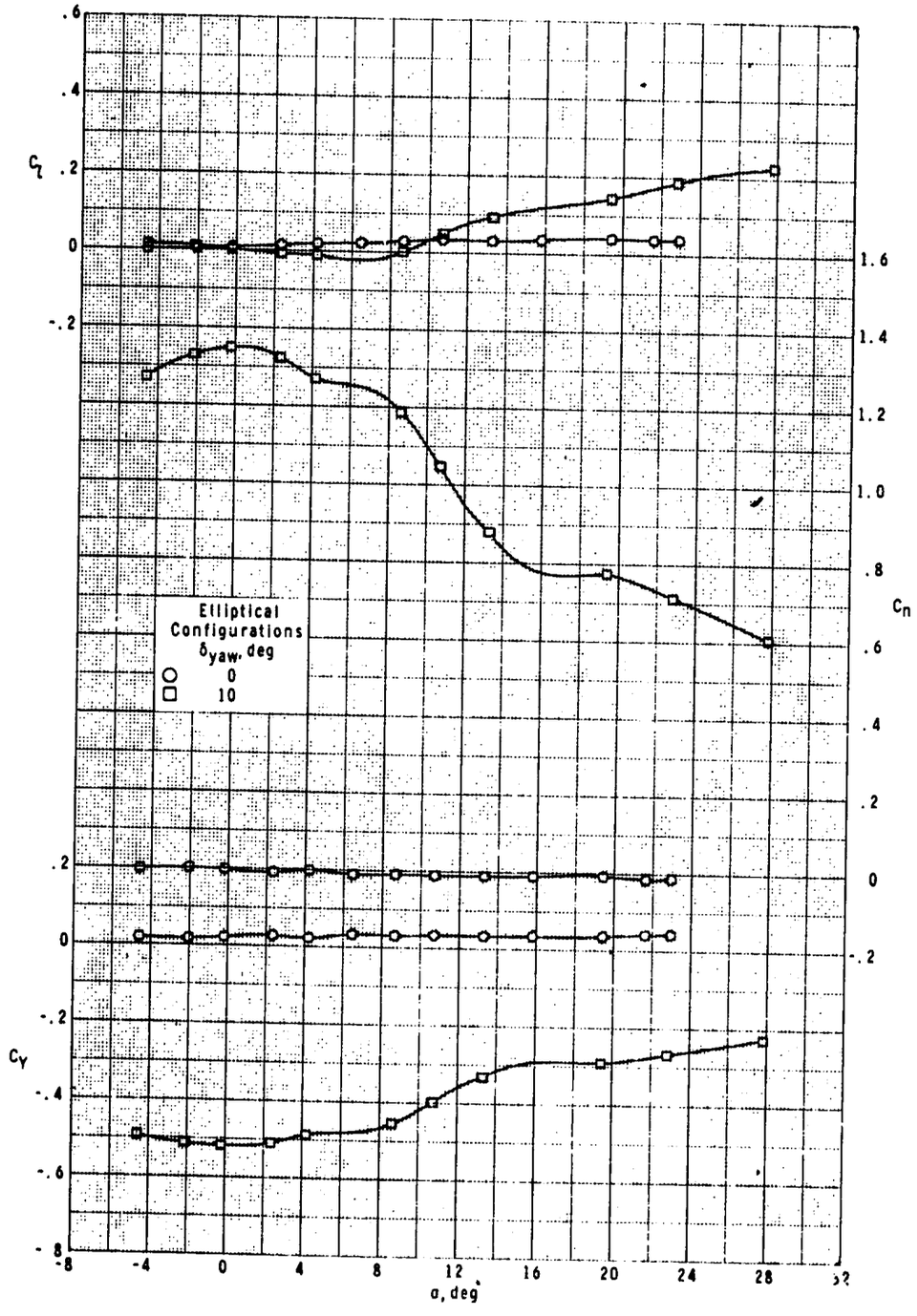

(a) M = 1.60.

Figure 20.- Yaw-control effectiveness of elliptical cross-section body-wing-tail configuration with variation in angle of attack.

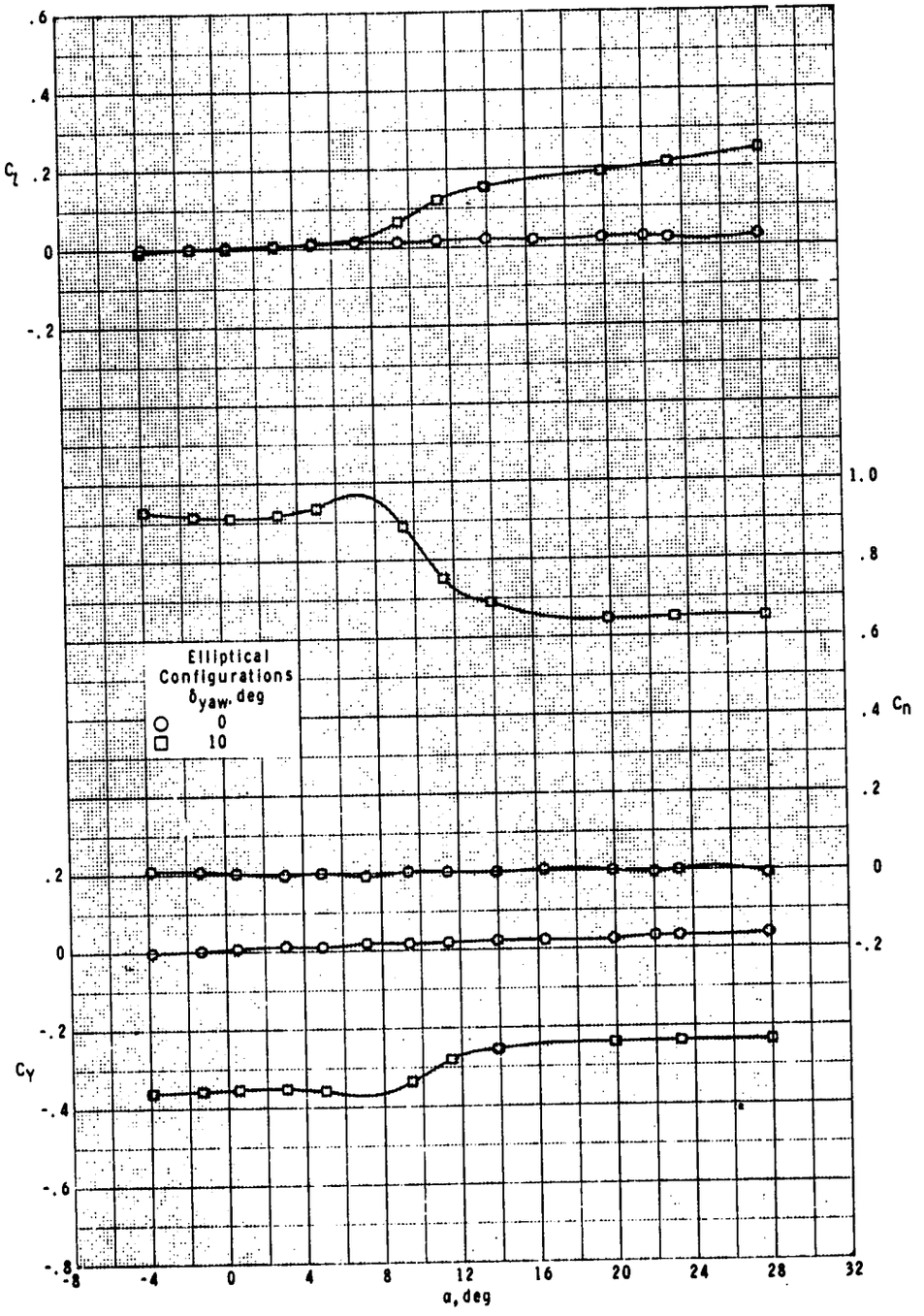

(b) M = 2.00.

Figure 20.- Continued.

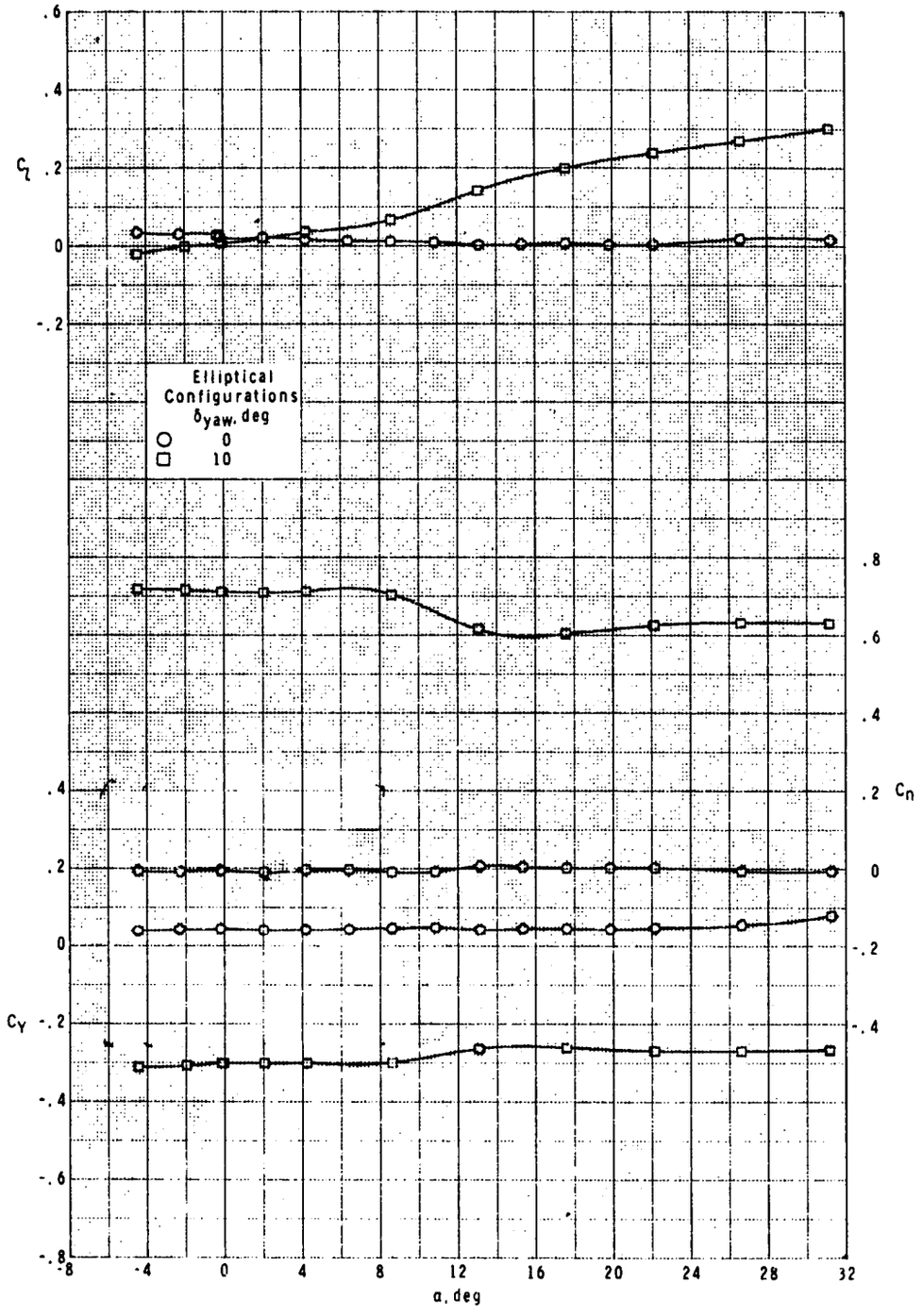

(c) M = 2.50.

Figure 20.- Continued.

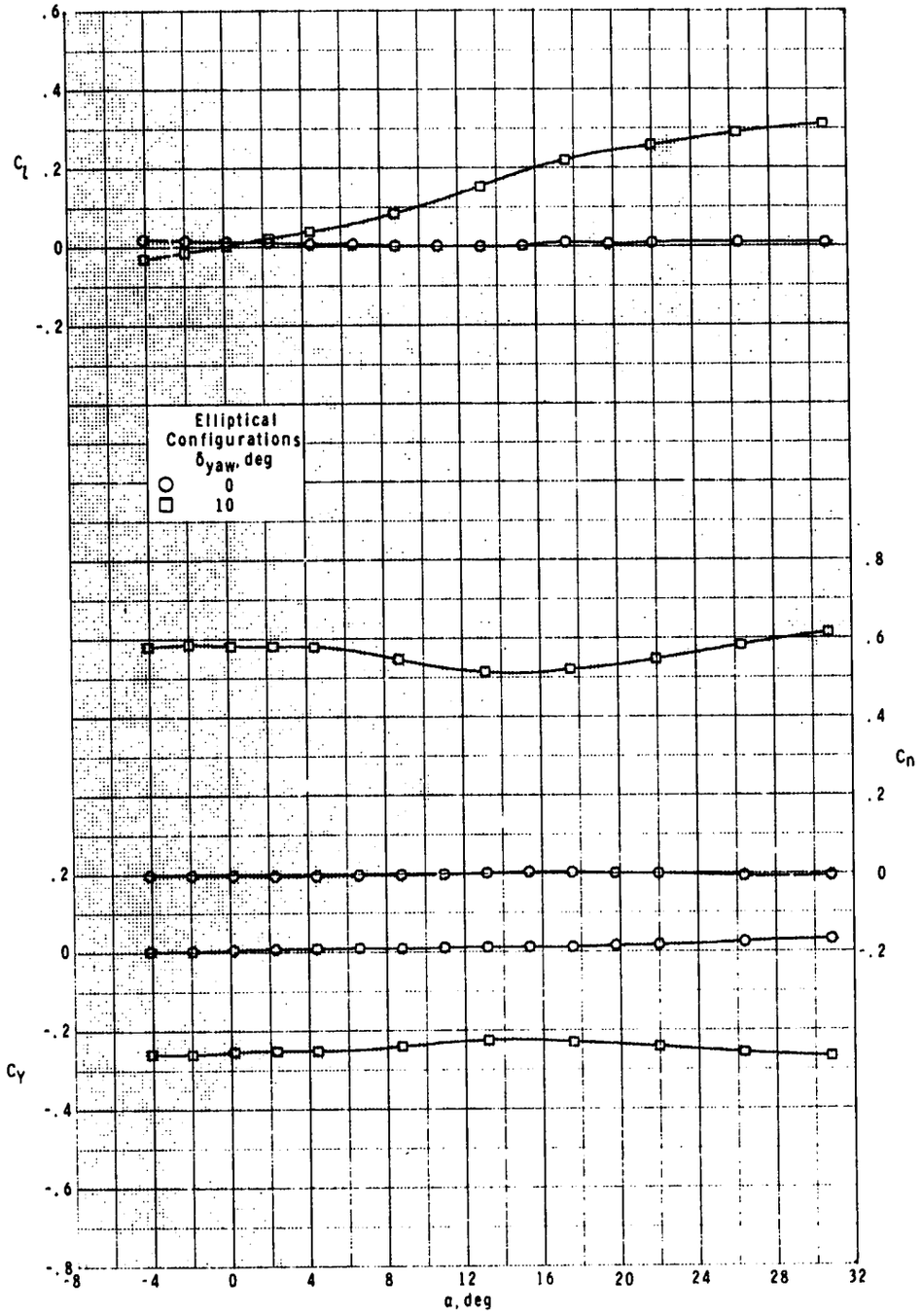

(d) M = 2.96.

Figure 20.- Continued.

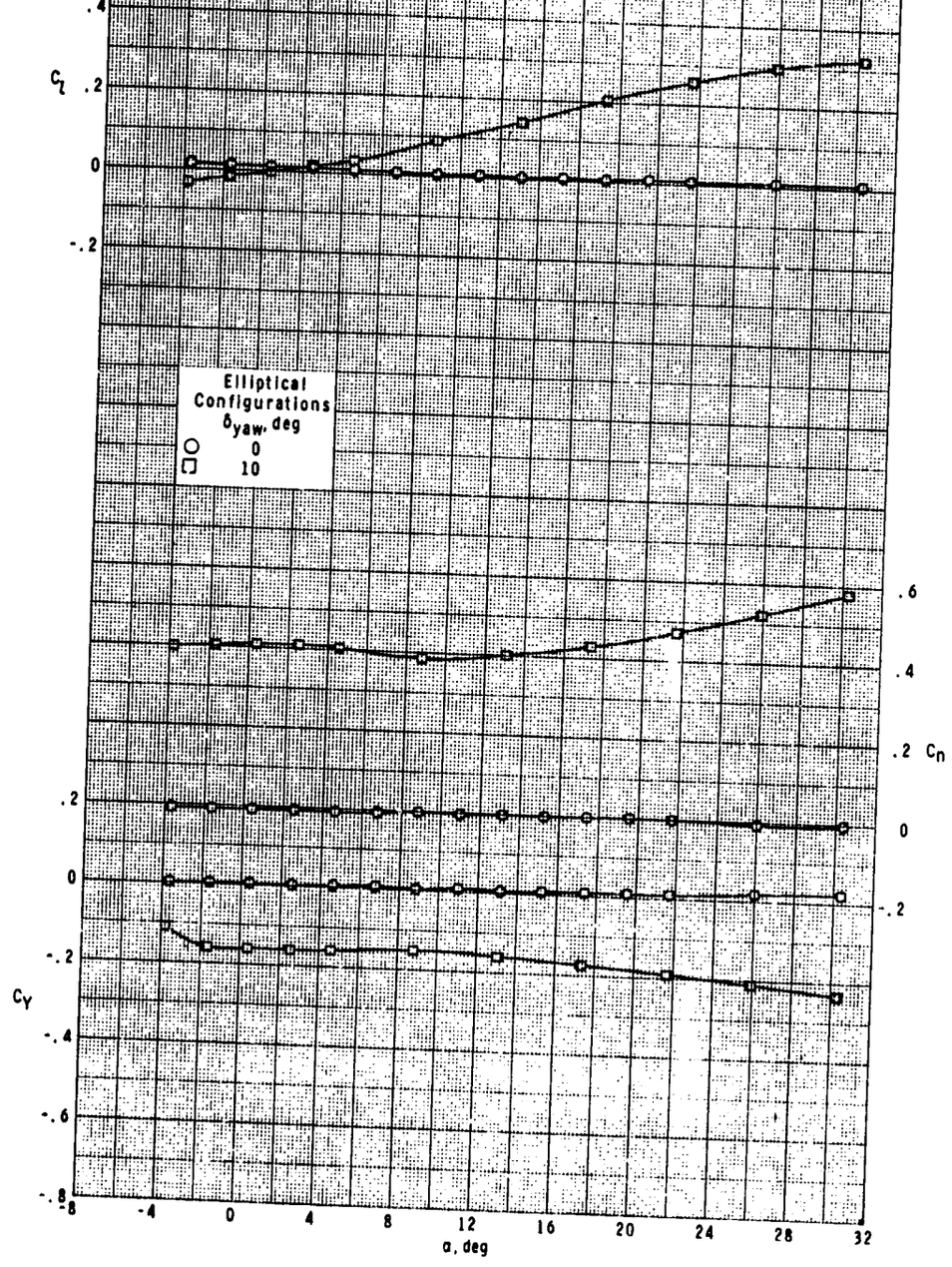

(e) M = 3.95.

Figure 20.- Continued.

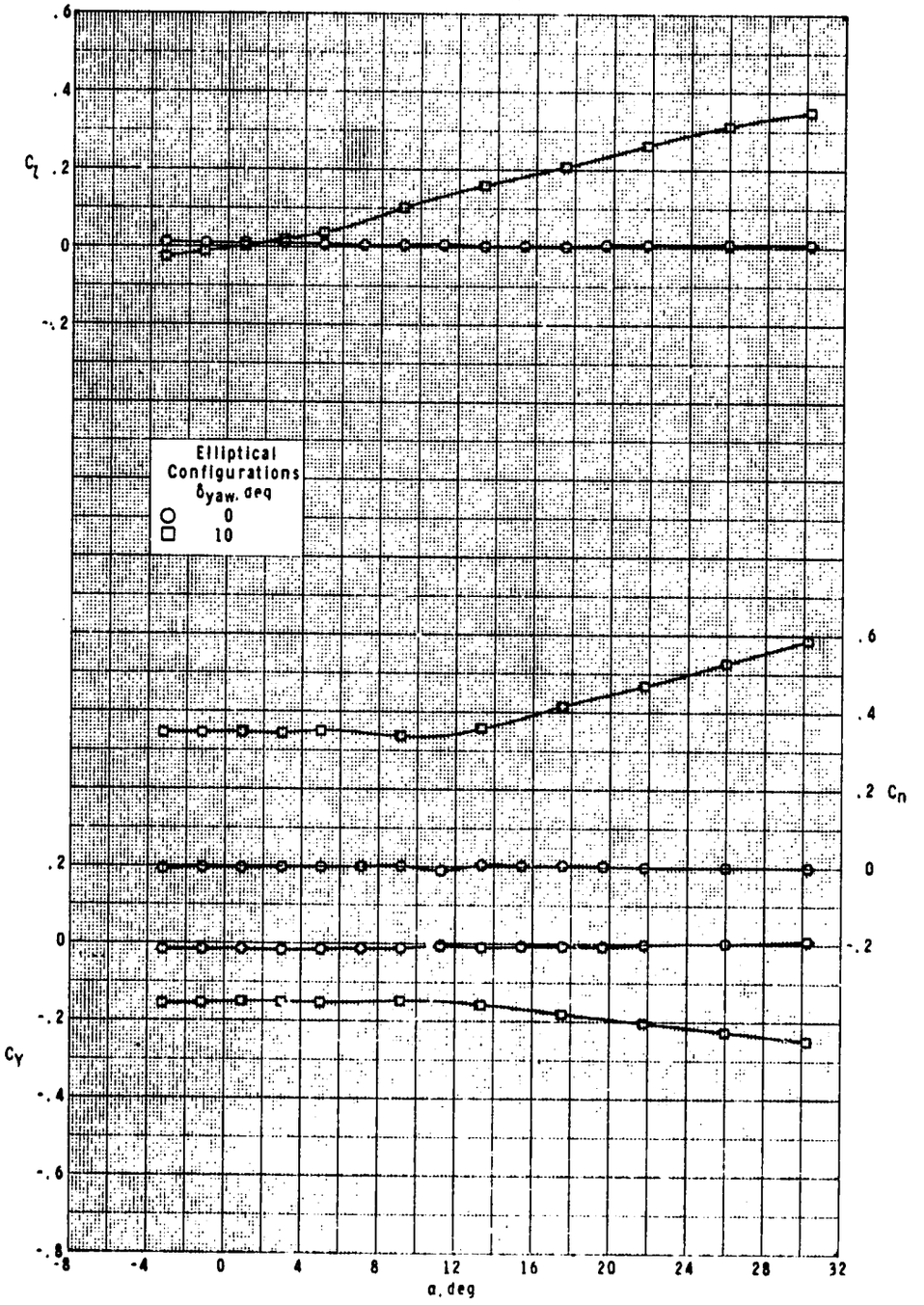

(f) M = 4.63.

Figure 20.- Concluded.

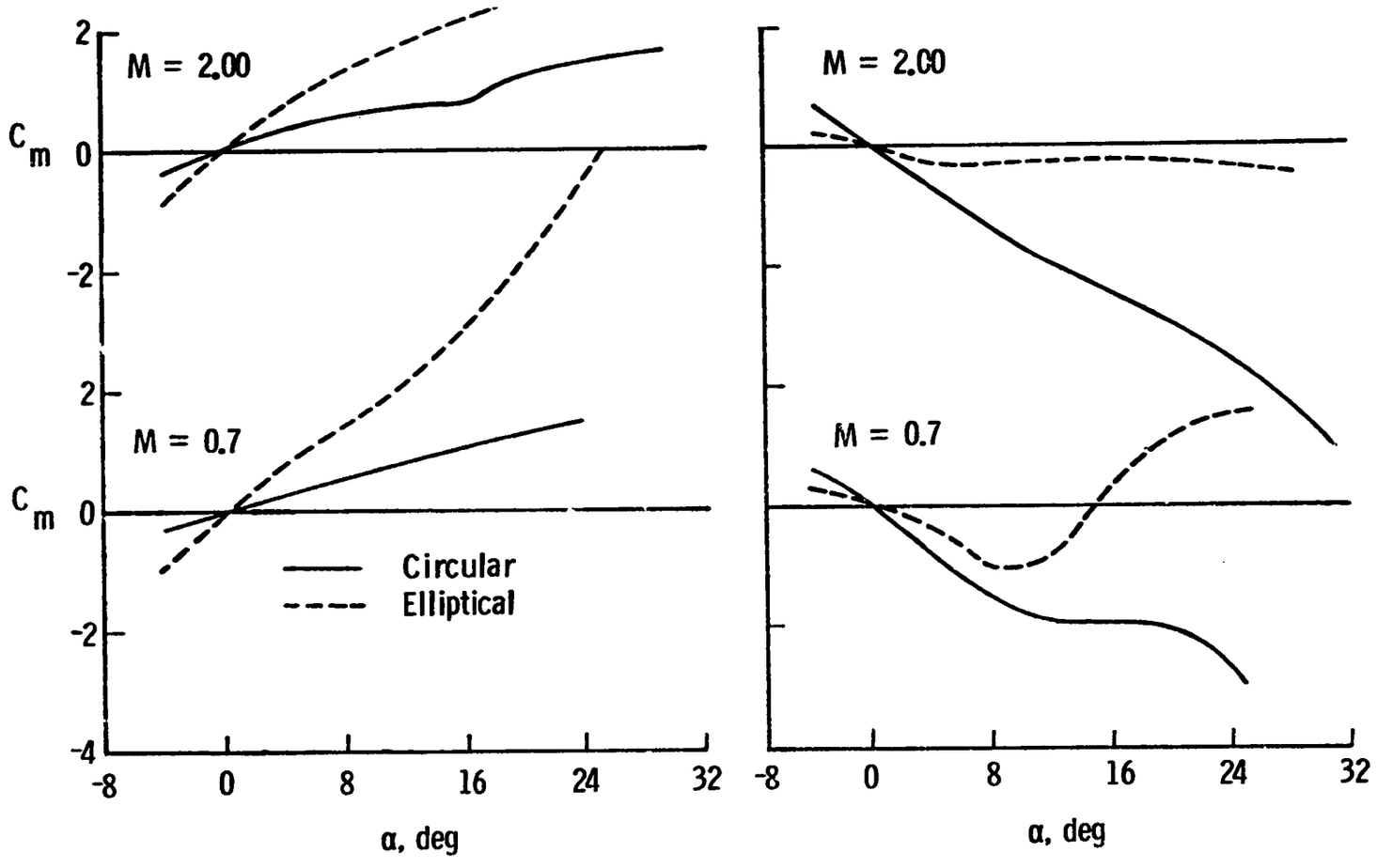

(a) Bodies.

(b) Missile concepts.

Figure 21.- Comparison of pitching moments.

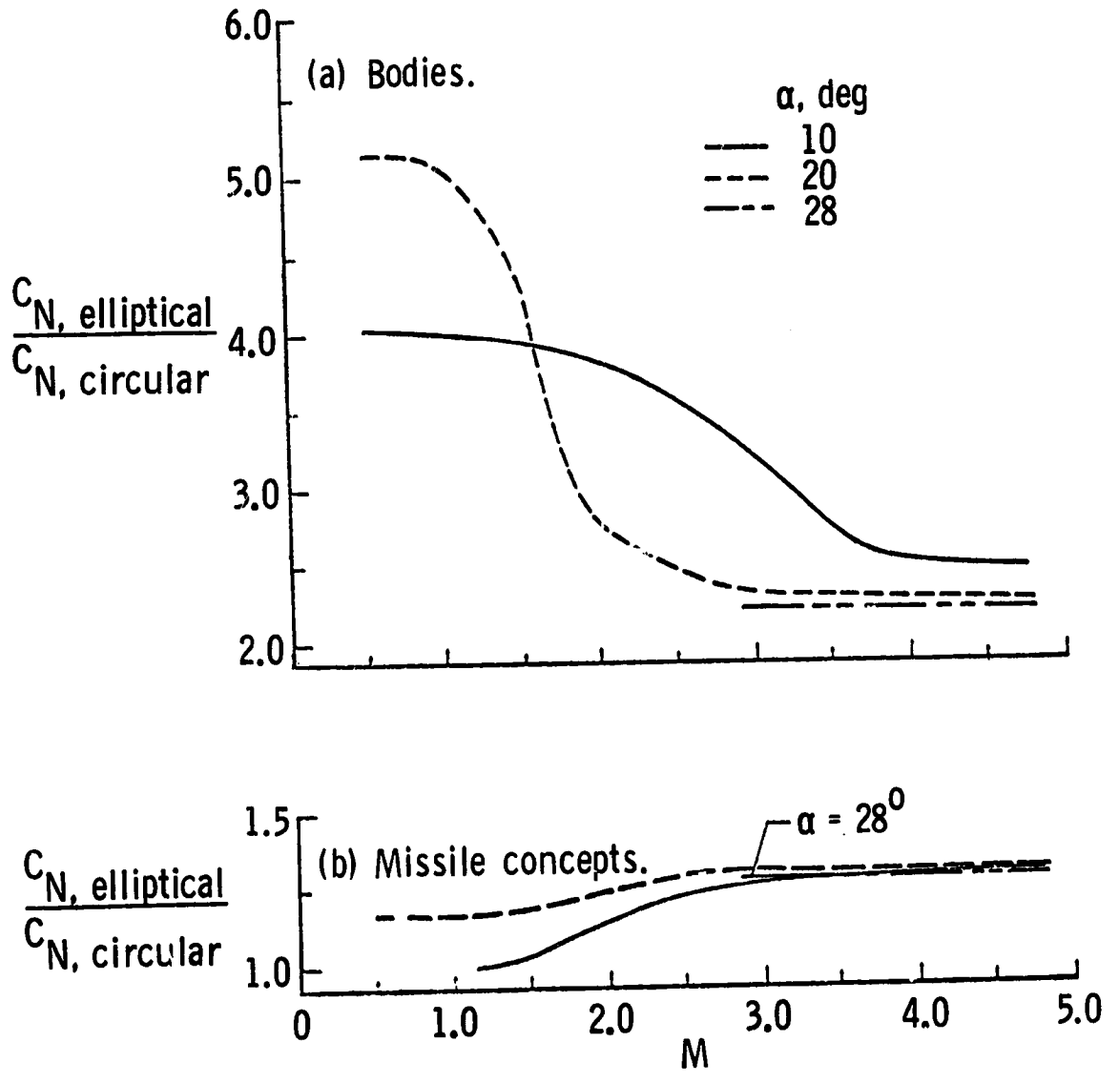

Figure 22.- Relative normal-force development.

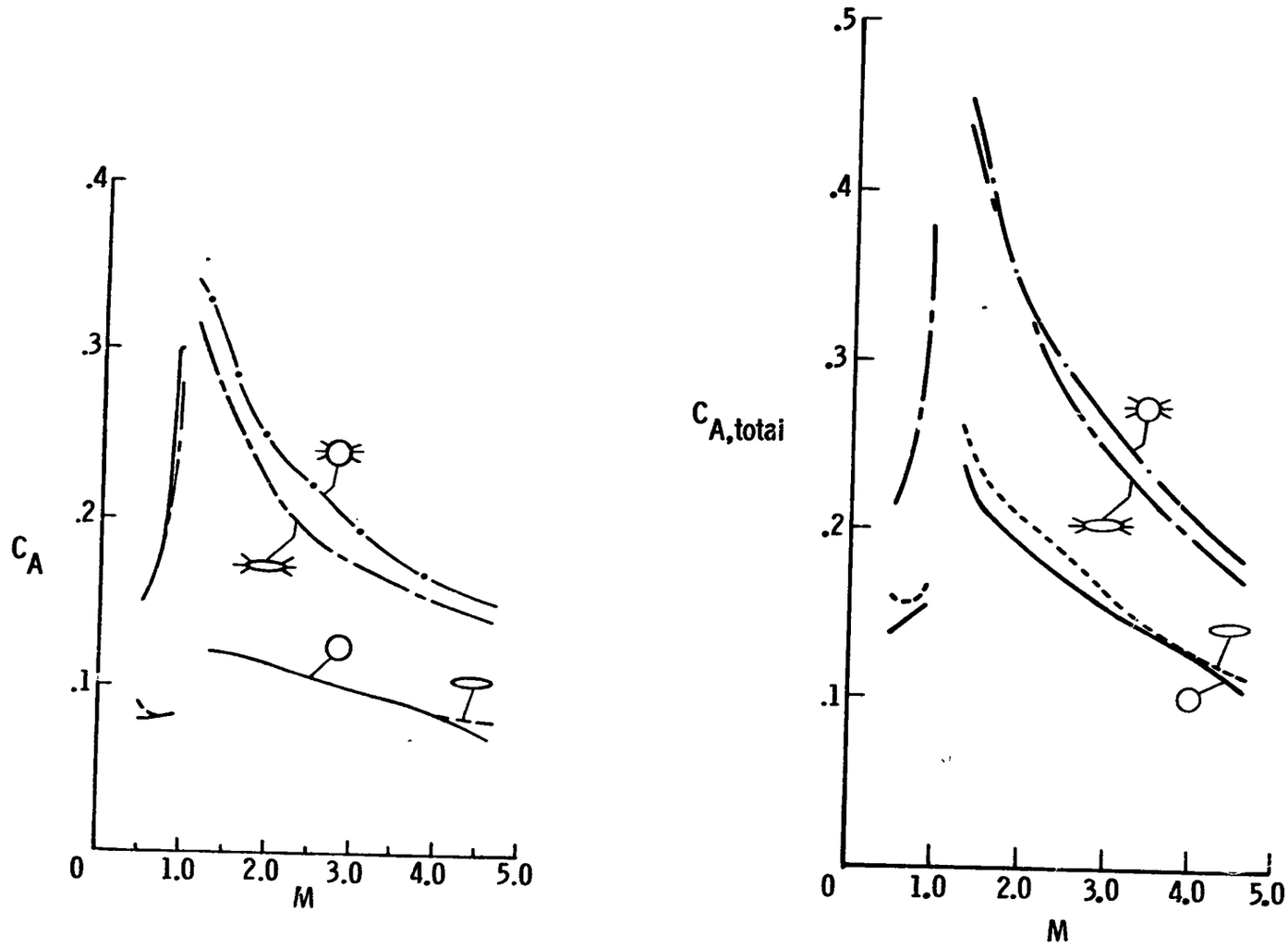

(a) Adjusted for base pressures.

(b) Gross axial force.

Figure 23.- Comparison of axial-force coefficients at zero angle of attack.

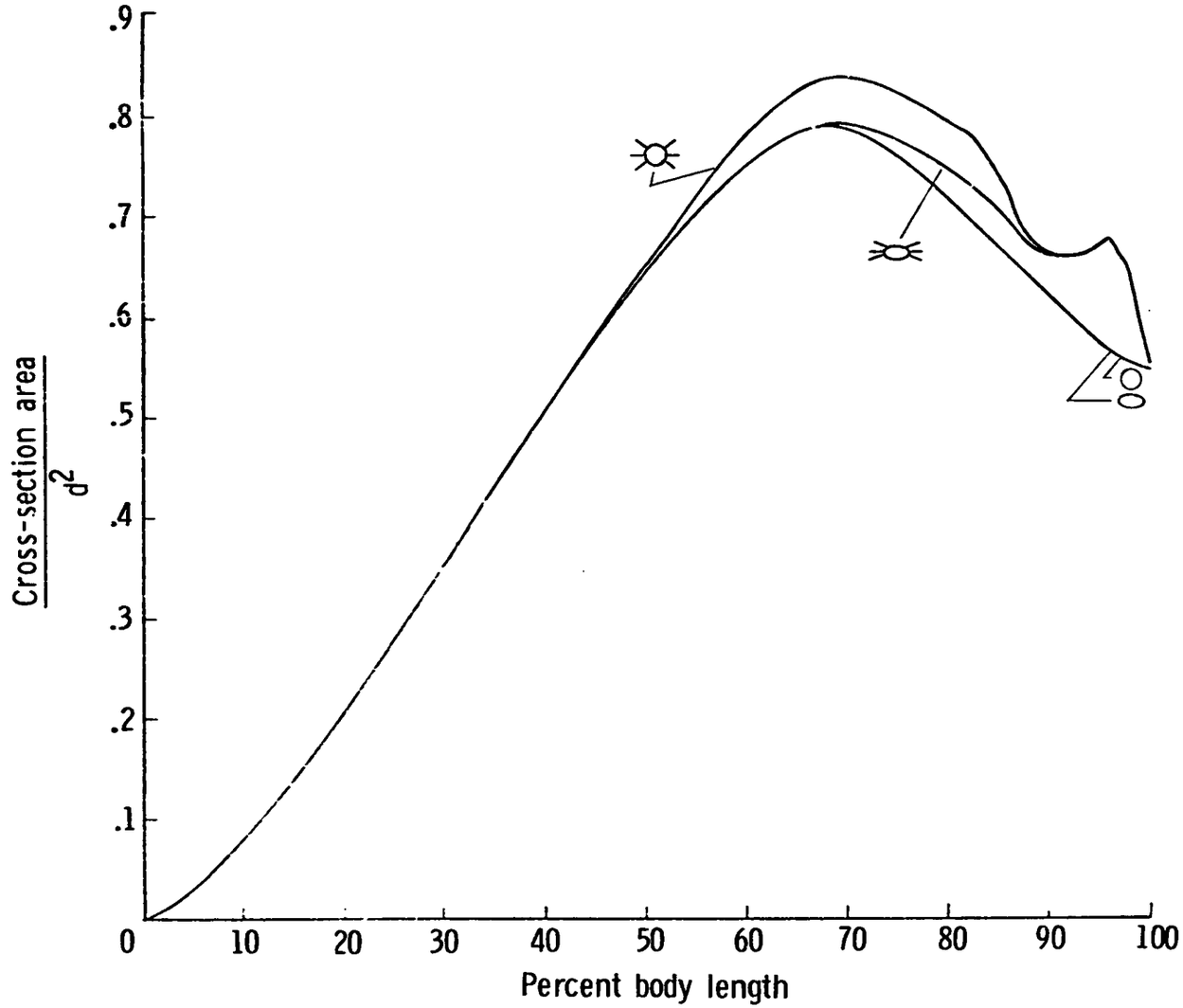

Figure 24.- Comparison of cross-section area distributions.

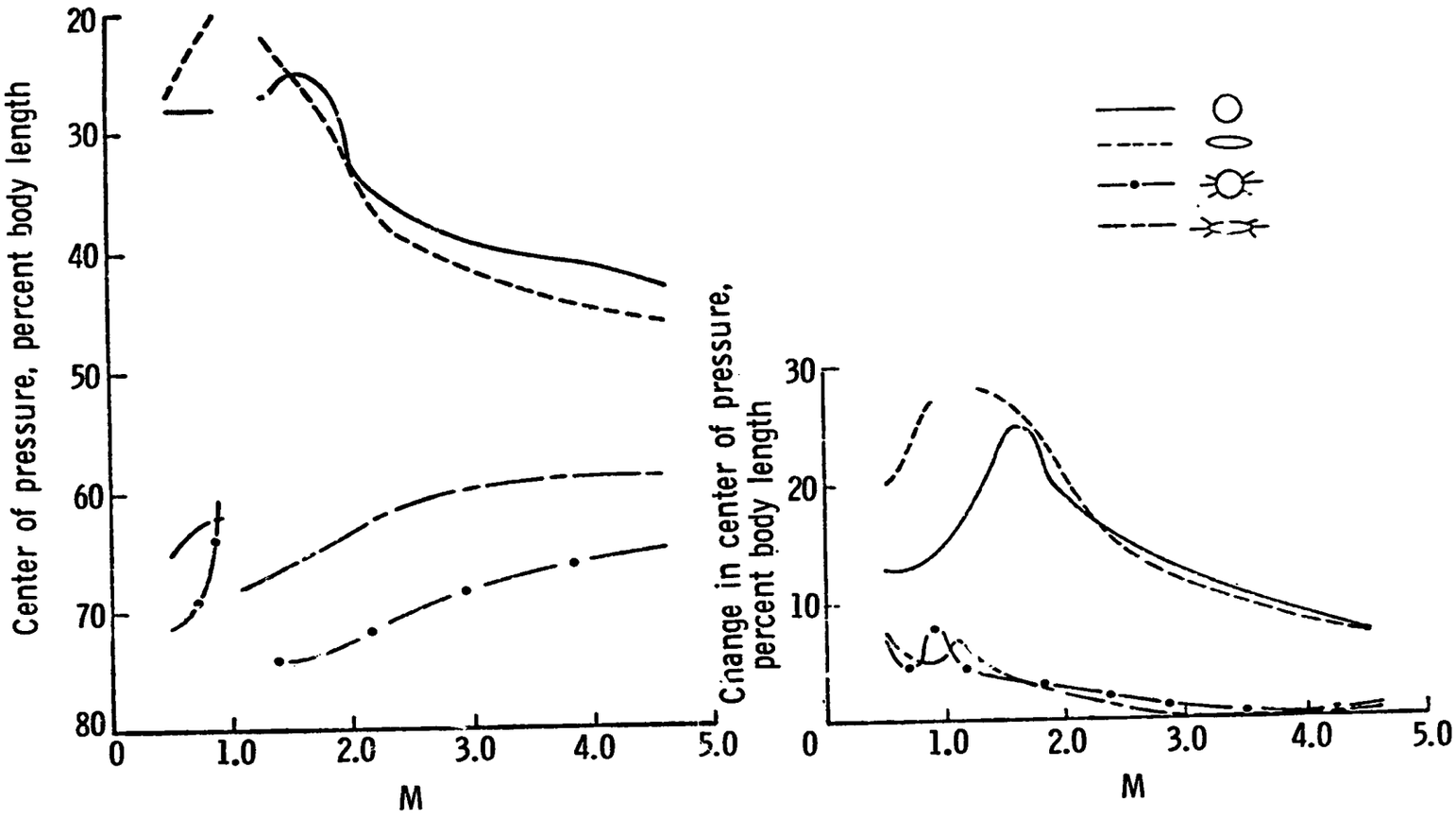

(a) Zero angle of attack.

(b) Angle of attack between 0° and 20°.

Figure 25.- Comparison of center-of-pressure travel.

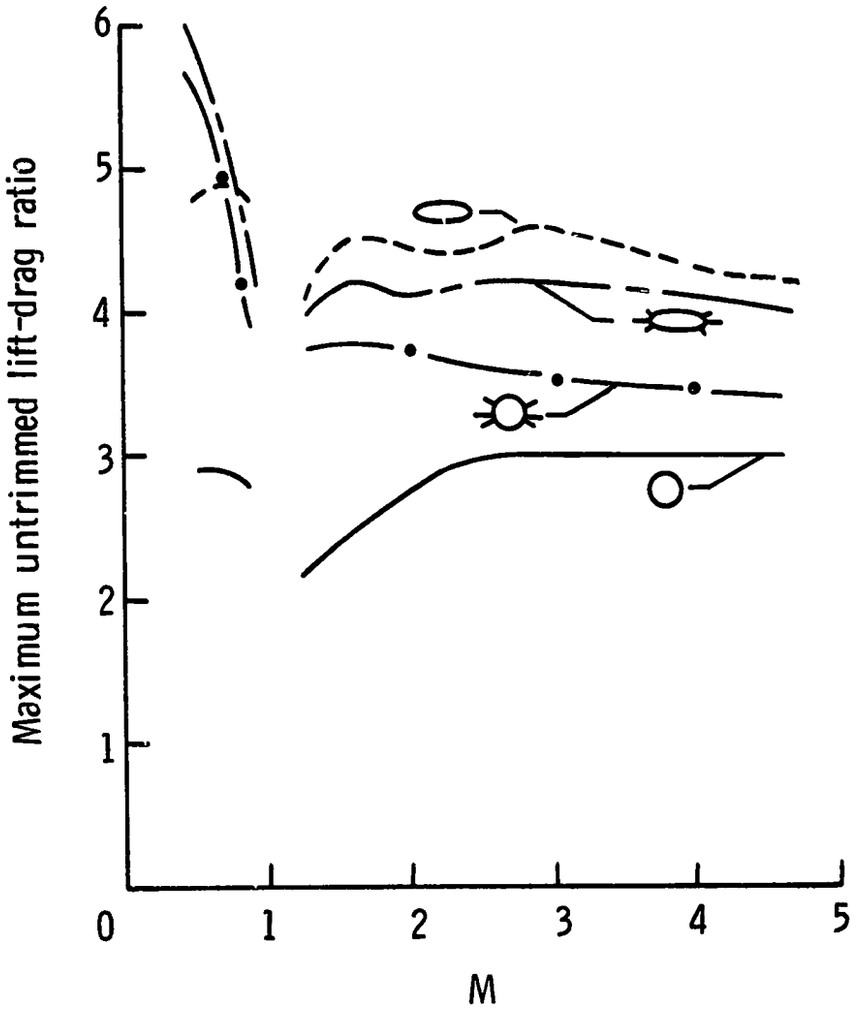

Figure 26.- Comparison of maximum lift-drag ratios.

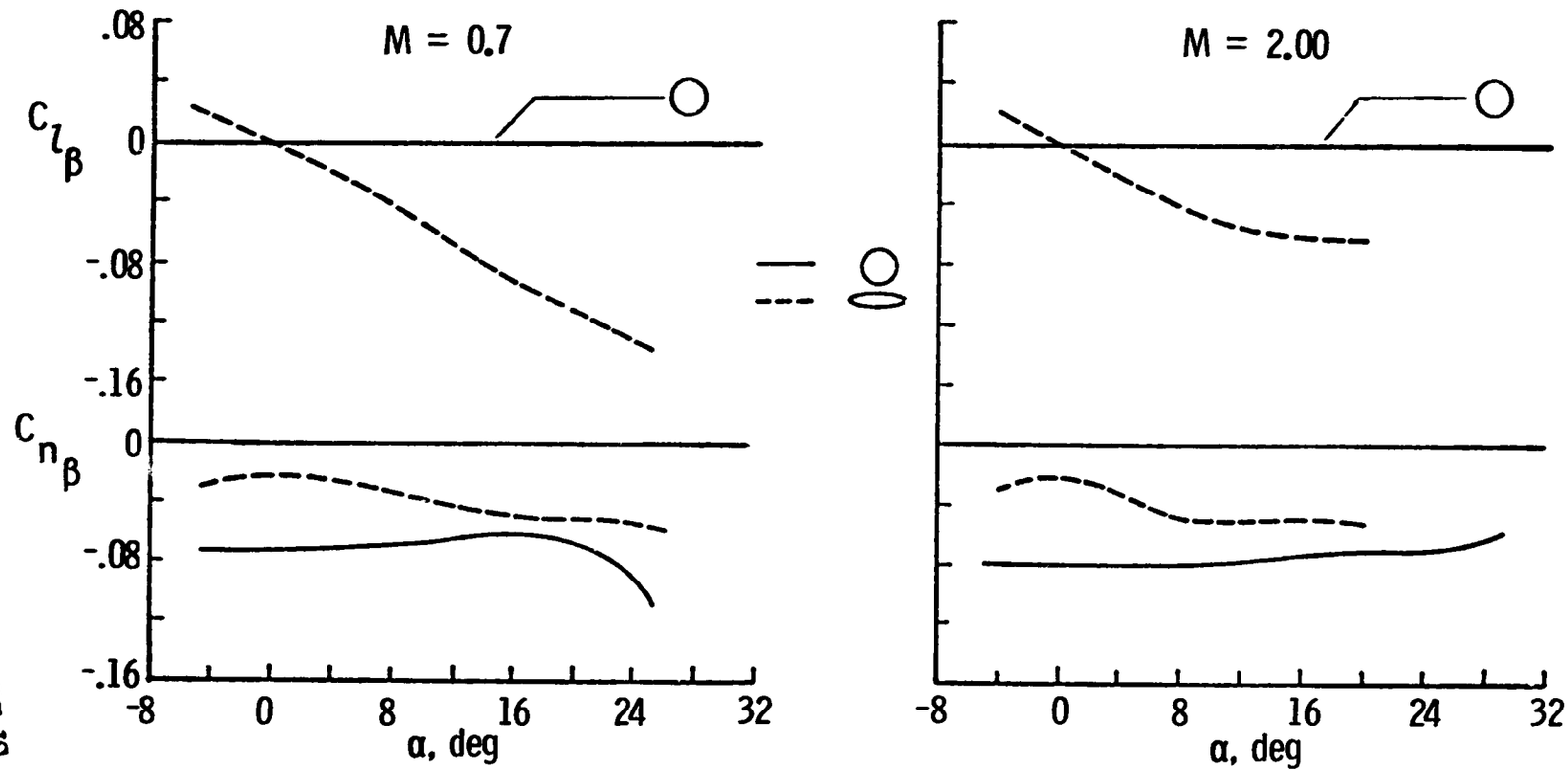

(a) Bodies.

Figure 27.- Comparison of lateral-directional stability parameters.

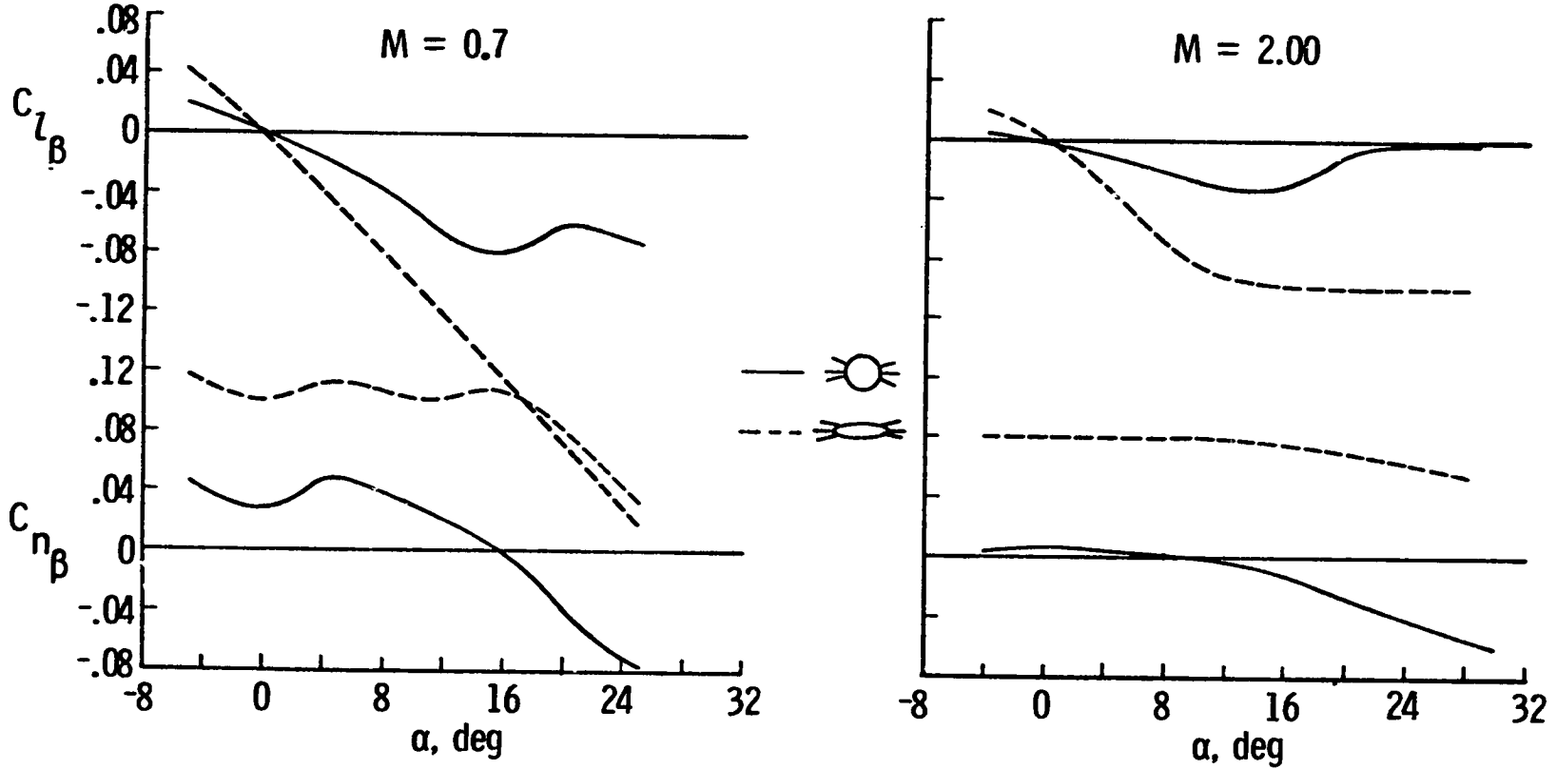

(b) Missile concepts.

Figure 27.- Concluded.

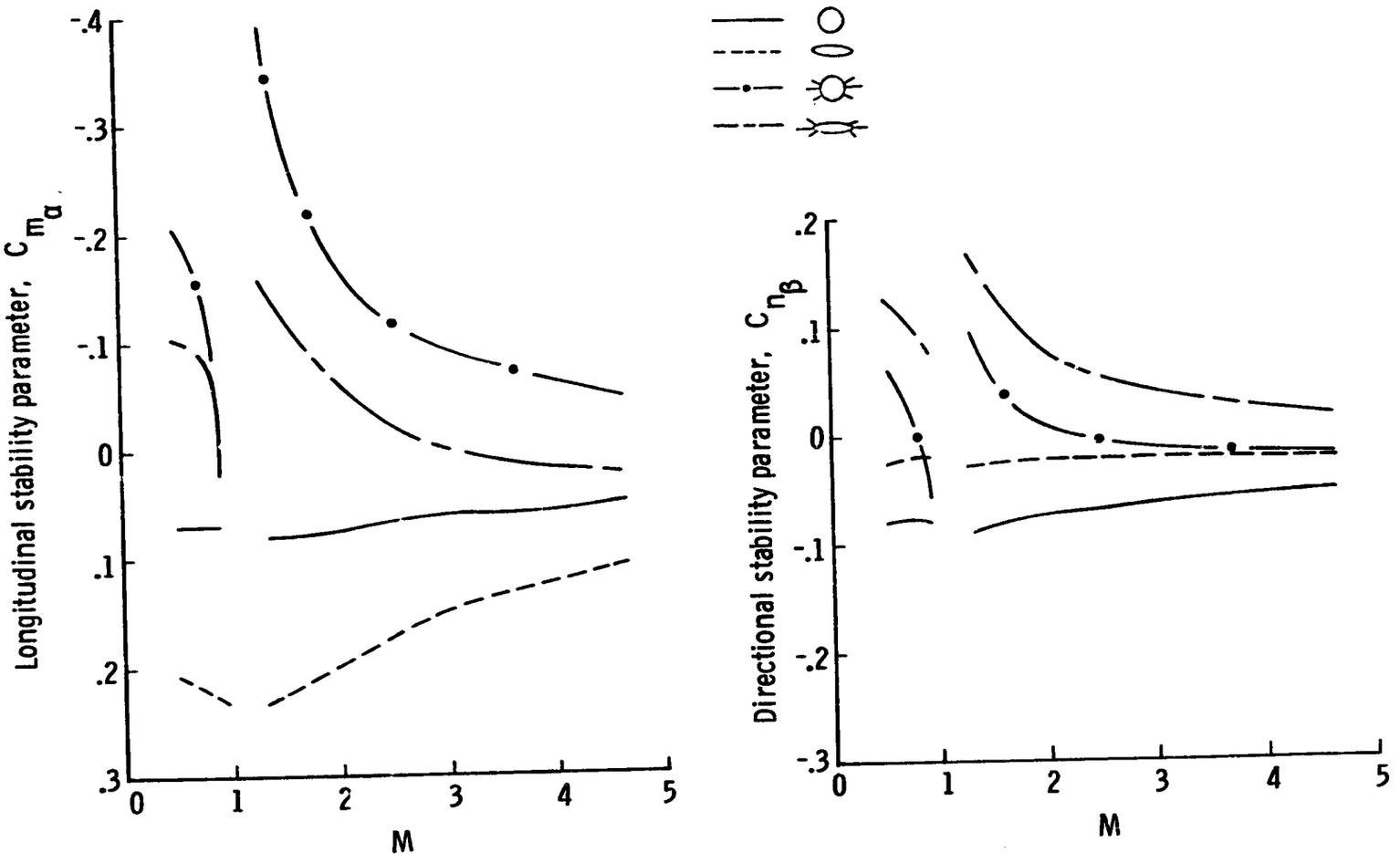

Figure 28.- Comparison of longitudinal and directional stability parameters.

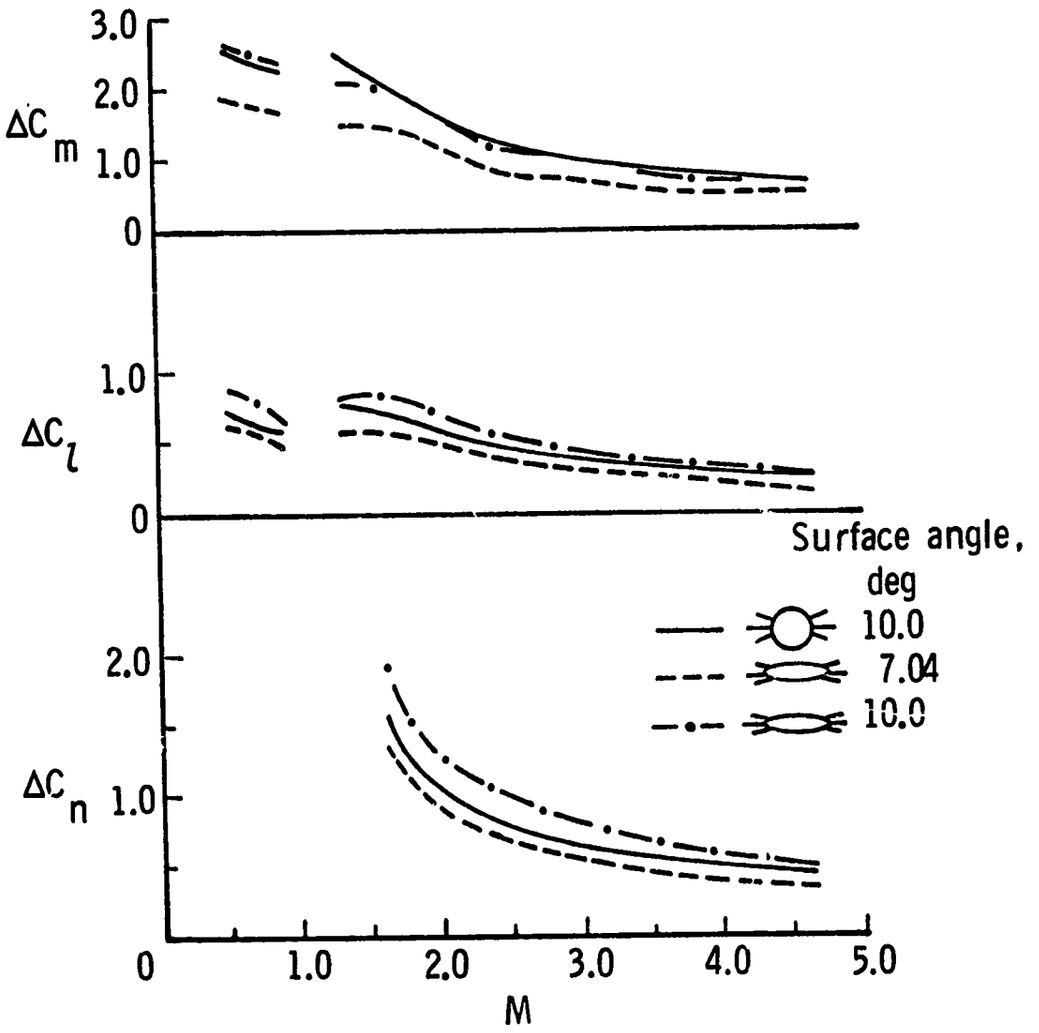

Figure 29.- Comparison of moment control parameters.

1. Report No.	2. Government Accession No.	3. Recipient's Catalog No.
NASA TM-74079		

4. Title and Subtitle	5. Report Date
AERODYNAMIC CHARACTERISTICS OF A NON-PLANAR MISSILE CONCEPT WITH BODIES OF CIRCULAR AND ELLIPTICAL CROSS SECTIONS	December 1977
	6. Performing Organization Code

7. Author(s)	8. Performing Organization Report No.
Ernald B. Graves	L-11963
	10. Work Unit No. 505-11-[illegible]-01

9. Performing Organization Name and Address	11. Contract or Grant No.
NASA Langley Research Center Hampton, VA 23665	
	13. Type of Report and Period Covered
12. Sponsoring Agency Name and Address	Technical Memorandum
National Aeronautics and Space Administration Washington, DC 20546	14. Sponsoring Agency Code

15. Supplementary Notes

16. Abstract

An investigation has been conducted to compare the experimental aerodynamic characteristics of a low-drag missile concept with a body of circular cross section to one with a body of 3:1 elliptical cross section, the bodies having identical cross-section area distributions. The concepts were of non-wing design with constant wing span. Tail surfaces were located flush at the body base with ±30° dihedral. Wind-tunnel tests were performed at Mach numbers from 0.5 to 4.63 and at angles of attack from about -[illegible]° to [illegible]°.

17. Key Words (Suggested by Author(s))	18. Distribution Statement
Aerodynamic characteristics Missiles Non-planar missile Elliptical body	Unclassified - Unlimited Subject Category [illegible]

19. Security Classif. (of this report)	20. Security Classif. (of this page)	21. No. of Pages	22. Price*
Unclassified	Unclassified	[illegible]	[illegible]

* For sale by the National Technical Information Service, Springfield, Virginia 22161